REPORT NO.
UCB/EERC-87/04
DECEMBER 1990

EARTHQUAKE ENGINEERING RESEARCH CENTER

EARTHQUAKE SIMULATOR TESTING OF A COMBINED SLIDING BEARING AND RUBBER BEARING ISOLATION SYSTEM

by

JAMES M. KELLY
MICHEL S. CHALHOUB

Report to the National Science Foundation

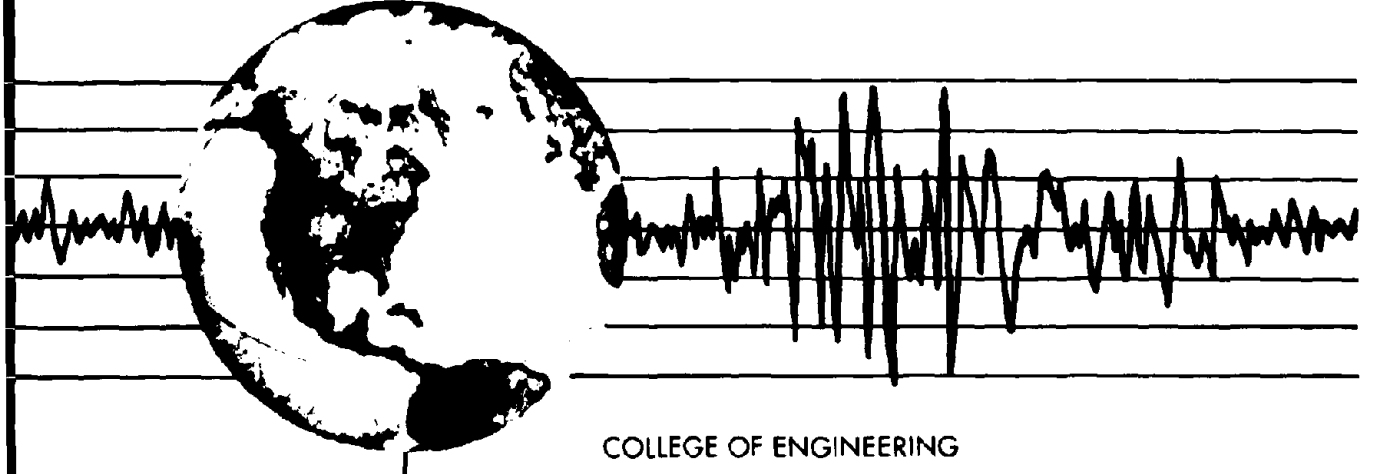

COLLEGE OF ENGINEERING

UNIVERSITY OF CALIFORNIA AT BERKELEY

For sale by the National Technical Information Service, U.S. Department of Commerce, Springfield, Virginia 22161

See back of report for up to date listing of EERC reports.

50272-101

REPORT DOCUMENTATION PAGE	1. REPORT NO. NSF/ENG-87049	2.	3. PB92-192962
4. Title and Subtitle: Earthquake Simulator Testing of a Combined Sliding Bearing and Rubber Bearing Isolation System			5. Report Date: December 1990 6.
7. Author(s): James M. Kelly and Michel S. Chalhoub			8. Performing Organization Rept. No. UCB/EERC-87/04
9. Performing Organization Name and Address: Earthquake Engineering Research Center, University of California, Berkeley, 1301 So. 46th Street, Richmond, Calif. 94804			10. Project/Task/Work Unit No. 11. Contract(C) or Grant(G) No. (C) (G)ECE-8414036
12. Sponsoring Organization Name and Address: National Science Foundation, 1800 G Street, N.W., Washington, D.C. 20550			13. Type of Report & Period Covered 14.

15. Supplementary Notes

16. Abstract (Limit: 200 words)

Essential requirements of a base isolation system include wind restraint, stability, and fail-safe capacity. A new base isolation system combining sliders and rubber bearings inherently satisfies all three requirements, and possesses other advantages. The system was tested on the Earthquake Simulator at the University of California at Berkeley by installing it under the base of a one-fourth scale nine-story steel structure and subjecting it to different earthquake inputs. The base behaves as fixed for low magnitude inputs. When sliding starts the rubber bearings provide additional stiffness and recentering. Under very severe inputs the tension devices reach their locking limit and cause a large increase in the stiffness of the system. Areas of base shear hysteresis loops are drastically enlarged by the addition of sliders. Displacements are better controlled than the ones for a purely elastomeric isolation system. Vertical deflections due to large horizontal drift encountered in solely rubber systems, are eliminated. The fail-safe capacity is provided by the tension restrainers and by the constant contact of the sliders with the base. The sliders were also tested separately on a static rig. The friction coefficient for teflon-stainless steel increases with sliding velocity and decreases with pressure. Teflon sustains high pressures without remarkable changes in its properties. The main aspect of its wearing is delamination.

17. Document Analysis a. Descriptors

b. Identifiers/Open-Ended Terms

c. COSATI Field/Group

18. Availability Statement: Release Unlimited	19. Security Class (This Report): Unclassified	21. No. of Pages: 184
	20. Security Class (This Page): unclassified	22. Price

(See ANSI-Z39.18) See Instructions on Reverse

OPTIONAL FORM 272 (4-77)
(Formerly NTIS-35)
Department of Commerce

EARTHQUAKE SIMULATOR TESTING OF A COMBINED SLIDING BEARING AND RUBBER BEARING ISOLATION SYSTEM

by

James M. Kelly

and

Michel S. Chalhoub

Report to the National Science Foundation

Report No. UCB/EERC-87/04
Earthquake Engineering Research Center
College of Engineering
University of California at Berkeley

December 1990

ABSTRACT

Essential requirements of a base isolation system include wind restraint, stability, and fail-safe capacity. A new base isolation system combining sliders and rubber bearings inherently satisfies all three requirements, and possesses other advantages. The system was tested on the Earthquake Simulator at the University of California at Berkeley by installing it under the base of a one-fourth scale nine-story steel structure and subjecting it to different earthquake inputs. The base behaves as fixed for low magnitude inputs. When sliding starts the rubber bearings provide additional stiffness and recentering. Under very severe inputs the tension devices reach their locking limit and cause a large increase in the stiffness of the system. Areas of base shear hysteresis loops are drastically enlarged by the addition of sliders. Displacements are better controlled than the ones for a purely elastomeric isolation system. Vertical deflections due to large horizontal drift encountered in solely rubber systems, are eliminated. The fail-safe capacity is provided by the tension restrainers and by the constant contact of the sliders with the base. The sliders were also tested separately on a static rig. The friction coefficient for teflon-stainless steel increases with sliding velocity and decreases with pressure. Teflon sustains high pressures without remarkable changes in its properties. The main aspect of its wearing is delamination.

ACKNOWLEDGEMENTS

The research reported here was supported by the National Science Foundation under Grant No. ECE-8414036 and was carried out at the Earthquake Simulator Laboratory of the Earthquake Engineering Research Center of the University of California at Berkeley. The authors would like to thank the National Science Foundation for its support, especially Dr. A. J. Eggenberger.

The isolation bearings used in the experimental work were provided to the project by Oil States Industries, Athens, Texas (now Bearing Pad Division of Fluorocarbon Inc.) and by the Malaysian Rubber Producers' Research Association, Hertford, England.

TABLE OF CONTENTS

LIST OF TABLES

LIST OF FIGURES

Figure **Page**

CHAPTER ONE

TEFLON AND RUBBER FOR BASE ISOLATION

Base isolation is a seismic design strategy based on the concept that a structure can be partially protected from earthquakes by uncoupling it from the ground. This can be achieved by mounting the structure on horizontally flexible foundations capable of accommodating relatively large displacements and thus acting as shock absorbers. The debate among engineers whether to attach a structure rigidly to the ground or to let it move at very low frequency has existed since 1909 [1]. The more conventional method has almost always been chosen.

Base isolation is rapidly gaining acceptance, however, and many systems have been proposed in recent years. The buildings which have been constructed world-wide using the concept have in the main been built using laminated elastomeric bearings of natural or artificial rubber, often with additional elements for the purpose of enhanced energy dissipation and control of displacements under wind loading [2, 3, 4]. A three-story school in Lambesc near Marseilles, France, consisting of three buildings separated by seismic gaps, uses 152 multilayered elastomeric isolators [5]. The isolators are 12 inch diameter circular pads containing 20 layers of rubber for a total rubber thickness of 1.6 inches. A government office building in Wellington, New Zealand, is built on laminated natural rubber bearings with cylindrical lead plugs pressed in a central hole. The effect of the lead is to increase the damping and to provide displacement control. In South Africa, a nuclear power plant rests on an isolation system using neoprene bearings with bronze-stainless steel sliders installed on top of the bearings, designed by a French construction company [6]. When the neoprene bearings can no longer accept the increasing horizontal displacement, sliding starts. Interest in base isolation is extremely high in Japan, and there are now several buildings in that country on isolation systems, mostly of the elastomeric bearing type with additional damping elements.

In the United States, the first building using laminated elastomeric pads for seismic protection is the Foothill Communities Law and Justice Center in Rancho Cucamonga [7]. It was dedicated on 20 March 1986. In Salt Lake City, the City and County building is in the process of being rehabilitated by the insertion of elastomeric isolators between its base and the ground [8]. Base isolation seems to be

the best solution for the rehabilitation of old buildings that contain precious architectural detailing.

There are several important requirements for base isolation systems. They have to provide a low frequency motion with relatively high damping in order to limit the displacements to an acceptable value. The system must incorporate a wind restraint and have a recentering effect. In the case of an unexpectedly severe earthquake, the system must provide a fail-safe capacity.

Sliding systems have been proposed as aseismic isolation systems because of their inherent simplicity and their relatively low cost. However, they present problems such as excessive drift and lack of fail-safe constraints. This is mainly due to their force-deflection characteristics which show no resistance once the sliding threshold is overcome. In addition, they may produce a very low effective frequency, because of the magnitude of the input, leading to extremely large relative displacements.

The arrangement tested in the present research combines sliders with elastomeric springs, and thereby produces a system with the desirable features of a base isolation system and none of the disadvantages of a purely sliding system. The damping needed in a base isolation system is here provided by friction energy dissipation. The high energy dissipation capacity of the system, shown by the large area of its hysteresis loops, is caused by the addition of the sliders.

Sliding bearings are used in large reinforced concrete structures to control shrinkage cracking and thermal deformations, but in that application, they include a mechanism that locks up the building at one end, so that the sliding elements play no role in the seismic response of the structure. The present system replaces the lock-up mechanism by flexible rubber bearings arranged around the periphery of the building, and incorporates the sliding elements into the seismic response.

Since this system is but a slight modification of an existing practice, it is possible that resistance to the use of such a system by civil engineers will be less than that which has been shown against the rubber bearing isolation system which is a more radical departure from conventional engineering.

CHAPTER TWO

TEST STRUCTURE AND ISOLATION SYSTEM

1. Test Structure

A one-fourth scale, nine-story steel frame was used in this experiment. The structure comprised four one-bay frames in the transverse direction and two three-bay frames in the longitudinal direction. An eccentric K-bracing system was placed in both directions. In the middle bays of the longitudinal frames, the braces had an eccentricity of 6 inches and consisted of double angles $1\frac{1}{2} \times 1\frac{1}{2} \times \frac{1}{4}$ inch at the first and fifth to ninth floors, and consisted of double angles $1 \times 1 \times \frac{1}{4}$ inch at the second, third and fourth floors. On the two exterior transversal frames, the braces had an eccentricity of 16 inches and consisted of double angles $1\frac{1}{2} \times 1\frac{1}{2} \times \frac{1}{8}$ inch for the upper seven stories and double angles $2 \times 2 \times \frac{3}{16}$ inch for the lower two stories. For the girders, single angles $3 \times 3\frac{1}{2} \times \frac{1}{4}$ inch were used to make an X-shaped brace system. The floors were about 3 feet high each, except for the first floor which was 4 feet high. The structure and its dimensions are shown in Figure 2.1, and the scale factors are tabulated in Table T-2.1.

As a rule of thumb, the fundamental period of a structure in seconds is close to one tenth of its number of stories. There is no risk of resonance between the fundamental frequency of a stiff building and that of the isolation system. For this reason, base isolation is well suited to low-rise buildings. The center of gravity of a short building is relatively low and, thus, so is its overturning moment, so that the elastomeric pads on which a base-isolated structure rests would always be in compression. Very tall buildings of more than 20 stories have a fundamental period above 2 seconds, and therefore do not need to be base isolated. Hence, there is a critical category of medium-size structures between 9 and 20 stories, for which isolation can be effective but for which uplift can play a role in the performance of the isolation system. The structure simulated in the present experiment falls into this category. Its fixed base fundamental frequency was 3.4 Hz, corresponding to 1.7 Hz in the prototype. For this reason, it was well suited to examine the possibility of extending the concept of base isolation further for medium rise buildings.

2. Mass Distribution

In order to introduce the desired inertia forces and overturning moment, concrete slabs were attached to the frame girders. The distribution of the concrete weights was limited by the shaking table load capacity of about 130 kips and its overturning moment capacity of about 1,700 kip-ft. The mass distribution is shown in Figure 2.1. The weight of the structure was about one kip per story, and after addition of the concrete slabs, the weight was distributed in a pattern of 1 - 9 - 9 - 9 - 9 - 13 - 9 - 9 - 9.2 - 14 kips, from top to bottom, leading to a total of about 91 kips for the entire model. At the fourth floor, a slightly higher mass was provided to increase the overturning moment effect in the response. The large mass at the base simulates the bottom slab of a real building which is generally heavy and rigid in order to distribute the vertical loads transmitted from the upper stories to the foundations uniformly.

3. Elastomeric Bearings

The idea of base isolation was proposed many years ago. However, it did not become practical until recent developments in the use of elastomers.

Rubber-like materials have been widely used in engineering applications, for purposes other than earthquake protection of buildings. Elastomeric blocks have been installed under bridge decks to accommodate slow differential movements; they have found application in the isolation of buildings against high frequency vibrations caused by traffic and they have also been used as elastic foundations for machinery and motors.

For the seismic protection of structures, elastomeric bearings have to fulfill different conditions. It is commonly accepted that vertical components of earthquake motion are much less severe in their effects than horizontal ones. Damage to a structure is mainly due to amplification in the horizontal direction. For this reason, seismic isolation uses elastomeric bearings that are very stiff in the vertical direction, but can accommodate large horizontal deflections. Large vertical stiffness avoids the amplification of rocking motion. Large horizontal flexibility causes the building to behave roughly as a single degree of freedom oscillator in the horizontal direction. Its motion will have a very low

frequency because of the large mass and the low stiffness. By careful design of the bearings in relation to the mass of the building, this frequency can be brought to a value low enough to be outside the range of frequency content of earthquake excitation.

The pads used in this experiment were multilayered elastomeric bearings made of thin rubber layers interleaved by thin steel plates. In the fabrication process, the rubber and steel are bonded together under high temperature and high pressure. The effect of the bond is a substantial increase in the compression modulus [9, 10], which prevents the rubber from bulging when subjected to a vertical load.

For the same mass distribution on the model, yielding 91 kips of total weight, two isolation systems using elastomeric bearings were used. A previous isolation system consisted of a set of eight filled rubber bearings provided by the Malaysian Rubber Producers' Research Association (MRPRA set #1), Hertford, England. Then steel-teflon sliders were used under the four internal columns of the structure and four natural rubber bearings with cylindrical central holes were installed under the corners. The central holes were initially designed to lodge a lead plug in each bearing to increase its stiffness and damping and thus provide better displacement control. In their present use, however, tension devices were installed in the holes instead of the lead plugs.

Properties of the Elastomeric Bearings

The MRPRA set #1 bearings had a 5.75×5.75 inch square cross section and consisted of 16 layers of rubber each 0.21 inch thick, yielding a total height of rubber of 3.4 inches, interleaved by 15 steel shims each 0.06 inch thick. The two extreme plates at the top and bottom of the bearing were each 5/8 inch thick. A 1/16 inch thick protective layer of rubber was glued on their lateral areas (Figure 2.2). These are used in real construction for the protection of the elastomer against external factors such as fire and oil. Their measured vertical stiffness was around 420 k/in. at 1.6% vertical strain and their horizontal stiffness around 1.1 k/in. at 60% shear strain. The shear modulus of the elastomer was 100 psi.

The natural rubber bearings used with the sliders had a 5.75×5.75 inch square cross section and consisted of 6 layers of rubber 3/8 inch thick each interleaved by 5 steel shims each 0.2 inch thick. The top and bottom limiting plates were 1 inch thick. The bearings had a 1.25 inch diameter central hole. A 1/8 inch thick protective rubber layer was glued to their lateral surface (Figures 2.5 and 2.6). Their horizontal stiffness was about 1.3 k/in. at 50% shear strain. Elastomeric bearings do not have a linear force-deflection relationship and the non-linearity increases with the level of strain and the applied axial load. For practical purposes, however, a linear relationship can be satisfactorily used. When installed under the structural model, each of the external bearings carried 9 kips while each of the internal ones carried about 14 kips.

Results obtained from static rig tests for the elastomeric bearings at different axial loads and different shear strain levels, are tabulated in Table T-2.2 and plotted in Figures 2.3 and 2.4. It is noticed that the effective stiffness drops with amplitude of excitation and with axial load. The amount of damping in the bearings was also determined to be around 5% for both types. Typical hysteresis loops for MRPRA set #1 bearings and for the combined system while tested under the model are shown in a later section.

4. Uplift Restrainers

The taller a structure is, the larger is its overturning moment, and the greater is the risk of inducing tension in its foundations. Since excessive tension could be destructive for multilayered rubber bearings, a device was installed inside each of the outer corner bearings. The role of the device was to control uplift and horizontal drift. The restrainer consisted of a short steel sleeve and two steel bolts. The bolts were connected to the two limiting plates of the bearing. The assemblage locks when the bolts are pulled a certain distance apart. Its tension capacity was about 18 kips. The horizontal displacement of the bearing at which the restrainer locks can be adjusted by appropriate tightening of the bolts. The behavior of the bearing is influenced by the presence of the tension devices only when the deflection is large. At the level of horizontal displacement corresponding to the locking of the restrainers, the stiffness of the unit increases substantially. A tension device with its dimensions is

shown in Figure 2.7. A typical hysteresis loop for a natural rubber bearing equipped with a tension device is shown in Figure 2.8.

It should be noted that the restrainer system does not act as a sudden stop. Although the restrainer is effectively rigid when it acts, the bearing can continue to displace horizontally by shortening vertically, thus the normally low horizontal stiffness is replaced by a stiffness that is related to the much higher vertical stiffness.

5. Sliding Bearings

The basic components of a slider consisted of a teflon layer bearing against a stainless steel plate, see Figure 2.9. The teflon layer had a thickness of about 1/25 inch, backed by a 1/2 inch thick layer of Fabreeka® pad bonded to a 1/8 inch thick steel plate. This component was mounted on a rubber bearing constrained against horizontal movement. The stainless steel component consisted of a 1/32 inch thick stainless steel mirror, point welded to a 1/8 inch thick steel plate. Their areas were 10×7 and 10.5×7.5 square inches, respectively.

The coefficient of friction for the teflon-steel units, as provided by the manufacturer, was about 5%, however, a separate testing of the sliders showed a higher coefficient of friction, namely around 17%. This caused concern about the isolation effectiveness that would be provided by sliders of such a high coefficient of friction, since the threshold of the base shear at which the sliding would start was correspondingly increased. For this reason, after the structure was tested with the system described above, the area of the teflon was reduced from 6×6 to 4×4 square inches. This was done since the coefficient of friction of the teflon with other surfaces decreases with increased pressure in the material. When the area was reduced to 4×4, the coefficient of friction dropped to about 12%. The reason for the discrepancy between the specified and measured coefficients of friction was mainly the effect of the sliding velocity and the pressure in the material.

The amplitude of travel of the teflon on the steel before it reaches the edge of the plate, was 3 inches for the 4×4 sliders and 2 inches for the 6×6.

6. The Combined Isolation System

In general, an isolation system consists of a group of devices mounted together in order to decouple the building from the ground motion. The present system using a combination of elastomeric bearings, sliders, and uplift restrainers (Figure 2.10), was designed to fulfill three important goals:

(1) **Providing Threshold for Base Motion**. The friction of the sliders keeps the structure from moving under wind loading and small earthquakes. The base shear must exceed a certain limit in order to start sliding. This limit is proportional to the friction coefficient, and to the fraction of the weight of the model carried by the sliders. This wind restraint capacity was experimentally verified by applying earthquake signals of very small spans. Figure 7.6 shows the base shear hysteresis loops for the Mexico City earthquake input at a horizontal span of 150; very little relative motion was recorded for this level of excitation. By examining the Fourier transforms of the corresponding floor accelerations (Figure 7.3), it was noticed that they were similar to the ones for the fixed base case. The ability of an isolation system to ensure a certain fixity for low level dynamic loading renders it practical and avoids unnecessary movement of the structure when seismic isolation is not yet needed.

(2) **Additional Stiffness and Restoring Effect**. Once the shear force that activates the sliders is reached, their horizontal stiffness drops from a very large value to zero, causing an unrestrained displacement. For this reason, sliders were combined with elastomeric bearings that would provide an additional stiffness. The force-deflection relationship of the combined system would be theoretically bilinear with infinite initial stiffness, followed by a finite stiffness provided by the rubber bearings, which are kept free to deflect horizontally, instead of the zero stiffness that would otherwise characterize the sliders. This arrangement also ensures a restoring force that will bring the structure to almost its original at rest location. A series of experiments performed on a rigid block to study its sliding response under earthquake signals is described in reference [11]. The large displacement offset that remains at the end of the signal shows the need for a restoring spring. For the combined system, the base relative displacement time series under different earthquakes are shown in Figures 7.16 through 7.19. It is noticed that the offset is

reduced to a practically negligible value.

(3) **Control of Drift and Overturning.** The presence of tension devices inside the bearings, limits the horizontal drift of the base and the uplift of the columns. If a medium-rise building were to be base isolated, it would be essential to control its uplift; tension devices would prevent ca.: strophical overturning in the case of an unexpectedly severe earthquake. Also, they provide stiffening as they come close to locking: this compensates for the softening of the rubber bearings.

It is also worthwhile mentioning the inherent fail-safe capacity that the present system possesses. The horizontal stiffness of rubber bearings decreases with shear strain and axial load, and at a certain level of axial load they become unstable. For this reason systems consisting of solely rubber bearings use other accessories to provide fail-safe action on which the structure can depend in case of bearing buckling or bearing roll out. For the combined rubber-sliders system this problem is solved by having the structure constantly resting on the sliders and when the base drift is very large some of the axial load that was initially carried by the rubber bearings is transferred to the sliders.

The system, by combining sliders, elastomeric bearings, and tension devices, provides all the functions needed for the seismic protection of a structure.

Table T-2.1 Scale factors.

PARAMETER	$\frac{1}{4}$ scale $\frac{model}{prototype}$	
LENGTH	L	$\frac{1}{4}$
TIME	$\sqrt{L}$	$\frac{1}{2}$
MASS	L^3	$\frac{1}{16}$
DISPLACEMENT	L	$\frac{1}{4}$
ACCELERATION	1	$\frac{1}{1}$
STRESS	1	$\frac{1}{1}$
STRAIN	1	$\frac{1}{1}$
FORCE	L^2	$\frac{1}{16}$
AREA	L^2	$\frac{1}{16}$

Table T-2.2 MRPRA SET #1 bearings - static rig tests.
Change in effective stiffness with axial load and horizontal shear strain.

-	MRPRA SET # 1 BEARINGS - EFFECTIVE STIFFNESS		
-	30% shear strain	60% shear strain	100% shear strain
AXIAL LOAD (k.)	K_{eff} ($k.in^{-1}$)	K_{eff} ($k.in^{-1}$)	K_{eff} ($k.in^{-1}$)
5	1.48	1.11	-
10	1.44	1.08	0.91
20	1.30	0.96	0.77
30	1.15	0.84	0.62
40	1.00	0.69	0.42
45	0.95	0.64	-
50	0.95	0.54	-
60	0.85	-	-

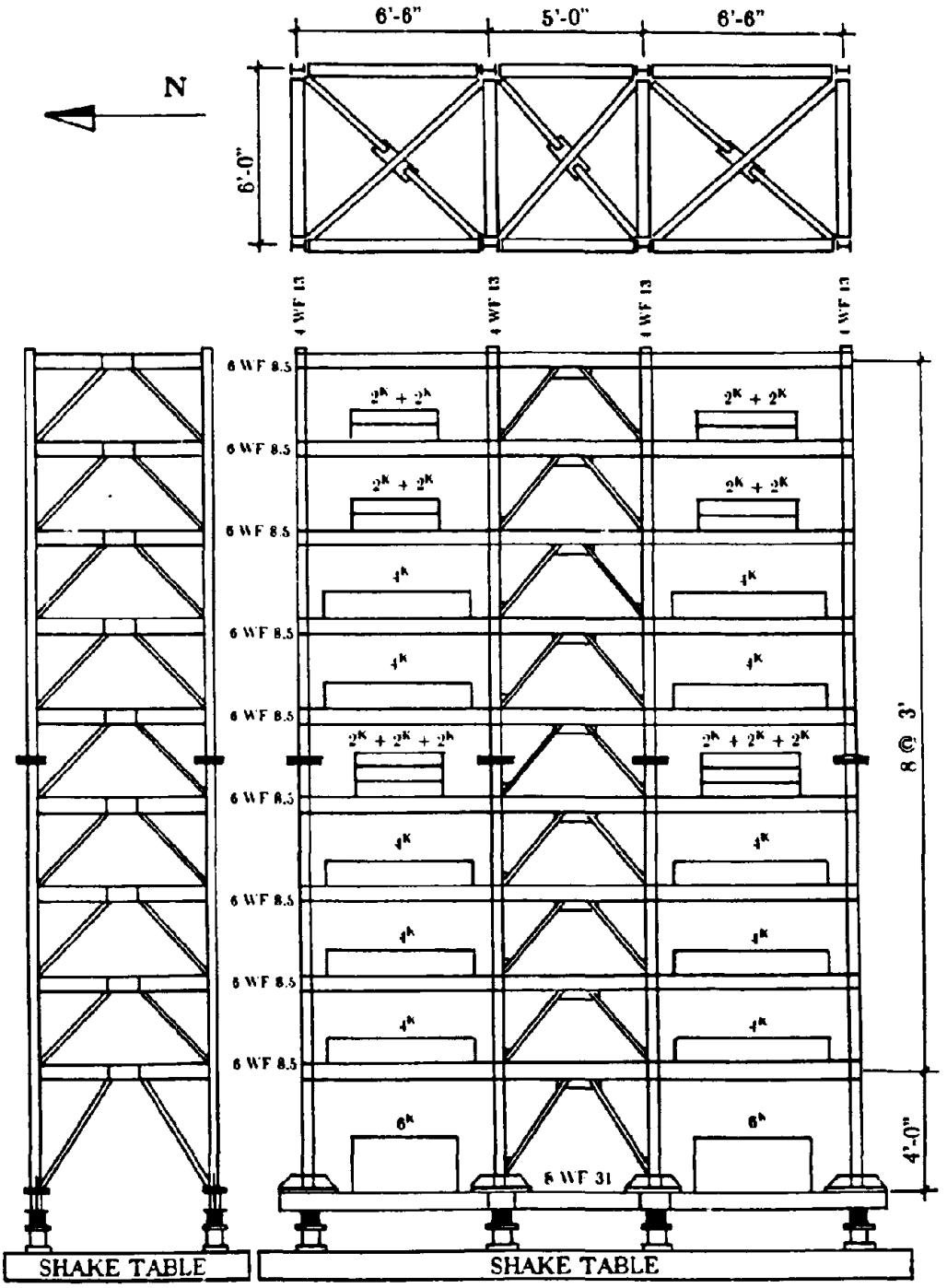

Figure 2.1 Nine story steel frame showing dimensions and mass distribution.

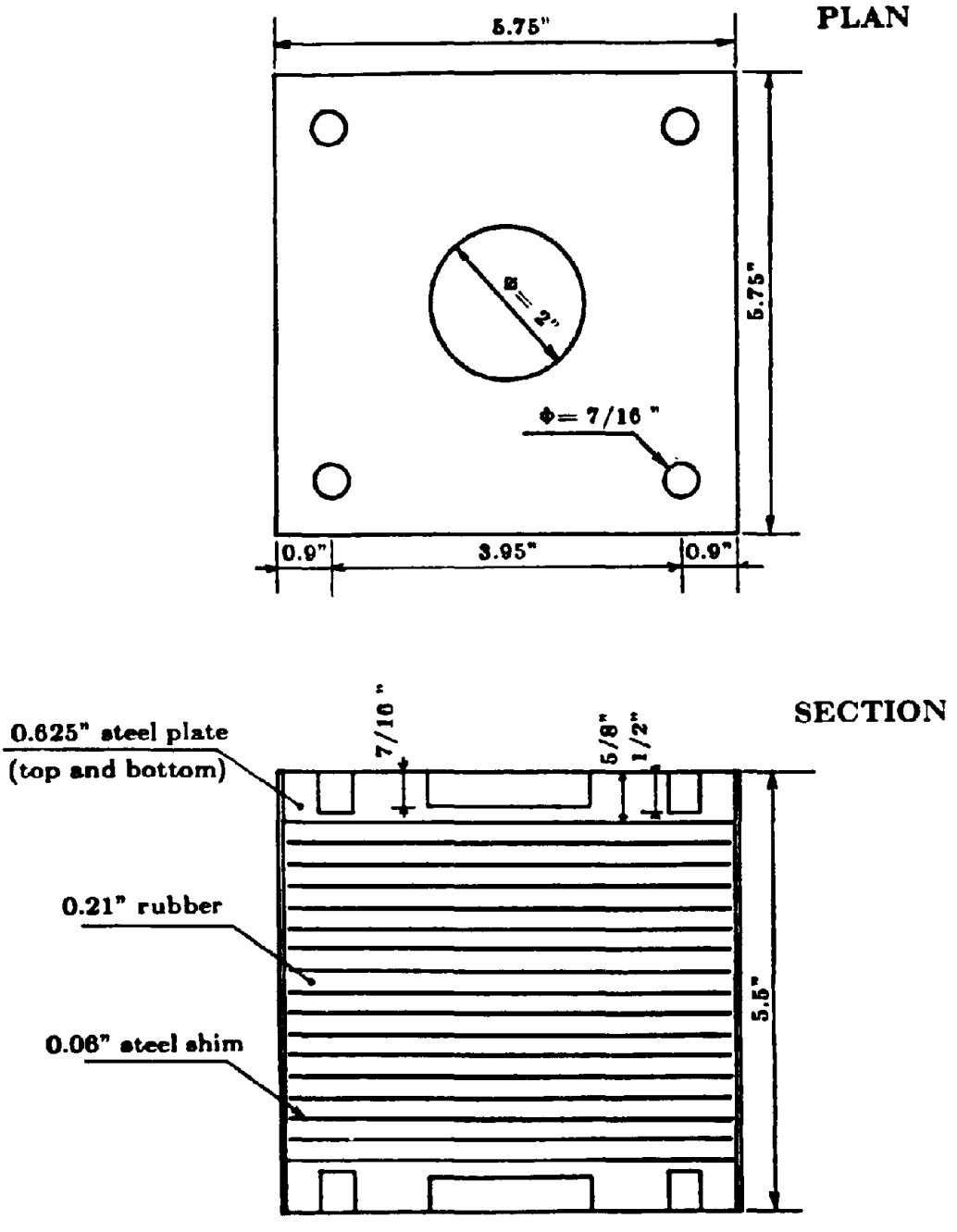

Figure 2.2 MRPRA SET #1 bearing showing dimensions.

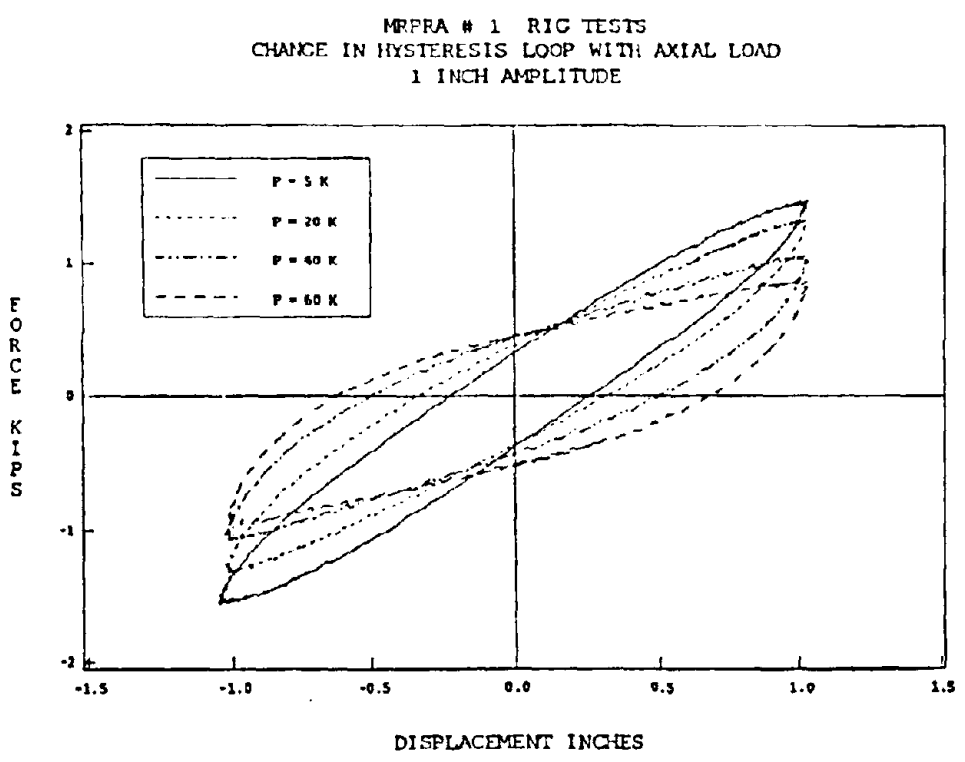

Figure 2.3a Change of hysteresis loop with axial load (30% shear strain).

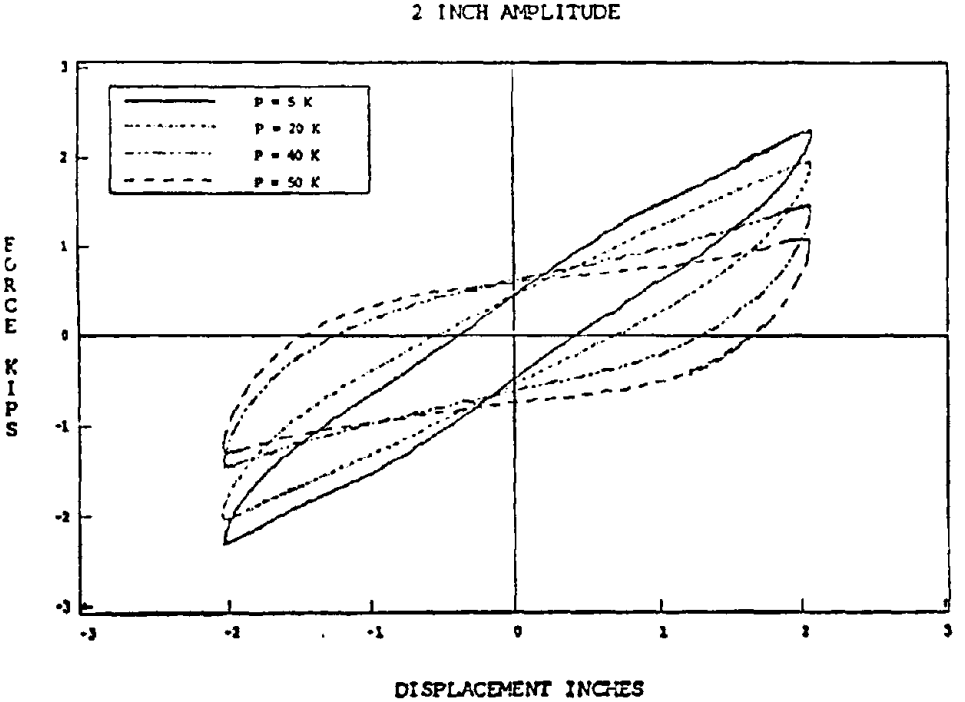

Figure 2.3b Change of hysteresis loop with axial load (60% shear strain).

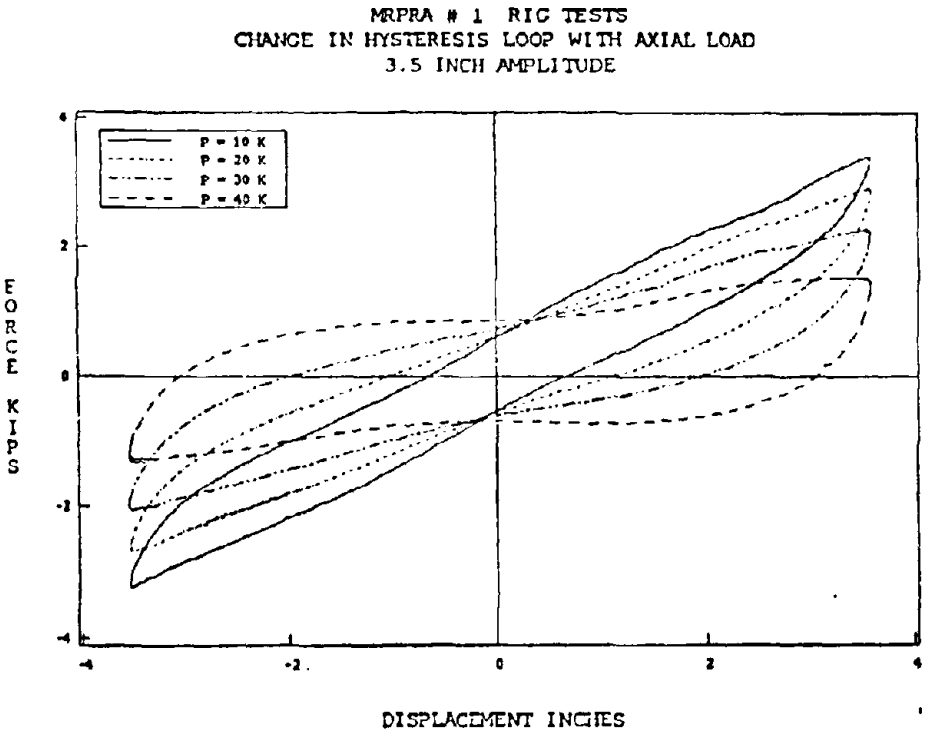

Figure 2.3c Change of hysteresis loop with axial load (100% shear strain).

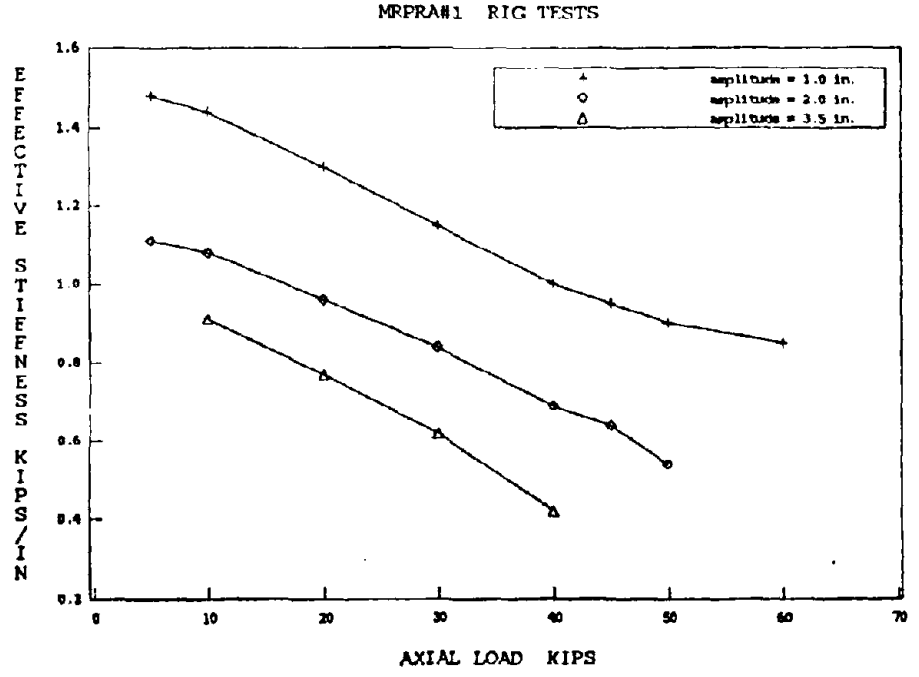

Figure 2.4 Change in effective stiffness with axial load and shear strain.

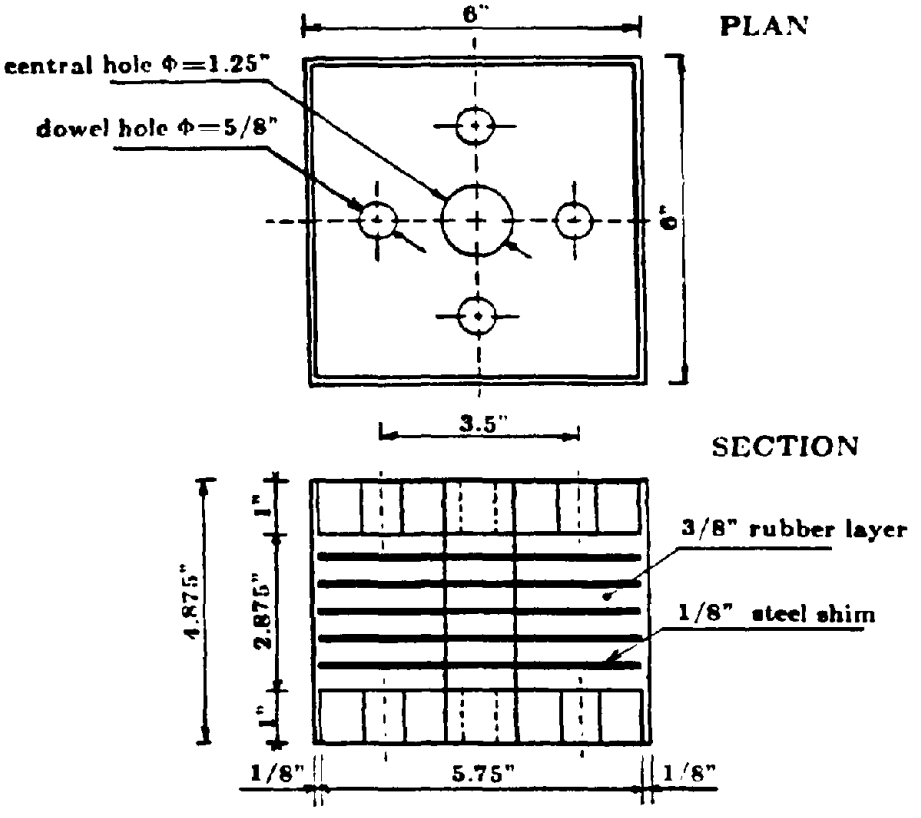

Figure 2.5 Natural rubber bearing showing details.

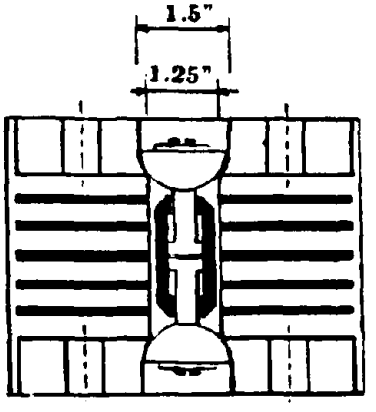

Figure 2.6 Modification of central hole to accommodate tension device.

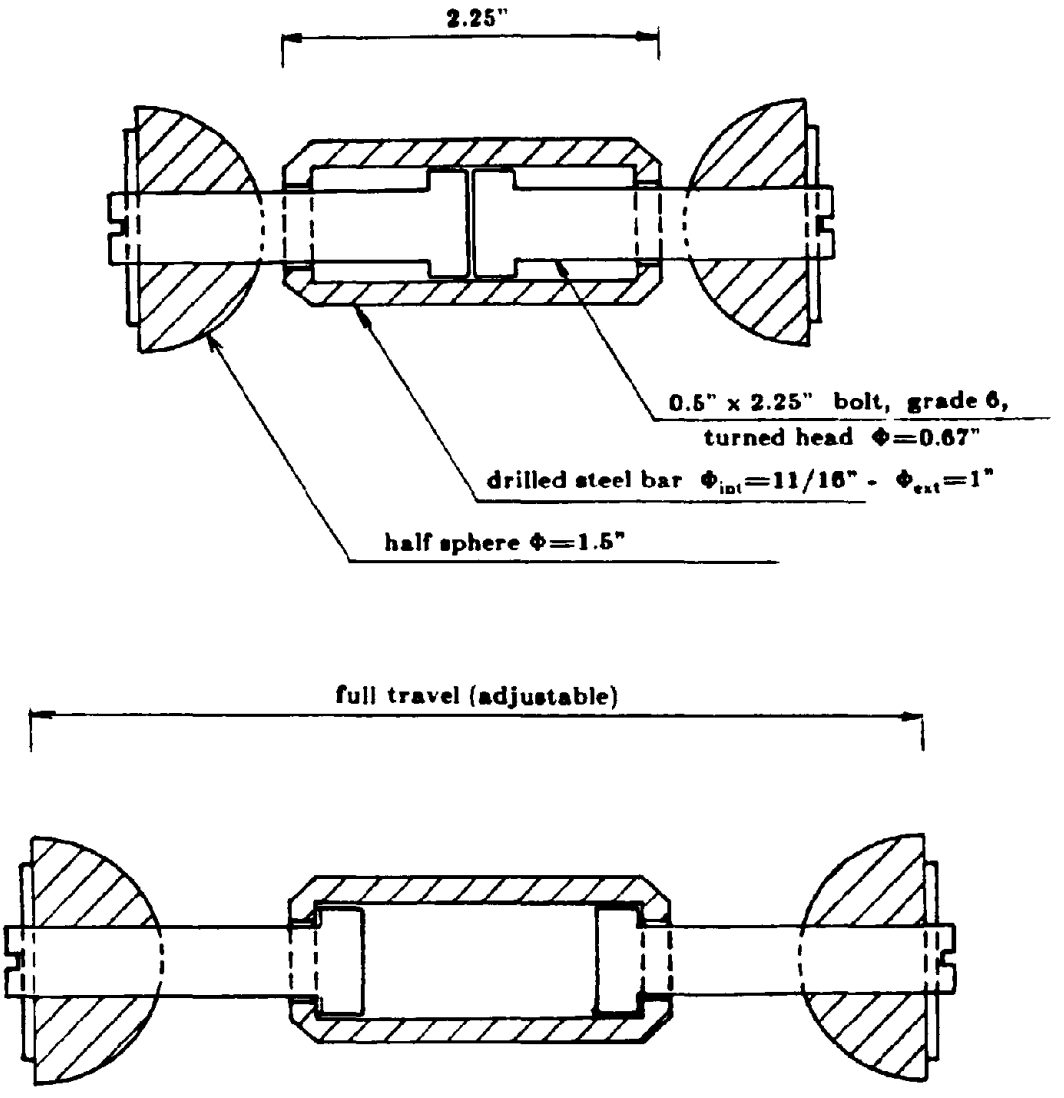

Figure 2.7 Tension restraint showing dimensions.

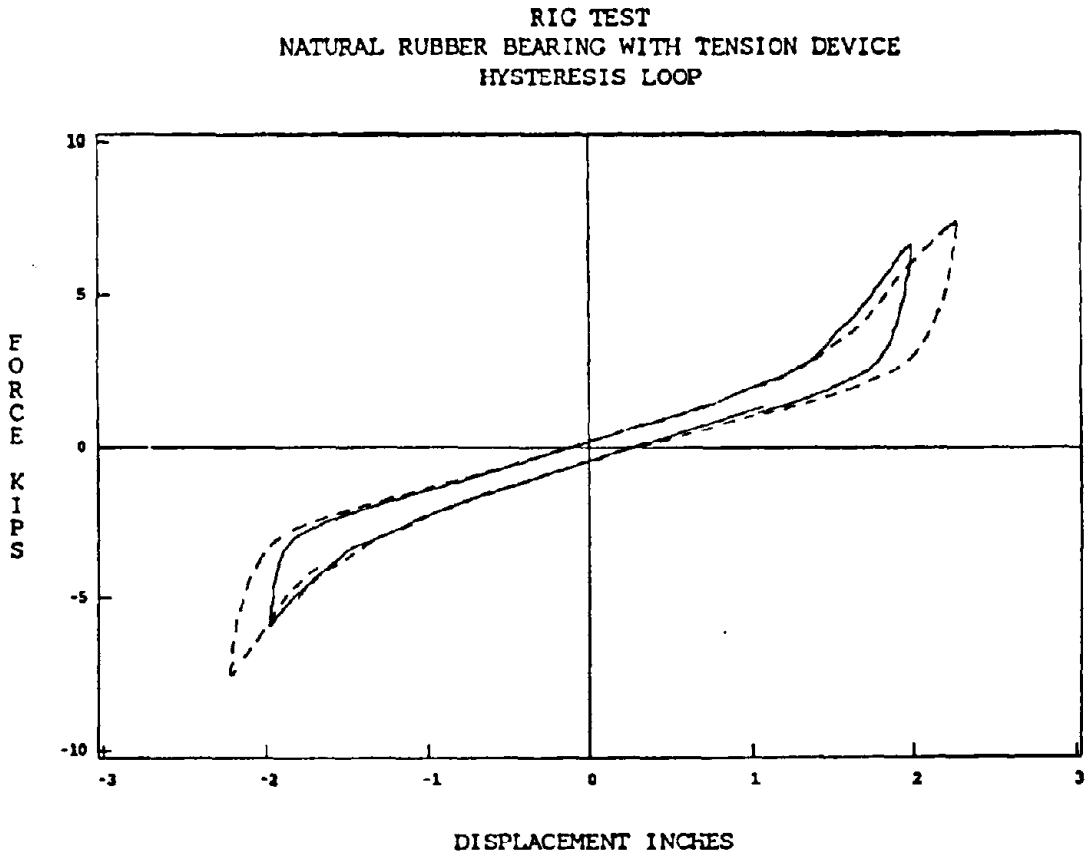

Figure 2.8 Effect of tension device on horizontal stiffness.

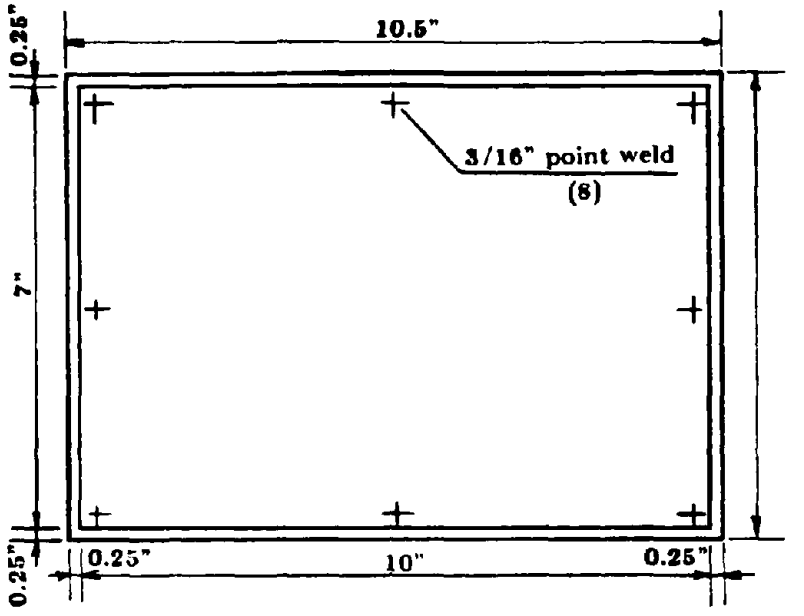

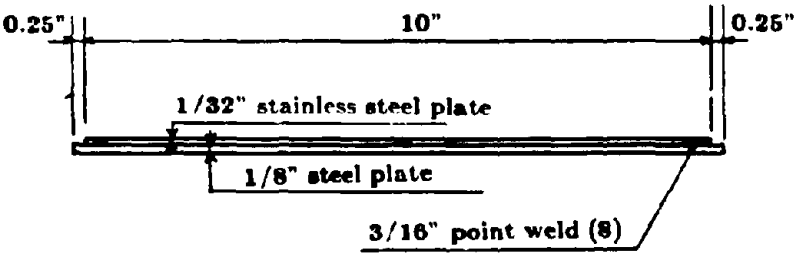

Figure 2.9 Teflon-stainless steel slider showing dimensions.

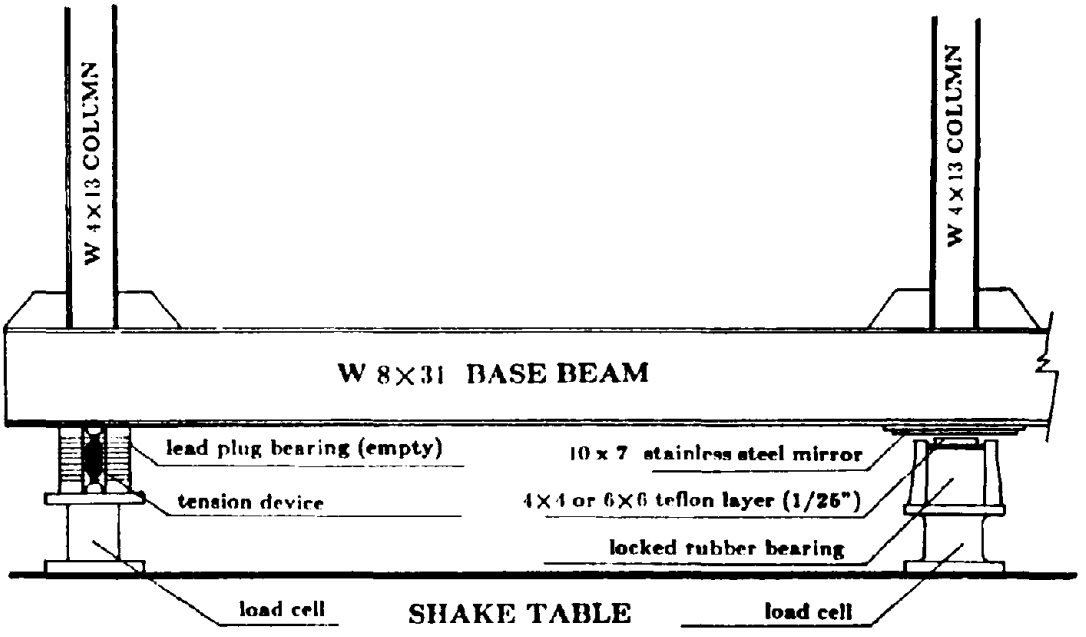

Figure 2.10 **Disposition of tension controlled bearing under corner column and teflon-stainless steel slider under adjacent interior column, repeated 4 times for the entire model.**

CHAPTER THREE
TEST FACILITIES

1. Earthquake Simulator

The present experiment was conducted at the Earthquake Simulator Laboratory at the University of California. The main facility is a shake table made of a 20×20×1 foot prestressed concrete slab weighing around 100 kips. For the model used, the table efficiency dropped for frequencies higher than 10 Hz. Vertical and horizontal motions can be independently applied. This is realized by three horizontal 50 kip and four vertical 25 kip hydraulic actuators. The actuators are located under the table in a 22×22×10 foot pit, built on massive foundations, and having a wall thickness of 5 feet. Air pressure of up to 4 psi can be created in the chamber underneath the table. This carries the vertical load of the table and the model and allows the vertical actuators to produce only the dynamic loads.

The total travel of the table is limited to 10 inches horizontally and 4 inches vertically. The table velocities and accelerations are limited by the flow rate and the oil column resonance in the actuators, respectively.

2. Input Signals

The signals used are derived from previously recorded earthquakes, stored as digitized accelerations. They are described in chapter 5. Since the table is displacement controlled, these accelerations are double integrated and converted from digital to analog before being applied to the table actuators through the MTS table controller.

Extensive work has previously been done on the repeatability of the table and its fidelity in reproducing the signal as close to the original record as possible. The table motion characteristics are not exactly the same whether the table is loaded or not. Also, since the original accelerogram is filtered below 0.1 and above 24 Hz before being applied to the table, it may be more effective in exciting very low and relatively high frequencies than is the table motion. Nevertheless, the main characteristics of each earthquake were satisfactorily preserved.

3. Data Acquisition System

The main component in the data acquisition system is a VAX 750 computer connected to a S-100 minicomputer that performs a digital to analog conversion. After the conversion is done, the command signal is sent from the S-100 to the MTS controller. The MTS controls the table displacements interactively.

Each measuring device installed on the structural model was connected to a channel. The channels were read by a MULTIPLEXER that converts from analog to digital. The digitized readings were then stored on the VAX 750 disk, then backed up on 9 track tapes.

The data acquisition capacity of the multiplexer is 50 KHz throughput and its burst rate is 300 KHz, in the sense that it scans the channels at the rate of 300,000 channels per second, and can read up to 50,000 samples per second from each channel.

A maximum of 256 channels can be connected to a test model. In the present experiment, 128 channels were connected and data was acquired at the rate of 200 readings per second on each channel. The data was then processed on the VAX 750 and SUN workstations.

CHAPTER FOUR
INSTRUMENTATION

Accelerometers, potentiometers, and direct current displacement transducers (DCDT) were installed on the model, and force measurement devices under the base. Since the strains were expected to stay in the elastic range, no strain measurements were made. Preliminary analyses provided levels of response at which plastic deformations would be incipient. Nonlinear behavior can be detected by examining the interstory drifts and comparing them with the deflections at which yielding would start.

1. Accelerations

Horizontal accelerations in the longitudinal direction were measured at each floor, at the vertical plane of symmetry of the structure. Nine accelerometers were mounted on the steel girders for the upper nine stories, and one on the concrete block at the base level. On the north-east and south-east columns of the structure, two accelerometers were installed to measure transverse horizontal accelerations at the ninth floor. Another six accelerometers were mounted to measure vertical accelerations. Four of these were installed at the four outer corners of the base directly above the isolation bearings, and the other two on the middle plane of the ninth floor girder. The locations of the accelerometers with their channel numbers are shown in Figure 4.1.

2. Displacements

Displacements in the horizontal direction were measured at each floor using potentiometers. Nine of them were mounted on the upper nine steel girders, at the vertical plane of symmetry of the structure, on the north side. Since they were connected to a fixed reference frame external to the table, they were recording floor absolute displacements. Floor relative displacements, were obtained by subtraction from the table displacements. At the base, however, two potentiometers were installed between the outer north corners and the table. These measured base relative displacements at the north-west and north-east sides. Their average was used in the study of the relative base displacement

response. Another two potentiometers were mounted on the east side of the base, at 3 feet towards its center, from the outer north and south corners. They measured relative displacements in these directions. Their average was used in determining transverse base relative displacements, and their difference in examining torsional behavior. Displacements in the vertical direction were measured using eight DCDTs. Four of them were installed at the four base outer corners and connected between the top and bottom of the four external columns of the structure. These were intended to record any axial deformations. Another four were mounted at the same locations in plane view, but connected between the table and the top of the four external columns. These were intended to measure total vertical deformations at the outer corners. The difference between the two sets provided the vertical deflections in the bearings. However, since it was noticed that the axial deformations in the steel columns were negligible compared with the total vertical deflections, the latter set of DCDTs was directly used for bearing deflection calculations. They were also used to examine rocking movements of the model. potentiometers are shown in Figure 4.2 and DCDTs in Figure 4.3.

3. Forces

Force measurements were performed at the base level only. The four exterior bearings were mounted on load cells capable of measuring axial, shear, and bending forces. Two load cells were installed in parallel under each of the bearings at the outer corners. Single load cells were used for the four interior sliders. These internal ones, however, did not record either axial or bending forces due to some instrumentation limitations. The static axial loads on the interior bearings were obtained by calculation; since the measured axial loads carried by the external bearings were about 9 kips per bearing, it was concluded that the internal bearings were carrying about 14 kips each. Equal distribution of the axial loads among the outer bearings was achieved by careful shimming. Data was recorded for static tests consisting of jacking and unjacking the structure at these individual locations. Load cells locations and channel numbers are shown in Figure 4.4.

Table T-4.1 lists the channels assigned to the various measurement instruments installed on the model, with their functions. Note that channels 1 through 12 correspond to the shaking table

accessories.

The structure was also tested fixed base with no load cells under its columns and the channel numbering was changed. The fixed base structure instrumentation is shown in Figures 4.5 and 4.6.

Figures 4.7-4.11 show some photographs of the instrumentation on the base-isolated model.

Table T-4.1 Channel list for base isolated structure.

LIST OF CHANNELS FOR STRUCTURE ON:
- COMBINED RUBBER-SLIDERS SYSTEM
- MALAYSIAN RUBBER PRODUCERS RESEARCH ASSOCIATION (MRPRA) SET #1

CHANNEL	NAME	UNITS	REMARK
1	h1 disp	inches	table horizontal actuator1 displ.
2	h2 disp	inches	table horizontal actuator2 displ.
3	avg hacc	G's	table horizontal acceleration
4	avg vacc	G's	table vertical acceleration
5	pitch acc	rad/sec2	table pitch
6	roll acc	rad/sec2	table roll
7	twist acc	rad/sec2	table twist
8	v1 disp	inches	north-west vertical actuator displacem.
9	v2 disp	inches	north-east vertical actuator displacem.
10	v3 disp	inches	south-west vertical actuator displacem.
11	h span	inches	applied table horiz. displacement
12	hvel	in/sec	table horizontal velocity
13	no1ax	kips	north-west load cell #1/axial/bearing A2
14	no1sh	kips	north-west load cell #1/shear/bearing A2
15	no1mo	kip-inch	north-west load cell #1/momen/bearing A2
16	no2ax	kips	north-west load cell #2/axial/bearing A2
17	no2sh	kips	north-west load cell #2/shear/bearing A2
18	no2mo	kip-inch	north-west load cell #2/momen/bearing A2
19	no3ax	kips	north-east load cell #1/axial/bearing A1
20	no3sh	kips	north-east load cell #1/shear/bearing A1
21	no3mo	kip-inch	north-east load cell #1/momen/bearing A1
22	no4ax	kips	north-east load cell #2/axial/bearing A1
23	no4sh	kips	north-east load cell #2/shear/bearing A1
24	no4mo	kip-inch	north-east load cell #2/momen/bearing A1
25	so4ax	kips	south-east load cell #1/axial/bearing D1
26	so4sh	kips	south-east load cell #1/shear/bearing D1
27	so4mo	kip-inch	south-east load cell #1/momen/bearing D1
28	so3ax	kips	south-east load cell #2/axial/bearing D1
29	so3sh	kips	south-east load cell #2/shear/bearing D1
30	so3mo	kip-inch	south-east load cell #2/momen/bearing D1
31	so2ax	kips	south-west load cell #1/axial/bearing D2
32	so2sh	kips	south-west load cell #1/shear/bearing D2
33	so2mo	kip-inch	south-west load cell #1/momen/bearing D2
34	so1ax	kips	south-west load cell #2/axial/bearing D2
35	so1sh	kips	south-west load cell #2/shear/bearing D2
36	so1mo	kip-inch	south-west load cell #2/momen/bearing D2
37	ni2sh	kips	north-east load cell /shear/bearing B1
38	ni2mo	kip-inch	north-east load cell /momen/bearing B1
39	si2sh	kips	south-east load cell /shear/bearing C1
40	si2mo	kip-inch	south-east load cell /momen/bearing C1
41	si1sh	kips	south-west load cell /shear/bearing C2
42	si1mo	kip-inch	south-west load cell /momen/bearing C2
43	ni1sh	kips	north-west load cell /shear/bearing B2
44	ni1mo	kip-inch	north-west load cell /momen/bearing B2

LIST OF CHANNELS FOR STRUCTURE ON:
- COMBINED RUBBER-SLIDERS SYSTEM
- MALAYSIAN RUBBER PRODUCERS RESEARCH ASSOCIATION (MRPRA) SET #1

CHANNEL	NAME	UNITS	REMARK
45	no1 totax	inches	total axial deformation corner A2
46	no1 parax	inches	column axial deformation corner A2
47	no2 totax	inches	total axial deformation corner A1
48	no2 parax	inches	column axial deformation corner A1
49	so2 totax	inches	total axial deformation corner D1
50	so2 parax	inches	column axial deformation corner D1
51	so1 totax	inches	total axial deformation corner D2
52	so2 parax	inches	column axial deformation corner D2
53	no1 pdisp	inches	north lateral relative base displacement
54	so1 pdisp	inches	south lateral relative base displacement
55	so1 rdisp	inches	west longitudinal rel. base displacement
56	so2 rdisp	inches	east longitudinal rel. base displacement
57	1st hdisp	inches	1st story absolute horizon. displacement
58	2nd hdisp	inches	2nd story absolute horizon. displacement
59	3rd hdisp	inches	3rd story absolute horizon. displacement
60	4th hdisp	inches	4th story absolute horizon. displacement
61	5th hdisp	inches	5th story absolute horizon. displacement
62	6th hdisp	inches	6th story absolute horizon. displacement
63	7th hdisp	inches	7th story absolute horizon. displacement
64	8th hdisp	inches	8th story absolute horizon. displacement
65	9th hdisp	inches	9th story absolute horizon. displacement
66	no2 vacc	g's	Base north-east corner vertical acceler.
67	no1 vacc	g's	Base north-west corner vertical acceler.
68	so2 vacc	g's	Base south-east corner vertical acceler.
69	so1 vacc	g's	Base south-west corner vertical acceler.
70	base hacc	g's	Base horizontal acceleration
71	1st acc	g's	1st story horizontal acceleration
72	2nd hacc	g's	2nd story horizontal acceleration
73	3rd hacc	g's	3rd story horizontal acceleration
74	4th hacc	g's	4th story horizontal acceleration
75	5th hacc	g's	5th story horizontal acceleration
76	6th hacc	g's	6th story horizontal acceleration
77	7th hacc	g's	7th story horizontal acceleration
78	8th hacc	g's	8th story horizontal acceleration
79	9th hacc	g's	9th story horizontal acceleration
80	nc vacc9	g's	9th story north vertical acceleration
81	no pacc9	g's	9th story north, lateral horizon. acceler.
82	sc vacc9	g's	9th story south vertical acceleration
83	so pacc9	g's	9th story south, lateral horizon. acceler.

BASE ISOLATED

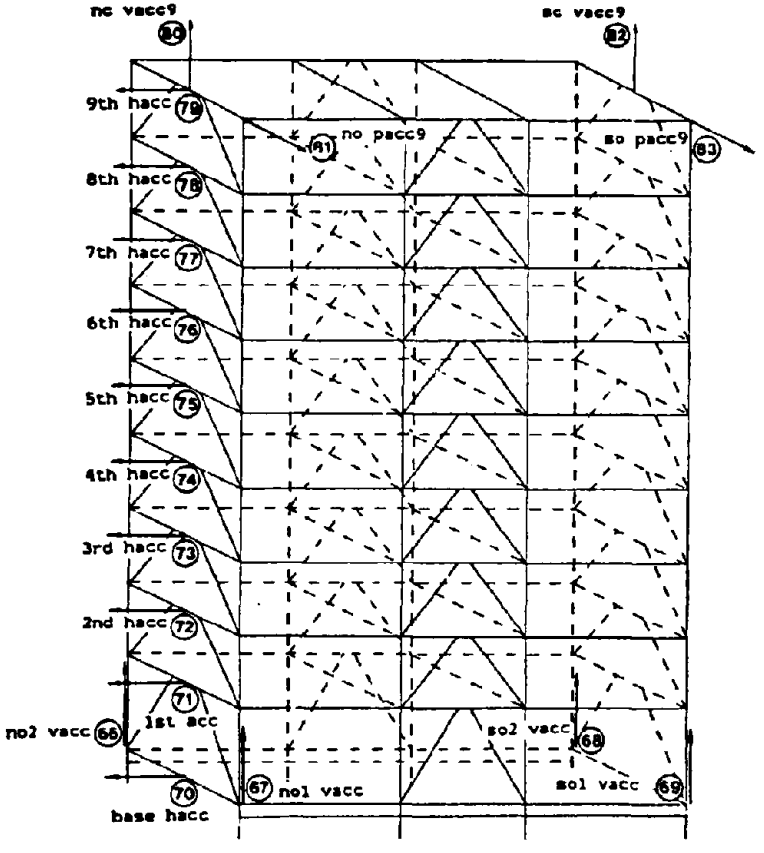

Figure 4.1 Location and channel numbers of accelerometers on base isolated structure.

BASE ISOLATED

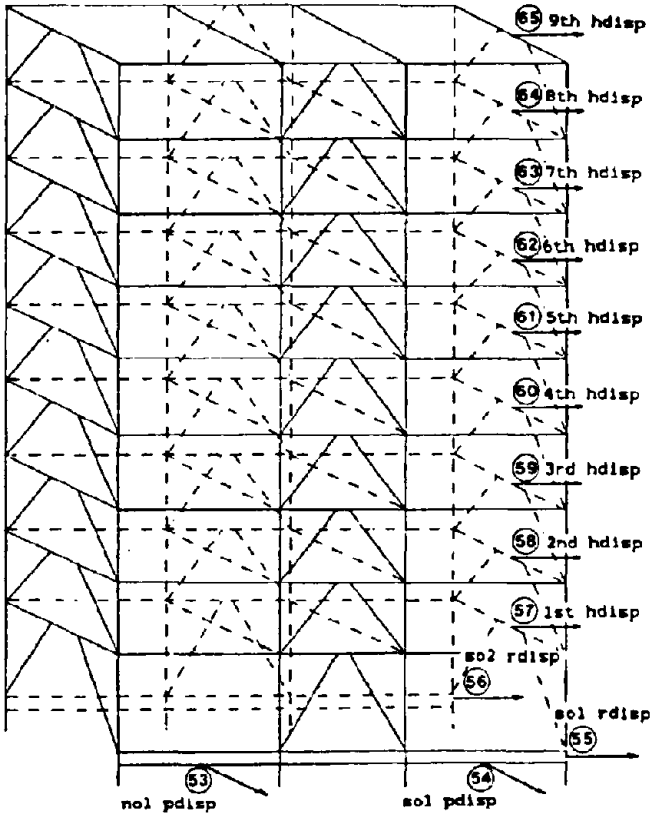

Figure 4.2 Location and channel numbers of potentiometers on base isolated structure.

BASE ISOLATED

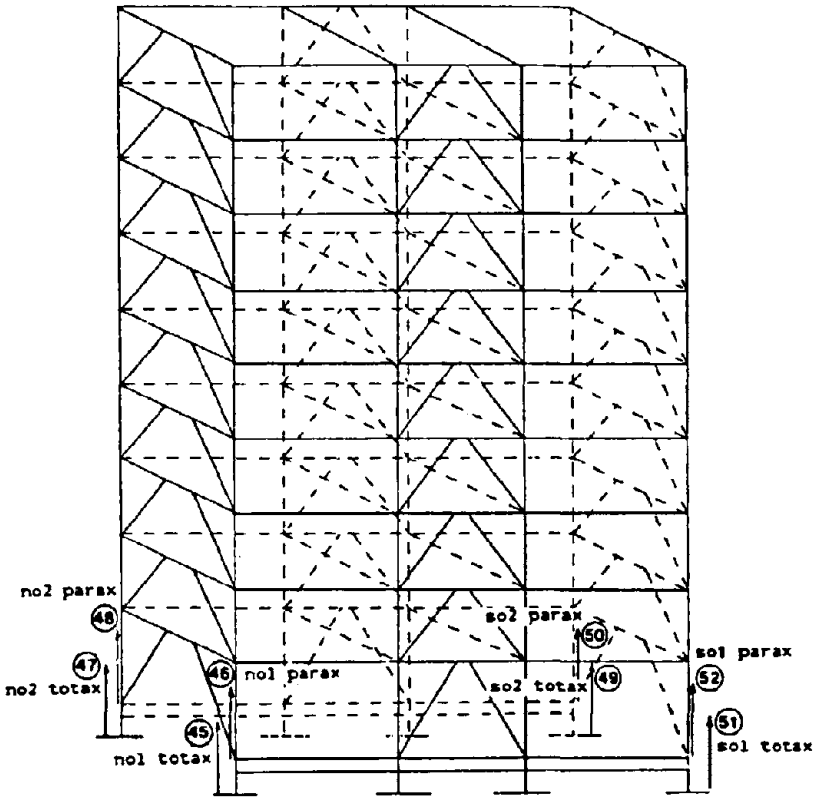

Figure 4.3 **Location and channel numbers of DCDTs on base isolated structure.**

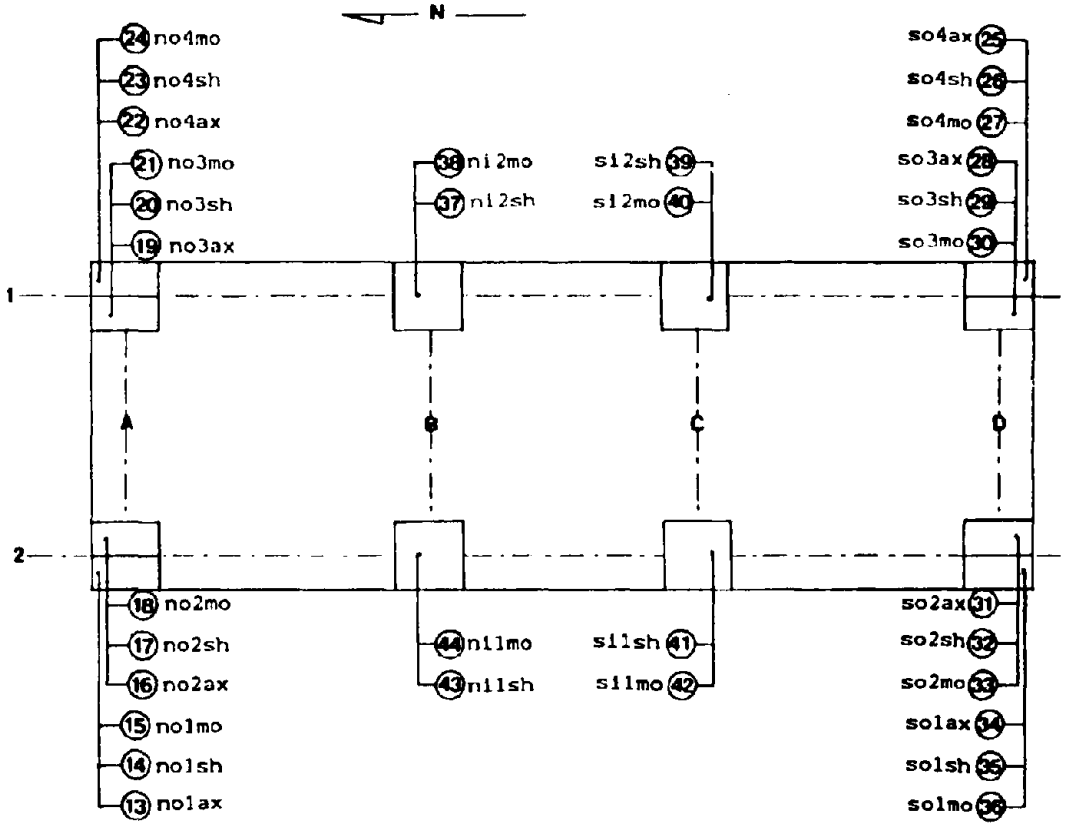

Figure 4.4 **Location and channel numbers of load cells under base isolated structure.**

FIXED BASE

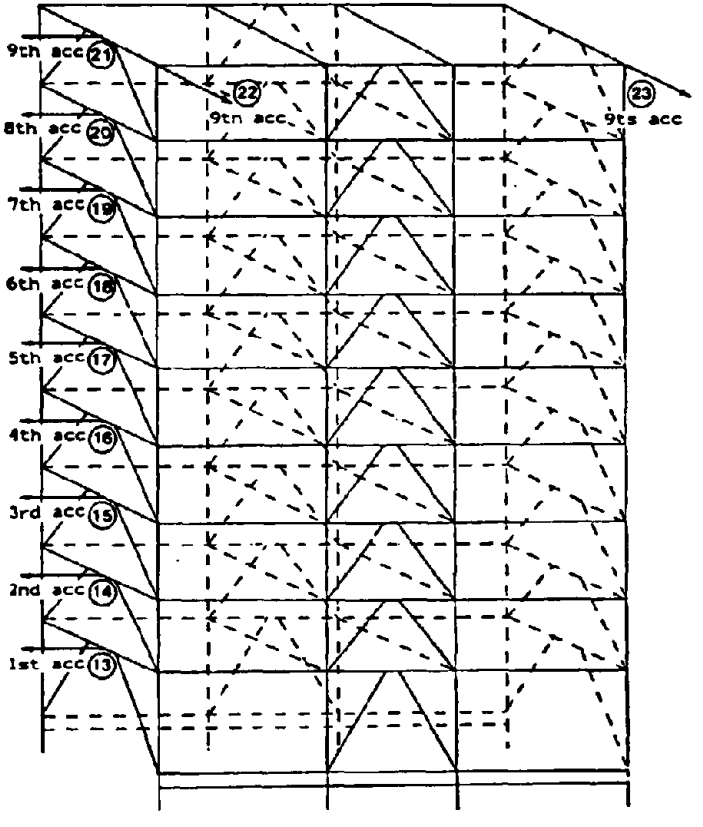

Figure 4.5 Location and channel numbers of accelerometers on fixed base structure.

FIXED BASE

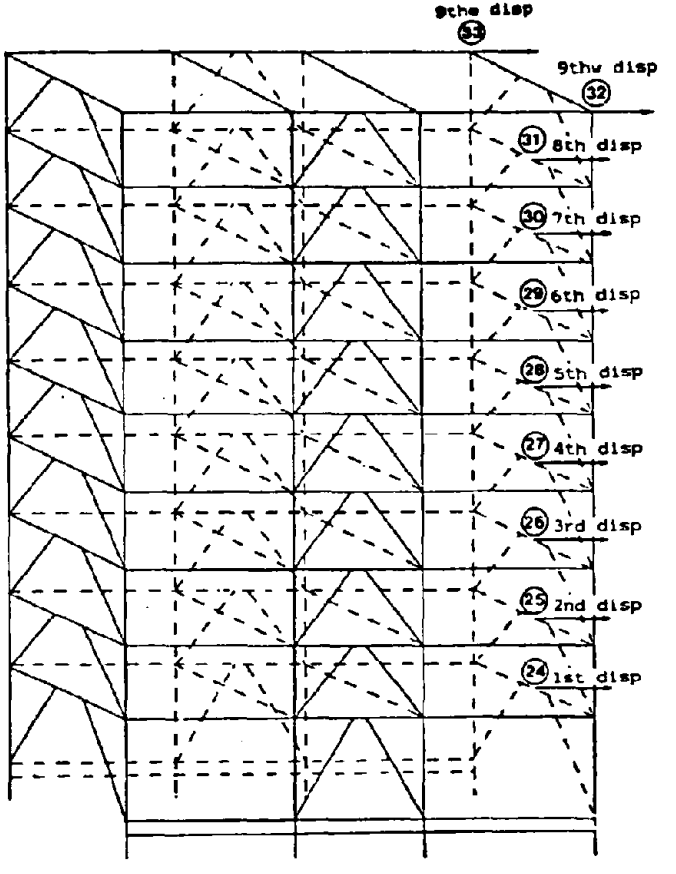

Figure 4.6 Location and channel numbers of potentiometers on fixed base structure.

Figure 4.7 Transversal (north) frame of the structure showing horizontal accelerometers.

Figure 4.8 North-east corner: rubber bearing on load cells, potentiometer measuring total vertical deformation, accelerometer measuring vertical base acceleration.

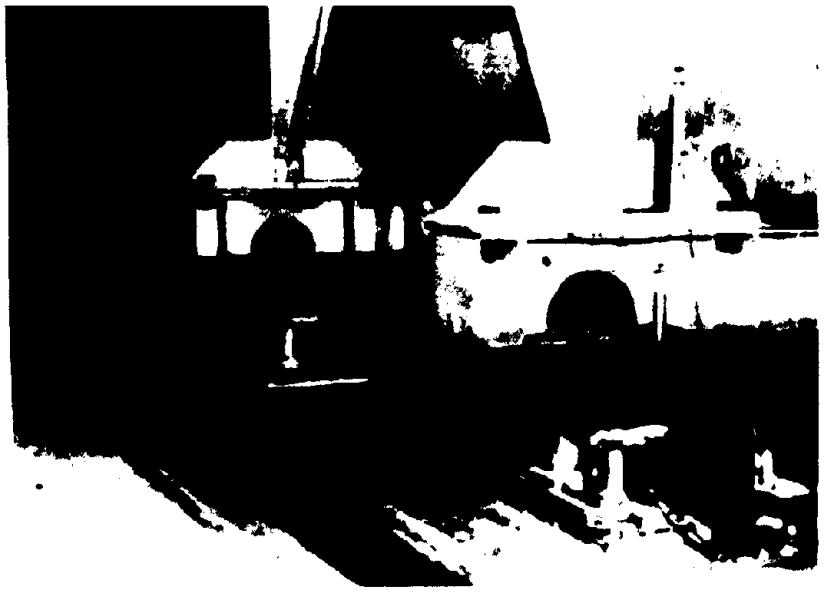

Figure 4.9 Side view of north rubber bearings.

Figure 4.10 Three channels of a corner load cell measuring axial, shear, and bending forces.

Figure 4.11 South-east corner: DCDTs measuring total (bottom DCDT) and column (top DCDT) vertical deformations.

CHAPTER FIVE
TEST PROGRAM

1. Table Motions

The table motions used were derived from eight different earthquake records. Horizontal and vertical excitations were applied separately and simultaneously at spans ranging from 50 to 425, where a span of 1000 corresponds to the maximum table displacement (±5 in. horizontal, ±2 in. vertical). But almost all inputs consisted of a horizontal component only. No rotational excitations were applied to the structure.

The signals used were the El Centro 1940, s00e; the San Fernando Pacoima Dam 1971, s16e; the Parkfield 1966, n65e; the San Francisco (Golden Gate Park station) 1957, s80e; the Taft (Lincoln School Tunnel station) 1952, s69e; the Mexico City 1985, s60e; the Bucharest (Romania) 1977, s00e; and the Miyagi-Ken-Oki (Japan) 1978, w00s horizontal components. Before being applied to the table, the original records were filtered (frequencies below 0.1 Hz and above 24 Hz were removed) then time scaled by $\sqrt{4}$ to maintain similitude. In the following description, the signal duration refers to the duration of the table movement, not to the actual earthquake.

Table displacement and acceleration time histories corresponding to these earthquake signals, their Fourier transforms, and their displacement, pseudo-velocity and pseudo-acceleration response spectras for damping values of 2%, 5%, and 20% are shown in Figures 5.1-5.8. The period range was between 0.1 and 10 seconds for the displacement response spectra and between 0.1 and 5 seconds for the pseudo-acceleration and pseudo-velocity. The eight inputs include earthquakes of varied frequency content, durations and intensities. For instance, the El Centro component has a relatively wide range of frequencies (between 1 and 5 Hz), and consists of about five significant cycles. It is commonly used by structural engineers and is considered a typical California earthquake record. When run at 375 horizontal span, the table peak acceleration and peak displacement were around 0.7 g and 2 inches, respectively. The Mexico City component is a low frequency, long duration (34 seconds) input. As can be seen from Figure 5.2a, significant spectral amplitude is shown at 1 Hz to 2 Hz. The table

signal consists of two sets of several cycles over a very long duration. When run at 375 horizontal span, a peak acceleration of 0.18 g was produced on the table, and the peak displacement was about 2 inches. Throughout the testing program, the Mexico City record was the most severe input for base isolation systems. The Bucharest record had relatively low frequency content (1 to 3 Hz) and short duration. It consisted of uniformly decreasing and uniformly spaced displacement cycles. At 300 horizontal span, the peak table acceleration and displacement were about 0.27 g and 1.6 inches, respectively. As for the Miyagi-Ken-Oki signal, the peculiarity was the large amount of energy at around 2 Hz. The Parkfield signal provided a good test of the re-centering effect in the system, since the table displacement time history for this signal consists of a large sway in one direction followed by small cycles. The signal is of medium duration with relatively wide spread frequencies. When run at 350 horizontal span, the peak table acceleration was around 0.4 g.

The highest frequency content was provided by the San Francisco signal. It consists of one pulse of very large acceleration, followed by a slow large sway. At a horizontal span of 200, the table acceleration reached 1.2 g. The table acceleration Fourier transform shows large spikes at about 5 Hz and up to 8 Hz. The duration of the signal is very short (about 10 seconds). The San Francisco input signal caused large base relative velocities able to activate the sliders at low spans.

This wide variety of input signals enabled different aspects of the isolation efficiency of the slider-bearing system to be studied.

2. Test Sequence

Table T-5.1 shows a complete chronological listing of the tests. They are identified by file names indicating the date of the test as year, month and day, followed by a sequence number. File names occupy the first column in Table 5.1. Column 2 shows the short names of the signals, they are self explanatory except "sct" which corresponds to the Mexico City earthquake of 1985. The third column lists the duration of each signal in seconds. The rate of data acquisition is shown in column 4, expressed as a fraction of a second between two consecutive readings. It was set to 0.005, which corresponds to 200 readings per second. The span of the table motion occupies column 5. The

geometric scale occupies column 6.

Since, to the knowledge of the authors, the new combined system had not been tested before, the sequence was started with low span sinusoidal signals. These were, however, unable to activate the sliders. The San Francisco signal for 50 and 100 horizontal spans was used next. It was noticed at this point that the coefficient of friction of the sliders was roughly 17 % which is about three times the value provided by the manufacturer. A detailed study of the coefficient of friction and its variation with velocity and axial load is presented in Chapter Six. The next table input was El Centro 150 horizontal span. The span was gradually increased to 350. In between, a test including the El Centro vertical component at 300 span was run. The vertical component was expected to introduce variations in the response since it affects the shear resistance of the sliders by changing the apparent weight of the structure. However, no significant difference was noticed. This was due to the decrease in the friction coefficient with increased pressure, resulting in a relatively constant resisting shear. Then, the entire series of earthquakes mentioned in the previous section was run at this level of horizontal displacement.

Because of the high coefficient of friction for the 6×6 inch sliders, the base shears were very high. Correspondingly, the model accelerations were relatively high. Since the coefficient of friction of the teflon-steel drops when the pressure in the teflon increases, the dimensions of the sliders were reduced to 4×4 inches. These were tested separately on a static rig before installation. For a pressure of around 900 psi and velocities between 1 and 10 in/sec., the average coefficient of friction was around 12 %.

The tension devices installed in the bearings did not engage because the displacements were decreased by the presence of the sliders. The initially allowed horizontal displacement of 2.25 inches was reduced to 1.75 inches by tightening the restrainers from 0.8 inch to 0.5 inch slack. This was done prior to the 861119 file series. Locking of the restrainers occurred for a low frequency, large displacement Mexico City input at 375 horizontal span. The locking effect on the base shear stiffness is shown in Figure 7.36 (right).

Throughout the entire test sequence, no significant damage of the teflon was noticed. However, some conclusions were drawn about the durability of the teflon sliders. A thin white film due to wearing of the teflon was noticed to appear on the stainless steel after repeated testing. It was periodically removed and the system retested. No difference, however, was noticed in the structural response. Under a real building awaiting an earthquake, the sliders are not expected to be used over periods of many hours as they were during the test program. For this reason, the durability of the sliders was considered very satisfactory for their purpose.

Table T-5.1 Test program: listing of test runs.

NINE STORY STEEL MODEL WITH K-BRACING
MASS DISTRIBUTION SHOWN IN FIGURE 2.1
TOTAL WEIGHT OF STRUCTURE 91 KIPS
BEARINGS: MALAYSIAN RUBBER PRODUCERS RESEARCH ASSOCIATION (MRPRA) SET # 1

FILENAME	SIGNAL	TIME	RATE	REMARKS
861015.01	ec2	19 secs	.005	sph=150 ts=1/4
861015.02	pac2	12 secs	.005	sph=150 ts=1/4
861015.03	park2	14 secs	.005	sph=150 ts=1/4
861015.04	sf2	12 secs	.005	sph=150 ts=1/4
861015.05	taft2	19 secs	.005	sph=150 ts=1/4
861015.06	buc1	12 secs	.005	sph=150 ts=1/4
861015.07	ec2	19 secs	.005	sph=200 ts=1/4
comment:	static tests were performed for shimming by jacking and lowering at individual locations and collecting data for axial load.			
861015.08	static	15 secs	.01	south end lift
861015.09	static	15 secs	.01	north end lift
FILENAME	SIGNAL	TIME	RATE	REMARKS
861016.01	static	15 secs	.01	south end lift
861016.02	static	15 secs	.01	north end lift
comment:	changed shims and jacking again.			
861016.03	static	15 secs	.01	north end lift
861016.04	static	15 secs	.01	south end lift
861016.05	ec2	19 secs	.005	sph=150 ts=1/4
861016.06	ec2	19 secs	.005	sph=150 ts=1/4
861016.07	ec2	19 secs	.005	sph=150 ts=1/4
861017.01	sf2	12 secs	.005	sph=150 ts=1/4
861017.02	ec2	19 secs	.005	sph=225 ts=1/4
861017.03	buc1	12 secs	.005	sph=150 ts=1/4
861017.04	pac2	12 secs	.005	sph=150 ts=1/4
861017.05	park2	14 secs	.005	sph=150 ts=1/4
861017.06	taft2	19 secs	.005	sph=150 ts=1/4
861017.07	pac2	12 secs	.005	sph=225 ts=1/4
861017.08	park2	14 secs	.005	sph=225 ts=1/4
861017.09	park2	14 secs	.005	sph=250 ts=1/4
861017.10	ec2	19 secs	.005	sph=250 ts=1/4
861017.11	sf2	12 secs	.005	sph=225 ts=1/4
861017.12	sf2	12 secs	.005	sph=250 ts=1/4
861017.13	taft2	19 secs	.005	sph=225 ts=1/4
861017.14	taft2	19 secs	.005	sph=250 ts=1/4
861017.15	pac2	12 secs	.005	sph=250 ts=1/4
861017.16	buc1	12 secs	.005	sph=225 ts=1/4
861017.17	buc1	12 secs	.005	sph=250 ts=1/4
861017.18	random30.d	35 secs	.005	sph=300

FILENAME	SIGNAL	TIME	RATE	REMARKS
861021.01	ec2	19 secs	.005	sph=150 ts=1/4
861021.02	ec2	19 secs	.005	sph=250 ts=1/4
861021.03	random30.d	35 secs	.005	sph=300
861021.04	random30.d	35 secs	.005	sph=600
861021.05	random30.d	35 secs	.005	sph=900
861021.06	ec2	19 secs	.005	sph=150 ts=1/4
861021.07	sf2	12 secs	.005	sph=150 ts=1/4
861021.08	pac2	12 secs	.005	sph=150 ts=1/4
861021.09	park2	14 secs	.005	sph=150 ts=1/4
861021.10	taft2	19 secs	.005	sph=150 ts=1/4
861021.11	sf2	102 sec	.005	sph=250 ts=1/4

comment: the following signals were run at low spans because the rigid body mode was at 0.75 Hz almost in resonance with first sloshing mode of water tank mounted on structure. Data mainly collected for water tank.

861023.01	ec2	19 secs	.005	sph=50 ts=1/4
861023.02	ec2	19 secs	.005	sph=75 ts=1/4
861023.03	ec2	19 secs	.005	sph=70 ts=1/4
861023.04	sf2	12 secs	.005	sph=50 ts=1/4
861023.05	sf2	12 secs	.005	sph=150 ts=1/4
861023.06	sf2	12 secs	.005	sph=75 ts=1/4
861023.07	pac2	12 secs	.005	sph=50 ts=1/4
861023.08	pac2	12 secs	.005	sph=75 ts=1/4
861023.09	park2	14 secs	.005	sph=50 ts=1/4
861023.10	park2	14 secs	.005	sph=75 ts=1/4
861023.11	taft2	19 secs	.005	sph=50 ts=1/4
861023.12	taft2	19 secs	.005	sph=75 ts=1/4
861023.13	bucl	12 secs	.005	sph=50 ts=1/4
861023.14	bucl	12 secs	.005	sph=25 ts=1/4
861023.15	sct	35 secs	.005	sph=25 ts=1/4
861023.16	sct	35 secs	.005	sph=50 ts=1/4

SLIDING BEARINGS, RUBBER BEARINGS, AND TENSION RESTRAINTS COMBINED AS A NEW ISOLATION SYSTEM.

FOUR INTERIOR BEARINGS WERE 6X6 TEFLON-STAINLESS STEEL SLIDERS
FOUR CORNER BEARINGS WERE NATURAL RUBBER BEARINGS WITH TENSION DEVICES IN CENTRAL HOLES.

FILENAME	SIGNAL	TIME	RATE	REMARKS
861028.03	static	15 secs	.01	south end lift
861028.04	static	15 secs	.01	north end lift

comment: some sine signals were applied before the following series. No sliding. Since expected high relative velocities to cause sliding, started with San Francisco high frequency record.

861029.01	sf2	12 secs	.005	sph=50 ts=1/4
861029.02	sf2	12 secs	.005	sph=100 ts=1/4
861029.03	sf2	12 secs	.005	sph=150 ts=1/4
861029.04	sf2	12 secs	.005	sph=200 ts=1/4
861029.05	sf2	12 secs	.005	sph=150 spv=150 ts=1/4
861029.06	ec2	19 secs	.005	sph=150 ts=1/4
861029.07	ec2	19 secs	.005	sph=200 ts=1/4

FILENAME	SIGNAL	TIME	RATE	REMARKS
861030.01	ec2	19 secs	.005	sph=200 ts=1/4
861030.02	ec2	19 secs	.005	sph=250 ts=1/4
861030.03	ec2	19 secs	.005	sph=300 ts=1/4
861030.04	ec2	19 secs	.005	sph&v=300 ts=1/4
861030.05	ec2	19 secs	.005	sph=350 ts=1/4
861030.06	miyagi	13 secs	.005	sph=350 ts=1/4
861030.07	park2	14 secs	.005	sph=350 ts=1/4
861030.08	taft2	19 secs	.005	sph=350 ts=1/4
861030.09	buc1	12 secs	.005	sph=250 ts=1/4
861030.10	buc1	12 secs	.005	sph=300 ts=1/4
861030.11	pac2	12 secs	.005	sph=350 ts=1/4
861030.12	pac2	12 secs	.005	sph&v=350 ts=1/4
861030.13	sct	34 secs	.005	sph=150 ts=1/4
861030.14	sct	34 secs	.005	sph=250 ts=1/4
861101.01	ec2	19 secs	.005	sph&v=300 ts=1/4

FILENAME	SIGNAL	TIME	RATE	REMARKS
861105.01	sct.o	34 secs	.005	sph=300 ts=1/4
861105.02	sct.o	34 secs	.005	sph=350 ts=1/4
861105.03	sct.o	34 secs	.005	sph&v=350 ts=1/4
861105.04	ecatc.s1	23 secs	.005	sph=250 ts=1/4
861105.05	ecatc.s1	23 secs	.005	sph=300 ts=1/4
861105.06	taftatc.s1	23 secs	.005	sph=300 ts=1/4

comment: by inspection of base shear hysteresis loops, it was noticed that the coefficient of friction was about 5 times the one provided by the manufacturer. It was around 20 %. In order to lower it, it was decided to increase the pressure on the teflon by reducing its area to 4X4 inch.

INSIDE BEARINGS WERE 4X4 TEFLON-STAINLESS STEEL SLIDERS.

861117.01	ec2	19 secs	.005	sph=150 ts=1/4
861117.02	ec2	19 secs	.005	sph=200 ts=1/4
861117.03	ec2	19 secs	.005	sph=300 ts=1/4
861117.04	ec2	19 secs	.005	sph=350 ts=1/4
861117.05	ec2	19 secs	.005	sph=400 ts=1/4
861117.06	ec2	19 secs	.005	sph=425 ts=1/4
861117.07	sct.o	34 secs	.005	sph=200 ts=1/4
861117.08	sct.o	34 secs	.005	sph=300 ts=1/4
861117.09	sct.o	34 secs	.005	sph=350 ts=1/4
861117.10	sct.o	34 secs	.005	sph=375 ts=1/4
861117.11	ec2	19 secs	.005	sph=150 ts=1/4

FILENAME	SIGNAL	TIME	RATE	REMARKS
861118.01	ec2	19 secs	.005	sph=150 ts=1/4
861118.02	sct.o	34 secs	.005	sph=400 ts=1/4

comment: the displacement control provided by the sliders
was such that the restrainers were not locking
at their initial adjustment of 0.8 inch which
allowed 2.25 inch horizontal freedom.
Tension restaints were thus tightened to 0.5 inch
bolt travel corresponding to 1.75 inch
horizontal freedom.

comment: oscillators were installed on the third floor and their
accelerations recorded.

861119.01	ec2	19	secs	.005	sph=300 ts=1/4
861119.02	ec2	19	secs	.005	sph=350 ts=1/4
861119.03	ec2	19	secs	.005	sph=375 ts=1/4
861119.04	sct.o	34	secs	.005	sph=375 ts=1/4
861119.05	buc1	12	secs	.005	sph=300 ts=1/4
861119.06	miyagi	12	secs	.005	sph=350 ts=1/4
861119.07	pac2	12	secs	.005	sph=350 ts=1/4
861119.08	park2	14	secs	.005	sph=350 ts=1/4
861119.09	sf2	13	secs	.005	sph=200 ts=1/4
861119.10	taft2	19	secs	.005	sph=350 ts=1/4
861119.11	taftatc.s1	23	secs	.005	sph=325 ts=1/4
861119.12	ecatc.s1	23	secs	.005	sph=325 ts=1/4
861119.13	ec2	19	secs	.005	sph=150 ts=1/4
861120.01	ec2	19	secs	.005	sph=150 ts=1/4
861124.01	random30.d	32	secs	.005	sph=100
861124.02	square pulse	15	secs	.005	
861124.03	sf2	13	secs	.005	sph&v=250 ts=1/4
861124.04	pac2	12	secs	.005	sph&v=350 ts=1/4
861124.05	sct.o	34	secs	.005	sph&v=350 ts=1/4
861125.01	sct.o	34	secs	.005	sph&v=350 ts=1/4

NINE STORY STEEL MODEL WITH K-BRACING
MASS DUSTRIBUTION IN FIGURE 2.1
TESTED FIXED BASE

870622.01	random30.d	32	secs	.005	int=.02	sph=250
870622.02	ec2	18	secs	.005	int=.01	sph=50
870622.03	ec2	18	secs	.005	int=.01	sph=100
870622.04	ec2	18	secs	.005	int=.01	sph=75
870622.05	ec2	18	secs	.005	int=.01	sph=125
870623.01	sf2	12	secs	.005	int=.01	sph=50
870623.02	sf2	12	secs	.005	int=.01	sph=75
870623.03	sf2	12	secs	.005	int=.01	sph=100
870623.04	sct.o	32	secs	.005	int=.01	sph=100
870623.05	taft2	18	secs	.005	int=.01	sph=100
870623.06	park2	12	secs	.005	int=.01	sph=125
870623.07	pac2	12	secs	.005	int=.01	sph=125
870623.08	buc1	14	secs	.005	int=.01	sph=150
870623.09	buc1	14	secs	.005	int=.01	sph=175
870623.10	miyagi	12	secs	.005	int=.01	sph=150
870623.11	miyagi	12	secs	.005	int=.000905	sph=175
870623.12	random30.d	32	secs	.005	int=.02	sph=350

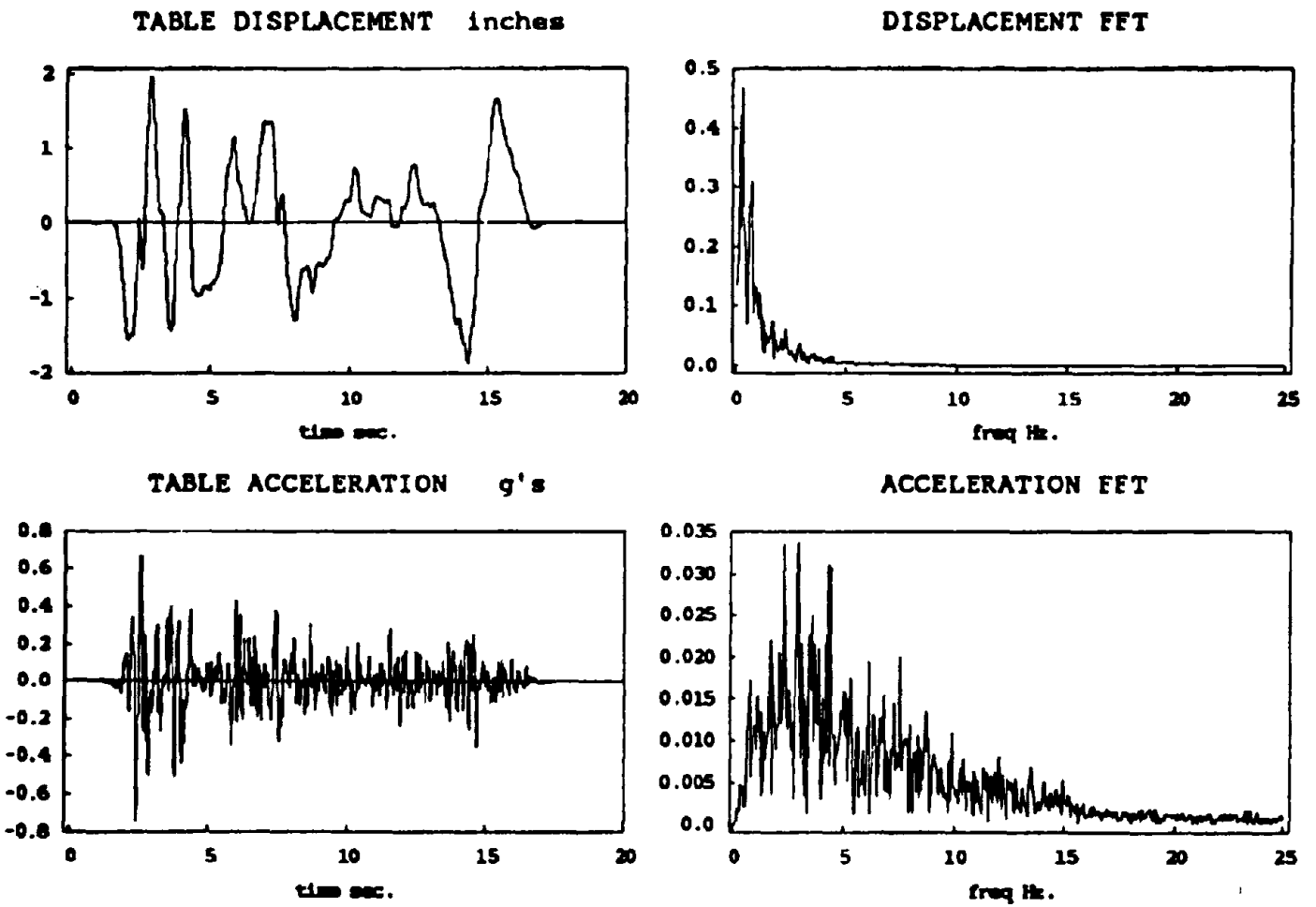

Figure 5.1a El Centro 1940 s00e, span=375, PTA=0.73 g.

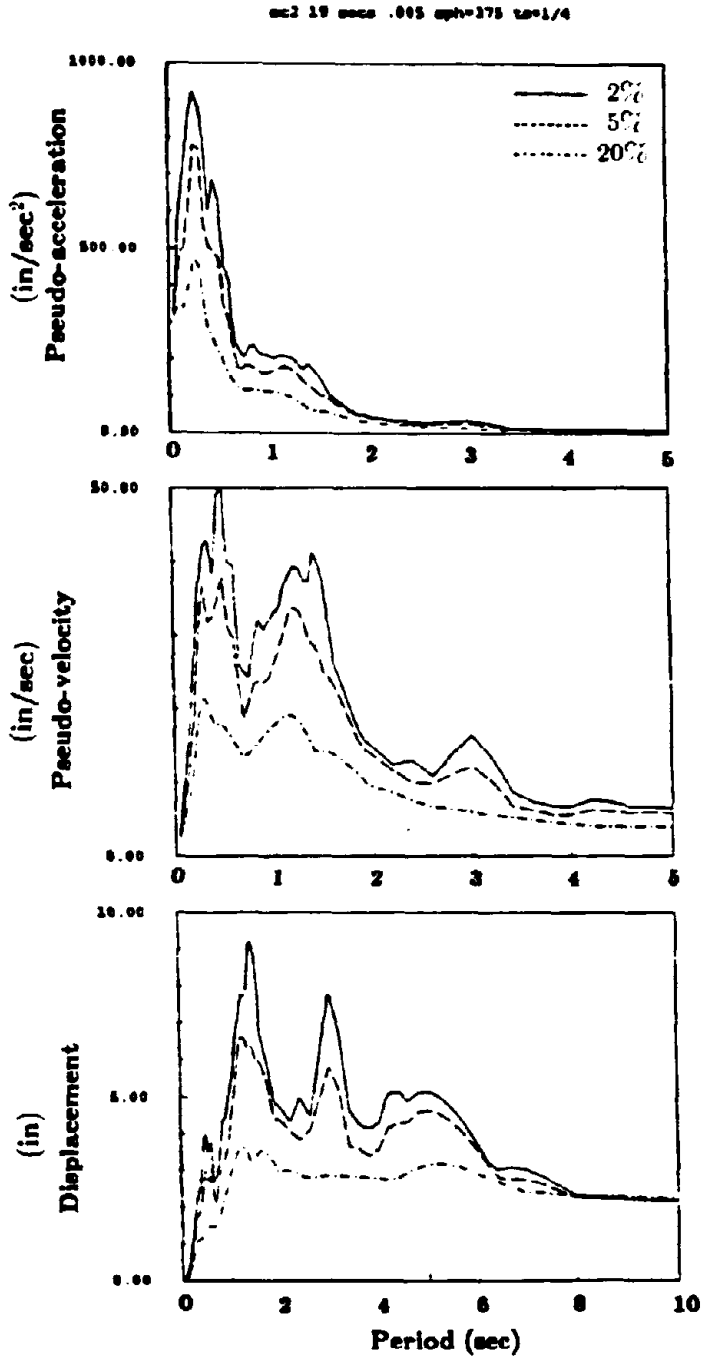

Figure 5.1b Response spectra. El Centro 1940 s00e, span=375, PTA=0.73 g.

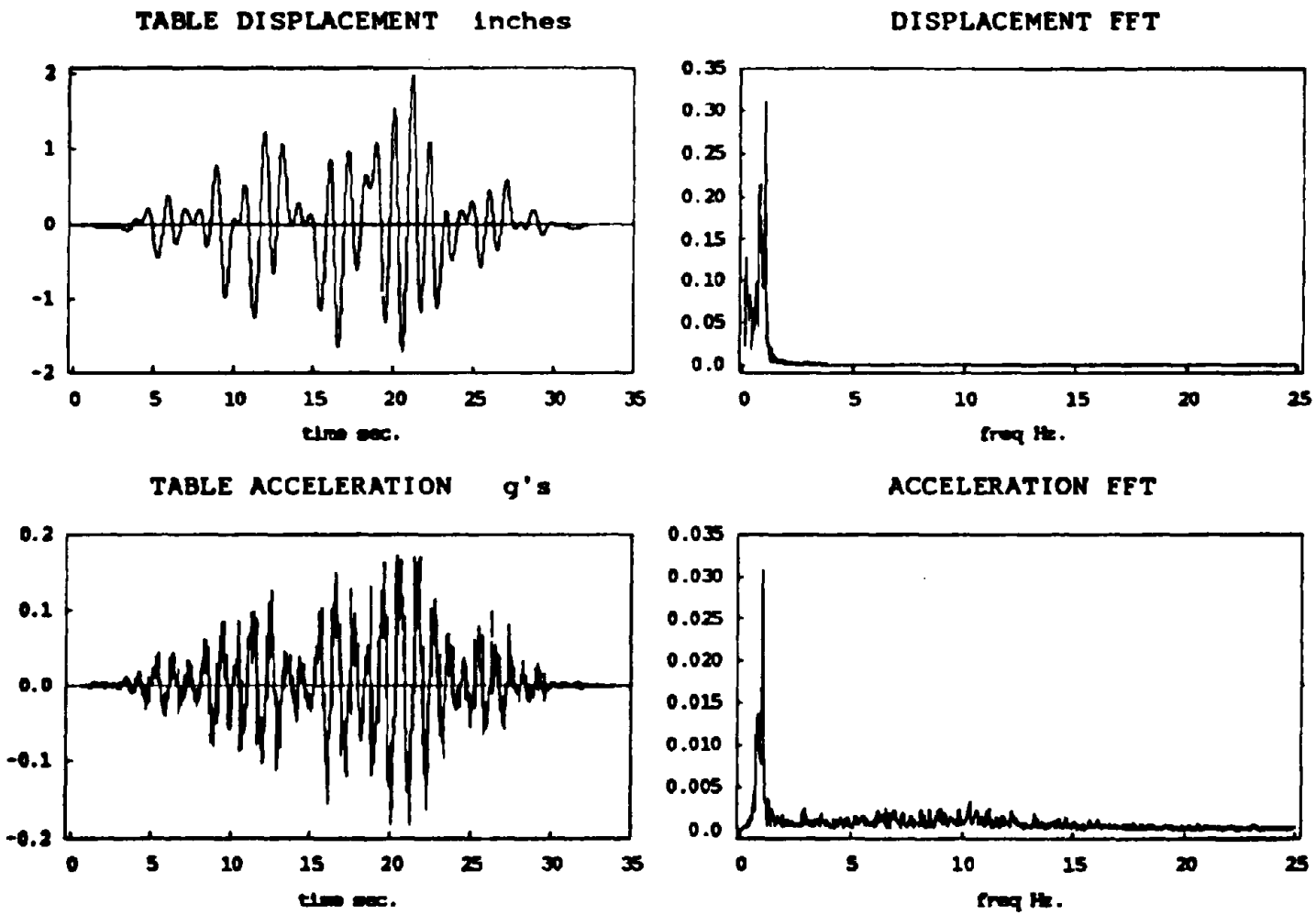

Figure 5.2a Mexico City 1985 s60e, span=375, PTA=0.18 g.

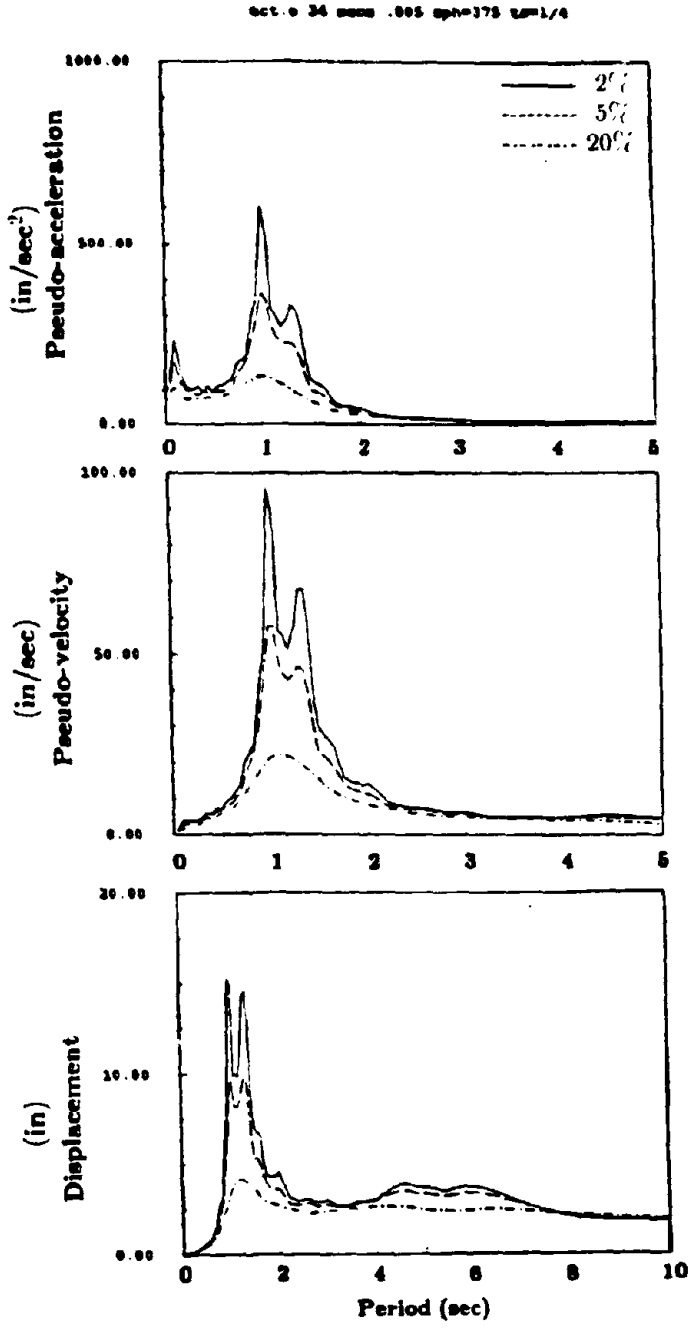

Figure 5.2b Response spectra. Mexico City 1985 s60e, span=375, PTA=0.18g.

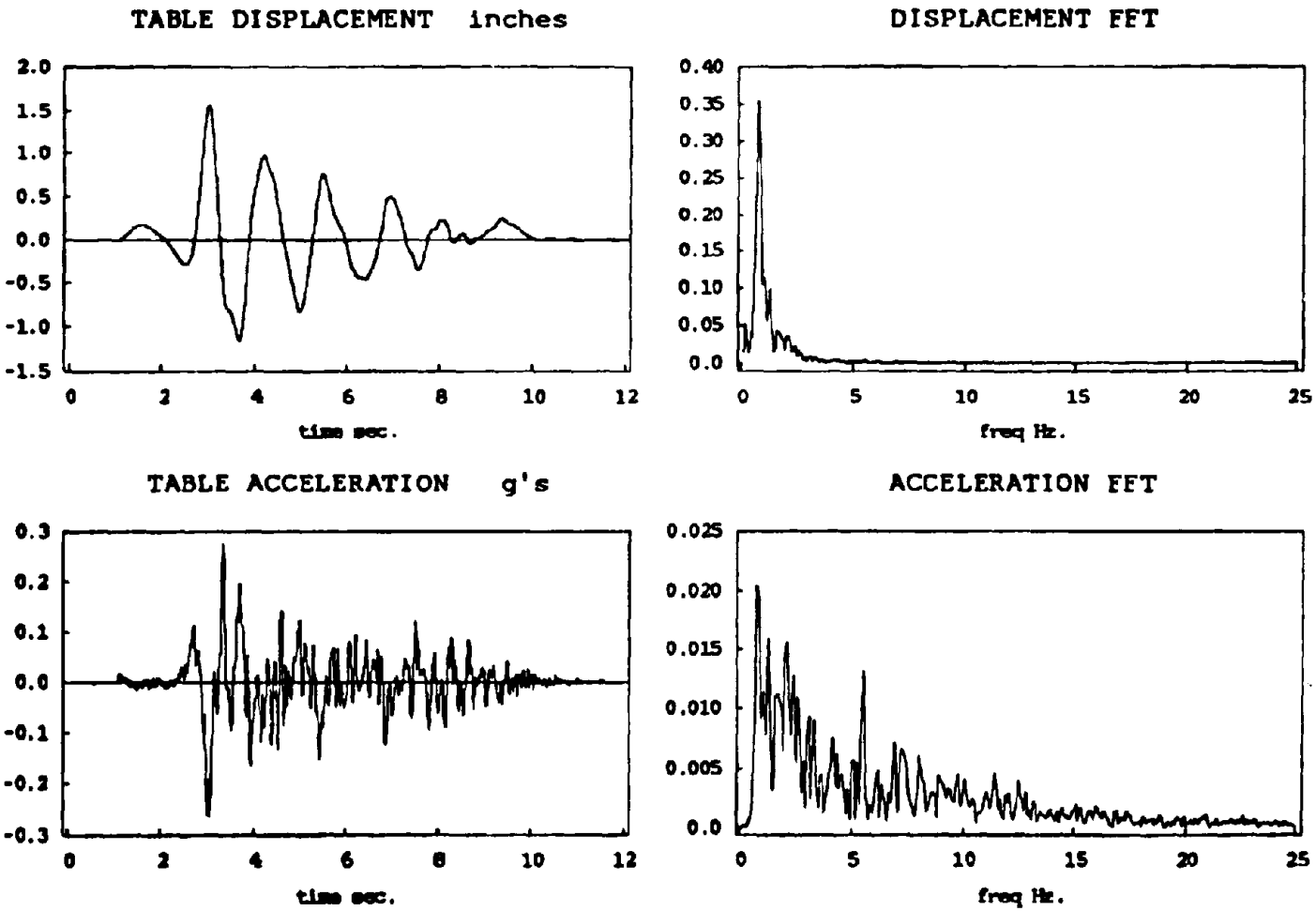

Figure 5.3a Bucharest 1977 s00e, span=300, PTA=0.27 g.

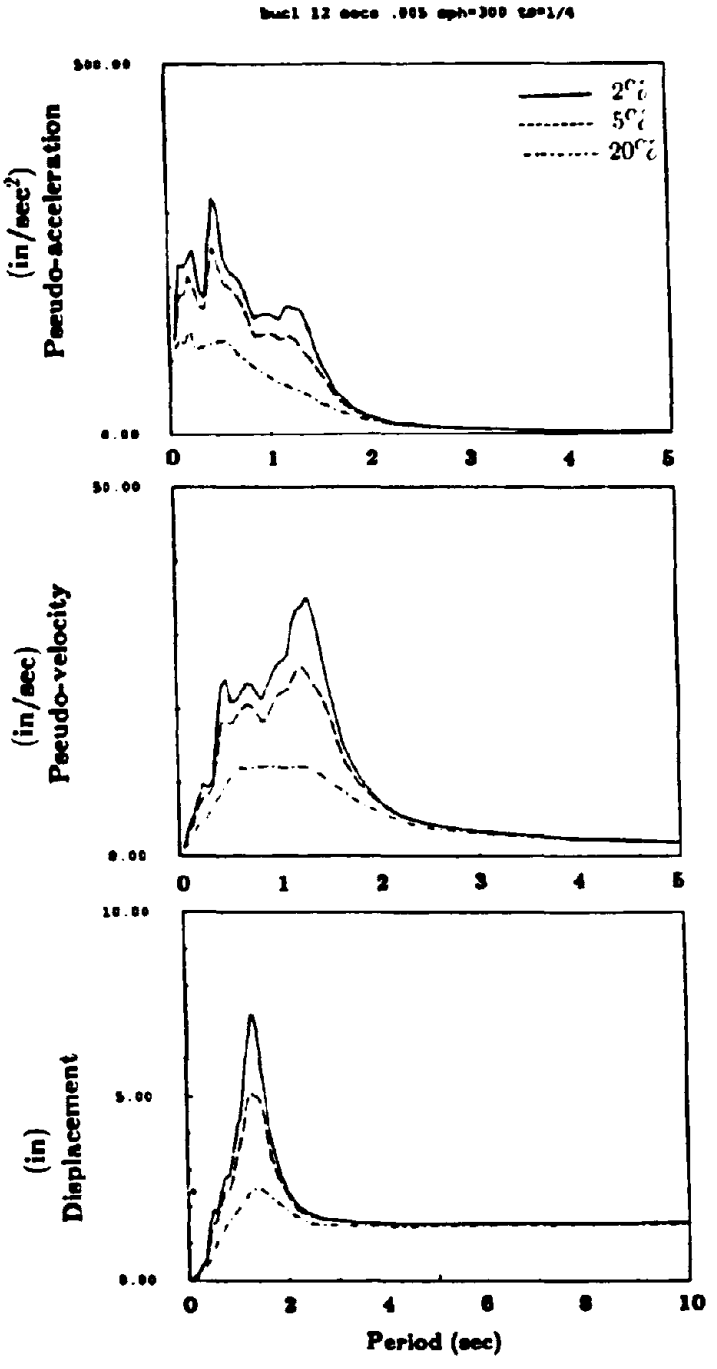

Figure 5.3b Response spectra. Bucharest 1977 s00e, span=300, PTA=0.27 g.

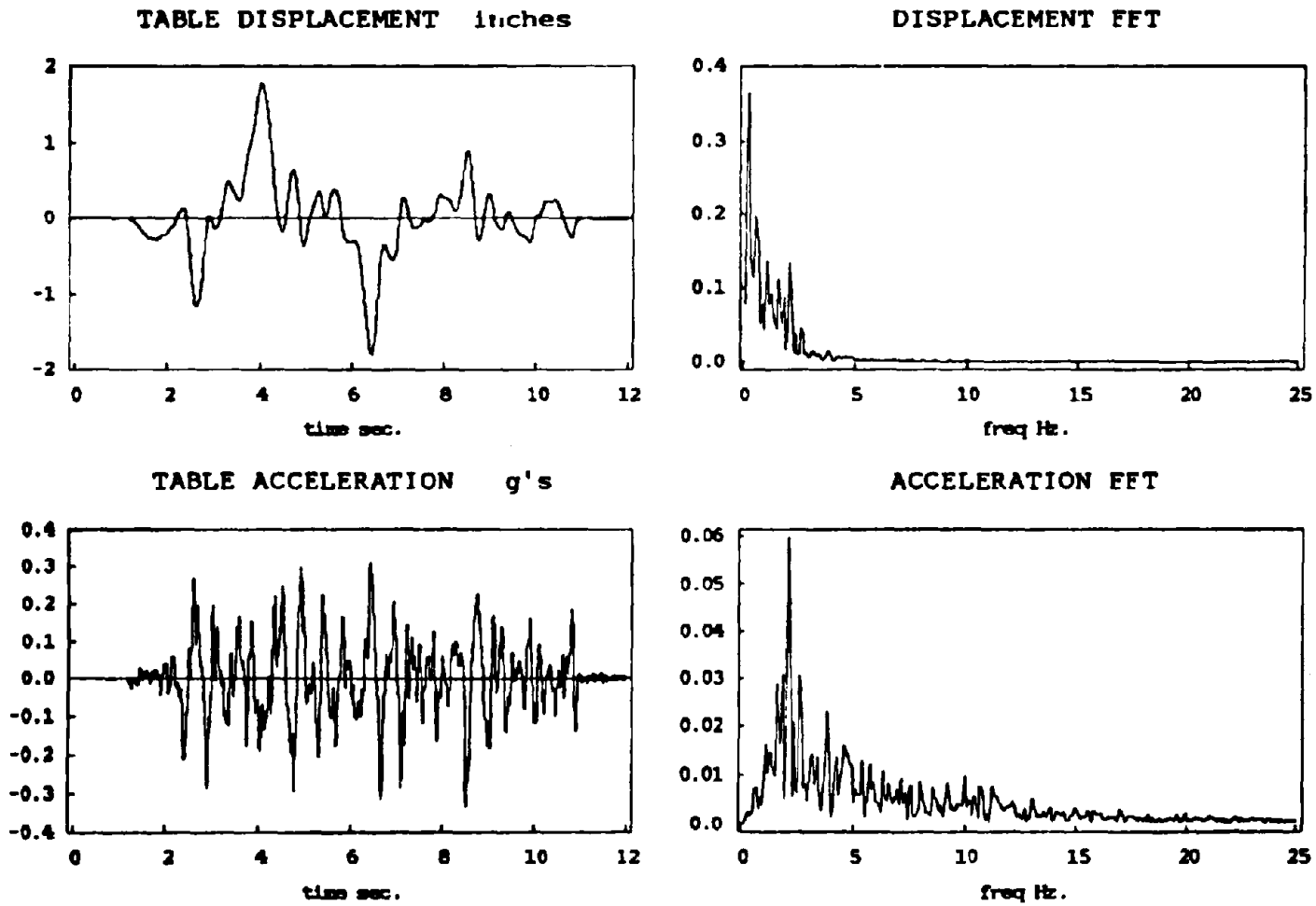

Figure 5.4a Miyagi-Ken-Oki 1978 w00s, span=350, PTA=0.33 g.

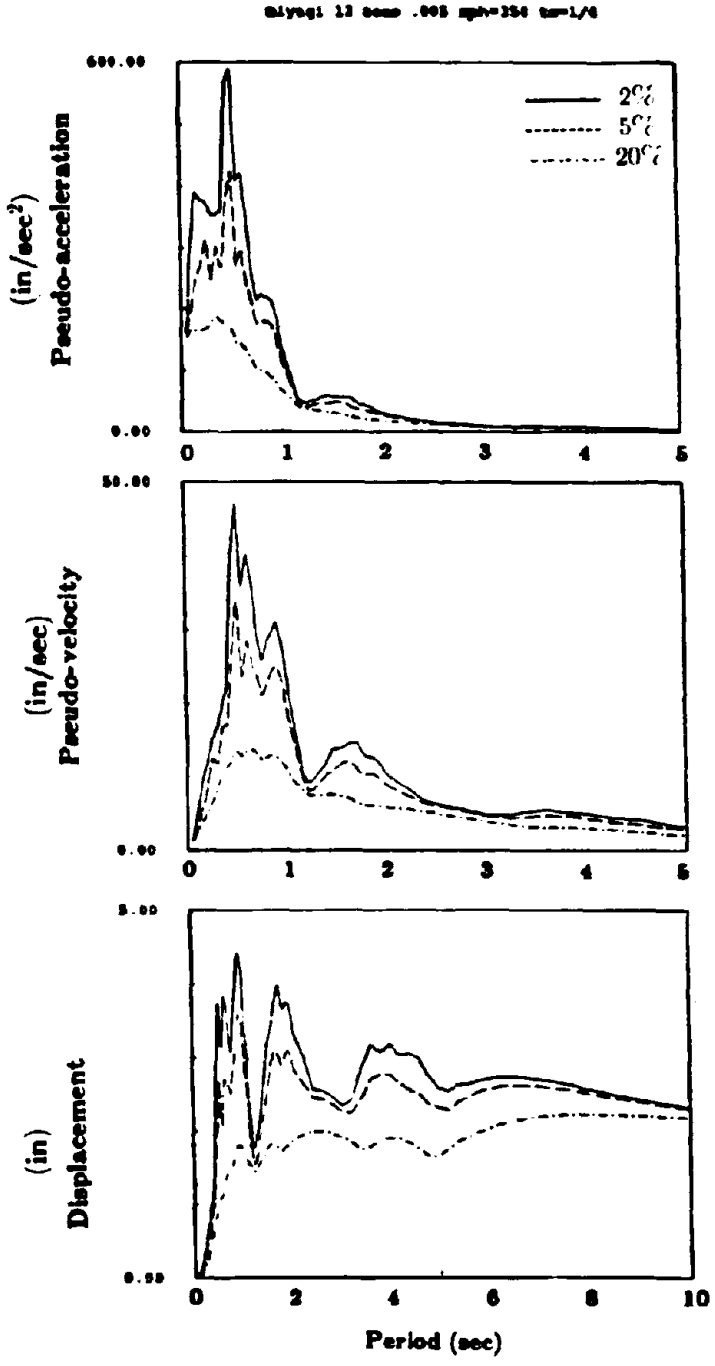

Figure 5.4b Response spectra. Miyagi-Ken-Oki 1978 w00s, span=350, PTA=0.33 g.

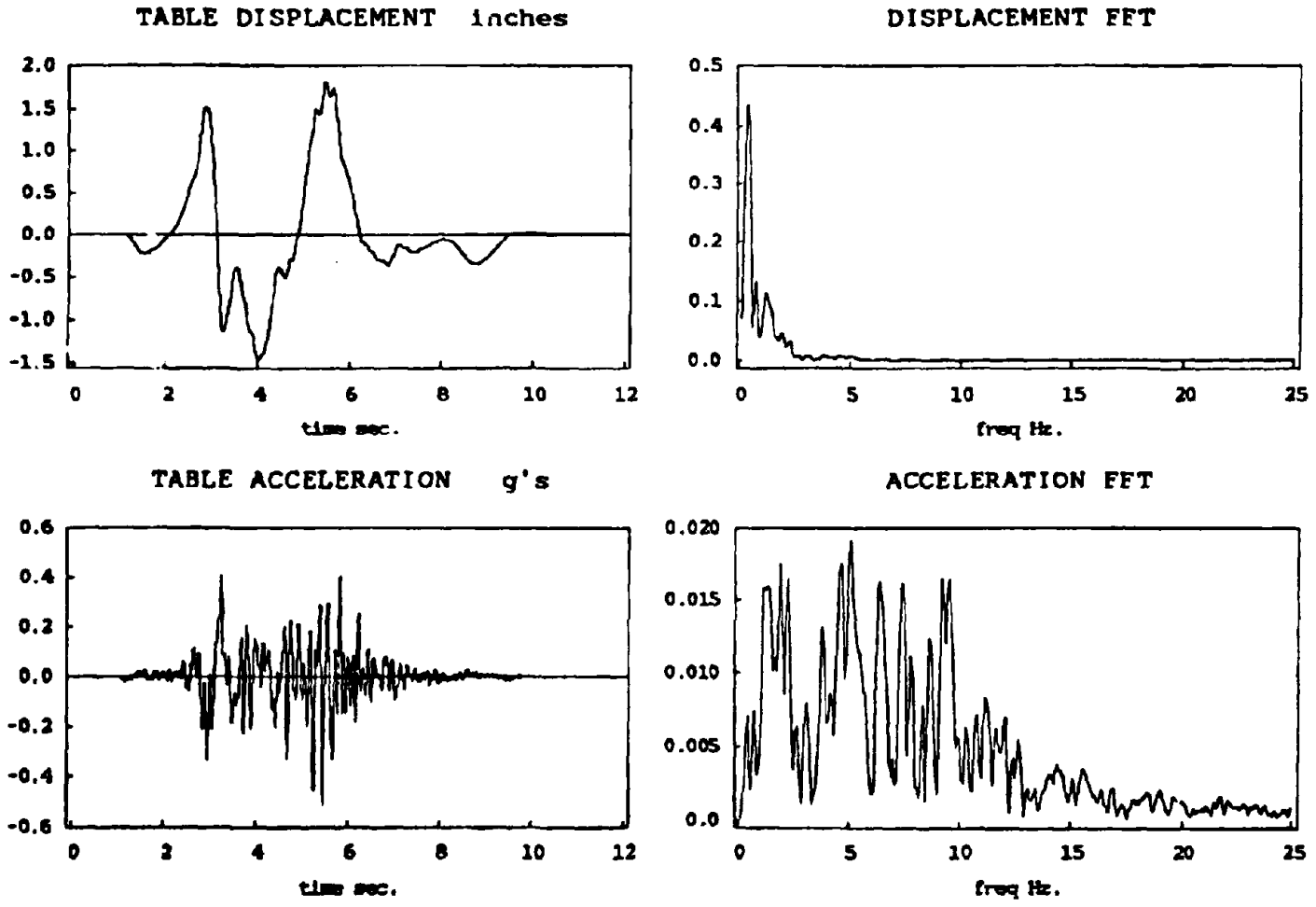

Figure 5.5a Pacoima Dam 1971 s16e, span=350, PTA=0.49 g.

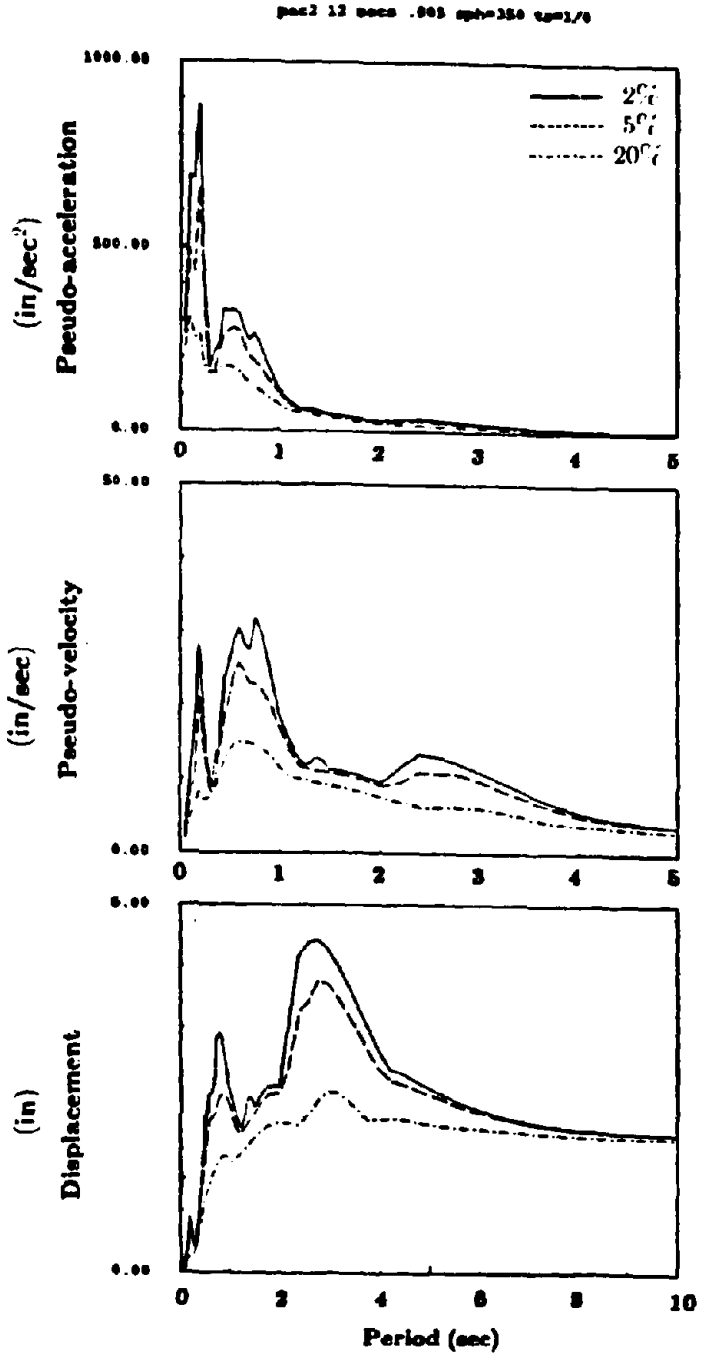

Figure 5.5b Response spectra. Pacoima Dam 1971 s16e, span=350, PTA=0.49 g.

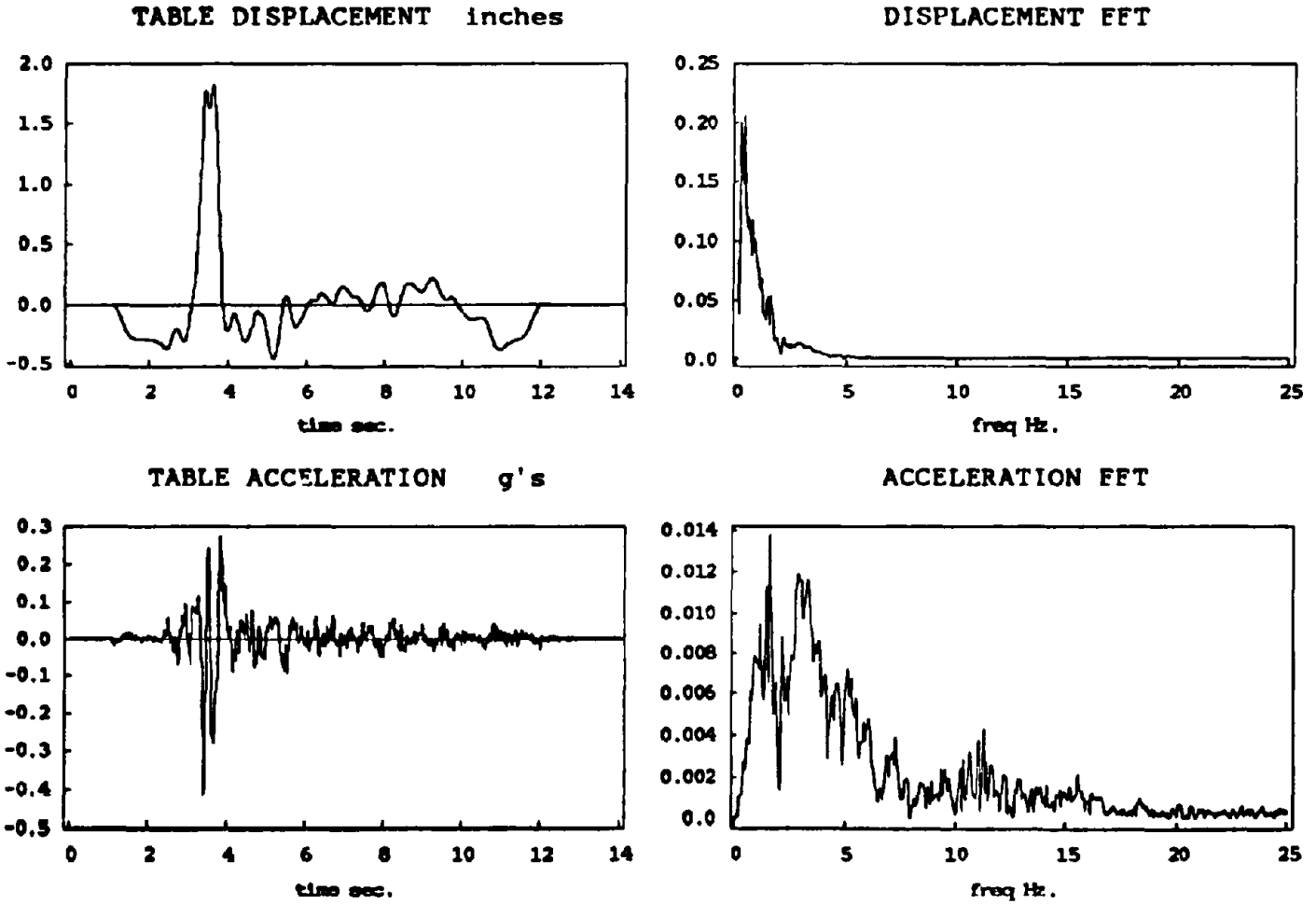

Figure 5.6a **Parkfield 1966 n65e, span=350, PTA=0.41 g**

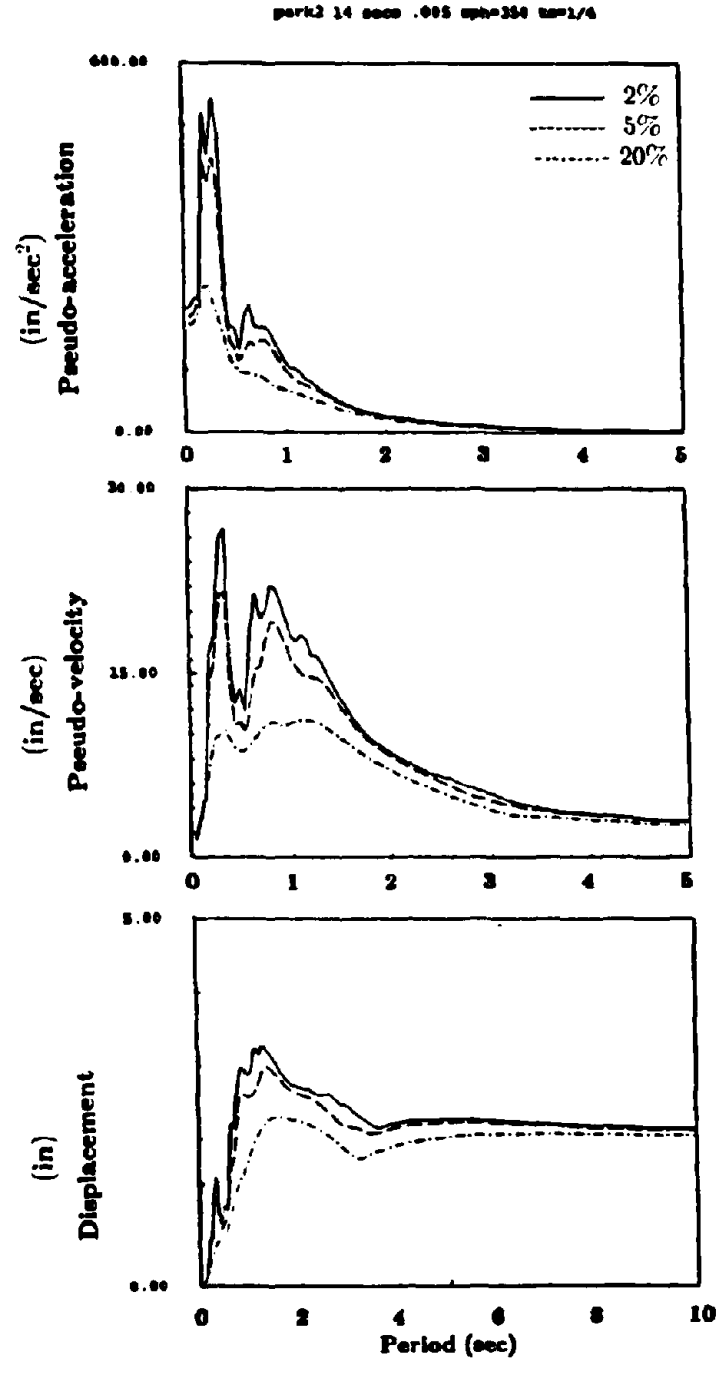

Figure 5.6b Response spectra. Parkfield 1966 n65e, span=350, PTA=0.41 g.

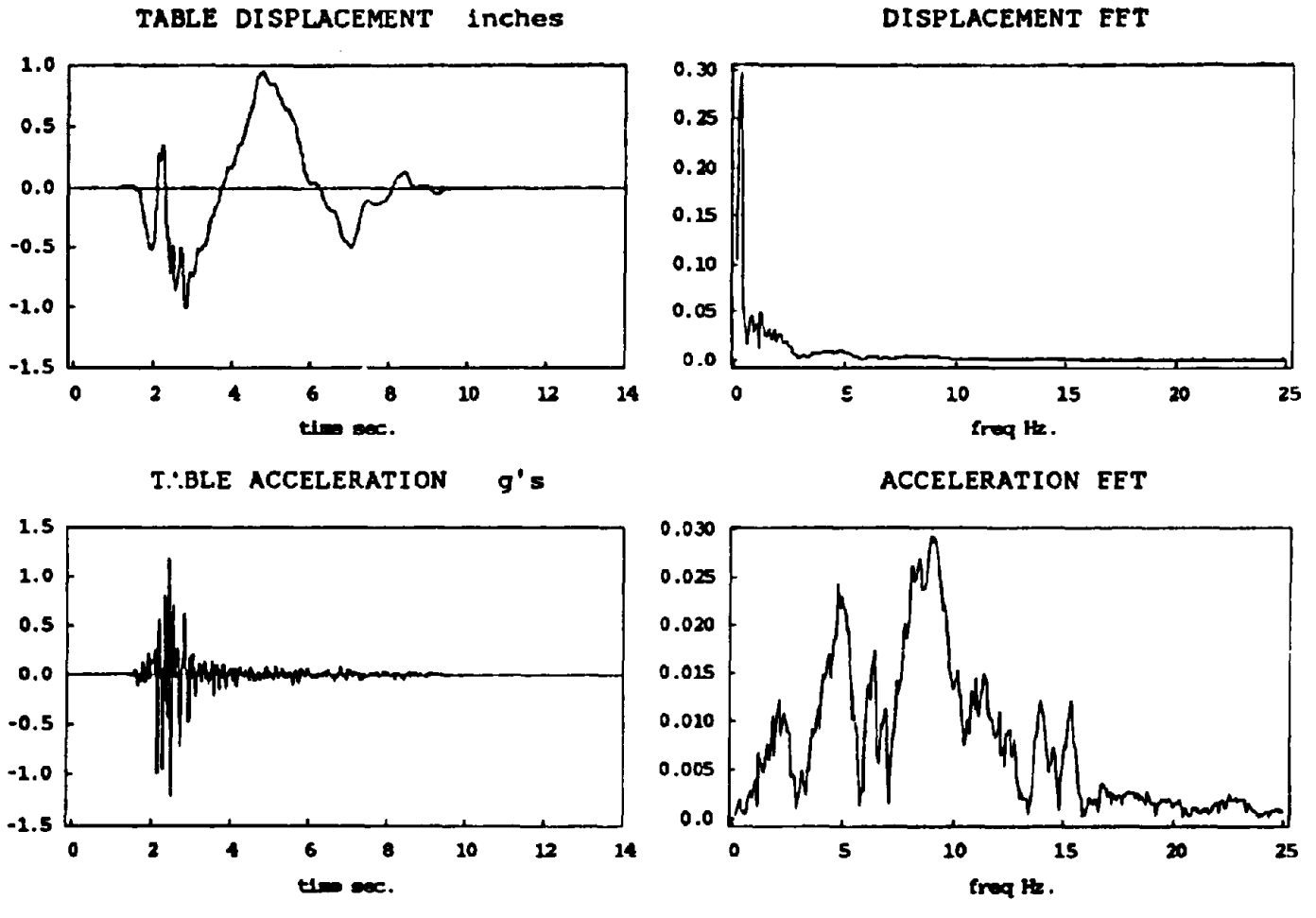

Figure 5.7a San Francisco 1957 s80e, span=200, PTA=1.20 g.

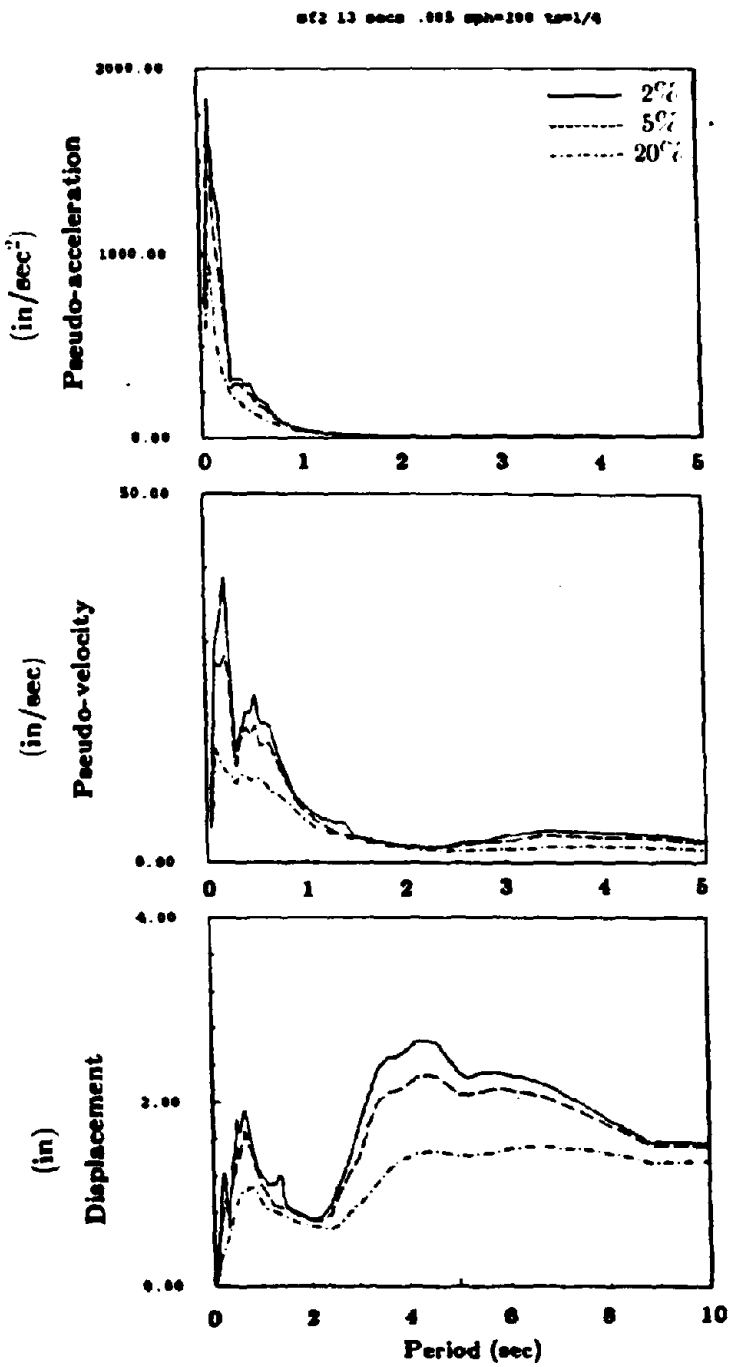

Figure 5.7b Response spectra. San Francisco 1957 s80e, span=200, PTA=1.20 g.

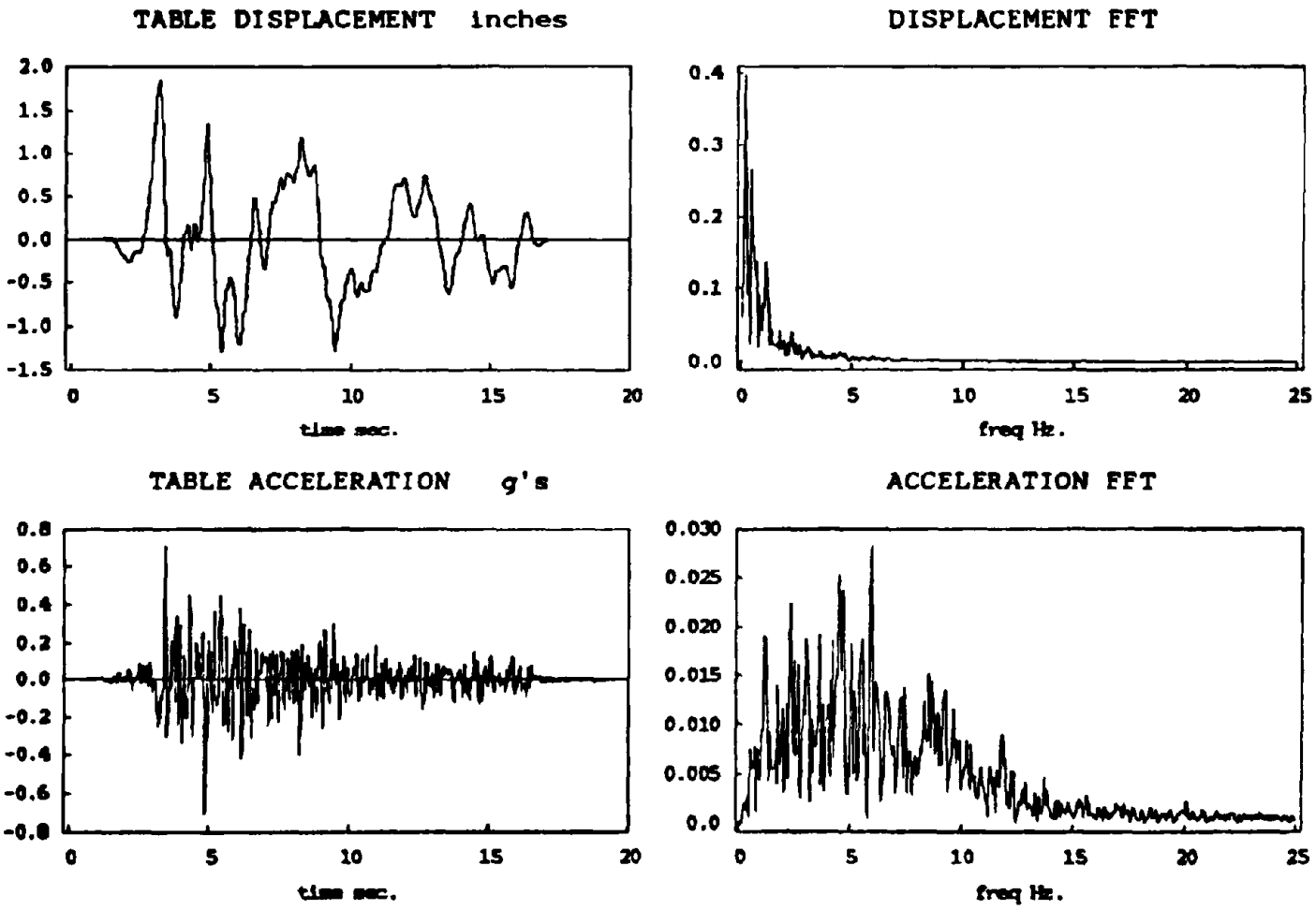

Figure 5.8a Taft 1952 s69e, span=350, PTA=0.72 g.

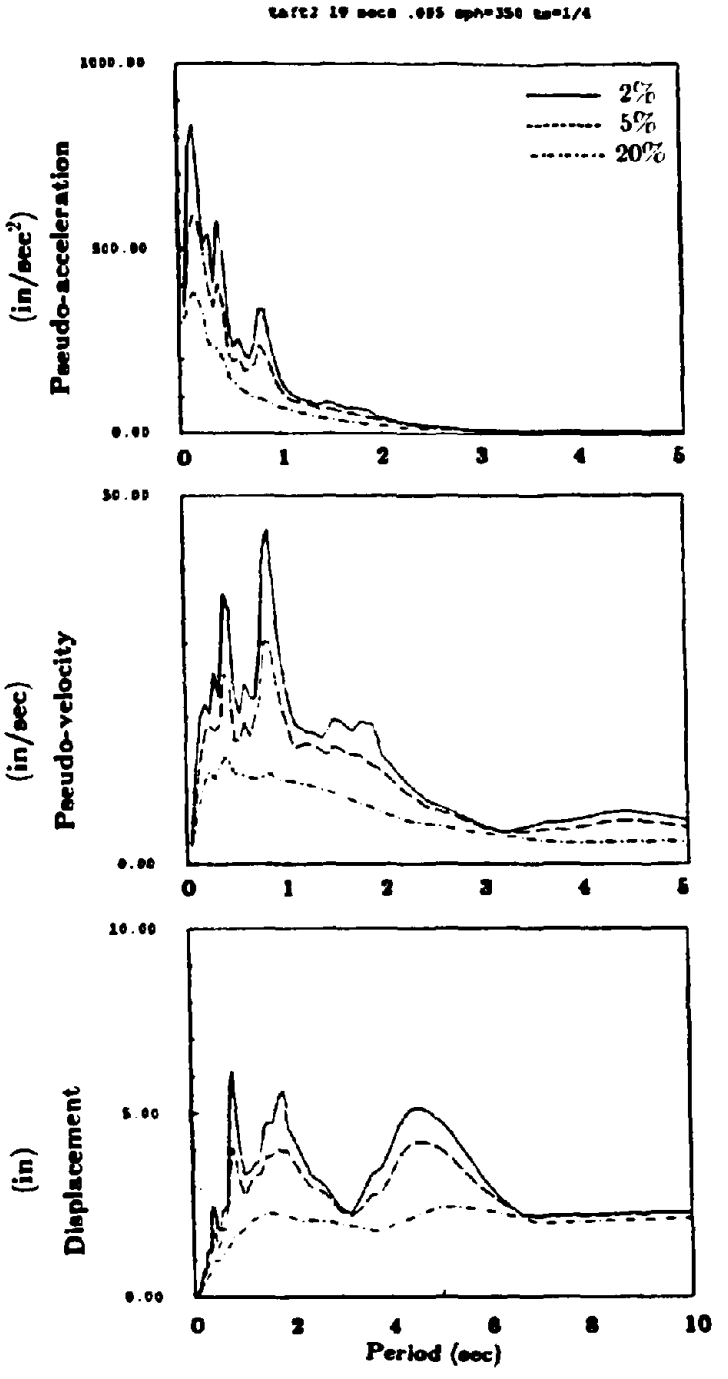

Figure 5.8b Response spectra. Taft 1952 s69e, span=350, PTA=0.72 g.

CHAPTER SIX

STATIC TESTS FOR SLIDING BEARINGS

1. General

Teflon sliders have been used in bridges and other structures to accommodate changes in member dimensions due to temperature and shrinkage effects. Since these movements are very slow, no conclusions have been drawn about the performance of sliders under earthquake loading. In the present experiment, sliders were combined with elastomeric pads, mounted under the structural model so that their behavior under earthquake loading could be better understood. In parallel with the shake table tests, the sliders were tested separately on a static rig to study their characteristics in more detail.

Of great interest, was the variation of the coefficient of friction μ, with the pressure in the material and the velocity of sliding. Generally, μ increased with velocity and decreased with pressure.

Changes in μ with the temperature and the cleanliness of the contacting surfaces are also a subject of interest and should be further investigated. In this experiment, however, these two factors were not studied since for sliders used in base isolation, the duration of activity is not long enough to make temperature changes a primary concern.

Wear of the slider would be an important topic in applications where a very large number of cycles is expected. This is not the case for an earthquake excitation. However, some results were drawn from repeated testing.

Previous work has been done on teflon sliders in different test conditions [12], [13]. In [12], the signal used was generated by the motor of a bulldozer and hence was not characterized by a constant velocity. A triangular signal provides a better description of the effect of velocity on the friction coefficient. In [13], tests of teflon consisted of extremely slow displacements and were mostly concerned with bridge joints. The sliding velocities used were of the order of 1% of the lowest velocity used in the present program.

2. Test Machine and Data Acquisition

The test machine is shown in Figure 6.1. The main structural parts consist of a stiff fixed base vertical column supported by two diagonal elements, and a horizontal beam located above the column and controlled by two vertical and one horizontal hydraulic actuator. The actuators can be either force controlled or displacement controlled. The two vertical actuators were force controlled. They were set to apply a constant force P' each, in order to ensure an axial load of $P = 2P'$ on the bearing, located under the center of the beam. The beam is very rigid in bending. Any vertical deflections in the bearing would be automatically followed by the vertical actuators so that P remains constant.

The horizontal actuator was displacement controlled, in the sense that it was set to provide a programmed signal. The nature of the displacement signal is chosen by the operator. In the present experiment, two types of displacements were used, a sinusoidal time series and a triangular time series. The force in the horizontal actuator was automatically changing correspondingly. At each actuator, two channels were connected to record forces and displacements.

The sliders tested were 6×6 inch and 4×4 inch teflon layers bearing against a stainless steel plate. The lower plate that carried the 1/25 inch thick teflon layer was mounted on a rubber bearing locked against horizontal movement (Figures 6.2 and 6.3). Between the bearing and the vertical column of the rig, a load cell was installed (Figure 6.4). The load cell measured shear, and bending forces.

Data was acquired through 15 channels. A list of the channel numbering and their functions is provided in Table T-6.1. The data acquisition system, that included an MTS board (Figure 6.5), was a part of the control instrumentation. A terminal permitted the display of all channels to check the correctness of the displacement input and the constancy of the applied axial load. A mechanical plotter, electrically connected to the shear and displacement channels produced simultaneously with the beam movement, the hysteresis loops of shear at the slider versus displacement of the horizontal beam. That was mainly intended to check if any deficiencies occurred during the test.

The rate at which the data samples are read is adjustable. For the slow runs, namely corresponding to 0.0125 Hz. the data was read at a rate of 10 readings a second. For the tests

corresponding to 0.125 Hz, 50 samples were acquired per second. For all higher frequencies of input displacement, 100 readings per second were performed. Each set of data acquired was temporarily stored on the disk of the computer until it was saved on tape, loaded on a VAX 750, and processed.

3. Test Sequence

The vertical loads and velocities used in the rig tests were intended to include their corresponding values encountered during shake table tests. While mounted under the structural model, the inner bearings carried about 14 kips each, and the outer ones around 9 kips each.

For the teflon sliders, the 6×6 inch layers were hence under a pressure of about 390 psi while installed under the structure. On the static rig, their pressure was varied from 100 psi to 1200 psi. The 4×4 inch layers were subjected to about 900 psi during the shake table tests, and their pressure on the static rig was varied from 100 psi to 3000 psi. The pressure was extended to that high value in order to detect any deficiencies that could result from accidental overloading of a slider during an earthquake.

Table T-6.2 provides a chronological listing of the series of tests performed on the static rig. In the first test series, which is not listed here, sinusoidal signals of various frequencies and amplitudes were used as horizontal displacement input. Since the slope of a sinusoidal signal is continuously changing, the sliding velocity was not fixed to a certain value. Furthermore, the shape of the hysteresis loops for those tests were close to elliptical, and thus did not show a constant shear force. That suggested that the friction coefficient depended greatly on the sliding velocity. The highest point of the hysteresis loops was located on the vertical axis, this showed that the coefficient of friction increased with velocity.

For the reasons mentioned above, it was decided to use a displacement signal with constant slope (triangular signal) to study the effect of the velocity on the coefficient of friction. The values that were used were intended to cover the range of velocities produced on the shake table. Integration of the structure base relative acceleration time series, produced relative velocities up to 12 in/sec for certain shake table tests.

4. Test Results

The displacement and shear time histories for the 3 or 4 main cycles of each test run along with the corresponding hysteresis loops are shown in Figures 6.8-6.22, for the 4×4 sliders. The values of the resulting coefficients of friction are summarized in Table T-6.3 and plotted in Figure 6.23. The test was mainly intended to study the coefficient of friction of the sliders and its dependence on the following factors:

Velocity

Even though it is commonly accepted that for most contacting surfaces, the static coefficient of friction is higher than the dynamic coefficient of friction, it was noticed that for very low velocities, namely 0.1 in/sec, the coefficient of friction was lower than the one obtained for higher velocities.

For instance, for the 4×4 sliders, μ changed from 7% to 17% when the velocity was increased from 0.1 to 10 in/sec, for a pressure of 100 psi, and from 6% to 15% for the same velocity variation, but under a pressure of 1200 psi in the teflon. However, this increase tends to a certain saturation at velocities around 12 in/sec. For velocities of above 12 in/sec, the shear level drops within the same test run, because of the increase in temperature at the contacting surfaces, producing a lower coefficient of friction. For these tests, the coefficient of friction adopted was the one that corresponded to the three full middle cycles in the input displacement time history. This coefficient was generally smaller than the one obtained at the first cycle of the signal.

Pressure

Another property of the teflon sliding on stainless steel is the dependence of its dynamic coefficient of friction on the pressure in the material. In general, for most sliding areas, the dynamic coefficient of friction is obtained from simply normalizing the shear resisted by the slider by the axial load, at a certain rate of sliding. In the present case, the value of the axial load had a large influence on μ. For instance, a change of 1100 psi in the pressure at 10 in/sec, caused a drop in μ from 17% to 7%.

On the other hand, the static coefficient of friction, which was adopted as corresponding to v = 0.1 in/sec, was not affected by the changes in axial load; for a difference of pressure of 1100 psi, μ stayed around 7%.

Temperature

Depending on the fabrication process and the composition of the teflon, the temperature has different effects on the coefficient of friction. This experiment gave only a general idea of the effects of temperature. The slider was estimated to be at room temperature before the test, and at around 110°F after the test, for velocities of 10 in/sec and above. Since it was not intended to study temperature effects for our present application, no instrumentation was installed to acquire the temperature time history. In sum, the effect was a slight drop in μ.

Contamination

It is commonly accepted that the presence of an external material between the contacting surfaces causes substantial changes in μ. In reference [12], data for greased sliders and dusted sliders is given. Since a building is expected to be always resting on its foundations, no other material will penetrate between the contacting surfaces. The area of steel which is not constantly covered by the teflon, can be regularly cleaned of a contaminating material as a part of the maintenance program.

Wear

After 60 test runs equivalent to about 250 cycles of an average amplitude of 1.2 inches, the teflon layer thickness was reduced by only 1/30 inch. The main type of wearing noticed was a delamination of the teflon layer (Figures 6.6 and 6.7). After tests of v = 10 in/sec and above were performed, very thin layers of teflon of areas of about 4 square inches detached from the sliders. Also, on the stainless steel plate, a white film was found after each test. This film was removed by each following test run and a white powder-like material was found on the steel at the limit of travel of the teflon.

For comparison, the teflon fragments were cleaned from the steel and the same test was rerun with a slight increase in the coefficient of friction. The difference, however, was negligible and the removal of the teflon film after each run was found unnecessary. There was some hesitation in identifying this delamination as damage, since it had almost no effect on the coefficient of friction. Also, the reduction in the thickness of the teflon was very small. Under earthquake excitation, the number of cycles is too small to cause a concern about the wearing in the slider.

Strength

At the end of the test program, the pressure on the teflon was increased to 3000 psi to test the strength of the slider. No noticeable change was observed, other than the decrease in the coefficient of friction in about the same proportion as for the previous pressure levels. No fracturing in the 1/30 inch thick teflon layer occurred. This showed that there is no risk of failure of the teflon or sudden changes in the slider properties in the case of an accidental overloading. At this level of pressure, however, the delamination was slightly increased.

Previous experience with teflon in slow movements, and recent research on its performance under dynamic excitations show its reliability and the possibility of using it as a component in base isolation systems.

Table T-6.1 List of channels for triangular signal rig testing.

LIST OF CHANNELS FOR TEFLON-STAINLESS STEEL SLIDERS
STATIC RIG TESTING.

CHANNEL	NAME	UNITS	REMARK
0	F.L.DCDT	INCHES	Front Left DCDT
1	B.L.DCDT	INCHES	Back Left DCDT
2	F.R.DCDT	INCHES	Front Right DCDT
3	B.R.DCDT	INCHES	Back Right DCDT
4	F.C.DCDT	INCHES	Front Center DCDT
5	B.C.DCDT	INCHES	Back Center DCDT
6	HOZ.LOAD	KIPS	Horizontal actuator force
7	HOZ.DISP	INCHES	Horizontal actuator displacement
8	VPM SHEAR	KIPS	Shear recorded on load cell
9	VPM MOMENT	KIP-IN	Moment recorded on load cell
10	VERT.LOAD1	KIPS	Vertical actuator #1 force
11	VERT.LOAD2	KIPS	Vertical actuator #2 force
12	VERT.DISP1	INCHES	Vertical actuator #1 displacement
13	VERT.DISP2	INCHES	Vertical actuator #2 displacement
14	VPM AXIAL	KIPS	Axial force recorded on load cell
15	VPM DISP	INCHES	Axial displacement between load cell and ground.

Table T-6.2 Sliders test sequence for triangular signal.

TEST SEQUENCE FOR 6x6 AND 4x4 TEFLON-STAINLESS STEEL
SLIDERS FOR TRIANGULAR HORIZONTAL DISPLACEMENT.
4 MINUTES REST BETWEEN SUCCESSIVE RUNS.

Collecting data at 10 samples/sec for 0.0125 Hz.,
50 samples/sec for 0.125 Hz.,
50 samples/sec for 0.625 Hz.,
100 samples/sec for other frequencies.

Testing 6x6 slider

FILENAME	VELOC in/s	FREQ Hz	AXIAL Kips	PRESS psi	AMPLIT in
870305.01	0.1	0.0125	3.6	100	2
870305.02	1.0	0.125	3.6	100	2
870305.03	5.0	0.625	3.6	100	2
870305.04	10.0	1.25	3.6	100	2
870305.05	12.0	1.50	3.6	100	2
870305.06	15.0	1.875	3.6	100	2
870305.11	0.1	0.0125	21.6	600	2
870305.12	1.0	0.125	21.6	600	2
870305.13	5.0	0.625	21.6	600	2
870305.14	10.0	1.25	21.6	600	2
870305.15	12.0	1.50	21.6	600	2
870305.16	15.0	1.875	21.6	600	2
870305.21	0.1	0.0125	32.4	900	2
870305.22	1.0	0.125	32.4	900	2
870305.23	5.0	0.625	32.4	900	2
870305.24	10.0	1.25	32.4	900	2
870305.25	12.0	1.50	32.4	900	2
870305.26	15.0	1.875	32.4	900	2
870305.31	0.1	0.0125	43.2	1200	2
870305.32	1.0	0.125	43.2	1200	2
870305.33	5.0	0.625	43.2	1200	2
870305.34	10.0	1.25	43.2	1200	2
870305.35	12.0	1.50	43.2	1200	2
870305.36	15.0	1.875	43.2	1200	2

The temperature for the previous tests raised from room temperature to around 100 F at the stainless steel face. The plate was warmer, but no other significant differences. Waited until cooling then started with 4x4 slider.

Testing 4x4 slider

FILENAME	VELOC	FREQ	AXIAL	PRESS	AMPLIT
870305.41	0.1	0.0125	1.6	100	2
870305.42	1.0	0.125	1.6	100	2
870305.43	5.0	0.625	1.6	100	2
870305.44	10.0	1.25	1.6	100	2
870305.45	12.0	1.50	1.6	100	2
870305.46	15.0	1.875	1.6	100	2
870305.51	0.1	0.0125	9.6	600	2
870305.52	1.0	0.125	9.6	600	2
870305.53	5.0	0.625	9.6	600	2
870305.54	10.0	1.25	9.6	600	2
870305.55	12.0	1.50	9.6	600	2
870305.56	15.0	1.875	9.6	600	2
870309.01	0.1	0.0125	14.4	900	2
870309.02	1.0	0.125	14.4	900	2
870309.03	5.0	0.625	14.4	900	2
870309.04	10.0	1.25	14.4	900	2
870309.05	12.0	1.50	14.4	900	2
870309.06	15.0	1.875	14.4	900	2
870309.11	0.1	0.0125	19.2	1200	2
870309.12	1.0	0.125	19.2	1200	2
870309.13	5.0	0.625	19.2	1200	2
870309.14	10.0	1.25	19.2	1200	2
870309.15	12.0	1.50	19.2	1200	2
870309.16	15.0	1.875	19.2	1200	2
980309.21	0.1	0.0125	32.0	2000	2
980309.22	1.0	0.125	32.0	2000	2
980309.23	5.0	0.625	32.0	2000	2
980309.24	10.0	1.25	32.0	2000	2
980309.25	12.0	1.50	32.0	2000	2
980309.26	15.0	1.875	32.0	2000	2
870309.31	0.1	0.0125	40.0	2500	2
870309.32	1.0	0.125	40.0	2500	2
870309.33	5.0	0.625	40.0	2500	2
870309.34	10.0	1.25	40.0	2500	2
870309.35	12.0	1.50	40.0	2500	2
870309.36	15.0	1.875	40.0	2500	2
870309.41	0.1	0.0125	48.0	3000	2
870309.42	1.0	0.125	48.0	3000	2
870309.43	5.0	0.625	48.0	3000	2
870309.44	10.0	1.25	48.0	3000	2
870309.45	12.0	1.50	48.0	3000	2
870309.46	15.0	1.875	48.0	3000	2

clockwise tilt of 0.04 rd. for 870309.47
counterclockwise tilt of 0.04 rd for 870309.48

870309.47	10.0	1.25	48.0	3000	2
870309.48	10.0	1.25	48.0	3000	2

Table T-6.3 Variation of friction coefficient for 4x4 inch teflon-stainless steel sliders with pressure and sliding velocity.

-	COEFFICIENT OF FRICTION (%) - 4 x 4 TEFLON SLIDER						
-	100 psi	600 psi	900 psi	1200 psi	2000 psi	2500 psi	3000 psi
0.1 $in.sec^{-1}$	6.9	6.8	6.4	6.4	5.5	5.3	5.0
1.0 $in.sec^{-1}$	11.7	11.5	11.1	11.1	10.2	8.8	7.9
5.0 $in.sec^{-1}$	16.9	16.7	14.5	13.2	10.3	9.0	8.3
10.0 $in.sec^{-1}$	17.5	17.2	15.9	15.0	11.0	9.5	8.7
12.0 $in.sec^{-1}$	17.2	16.7	15.0	14.6	10.7	9.4	8.3
15.0 $in.sec^{-1}$	17.1	16.6	14.9	14.2	10.2	9.1	7.9

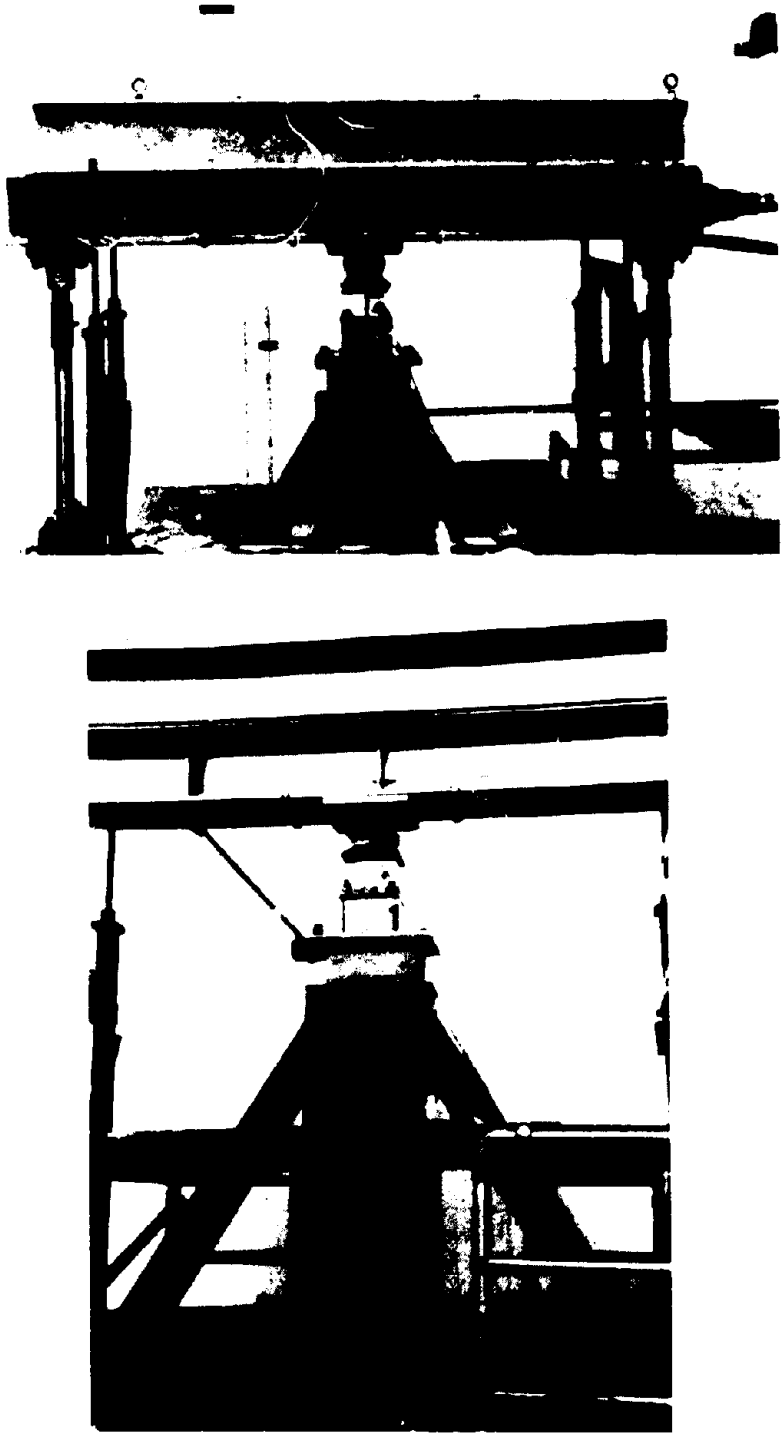

Figure 6.1 **Rig used for slider tests.**

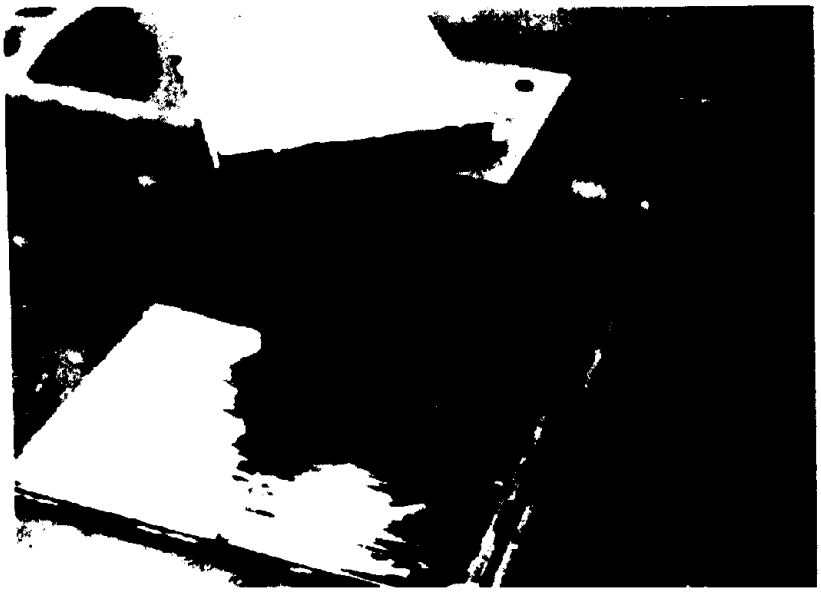

Figure 6.2 The three basic components: rubber bearing, teflon, stainless steel plate.

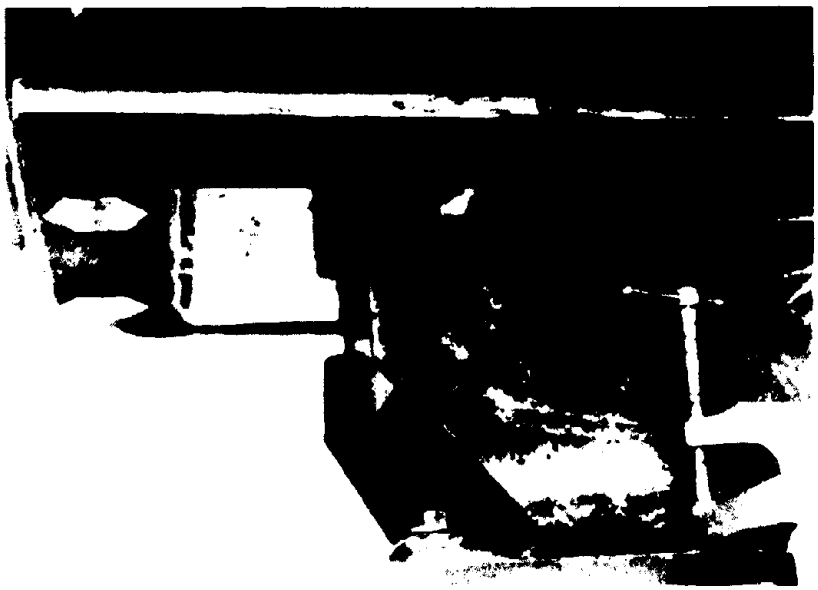

Figure 6.3 Slider as mounted on the static rig.

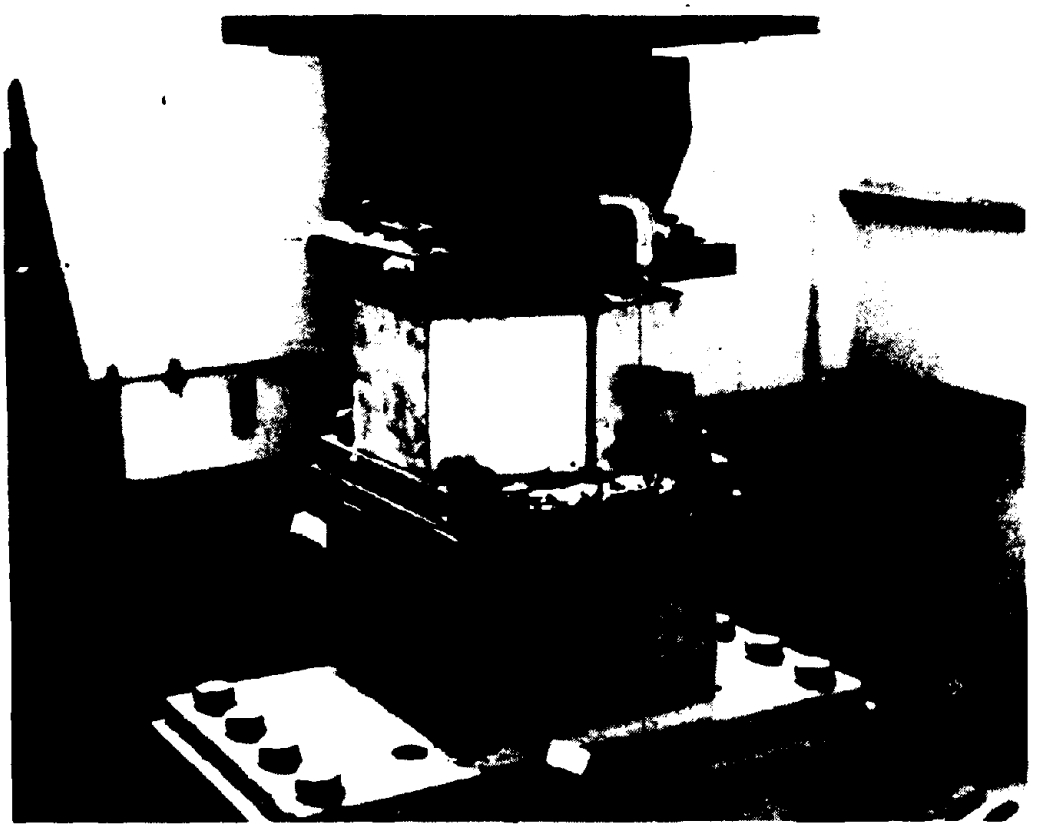

Figure 6.4 Slider on load cell.

Figure 6.5 Data acquisition and control system for static rig testing.

Figure 6.6 Teflon slider after repeated testing (250 cycles).

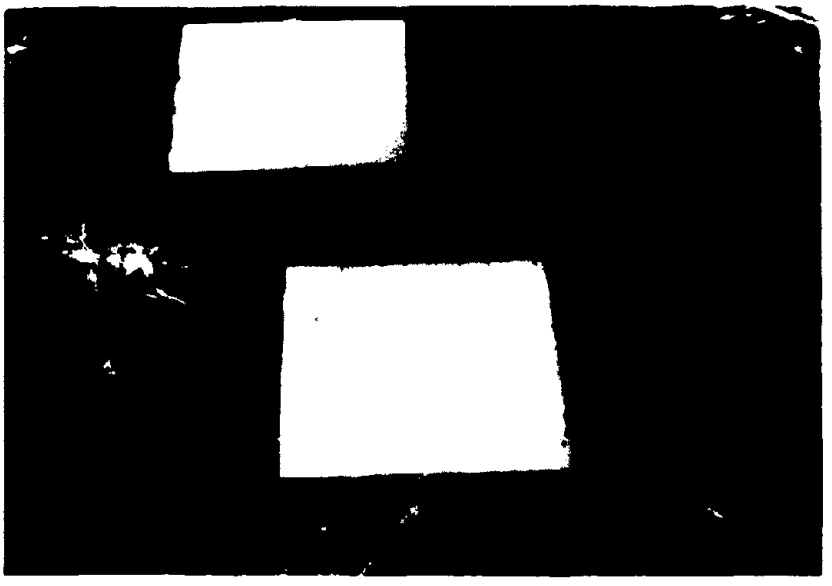

Figure 6.7 Teflon wearing by delamination.

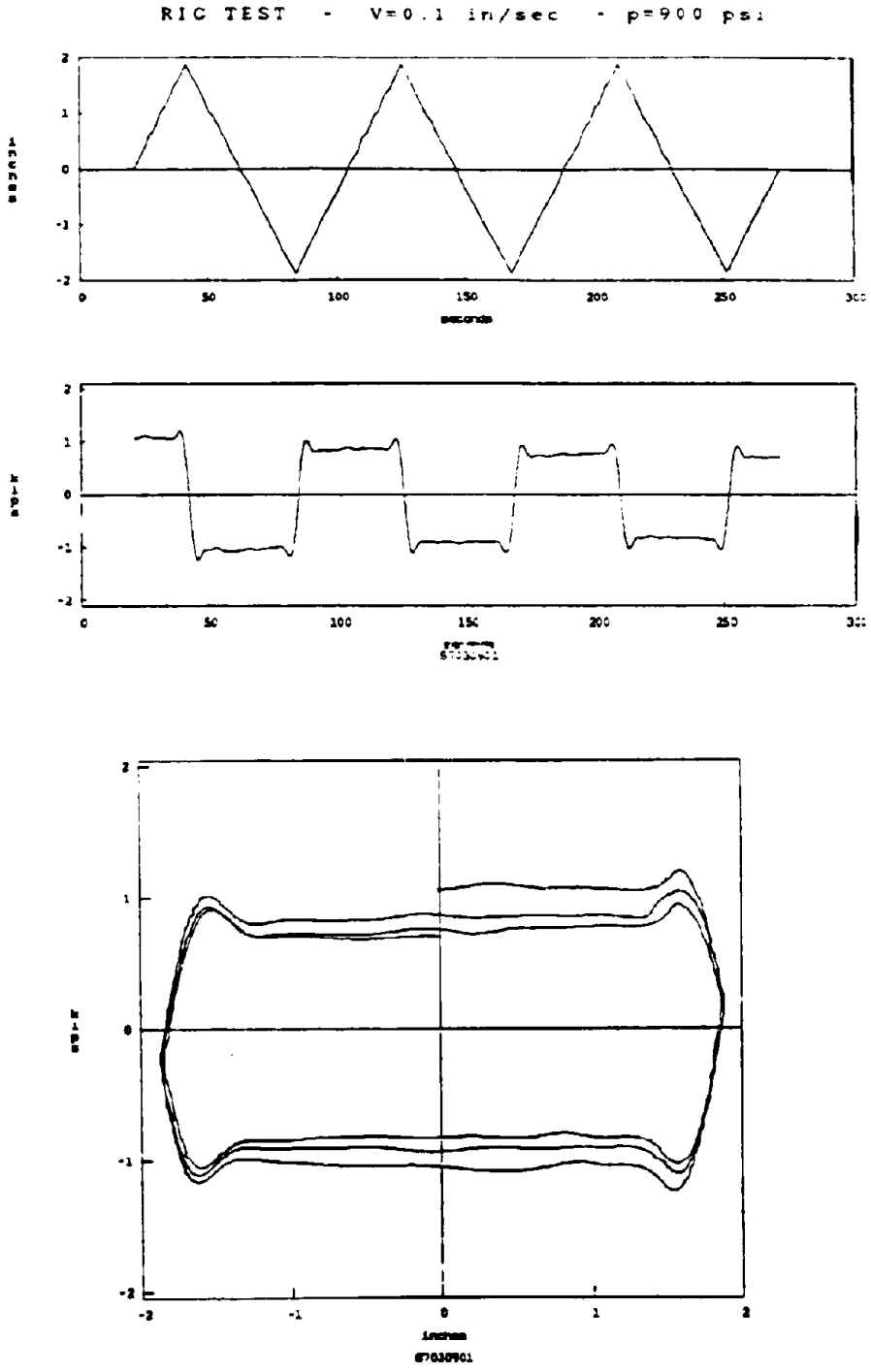

Figure 6.8 **Displacement, shear, and hysteresis loop for 4x4 inch slider, v=0.1 in/sec, p=900 psi.**

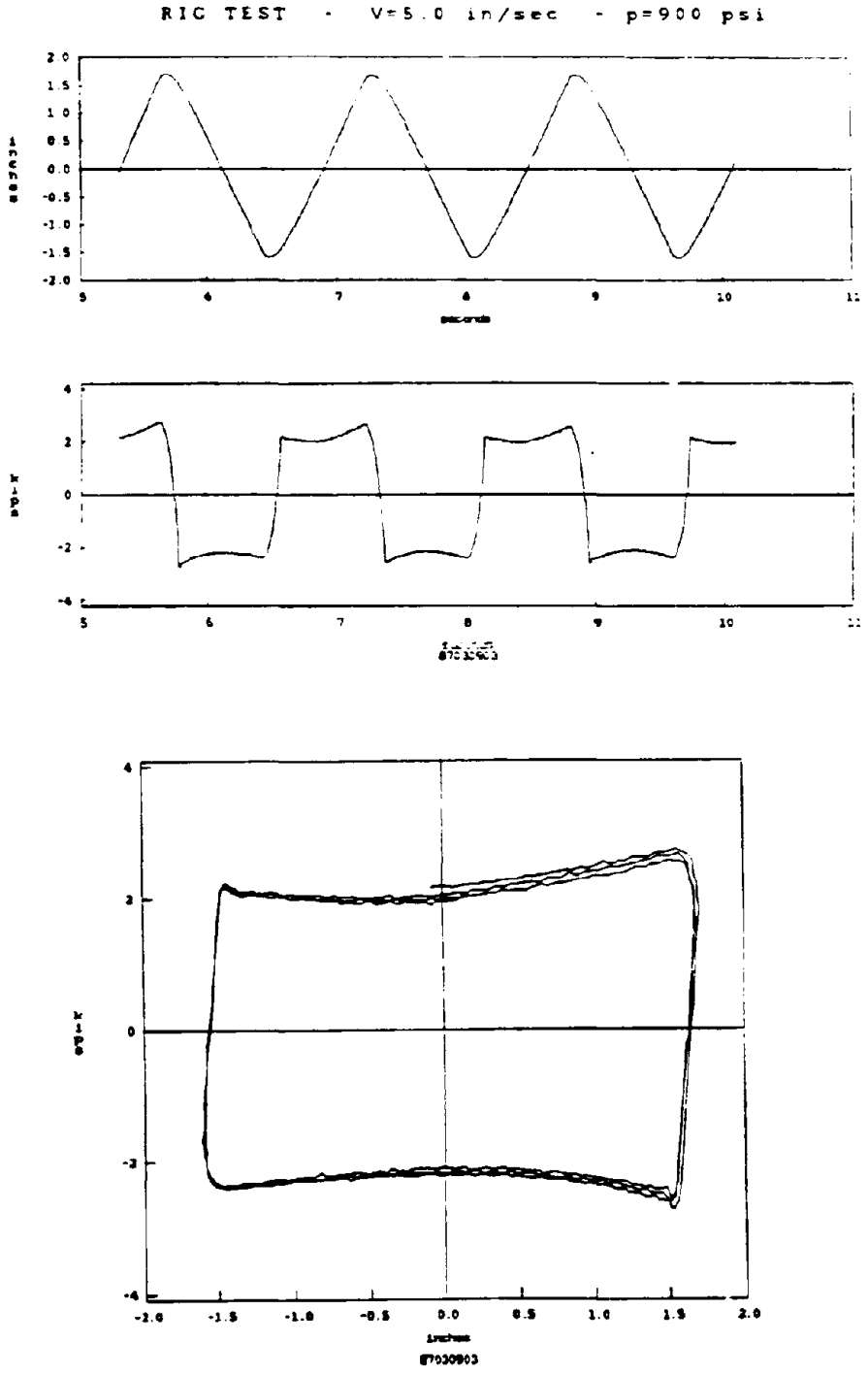

Figure 6.9 **Displacement, shear, and hysteresis loop for 4x4 inch slider, v=5.0 in/sec, p=900 psi.**

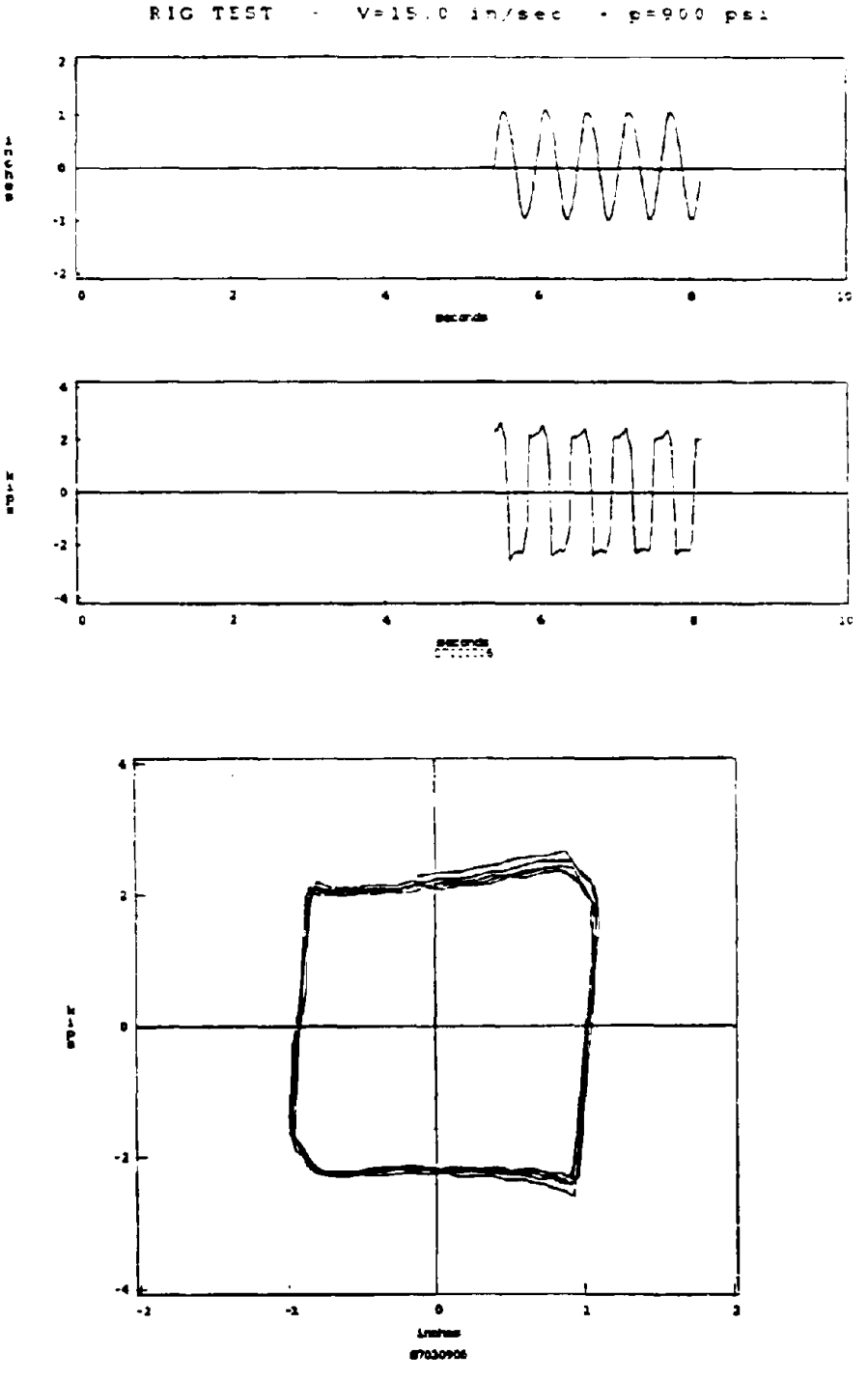

Figure 6.10 **Displacement, shear, and hysteresis loop for 4x4 inch slider, v=15.0 in/sec, p=900 psi.**

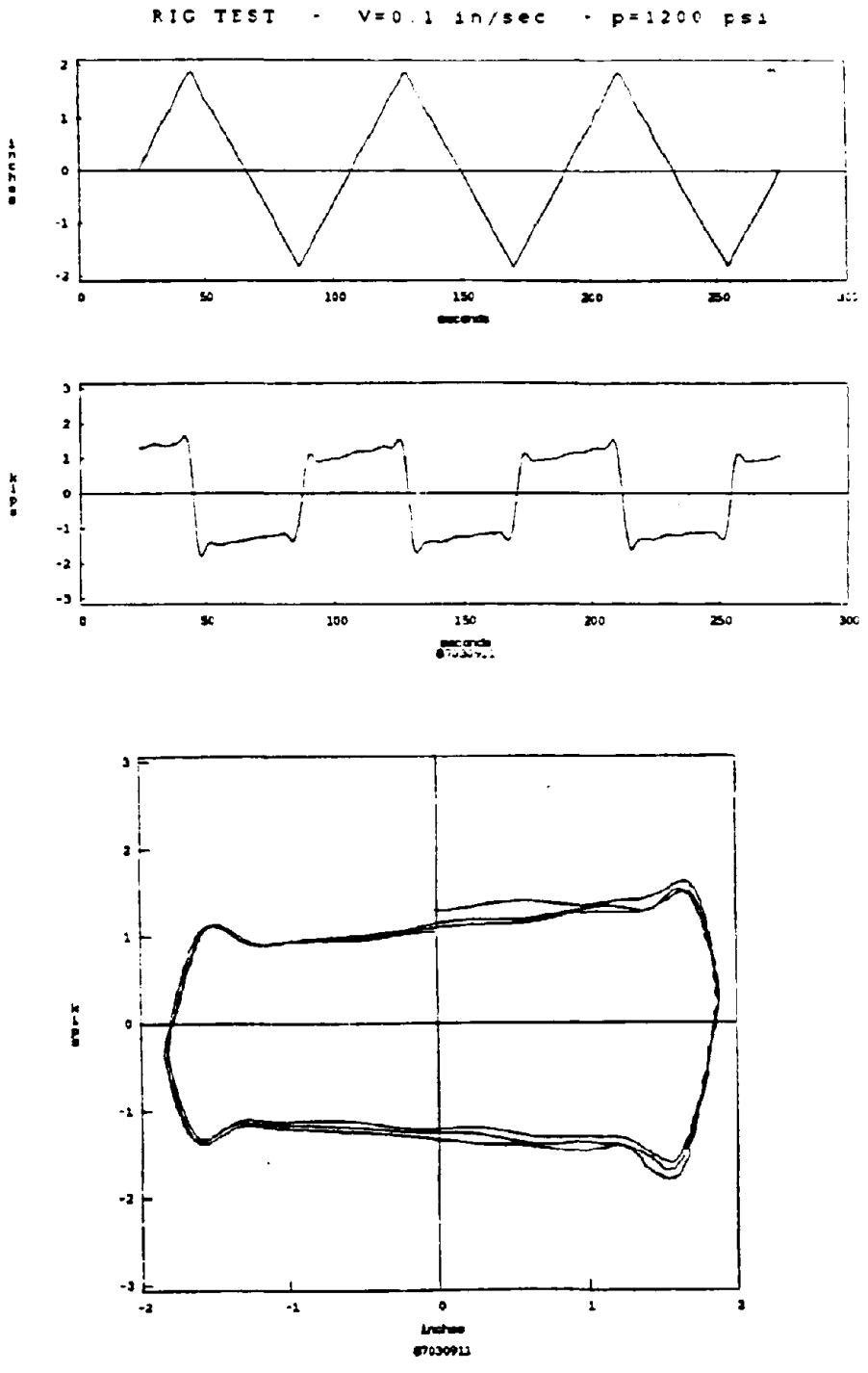

Figure 6.11 **Displacement, shear, and hysteresis loop for 4x4 inch slider, v=0.1 in/sec, p=1200 psi.**

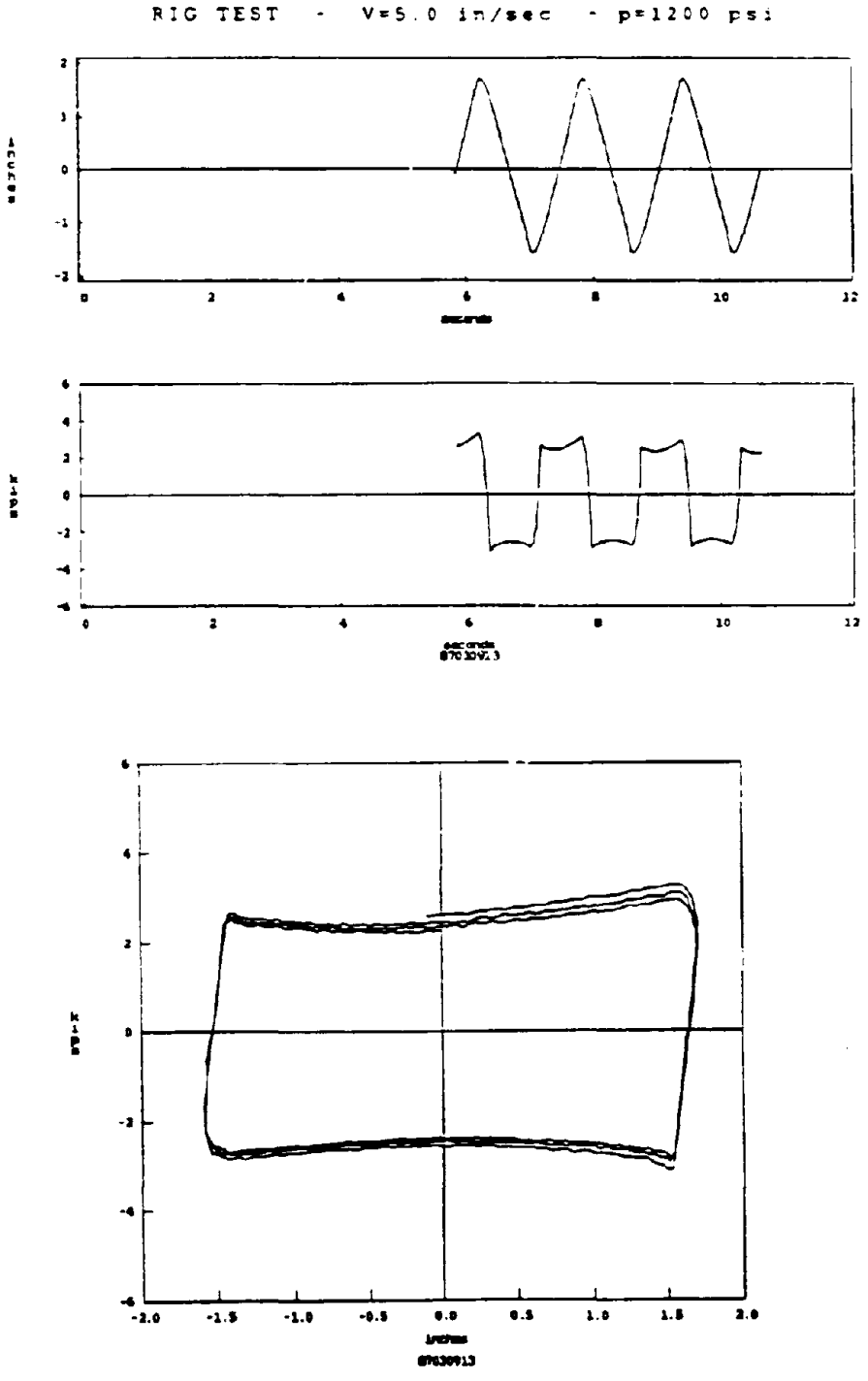

Figure 6.12 **Displacement, shear, and hysteresis loop for 4x4 inch slider, v=5.0 in/sec, p=1200 psi.**

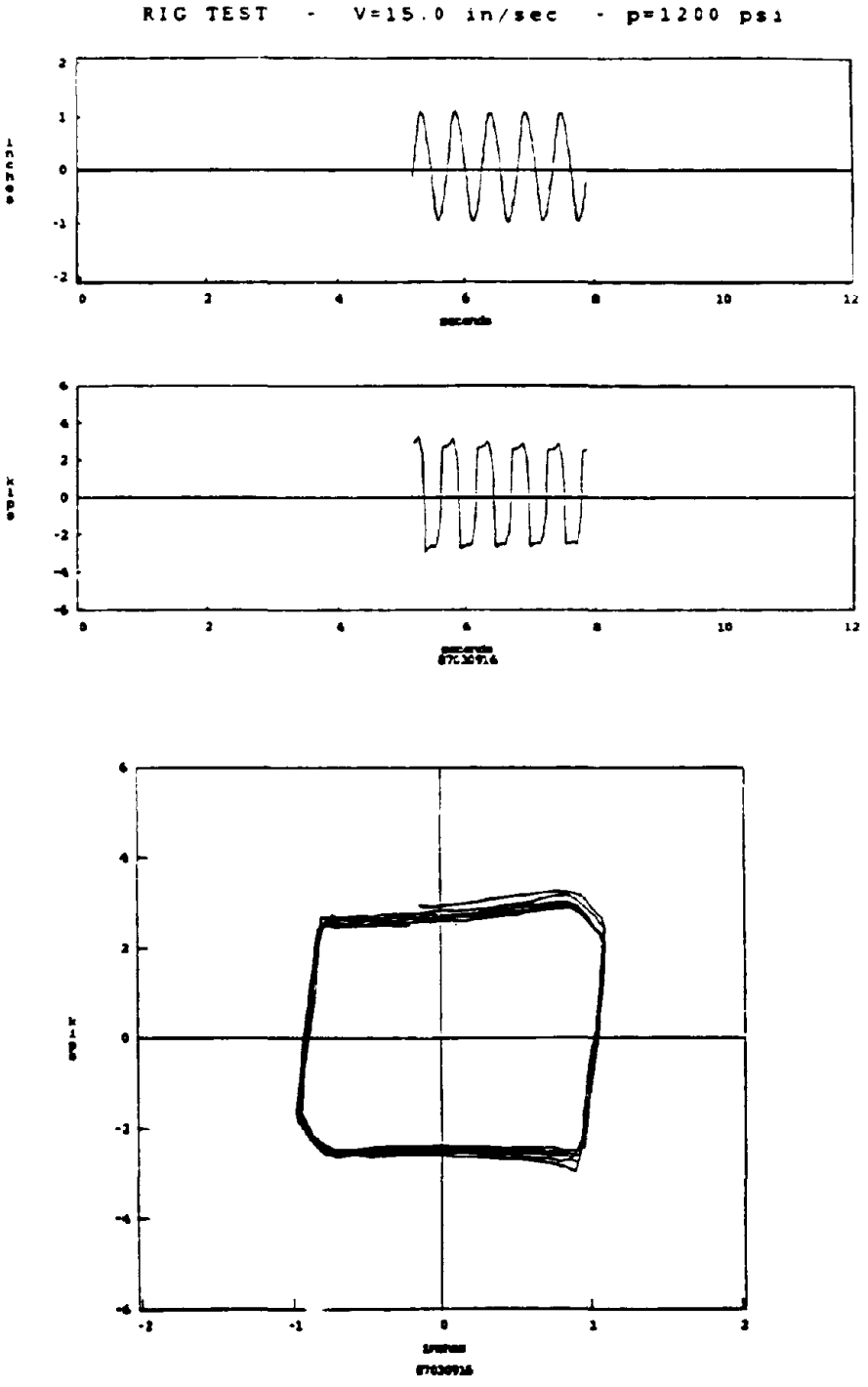

Figure 6.13 **Displacement, shear, and hysteresis loop for 4x4 inch slider, v=15.0 in/sec, p=1200 psi.**

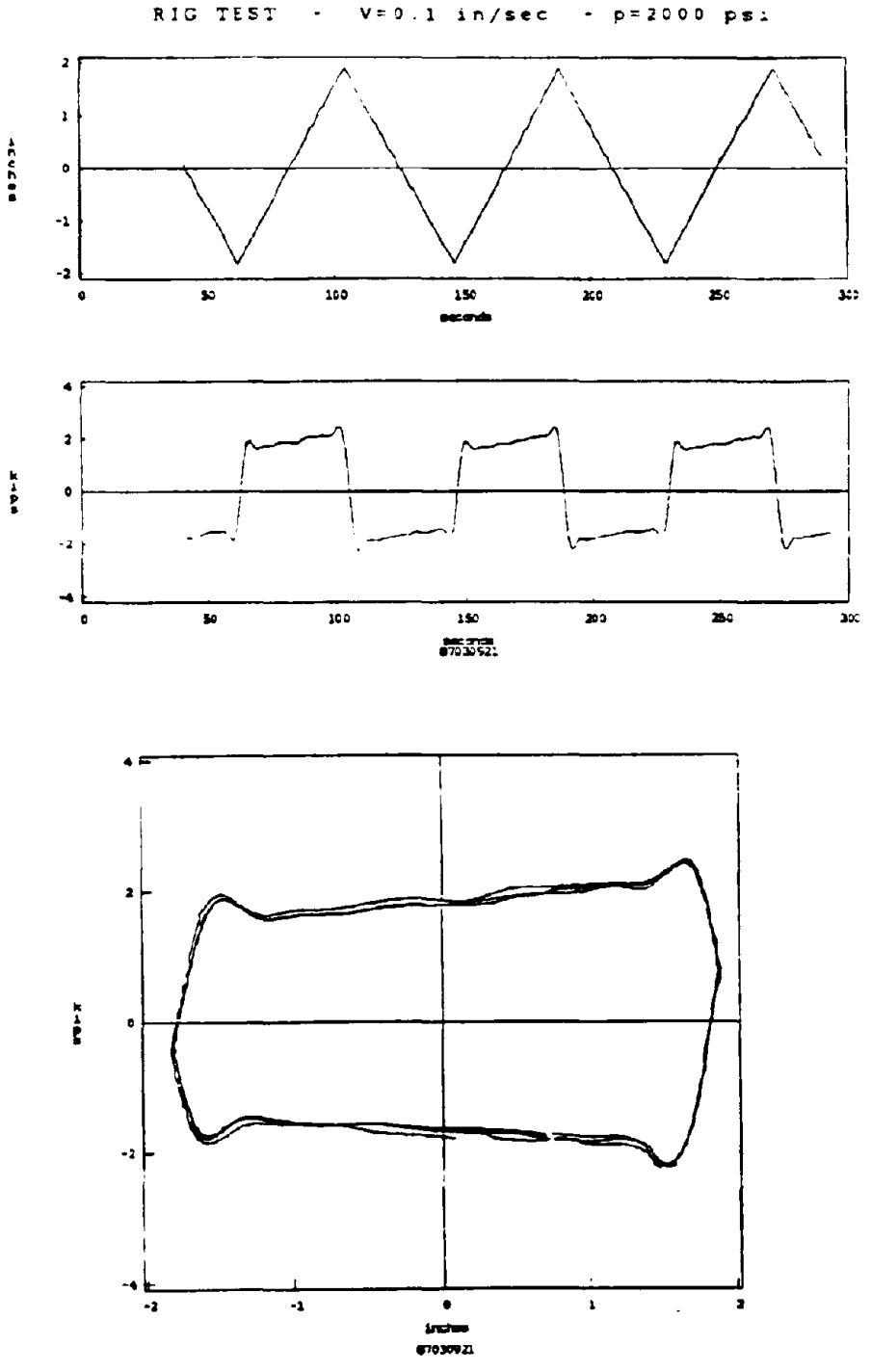

Figure 6.14 **Displacement, shear, and hysteresis loop for 4x4 inch slider, v=0.1 in/sec, p=2000 psi.**

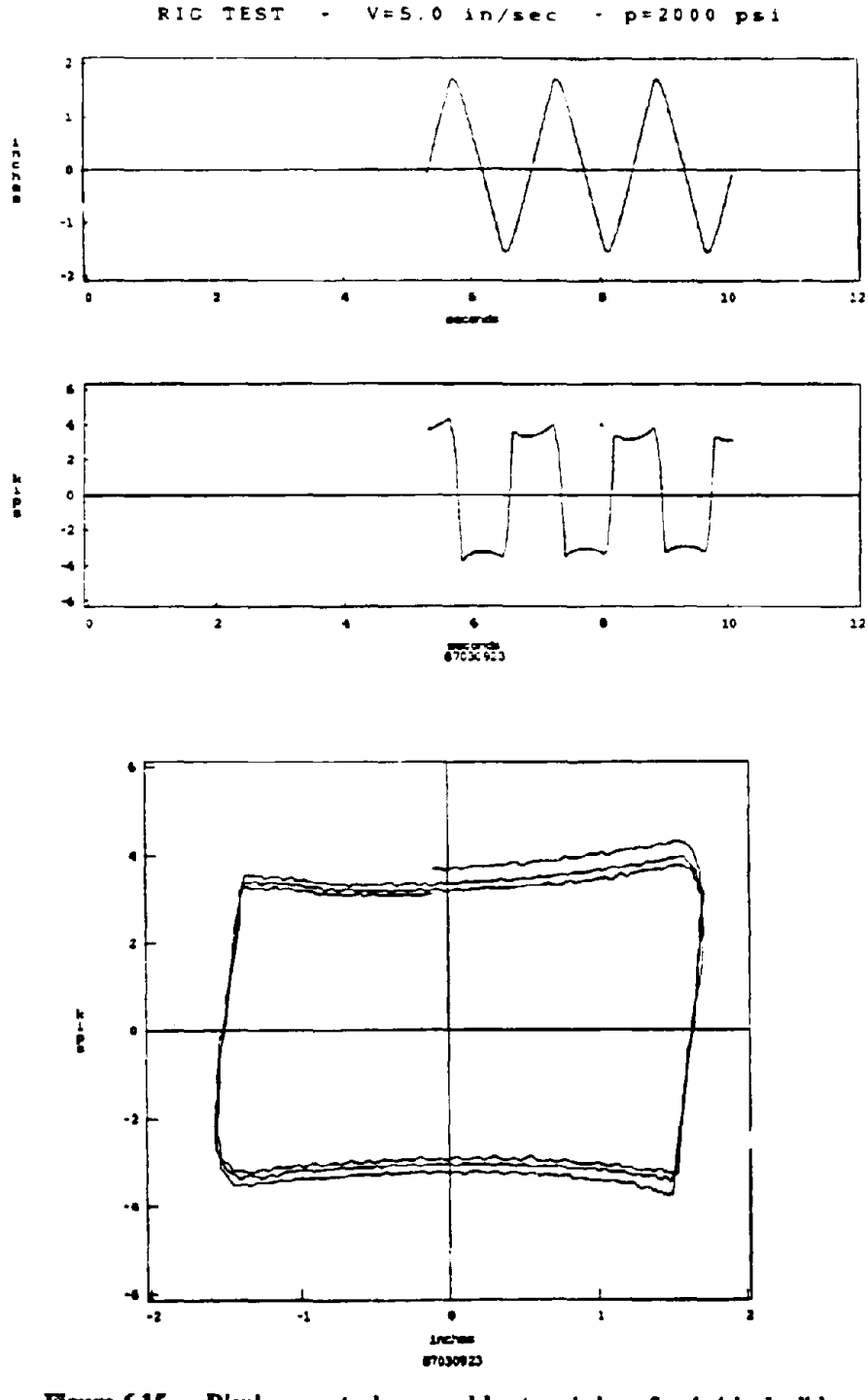

Figure 6.15 Displacement, shear, and hysteresis loop for 4x4 inch slider, v=5.0 in/sec, p=2000 psi.

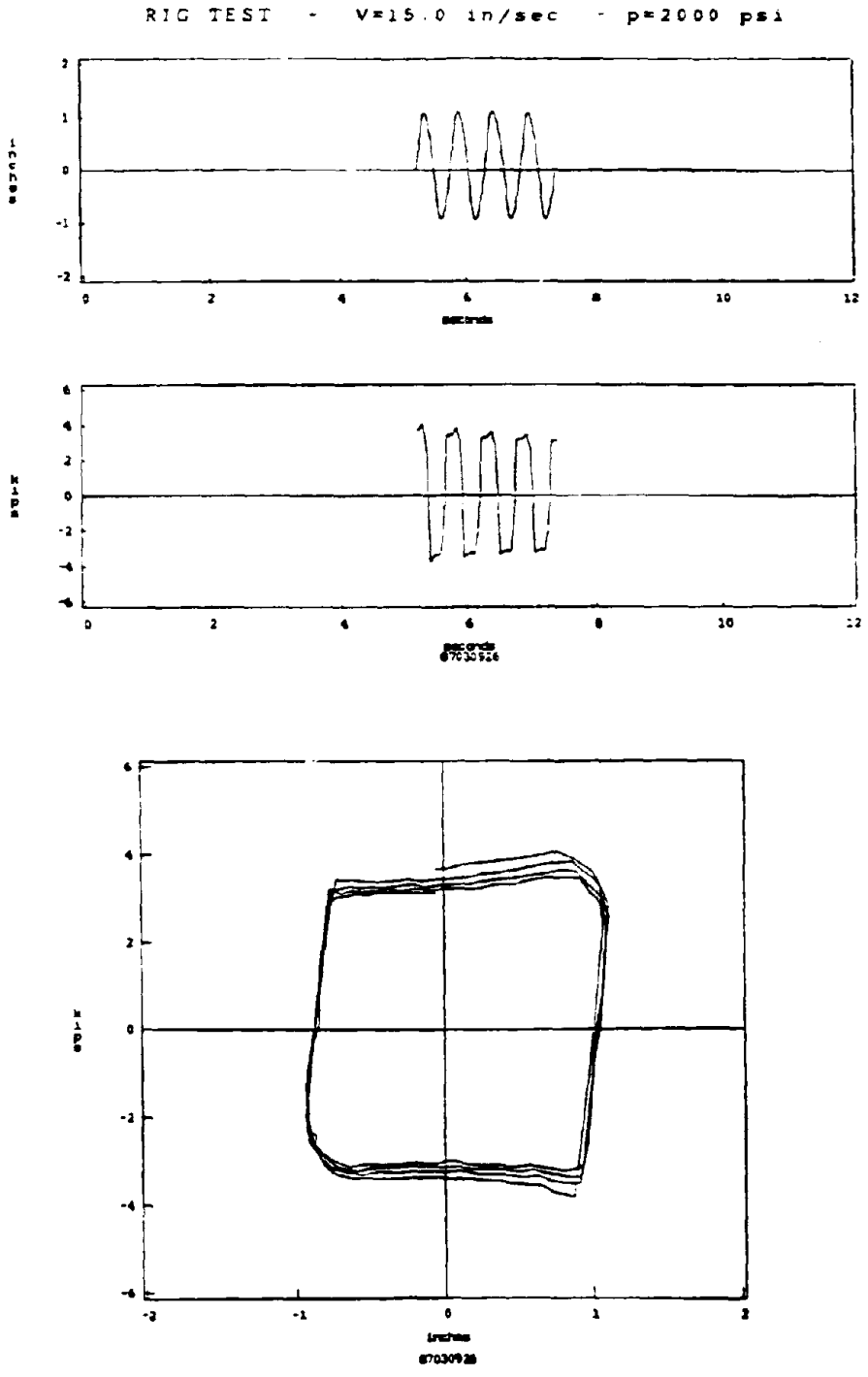

Figure 6.16 **Displacement, shear, and hysteresis loop for 4x4 inch slider, v=15.0 in/sec, p=2000 psi.**

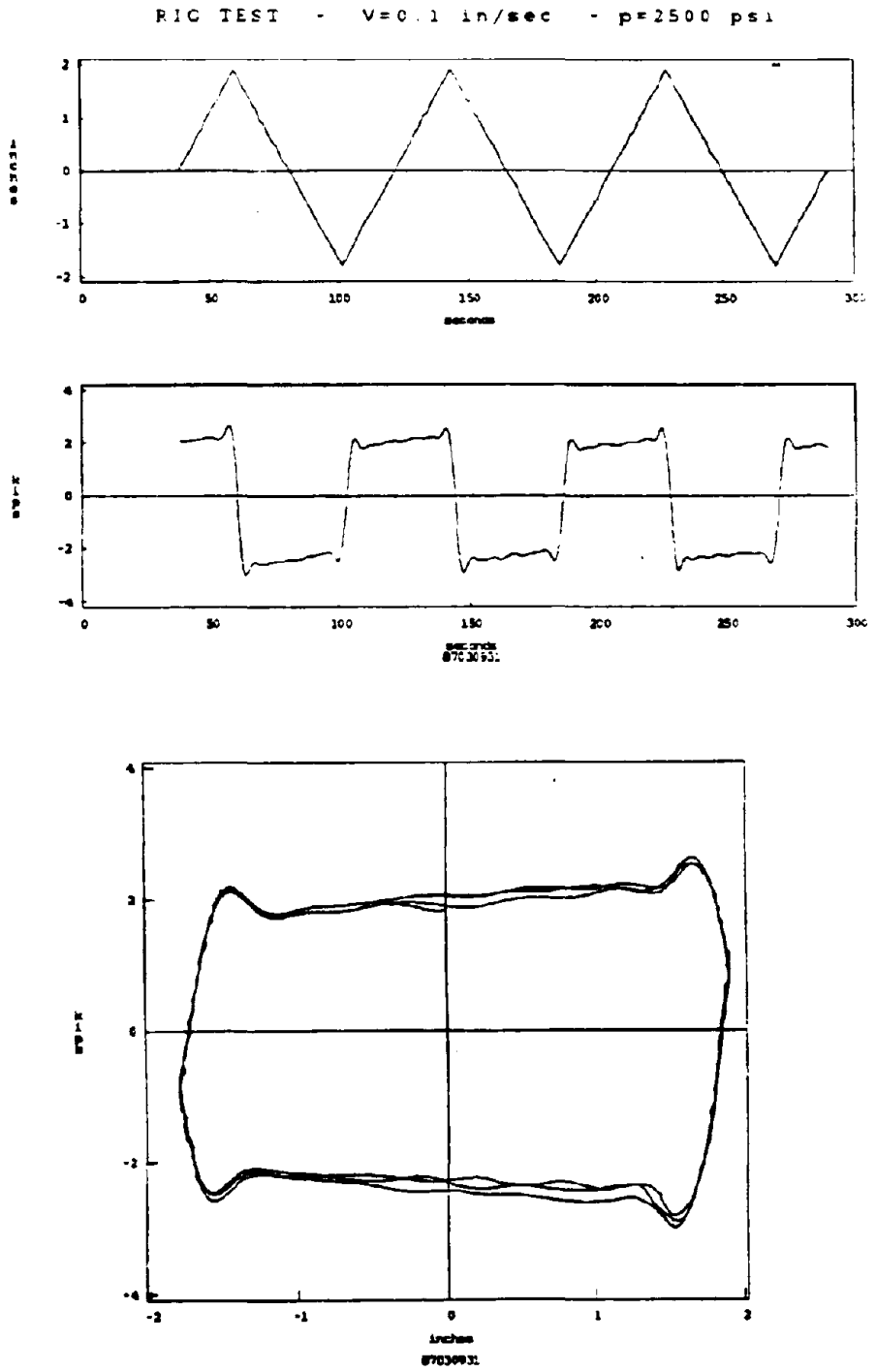

Figure 6.17 Displacement, shear, and hysteresis loop for 4x4 inch slider, v=0.1 in/sec, p=2500 psi.

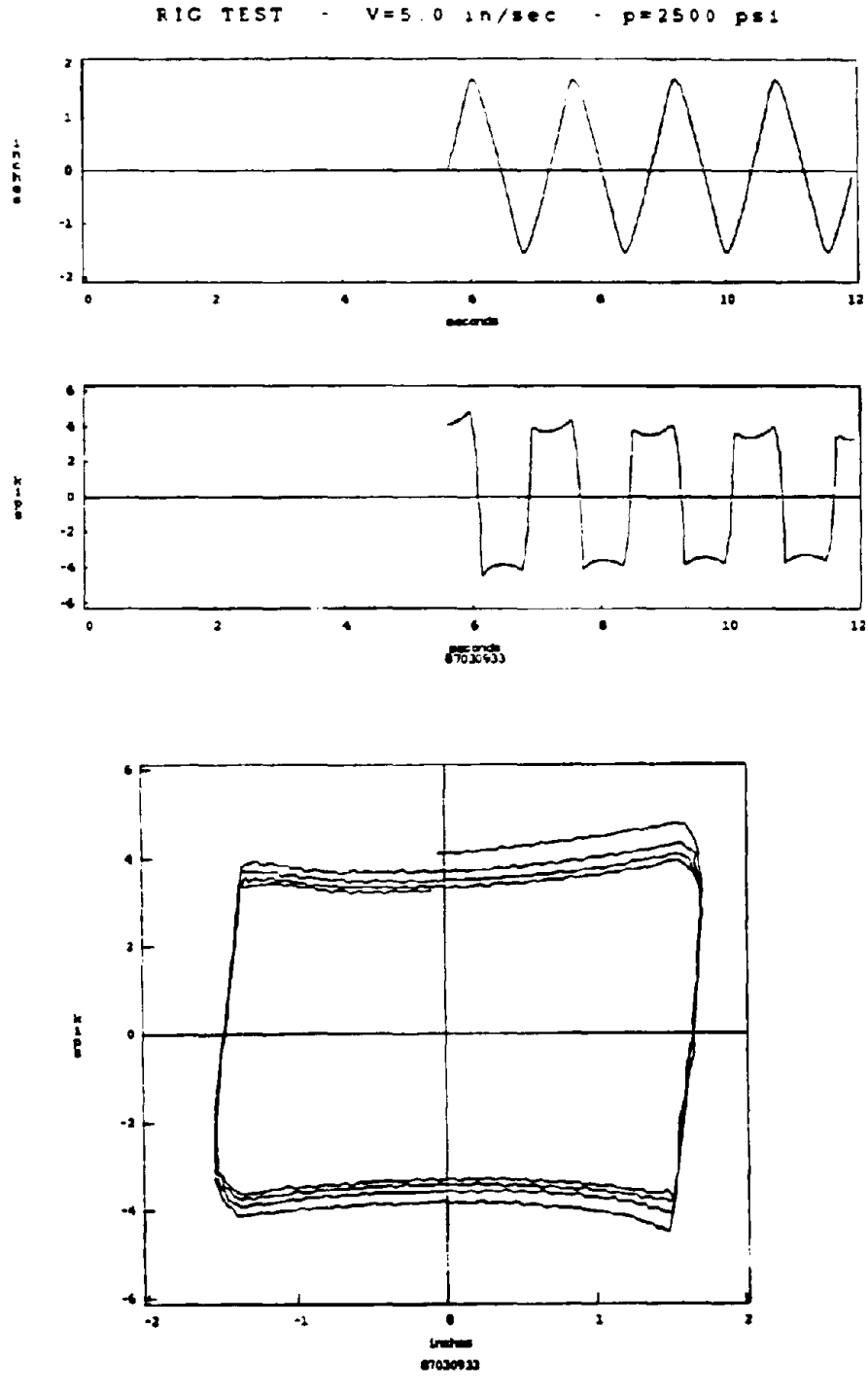

Figure 6.18 **Displacement, shear, and hysteresis loop for 4x4 inch slider, v=5.0 in/sec, p=2500 psi.**

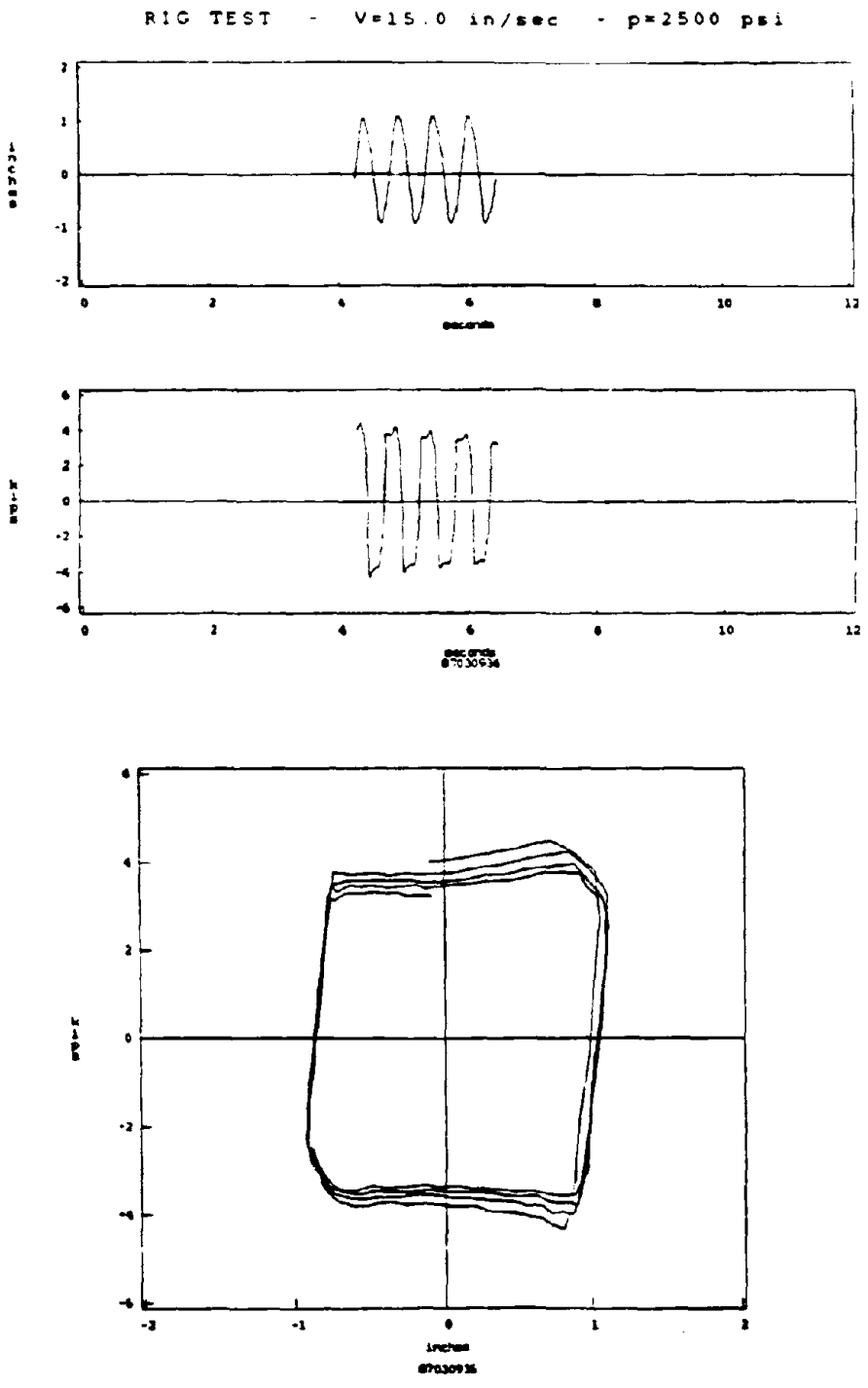

Figure 6.19 **Displacement, shear, and hysteresis loop for 4x4 inch slider, v=15.0 in/sec, p=2500 psi.**

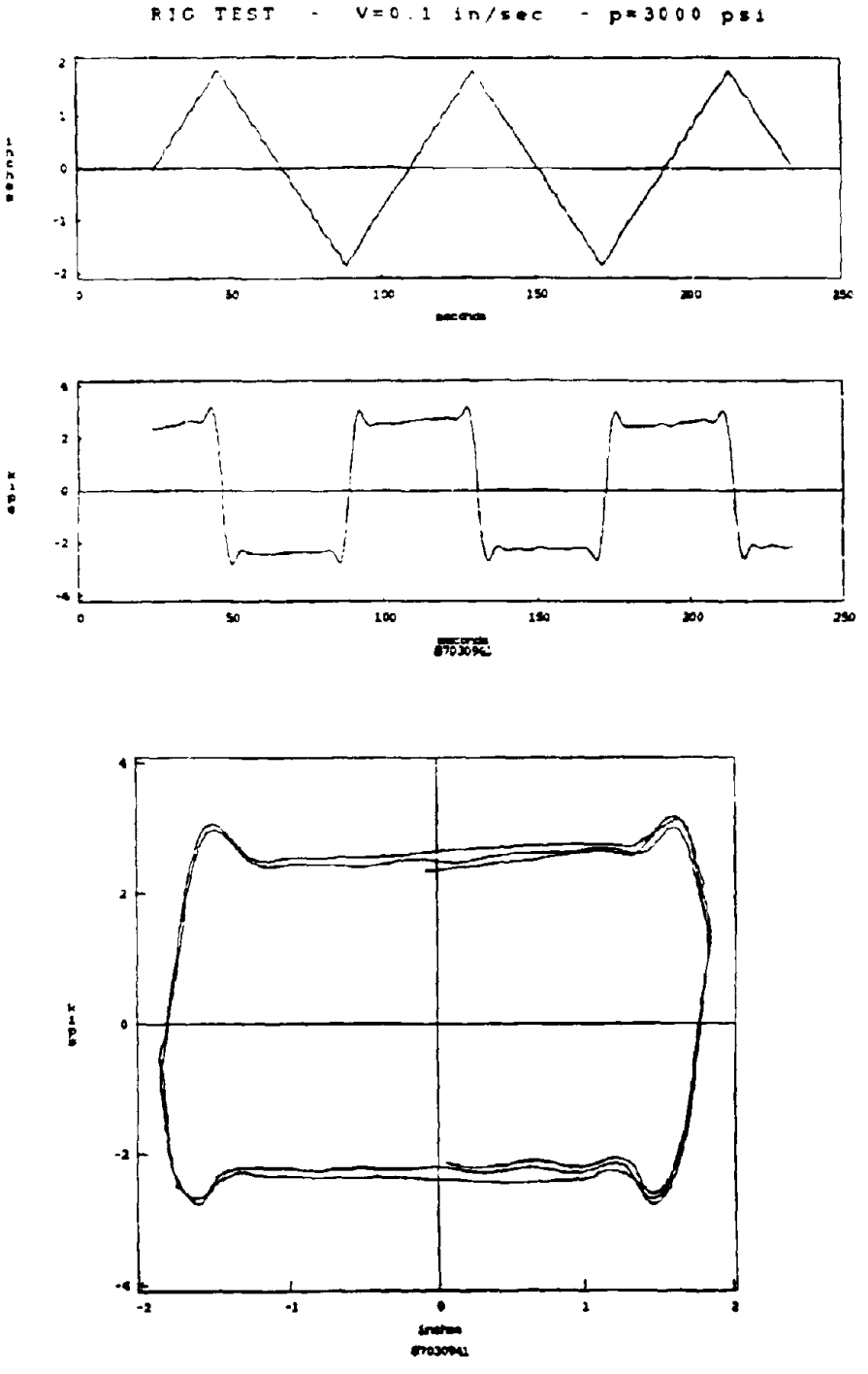

Figure 6.20 Displacement, shear, and hysteresis loop for 4x4 inch slider, v=0.1 in/sec, p=3000 psi.

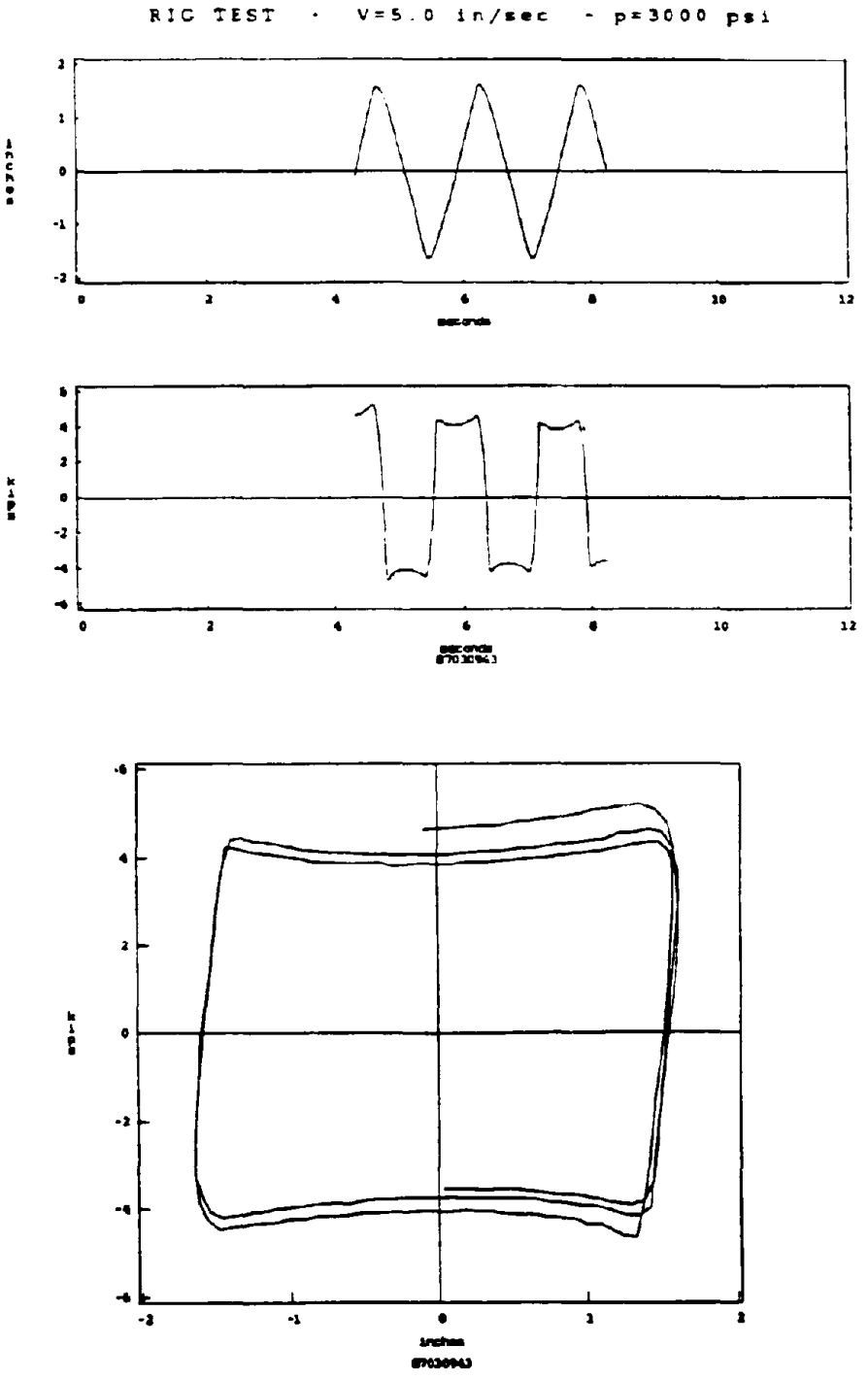

Figure 6.21 **Displacement, shear, and hysteresis loop for 4x4 inch slider, v=5.0 in/sec, p=3000 psi.**

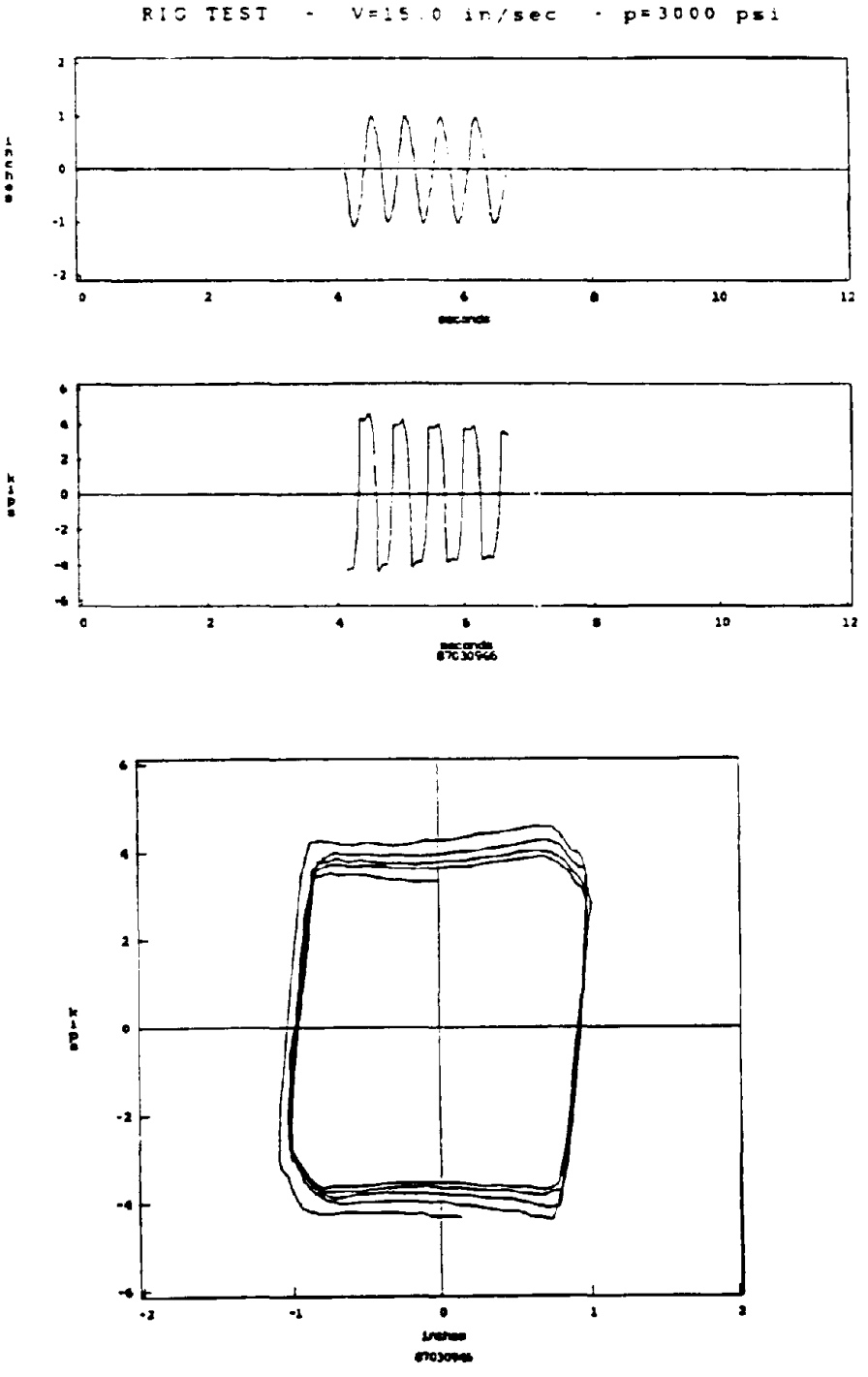

Figure 6.22 **Displacement, shear, and hysteresis loop for 4x4 inch slider, v=15.0 in/sec, p=3000 psi.**

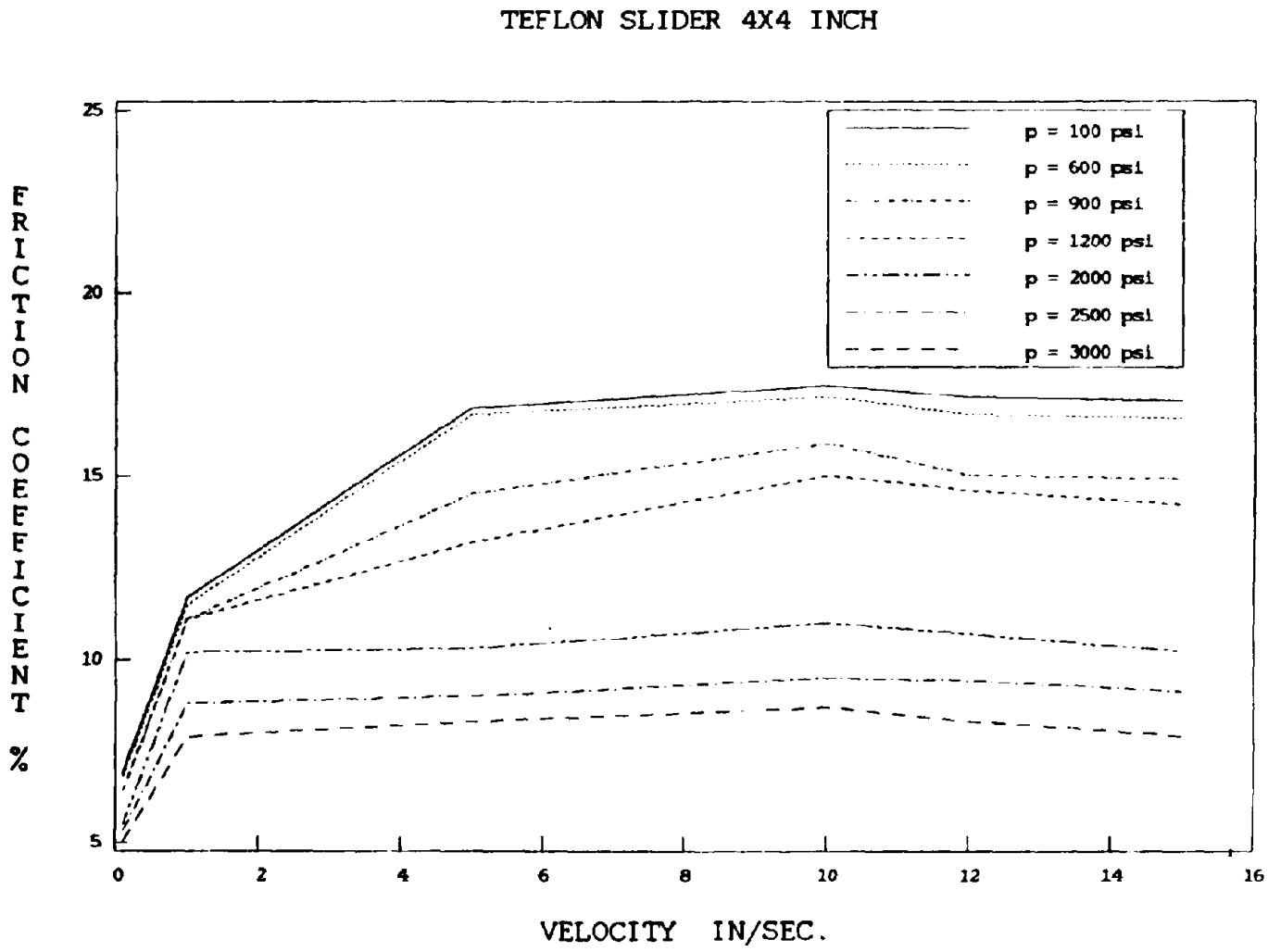

Figure 6.23 **Variation of friction coefficient with velocity and pressure.**

CHAPTER SEVEN

EARTHQUAKE SIMULATOR TEST RESULTS

1. General

It is commonly accepted that isolation systems consisting of solely rubber bearings provide substantial reduction in ground accelerations transmitted to the structure. However, this reduction in accelerations is accompanied by an increase in base drift and a lack of wind restraint. The system that combines sliders and rubber bearings provides a better displacement control and an inherent wind restraint. For the structure mounted on elastomeric bearings only (MRPRA SET #1), the mode corresponding to its fixed base fundamental frequency of 3.4 Hz was almost totally attenuated. The only significant peak in the Fourier transforms of the base and story accelerations corresponded to the frequency of rigid body motion of the structure at 0.7 Hz. When the sliders were added, the fixed base structure fundamental frequency appeared again. This is illustrated in Figures 7.1, 7.2 and 7.3 which show the Fourier transforms of table, base, third, sixth, and ninth story accelerations for El Centro at 200 span, Bucharest at 250 span, and Mexico City at 50 and 150 span, $\sqrt{4}$ time scaled records for the two isolation systems. That was due to the fact that the response of the structure had two distinct states; one corresponding to a base shear level below the sliding threshold, needed to activate the system, and the other to a base shear above it. In the first state the structure responded as if it were fixed base, while in the second state, the stiffness of the rubber bearings controlled and the first mode was the rigid body mode of the structure on a solely rubber isolation system. By comparing the responses between different spans for the isolation system that included sliders, it was noticed that the base relative displacement plays an important role in the pattern in which the energy is distributed between these two modes. When the span is larger, the combined system behaves more like a solely rubber system because of the increased participation of the rubber.

If an equivalent stiffness were to be determined, it would depend on the maximum base relative displacement and could be used only if an approximate idea were sought for a preliminary design phase. A different simple approach yields far more accurate results. A bilinear force displacement relationship with infinite initial stiffness followed by the stiffness of the four rubber bearings, was

found very adequate to model the combined isolation system. For the superstructure, static condensation can be used and the overall analysis can be performed on a simplified model where all elements are elastic except at the base.

2. Displacements

One of the advantages of the combined sliding bearing rubber bearing system was the reduction in the relative base displacements, due to the energy dissipation provided by friction, and to the increased base shear needed to start the base movement. Figures 7.4, 7.5 and 7.6 show base shear hysteresis loops for the MRPRA SET #1 and for the combined system. The respective peak base displacements for the MRPRA SET #1 system and the combined rubber-sliders system were 2.06 in. and 0.77 in. for the El Centro record at 200 horizontal span (1 in. peak table displacement) yielding 2.06 and 0.77 as base displacement amplification ratios for the two systems respectively; 2.57 in. and 0.94 in. for the Bucharest record at 250 horizontal span (1.25 in. peak table displacement) yielding 2.06 and 0.75 as respective base displacement amplifications. Under the Mexico City input, the peak base displacement for the MRPRA SET #1 was 0.11 in. at 50 horizontal span (0.25 peak table displacement), while it was 0.09 in. for the combined rubber-sliders system at 150 horizontal span (0.75 in. peak table displacement), yielding base displacement amplitudes of 0.44 and 0.12, respectively. In sum, the rubber system amplified the base drift about 3 times more than the combined rubber-sliders system did. Previous tests of rubber systems showed excessive base drift under low frequency inputs, like the Mexico City signal, and the span for those excitations had to be kept under 150. While using the slider-bearing system, we were able to apply horizontal spans up to 400 (2 in. peak table displacement) for the Mexico City record, resulting in a peak base displacement of only about two inches.

Deflected shapes of the structure at the instants when each story individually reached its maximum displacement are shown in Figures 7.7-7.14. It was noticed that the presence of the sliders in the proportion used (31 % of the total bearing area, carrying 60% of the total weight) did not change the main effect of an elastomeric base isolation system, that is causing the structure to move

like a rigid body. The deflected shapes at instants of maximum displacements also showed the predominance of a base-isolated first mode. For instance for the Mexico City signal at 375 span the story drifts at t=21.9 sec. were 0.13, 0.08, 0.08, and 0.07 in. for the first, second, third and ninth stories, respectively, while the base drift was 1.91 in. For the Bucharest table motion at 300 span the story drifts at t=3.2 sec. were 0.12, 0.04, 0.05, and 0.02 in. for the first, second, third and ninth stories while the base drift was about 1.3 in. For the San Francisco record at 200 span the story drifts at t=2.4 sec. were 0.07, 0.05, 0.05, and 0.03 in. for the first, second, third and ninth stories, respectively, with a base drift of 0.84 in. In sum, for most table motions, base displacements were larger than story drifts by a factor of 10 to 15. The magnitudes of the base displacements, however, depended on the type of signal applied. Table T-7.1 summarizes results for eight different earthquakes at different spans.

The structural model was also tested with its base fixed to the shake table. Time histories for the story drifts of the structure on the combined rubber-sliders isolation system were compared with the corresponding ones for the fixed base condition. The spans for all earthquake records applied to the isolated structure were larger than the ones applied to the fixed base structure by a factor of 2 to 3, yet resulting in story drifts of about the same magnitude. For instance, the maximum story drifts for the third, sixth and ninth stories under the San Francisco signal applied at 100 horizontal span (PTA=0.7 g) were 0.07, 0.07 and 0.04 in., respectively, for the fixed base condition, while they were of 0.06, 0.06 and 0.05, respectively, for the isolated structure on the combined system for the same signal at 200 horizontal span (PTA=1.2 g). This is illustrated in Figure 7.15. The choice of the quantity to which these values can be normalized in order to obtain a more precise comparison when the applied excitations have different magnitudes is debatable, especially because story drifts depend on both input displacements and input accelerations.

The relative base displacement time histories were of particular interest for studying the recentering provided by the rubber bearings. Figures 7.16-7.19 show the table acceleration, table displacement, and base drift time histories for the eight earthquake records used. The largest offset encountered throughout the whole testing program corresponded to the Mexico City input and yet was

only about 0.2 in. for a peak table displacement of 1.9 in. The recentering capacity of the system is particularly illustrated in Figure 7.18 (top, right) showing the base drift for the Parkfield input at 350 horizontal span. The table displacement time history shows a significant sway of 1.8 in. in one direction followed by small amplitude cycles of less than 0.5 in., the base, however, recentered with an offset of only 0.04 in. This shows that very small cycles are enough to recenter the system even if they are preceded by a strong ground motion in only one direction. The end-of-signal base offsets are shown in Table T-7.2 with their corresponding peak table displacement and peak table acceleration.

In a previous study of the sliding response of rigid blocks under earthquake excitations by Aslam et al. [11], a massive 3×2×1 ft concrete block weighing 935 lb was free to slide on a 6×6×0.5 protective concrete slab which was hydrostoned to the shake table. Various materials were used between the block and the slab to change the coefficient of friction which varied between 0.18 and 0.30. In that study the horizontal input acceleration was about 80% of the actual earthquake record (i.e., the Pacoima Dam s74w component of the 1971 earthquake accelerogram) applied simultaneously with various levels of the vertical component. Time histories of the block displacement relative to the table, given in [11], show extremely large end-of-signal offsets that reveal the need for a recentering spring.

3. Accelerations

One of the main purposes of base isolation is the reduction of ground accelerations transmitted to the structure. The acceleration reduction is expected to improve with softer systems like the ones consisting of rubber only. By the addition of sliders, the accelerations in the structure were slightly higher than the ones corresponding to a solely rubber system. The peak base acceleration to peak ground acceleration ratio increased from an average of 0.5 for the system using elastomeric pads, under input spans around 150, to an average value of 0.9 for the system that included sliders, for input spans as high as 375. As shown in Table T-7.1, the isolated base acceleration amplification ratio was highest for the Mexico City signal (about 1.7) and lowest for the San Francisco signal (about 0.6), because high frequency signals induced more sliding causing a softer equivalent system. Intermediate values

were found for most of the other earthquakes which had their input energy spread over a wider range of frequencies. Thus, there was almost no reduction in the ground accelerations, and the accelerations in the top stories were often slightly higher than the table accelerations for certain signals at low spans. However, the concept of isolation was still preserved, since for the fixed base case, these amplification ratios reached 4 or 5 for input spans of around 100. Figures 7.20-7.27 show acceleration time histories for the table and the fourth and ninth stories normalized to the peak table acceleration, for the fixed base structure and for the structure isolated on the combined system. They illustrate the reduction in accelerations provided by the combined rubber-sliders system. When the structure was tested as fixed base, the peak ninth story acceleration to the peak table acceleration reached 4.39 for El Centro input 125 span, 5.28 for Parkfield input 125 span, and was between 1.6 and 3 for the other records at similar spans, while for the isolated base case these ratios did not exceed 2.2. These values are summarized in Table T-7.3. Plots of the acceleration amplification along the elevation of the structure are shown in Figure 7.28 for the fixed base case and in Figure 7.29 for the base isolated case.

4. Effect of Input Magnitude

The effect of the magnitude of ground displacement on the acceleration and displacement model response was examined by using the El Centro record between 150 and 425 horizontal spans. It was noticed that the peak base relative displacement to the peak table displacement ratio increased with the span of the input up to a certain span level (around 300). After this level, the ratio started decreasing. The increase in the displacement amplification ratio for spans below 300 was due to the increased participation of the rubber bearings. At a horizontal span of about 300, the tension devices came close to locking and caused an increase in the stiffness, and hence a decrease in the base displacement (Figure 7.30). Figure 7.31 shows the hysteresis loops of the north bearings for horizontal spans of 150, 300 and 400. The effect of the restrainers can be seen for the 400 horizontal span. The same conclusion was drawn for the ninth story relative displacement. Generally, the displacement amplification ratio for the base was between 0.5 and 1.0 for all spans, and for the ninth story was between 0.9 and 1.5.

The amplification ratios for the accelerations generally decreased with increased span. However, the lowest value was for a horizontal span between 300 and 350, because of the stiffening caused by the restrainers close to locking. It is thus shown that the more the system is activated the lower the acceleration amplification ratio. These factors are summarized in Table T-7.4 and plotted in Figure 7.30, which shows the presence of an optimum span where the system provides the largest reduction in the accelerations.

If the building under consideration is expected to house equipment, sensitive to high frequencies and high accelerations, the proportion of sliders in the isolation system should be kept lower. However, if good isolation is required as well as reduction in the displacements, a high proportion of sliders can be used.

5. Base Shear

Since there were no instruments installed in the frame to measure member forces, the interstory shears were obtained by determining the inertia forces at each level. This is accurate enough for steel structures that are still in their linear elastic range, because they have very low damping, and the elastic force would practically equal the inertia force at each level.

The only check point between the statics and the inertia method was the base level, where the load cells for force measurement were installed. The limiting value F_{max} for the base shear was expected to be greatly influenced by the coefficient of friction of the sliders, since for a given displacement the additional shear provided by the rubber is constant. Assuming that the structure is moving as a rigid body, denoting by F_{max} the maximum base shear, and by γ_{max} the maximum base acceleration, the following equation holds:

$$F_{max}=M\gamma_{max}=\frac{W\gamma_{max}}{g}$$

where M and W are the total mass and total weight of the structural model. However,

$$F_s=\mu_{max}\alpha W$$

where μ_{max} is the maximum friction coefficient reached at maximum sliding velocity, F_s the maximum shear at the sliders, and α the fraction of total weight carried by the teflon. Thus, if the sliders were installed without the rubber bearings, the base acceleration would have had an upper bound of

$$\gamma_{max}=\mu_{max}\alpha g$$

With the presence of the rubber bearings, it is increased to

$$\gamma_{max}=g(\mu_{max}\alpha+\frac{K_r}{W}\delta_{max}) \tag{7.1}$$

where δ_{max} is the maximum base displacement.

Although the friction coefficient depends on the sliding velocity, μ_{max} can be fixed at a certain value obtained from tests (in our case 17%), and thus the maximum base acceleration corresponding to rigid body consideration of the structure is controlled by an appropriate combination of the two parameters α and K_r.

It was noticed that the frequency content of the different earthquakes is reflected in the accuracy of this approximation. The higher the frequency content of the earthquake is, the larger is the difference between the measured base shear and the one obtained from rigid body considerations.

6. Energy Dissipation Efficiency

It is commonly accepted that the total energy transmitted from the ground to a structure is absorbed in two different ways. The first one is due to the elastic strain, the second one is due to the plastic strain. The elastic strain energy is temporarily absorbed by the structure, part of it is transmitted back to the soil through the foundations and the other part released as kinetic energy causing amplification in the response quantities. For this reason, conventional design has a tendency to dissipate the major amount of the total energy absorbed by means of inelastic behavior of structural and non-structural elements. The need to increase the dissipated energy is satisfied by the use of sliders. It is shown here that the major portion of the total energy absorbed was dissipated by friction, minimizing the amplification in the response, and concentrating the deformations at the isolation

interface.

The efficiency of the combined rubber-sliders system in dissipating energy was investigated by examining the load-deflection relationship at the isolation interface. Hysteresis loops of total base shear versus relative base displacement were obtained for different earthquake signals and are shown in Figures 7.32-7.35. The total energy dissipated was calculated by numerical integration of the areas enclosed in these loops while the total input energy was obtained by integrating the product of the base shear with the table displacement time histories. Figures 7.36-7.43 show the cycles of energy dissipation (top), the cumulative input energy and the cumulative dissipated energy time histories (bottom). The proportion of the total input energy dissipated by hysteresis was above 90% for all eight table motions used. Table T-7.5 summarizes the results. It should be noted however that because of instrumentation resolution and because of numerical errors these values are valid to ±5%. Nevertheless, these plots show the efficiency of concentrating the energy dissipation at the isolation interface.

In an attempt to evaluate an equivalent damping, the total energy E dissipated for each test run, was divided by an estimated number of significant cycles N, read from the base drift time histories and from the instantaneous energy dissipation plots. Thus, $\omega_d = E/N$ provides an average value of energy dissipated per cycle. In order to determine an equivalent elastic work, ω_s, it was assumed that $\omega_s = F_m\delta_m/2$ where F_m is the maximum base shear and δ_m the maximum base relative displacement. An equivalent damping ratio was then evaluated by $\xi_e = \omega_d/4\pi\omega_s$. The values of E, N, and ξ_e are presented in Table T-7.6 for the eight earthquake records used. The values of ξ_e were about 20% for all signals.

Table T-7.1 **Peak values of base and ninth story response (top), with their corresponding amplification ratios (bottom).**

-	Table		Base		Ninth story	
filename	$D_{max}(in.)$	$A_{max}(g)$	$D_{max}(in.)$	$A_{max}(g)$	$D_{max}(in.)$	$A_{max}(g)$
861119.03 ELC375	1.96	0.73	1.36	0.43	2.01	0.64
861119.04 MEX375	1.97	0.18	1.91	0.31	2.55	0.39
861119.05 BUC300	1.56	0.27	1.27	0.32	1.75	0.31
861119.06 MIY350	1.81	0.33	1.22	0.38	1.72	0.46
861119.07 PAC350	1.82	0.49	1.30	0.52	1.87	0.59
861119.08 PAR350	1.82	0.41	1.09	0.37	1.46	0.46
861119.09 SFR200	1.01	1.20	0.84	0.68	1.23	0.63
861119.10 TAF350	1.83	0.72	1.36	0.39	1.62	0.68

-	Acceleration Amplification			Displacement Amplification		
filename	$\frac{A_{base}}{A_{table}}$	$\frac{A_{ninth}}{A_{table}}$	$\frac{A_{ninth}}{A_{base}}$	$\frac{D_{base}}{D_{table}}$	$\frac{D_{ninth}}{D_{table}}$	$\frac{D_{ninth}}{D_{base}}$
861119.03 ELC375	0.59	0.88	1.49	0.69	1.03	1.48
861119.04 MEX375	1.72	2.17	1.26	0.97	1.29	1.34
861119.05 BUC300	1.19	1.15	0.97	0.81	1.12	1.38
861119.06 MIY350	1.15	1.39	1.21	0.67	0.95	1.41
861119.07 PAC350	1.06	1.20	1.13	0.71	1.03	1.44
861119.08 PAR350	0.90	1.12	1.24	0.60	0.80	1.34
861119.09 SFR200	0.57	0.53	0.93	0.83	1.22	1.46
861119.10 TAF350	0.54	0.94	1.74	0.74	0.89	1.19

Table T-7.2 **Base displacement end-of-signal offsets for eight earthquake records with their corresponding peak table displacement and peak table acceleration.**

filename	signal	Base Offset (in.)	PTD (in.)	PTA (g)
861119.03	ELC375	-0.061	1.96	0.73
861119.04	MEX375	0.212	1.97	0.18
861119.05	BUC300	-0.006	1.56	0.27
861119.06	MIY350	0.119	1.81	0.33
861119.07	PAC350	-0.025	1.82	0.49
861119.08	PAR350	-0.011	1.82	0.41
861119.09	SFR200	0.037	1.01	1.20
861119.10	TAF350	0.057	1.83	0.72

Table T-7.3 **Acceleration amplification ratios at fourth and ninth stories for fixed base and base isolated structure.**

FIXED BASE STRUCTURE				BASE ISOLATED STRUCTURE			
signal	PTA (g)	4th story	9th story	signal	PTA (g)	4th story	9th story
ELC125	0.25	2.53	4.39	ELC375	0.73	0.42	0.88
MEX100	0.06	1.65	2.44	MEX375	0.18	1.64	2.17
BUC175	0.17	1.41	2.53	BUC300	0.27	0.70	1.15
MIY150	0.16	2.05	3.00	MIY350	0.33	0.63	1.39
PAC125	0.18	1.02	1.66	PAC350	0.49	0.45	1.20
PAR125	0.14	3.30	5.28	PAR350	0.41	0.53	1.12
SFR100	0.73	0.94	1.55	SFR200	1.20	0.23	0.53
TAF100	0.20	1.52	2.25	TAF350	0.72	0.38	0.94

Table T-7.4 Peak values of base and ninth story response (top), with their corresponding amplification ratios (bottom), for El Centro record with increasing span.

-	Table		Base		Ninth story	
filename	$D_{max}(in.)$	$A_{max}(g)$	$D_{max}(in.)$	$A_{max}(g)$	$D_{max}(in.)$	$A_{max}(g)$
861117.01 ELC150	0.78	0.27	0.49	0.19	0.75	0.31
861117.02 ELC200	1.04	0.39	0.76	0.21	1.04	0.38
861117.03 ELC300	1.56	0.58	1.41	0.29	1.92	0.48
861117.04 ELC350	1.83	0.68	1.53	0.35	2.14	0.55
861117.05 ELC400	2.07	0.80	1.71	0.41	2.33	0.64
861117.06 ELC425	2.22	0.85	1.82	0.48	2.50	0.67

-	Acceleration Amplification			Displacement Amplification		
filename	$\frac{A_{base}}{A_{table}}$	$\frac{A_{ninth}}{A_{table}}$	$\frac{A_{ninth}}{A_{base}}$	$\frac{D_{base}}{D_{table}}$	$\frac{D_{ninth}}{D_{table}}$	$\frac{D_{ninth}}{D_{base}}$
861117.01 ELC150	0.70	1.15	1.63	0.63	0.96	1.53
861117.02 ELC200	0.54	0.97	1.81	0.73	1.00	1.37
861117.03 ELC300	0.50	0.83	1.66	0.90	1.23	1.36
861117.04 ELC350	0.51	0.81	1.57	0.84	1.17	1.40
861117.05 ELC400	0.51	0.80	1.56	0.83	1.13	1.36
861117.06 ELC425	0.56	0.79	1.39	0.82	1.13	1.37

Table T-7.5 Energy dissipation efficiency of the combined rubber-sliders isolation system.

signal	Input Energy (E_I)	Dissipated Energy (E_D)	$\frac{E_D}{E_I}$
ELC375	221.1	205.4	93%
MEX375	246.5	250.8	102%
BUC300	56.0	54.6	97%
MIY350	166.2	157.5	95%
PAC350	75.5	72.3	96%
PAR350	44.6	41.9	94%
SFR200	38.7	34.9	90%
TAF350	146.3	137.2	94%

Table T-7.6 Equivalent damping and equivalent stiffness obtained from experimental hysteresis loops of base shear for eight records. ξ_{eq} around 20%.

filename	signal	E	N	$w_D = \frac{E}{N}$	w_S	$\xi_{eq} = \frac{w_D}{4\pi w_S}(\%)$	$K_{eff}\ (k.in^{-1})$
861119.03	ELC375	205.38	6	34.23	13.6	20	15.0
861119.04	MEX375	250.79	5	50.16	20.1	20	11.8
861119.05	BUC300	54.55	2	27.28	10.4	21	13.0
861119.06	MIY350	157.44	5	31.49	11.3	22	15.1
861119.07	PAC350	72.33	3	24.11	11.2	17	13.6
861119.08	PAR350	41.93	2	20.97	8.3	20	14.7
861119.09	SFR200	34.90	2	17.45	5.7	24	16.6
861119.10	TAF350	137.23	4	34.31	12.4	22	13.6
Average						21	14.2

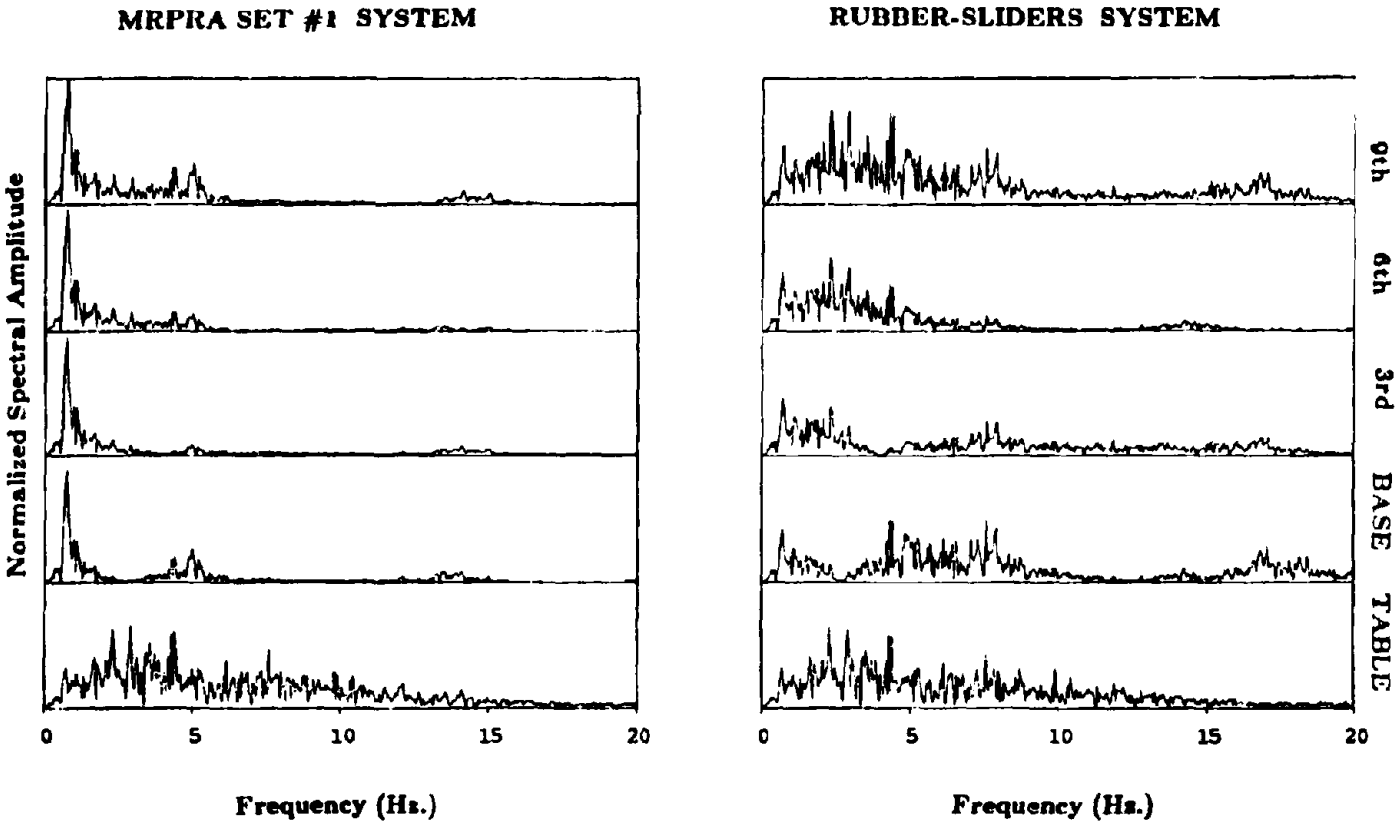

Figure 7.1 Acceleration Fourier transforms for El Centro record span 200.

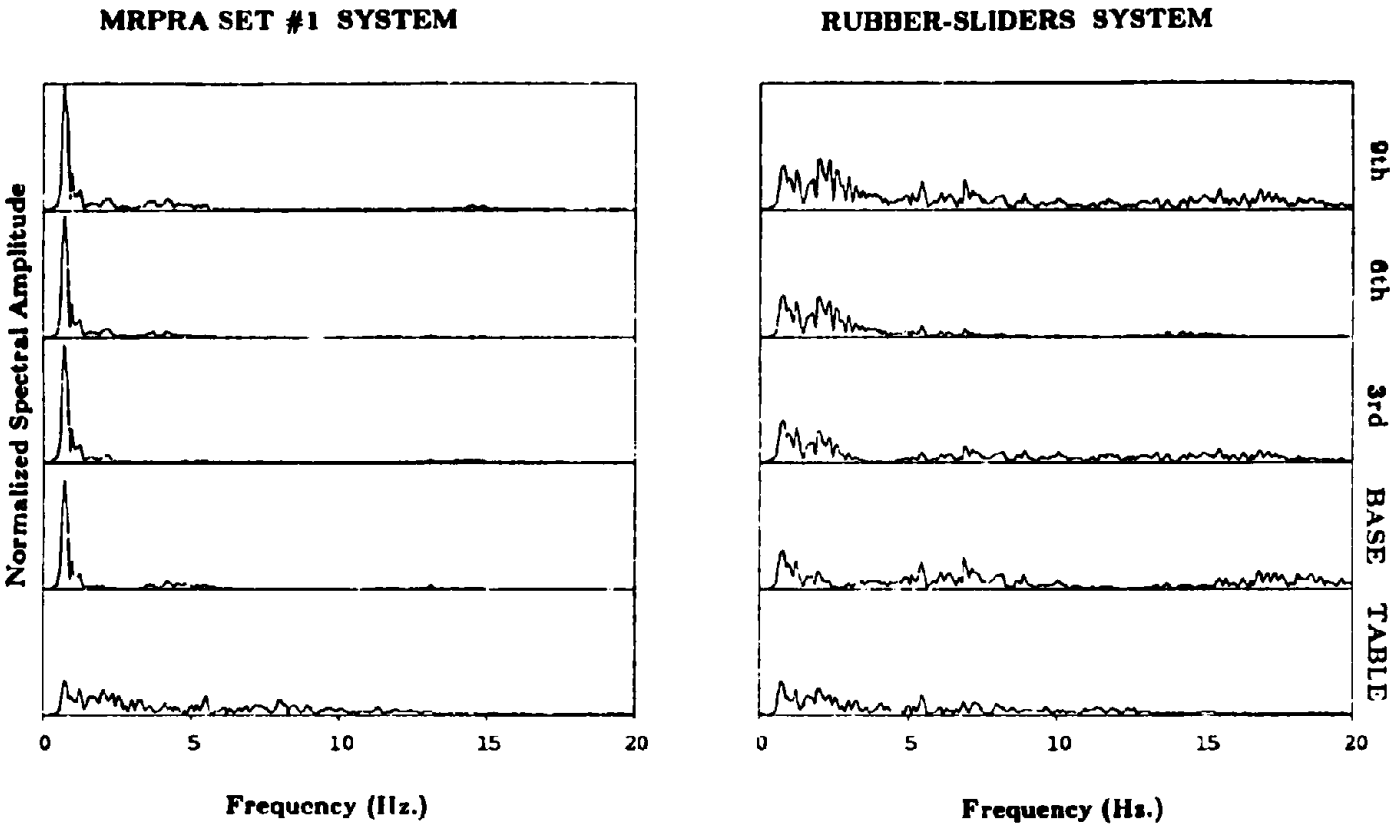

Figure 7.2 Acceleration Fourier transforms for Bucharest record span 250.

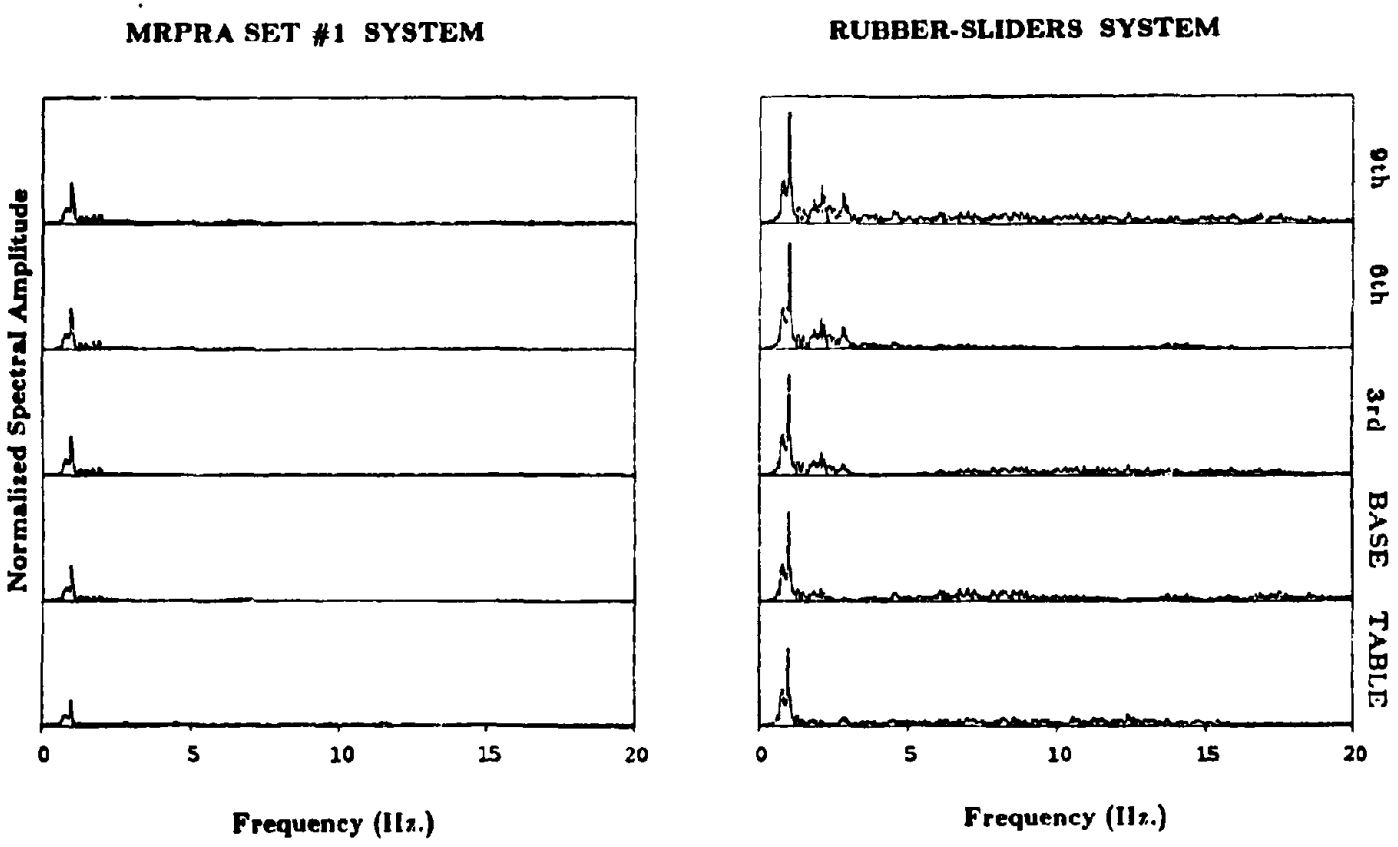

Figure 7.3 Acceleration Fourier transforms for Mexico City record span 50 (left) and span 150 (right).

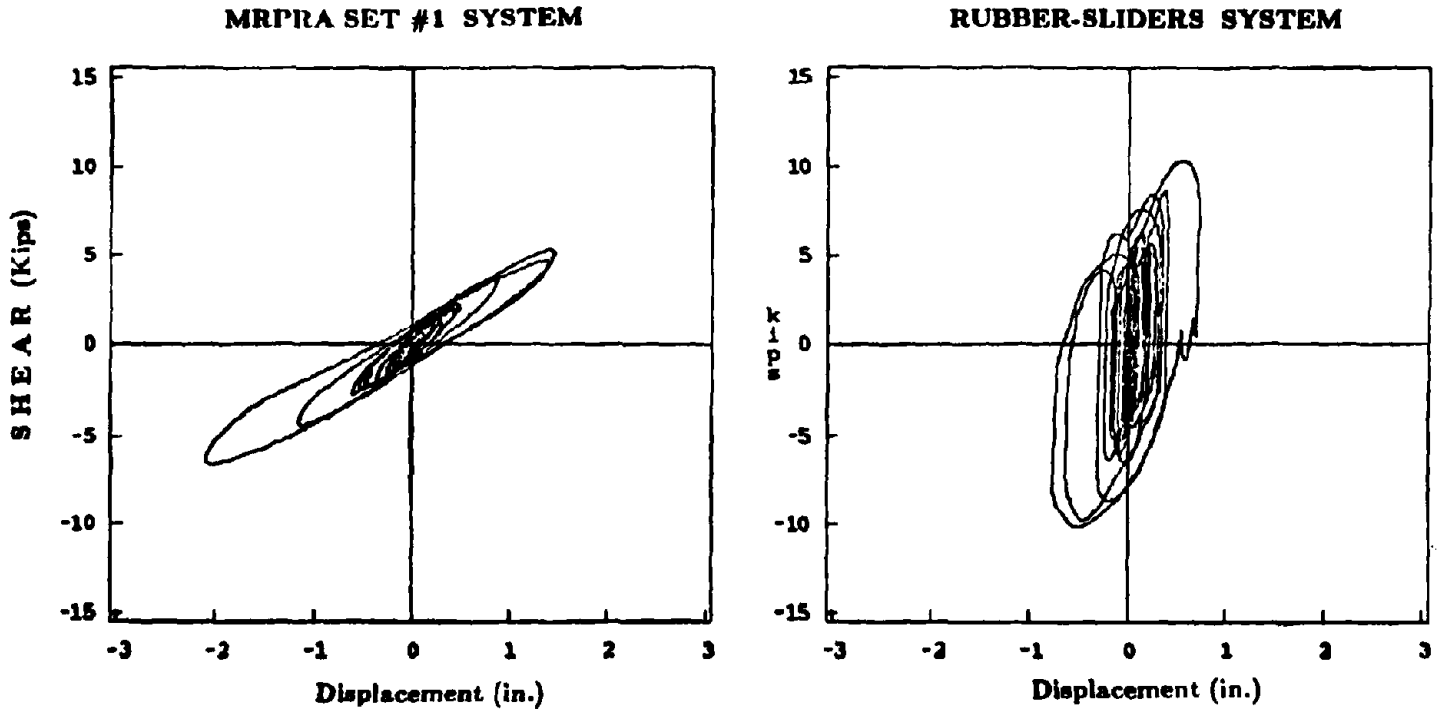

Figure 7.4 Base shear hysteresis loop for El Centro record span 200.

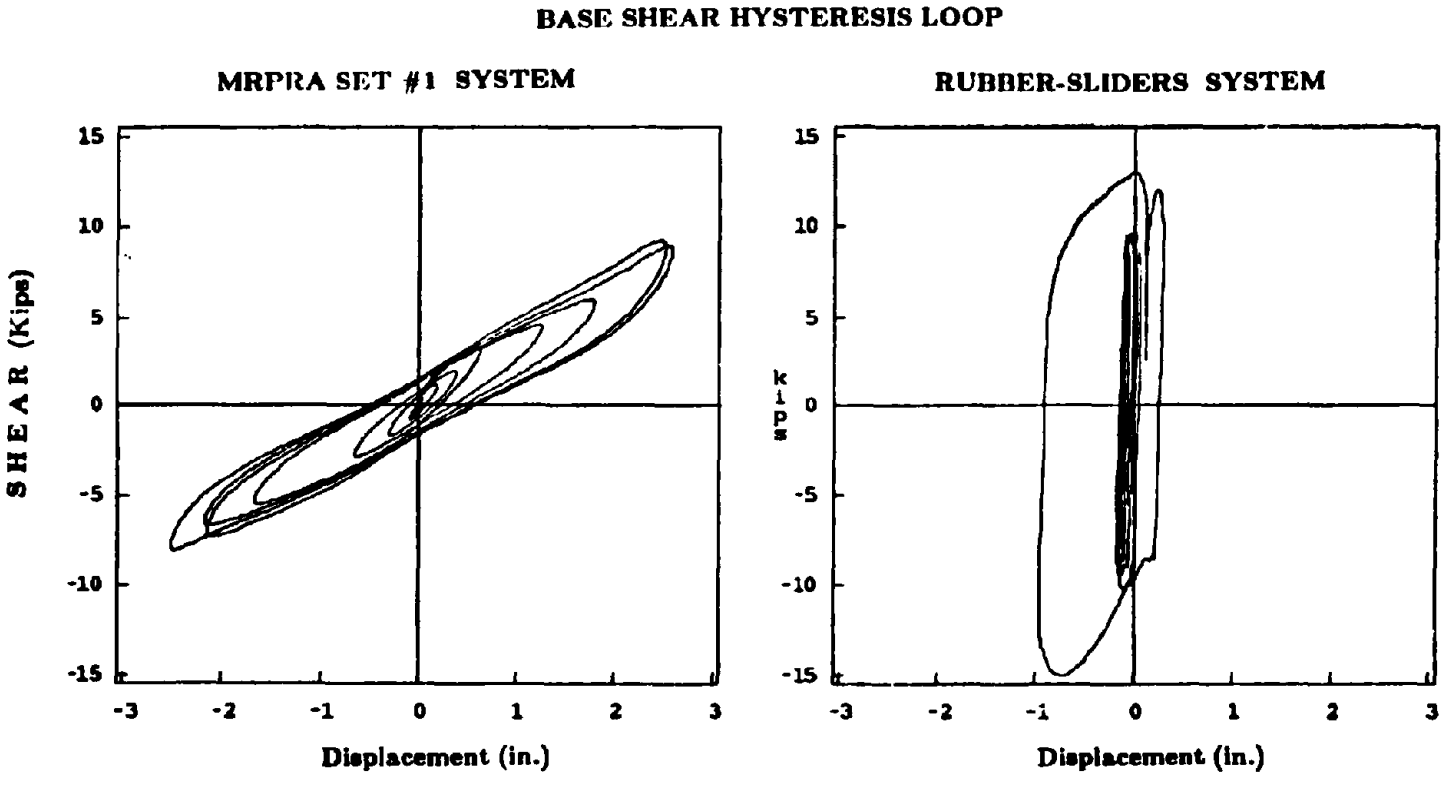

Figure 7.5 Base shear hysteresis loop for Bucharest record span 250.

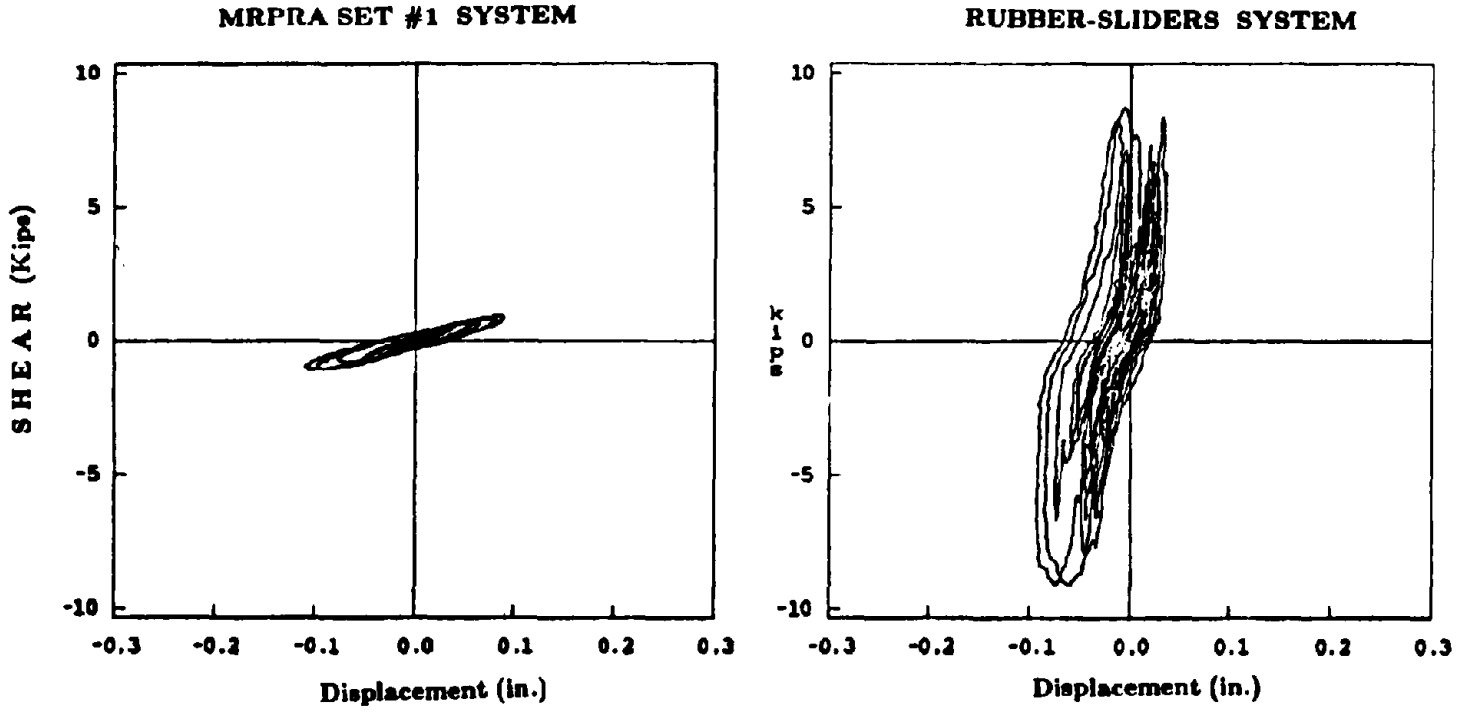

Figure 7.6 Base shear hysteresis loop for Mexico City record span 50 (left) and 150 (right).

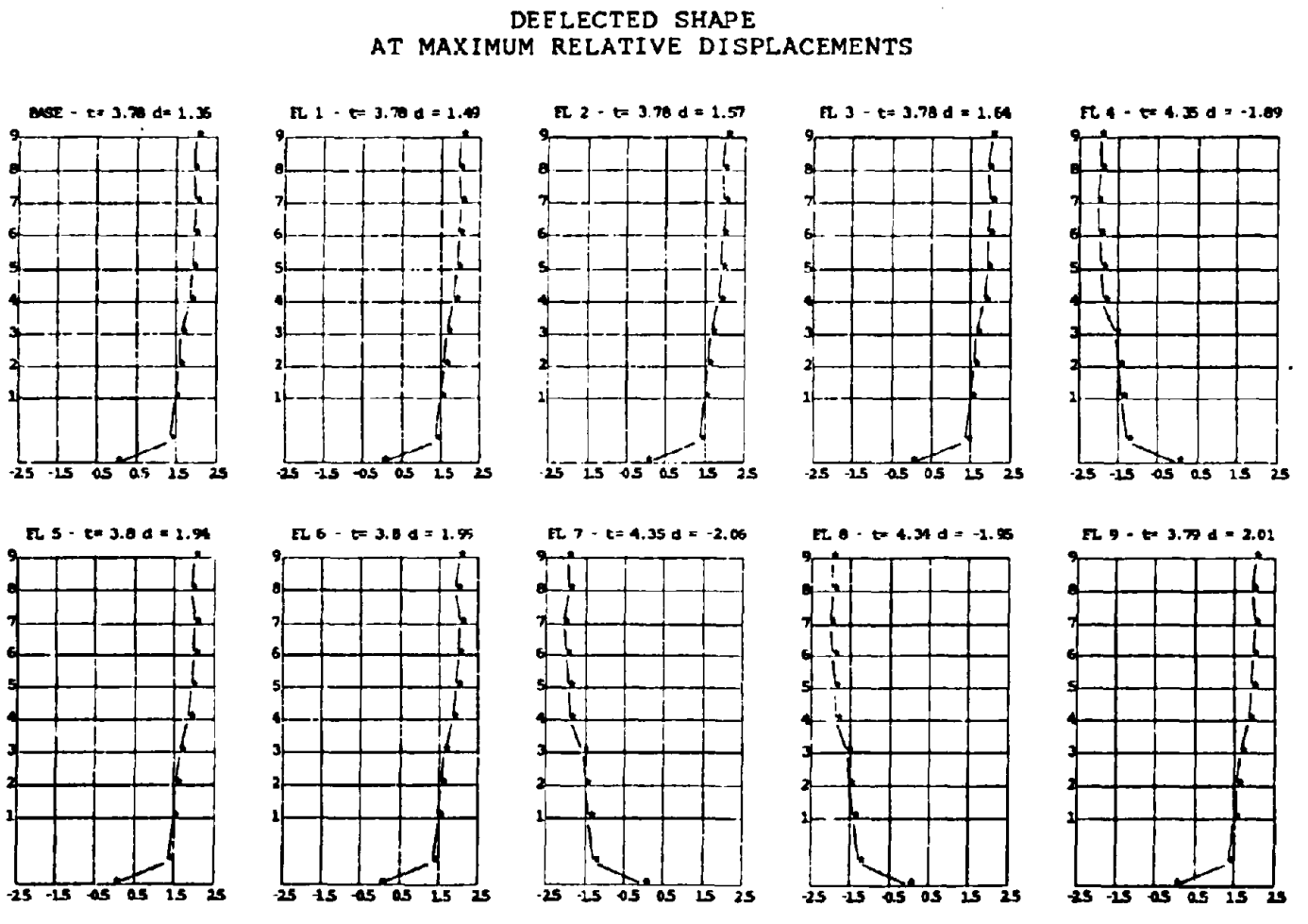

Figure 7.7 **Deflected shape of structure on rubber-sliders system, at maximum story displacements for El Centro signal 375 span.**

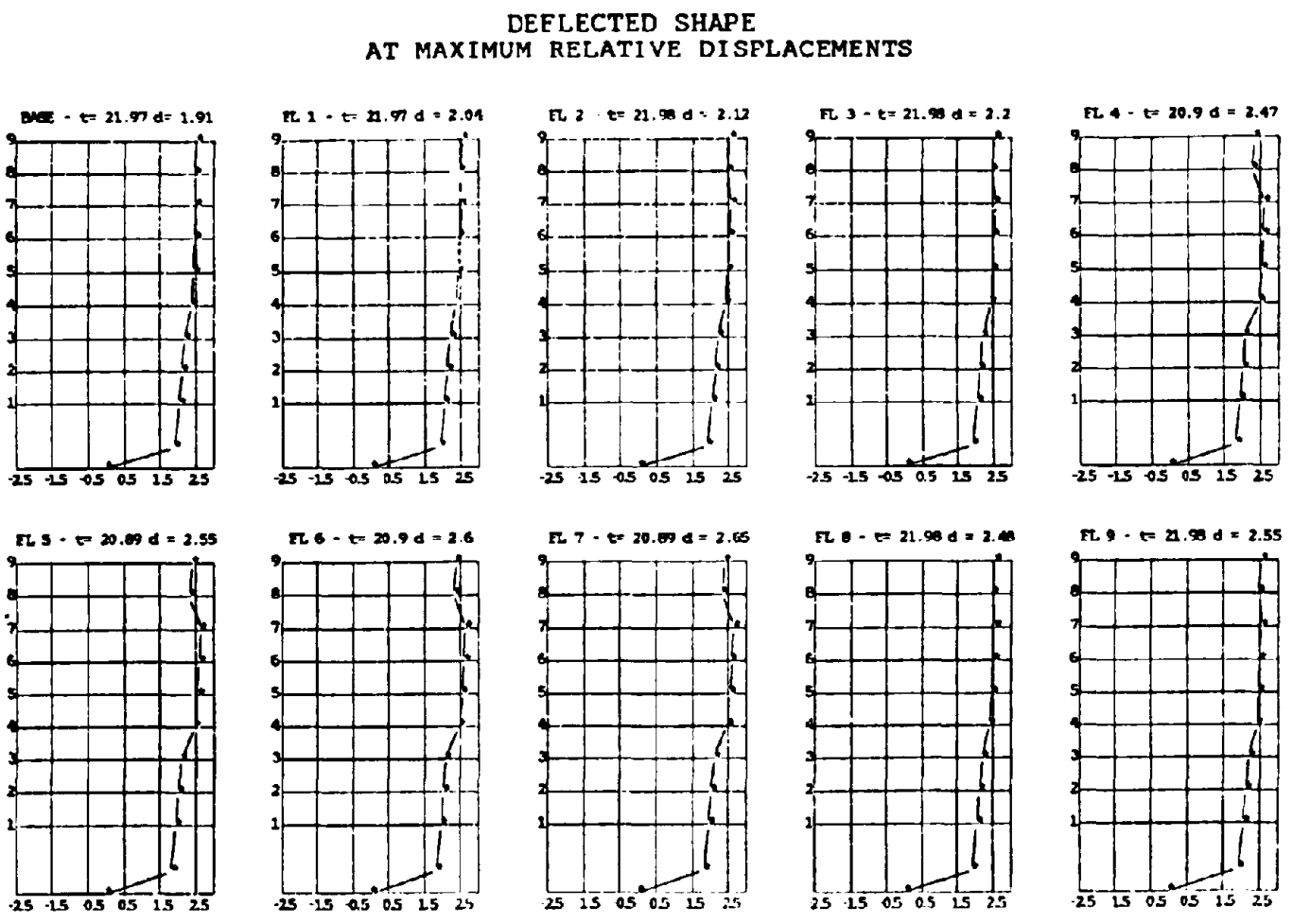

Figure 7.8 **Deflected shape of structure on rubber-sliders system, at maximum story displacements for Mexico City signal 375 span.**

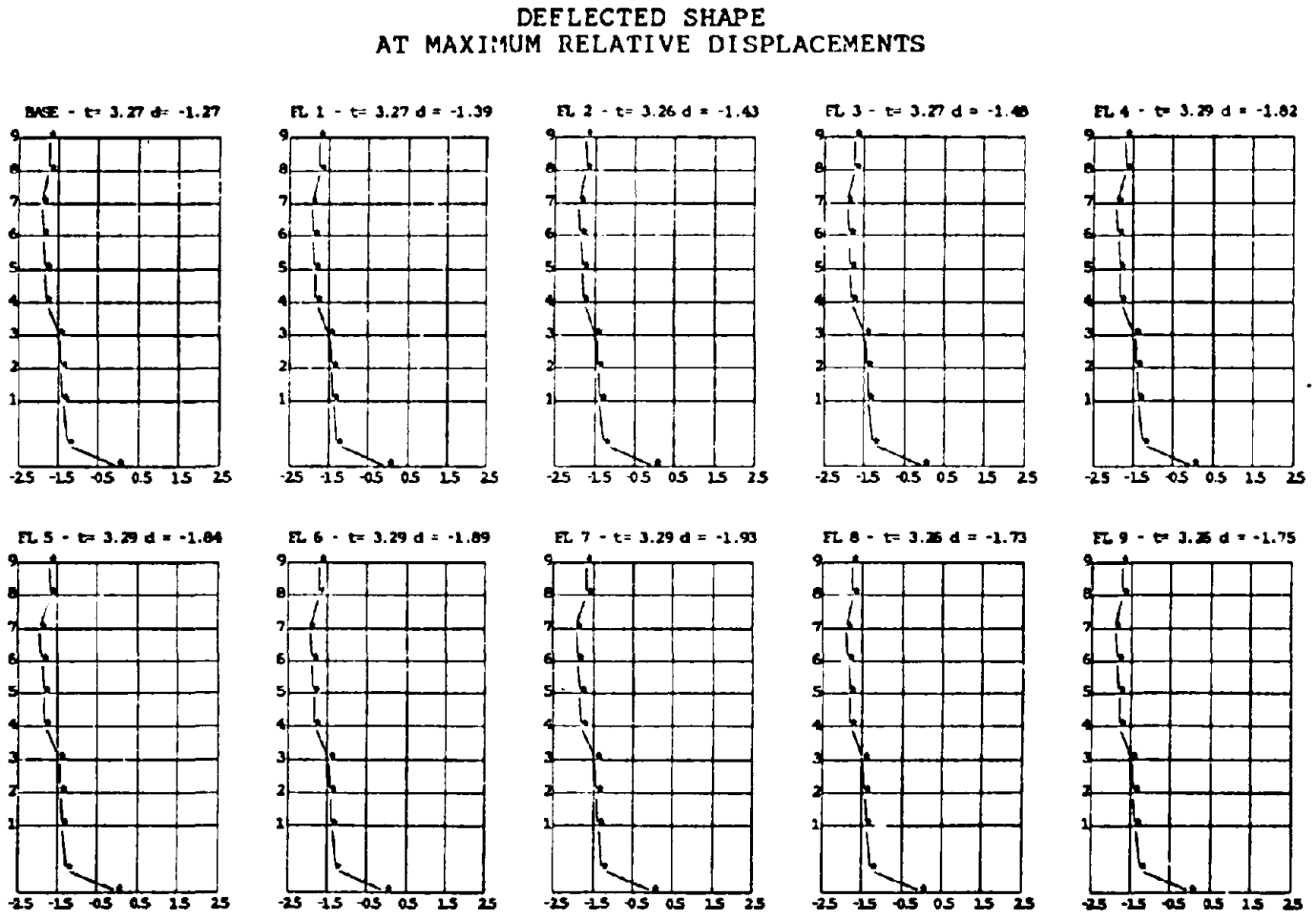

Figure 7.9 **Deflected shape of structure on rubber-sliders system, at maximum story displacements for Bucharest signal 300 span.**

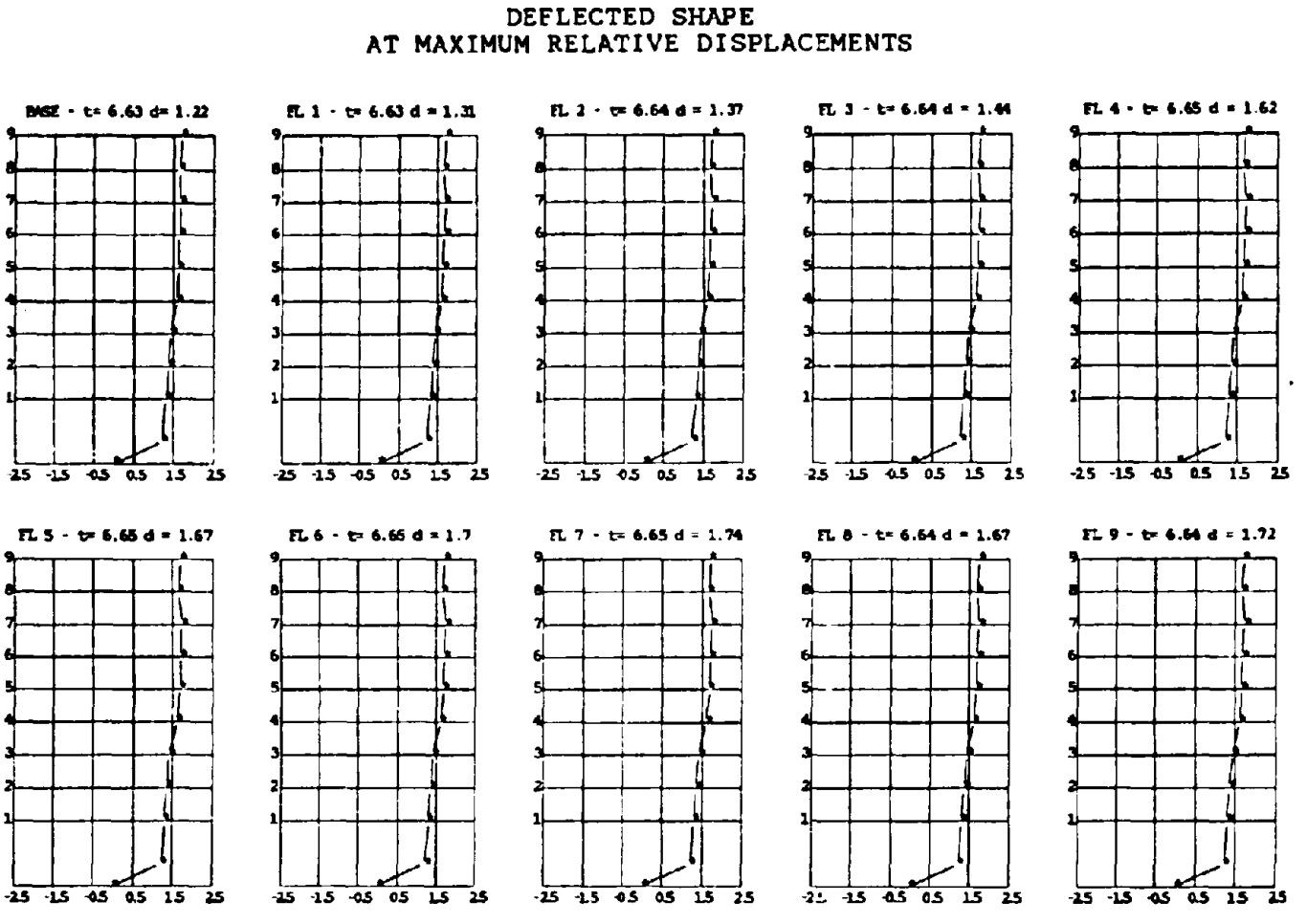

Figure 7.10 **Deflected shape of structure on rubber-sliders system, at maximum story displacements for Miyagi-Ken-Oki signal 350 span.**

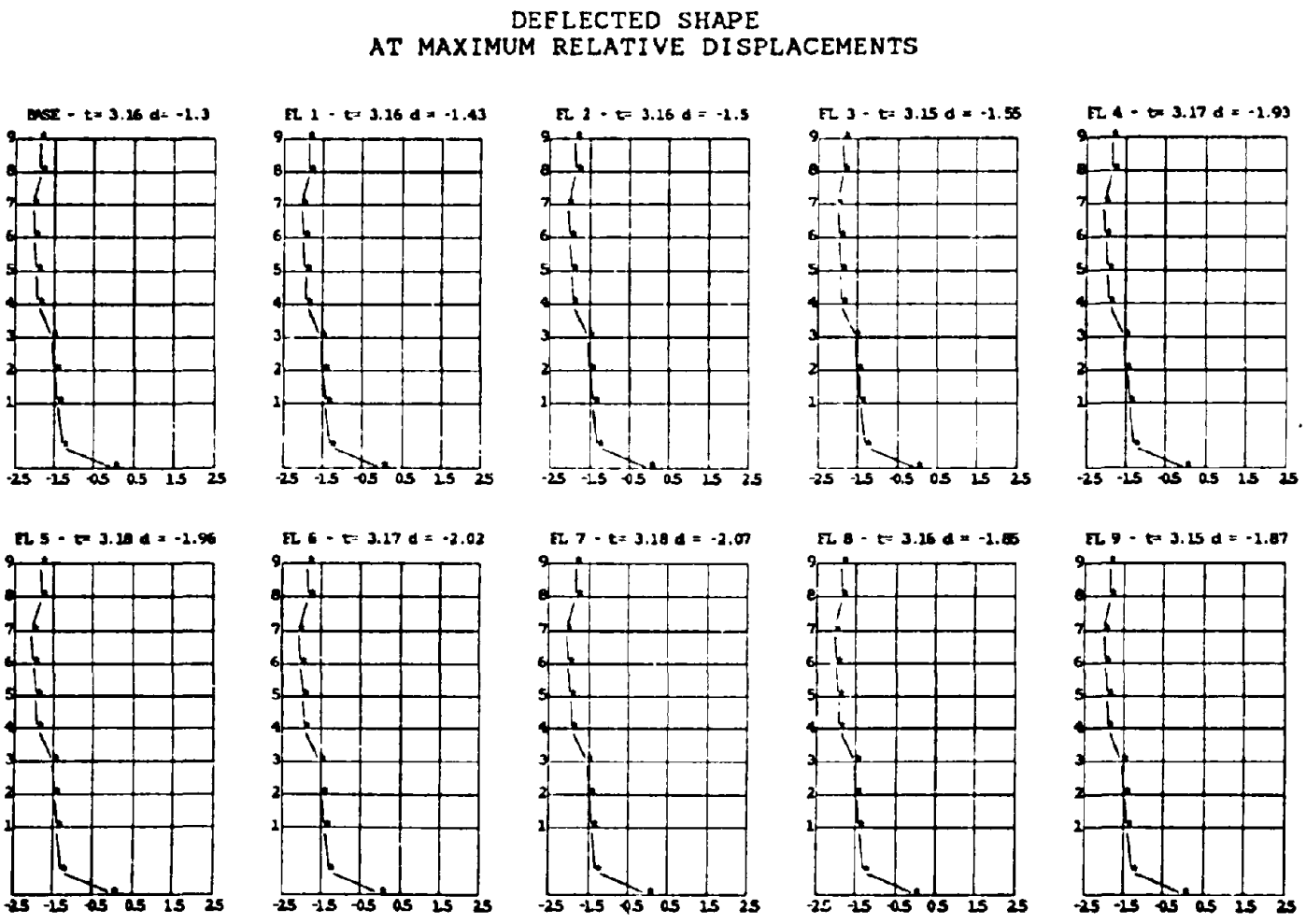

Figure 7.11 **Deflected shape of structure on rubber-sliders system, at maximum story displacements for Pacoima Dam signal 350 span.**

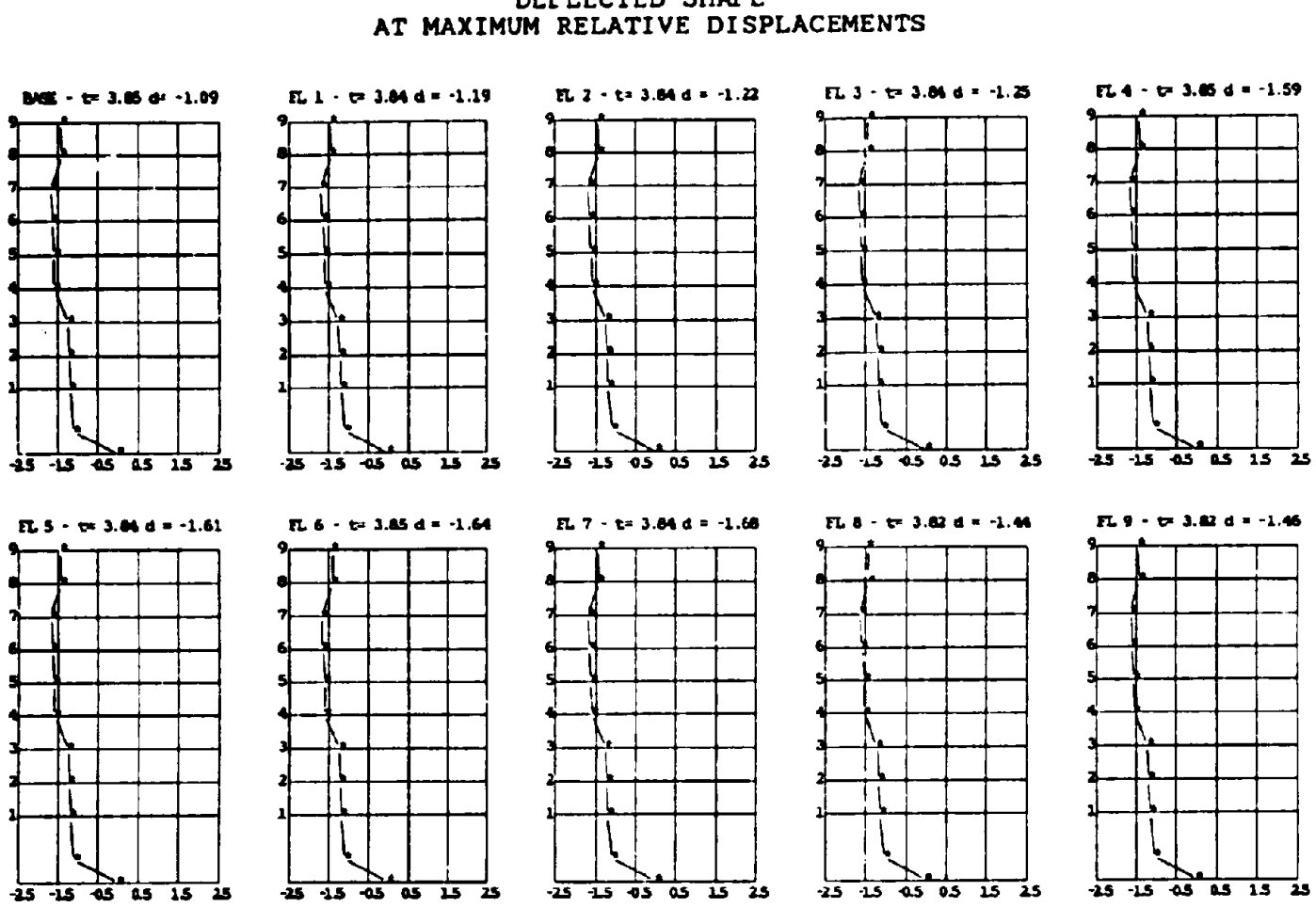

Figure 7.12 Deflected shape of structure on rubber-sliders system, at maximum story displacements for Parkfield signal 350 span.

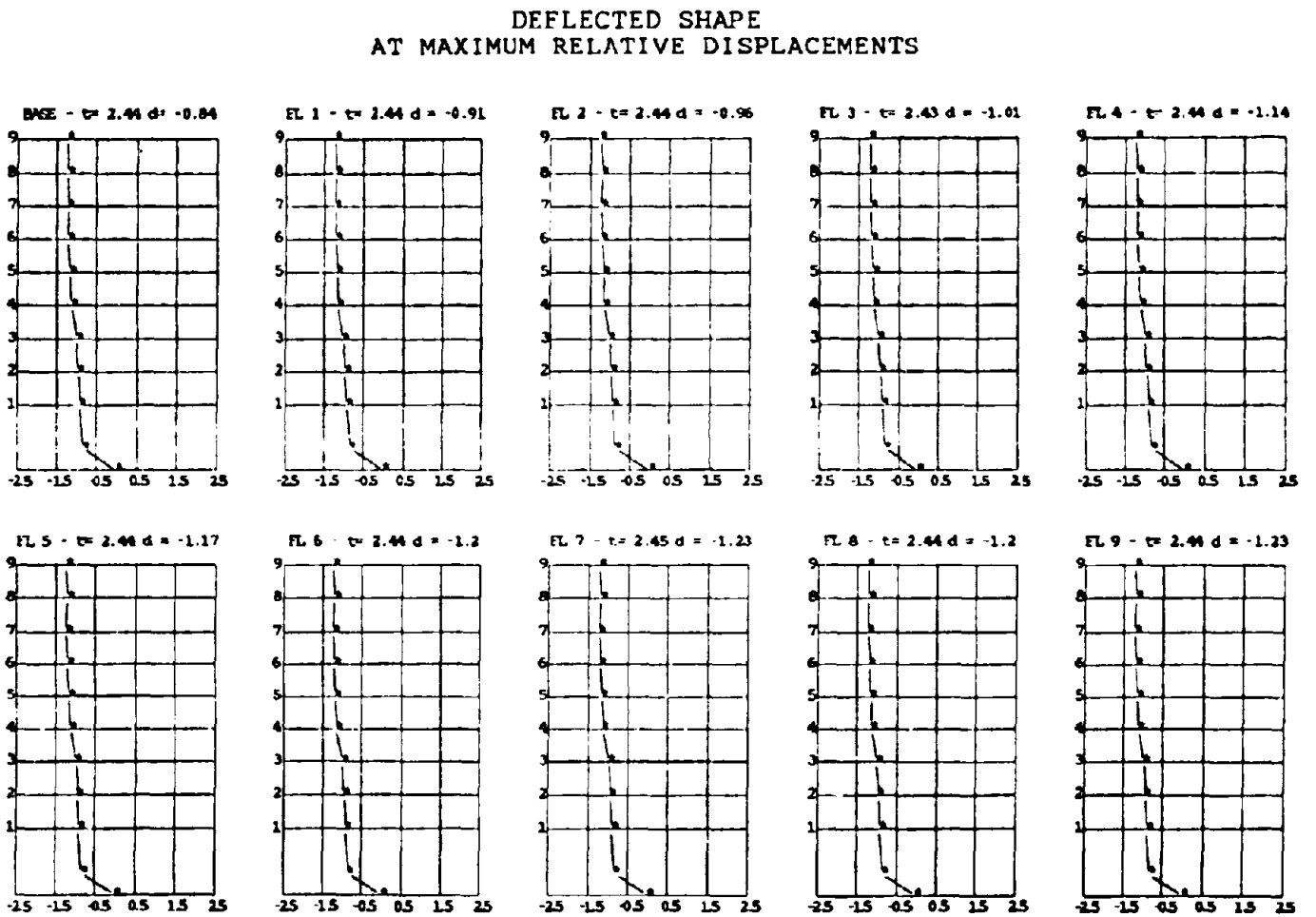

Figure 7.13 **Deflected shape of structure on rubber-sliders system, at maximum story displacements for San Francisco signal 200 span.**

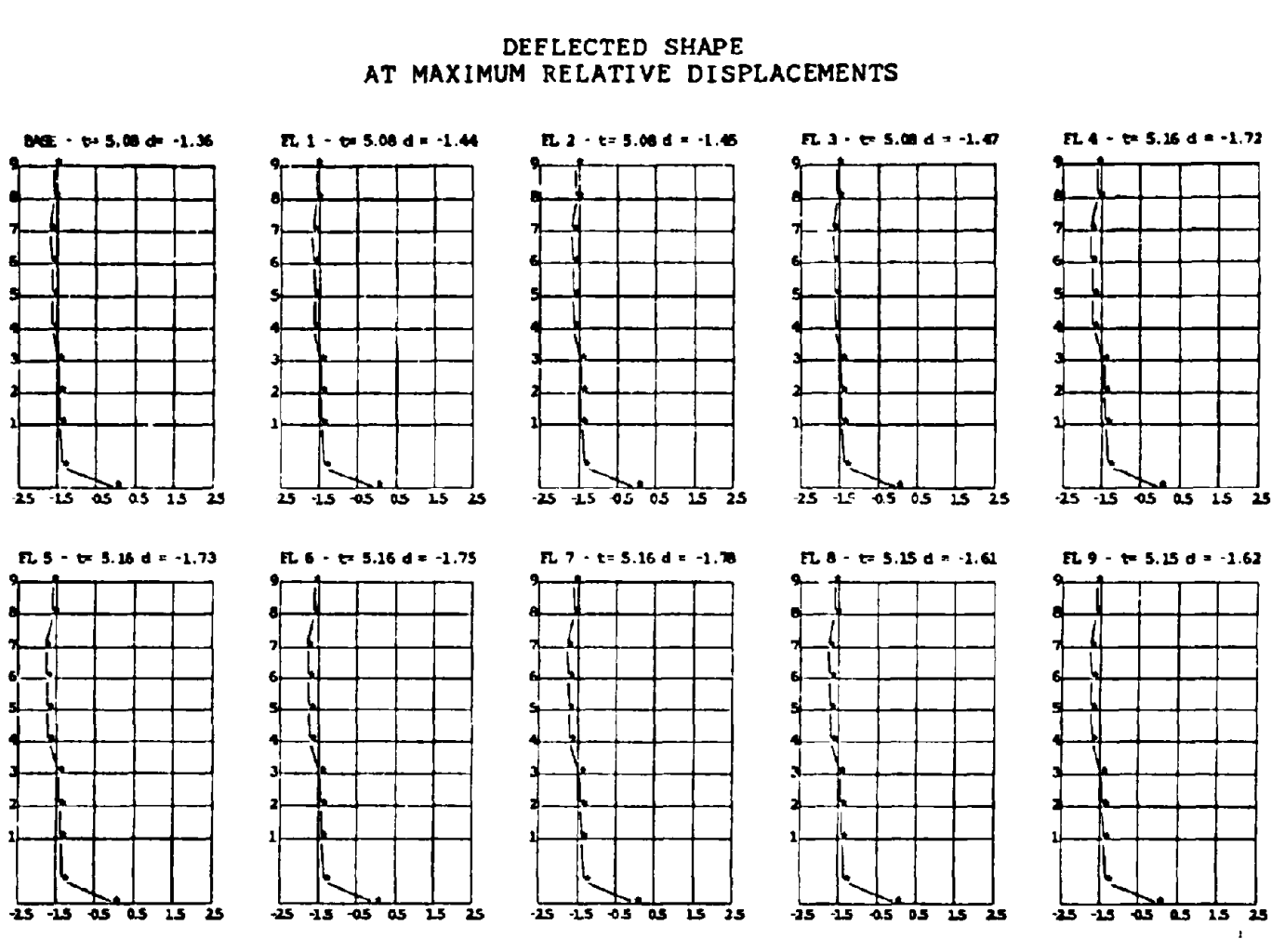

Figure 7.14 **Deflected shape of structure on rubber-sliders system, at maximum story displacements for Taft signal 350 span.**

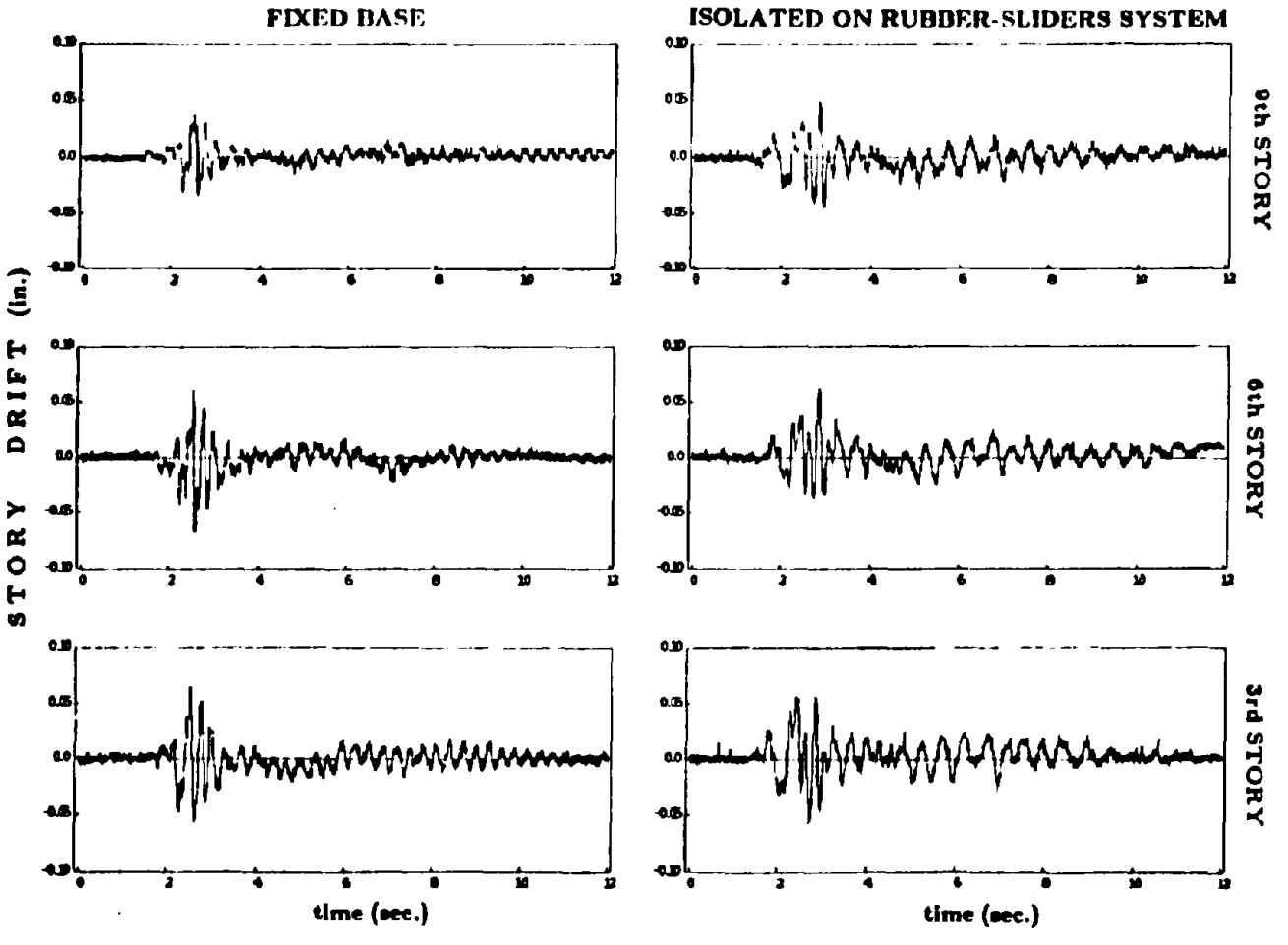

Figure 7.15 Story drift time history for San Francisco record at 100 horizontal span (PTA=0.7g, left) and 200 horizontal span (PTA=1.2g, right).

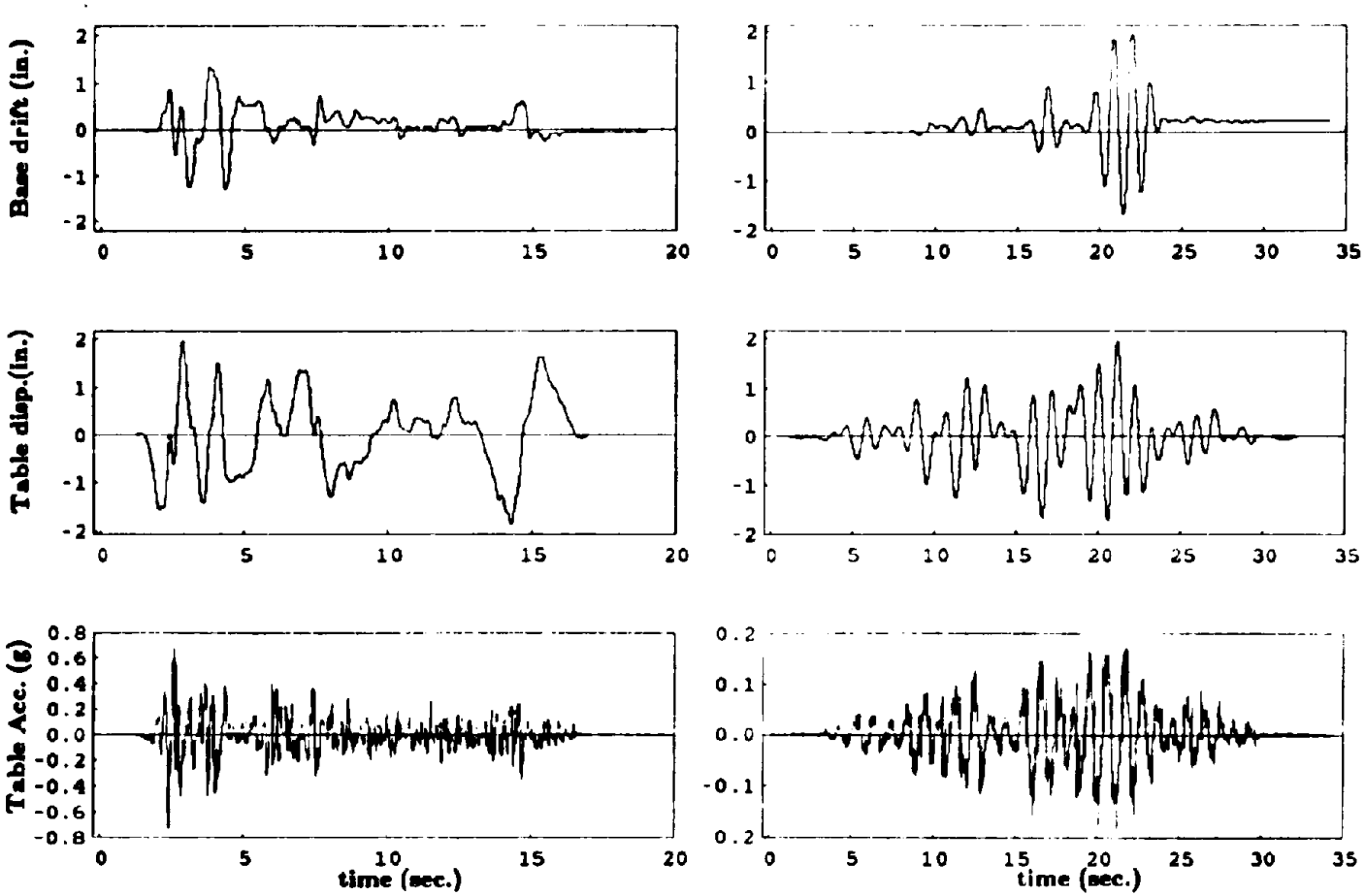

Figure 7.16 Top figure showing base drift final offset, El Centro 375 base offset=-0.06 in. (left), Mexico City 375 base offset=0.21 in. (right).

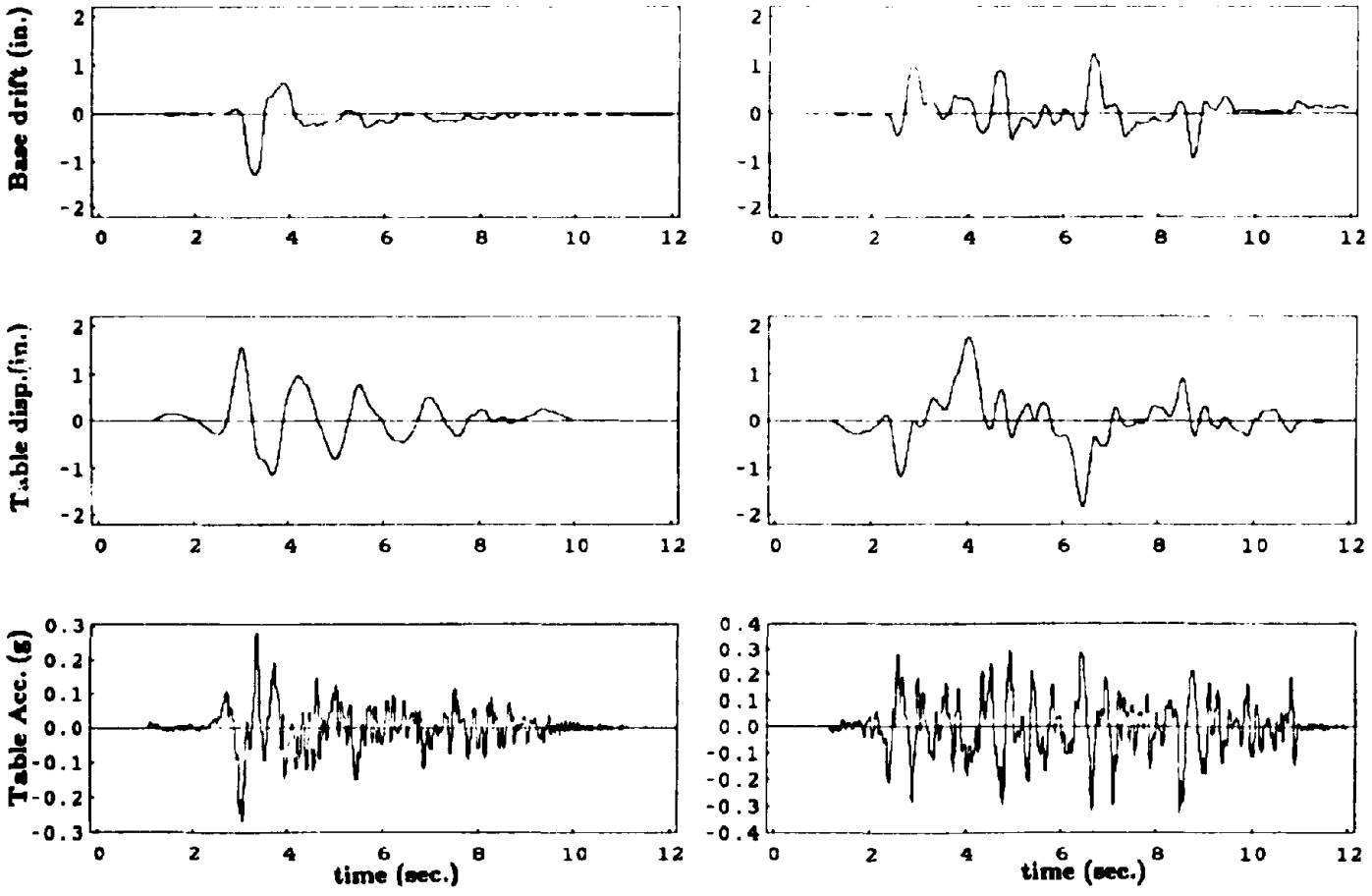

Figure 7.17 Top figure showing base drift final offset, Bucharest 300 base offset=-0.006 in. (left), Miyagi-Ken-Oki 350 base offset=0.19 in. (right).

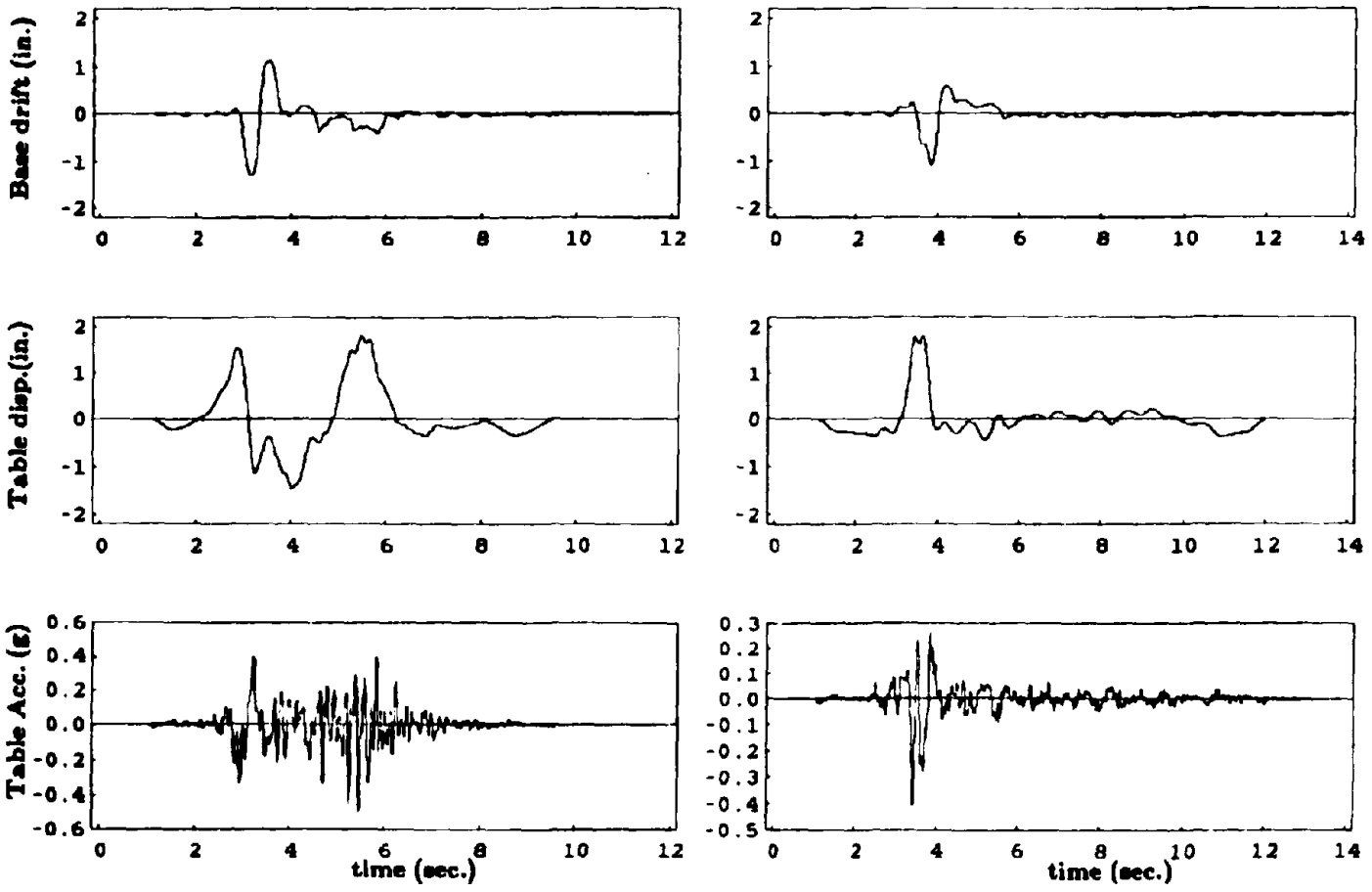

Figure 7.18 Top figure showing base drift final offset, Pacoima Dam 350 base offset=-0.025 in. (left), Parkfield 350 base offset=-0.041 in. (right).

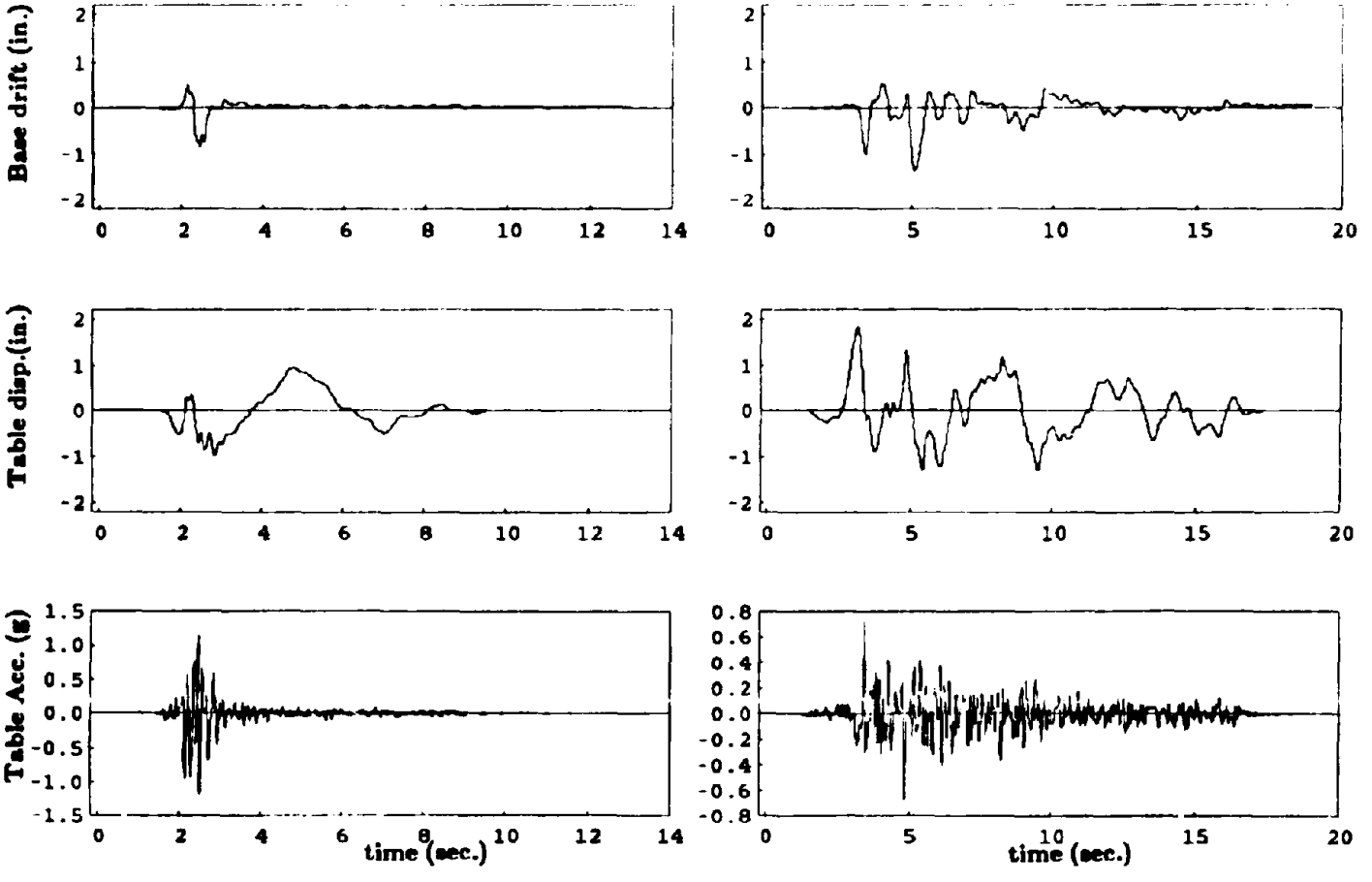

Figure 7.19 Top figure showing base drift final offset, San Francisco 200 base offset=0.037 in. (left), Taft 350 base offset=0.057 in. (right).

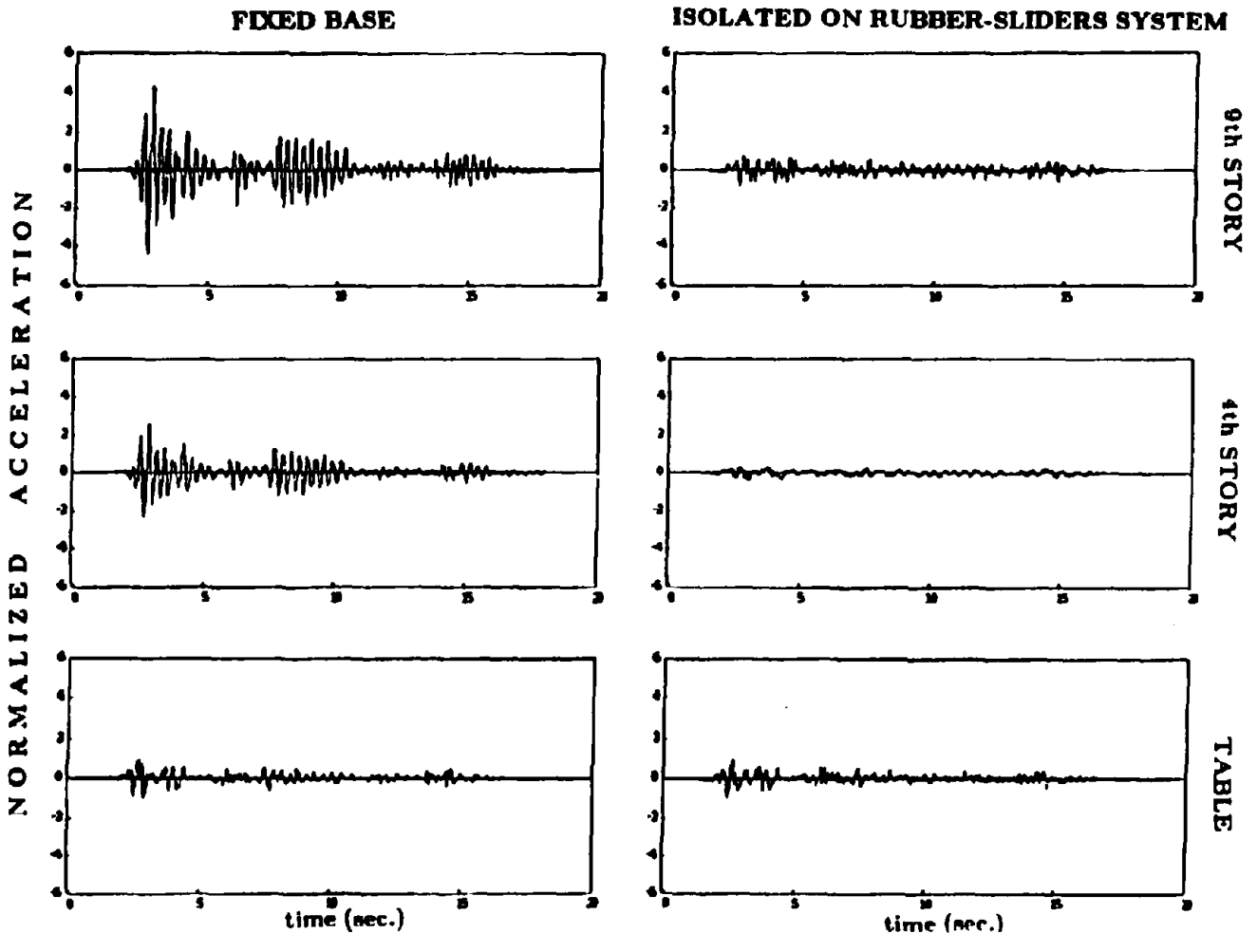

Figure 7.20 Acceleration Time histories normalized to peak table acceleration for El Centro record 125 horizontal span (PTA=0.25g, left) and 375 horizontal span (PTA=0.73g, right).

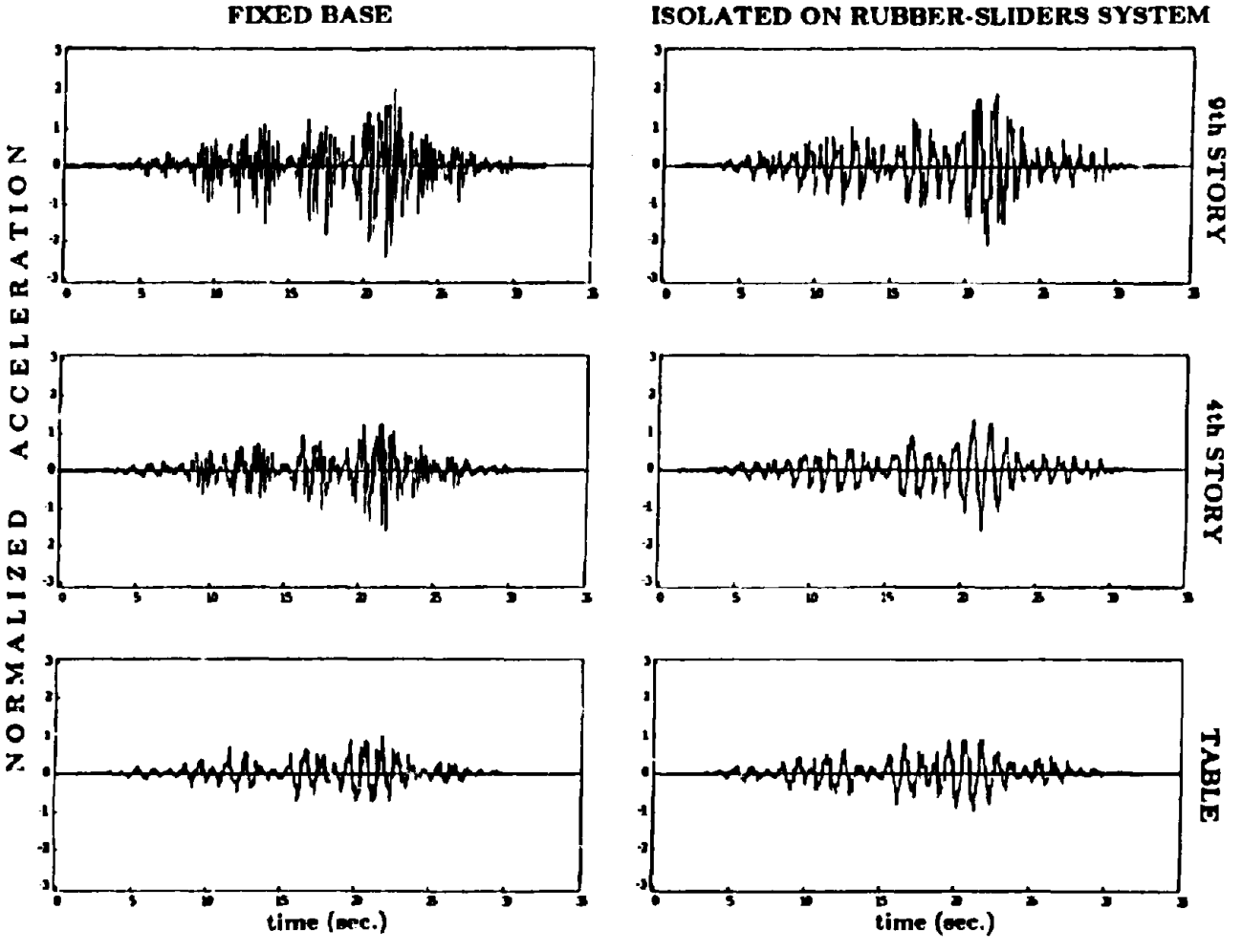

Figure 7.21 Acceleration time histories normalized to peak table acceleration for Mexico City record 100 horizontal span (PTA=0.06g, left) and 375 horizontal span (PTA=0.18g, right).

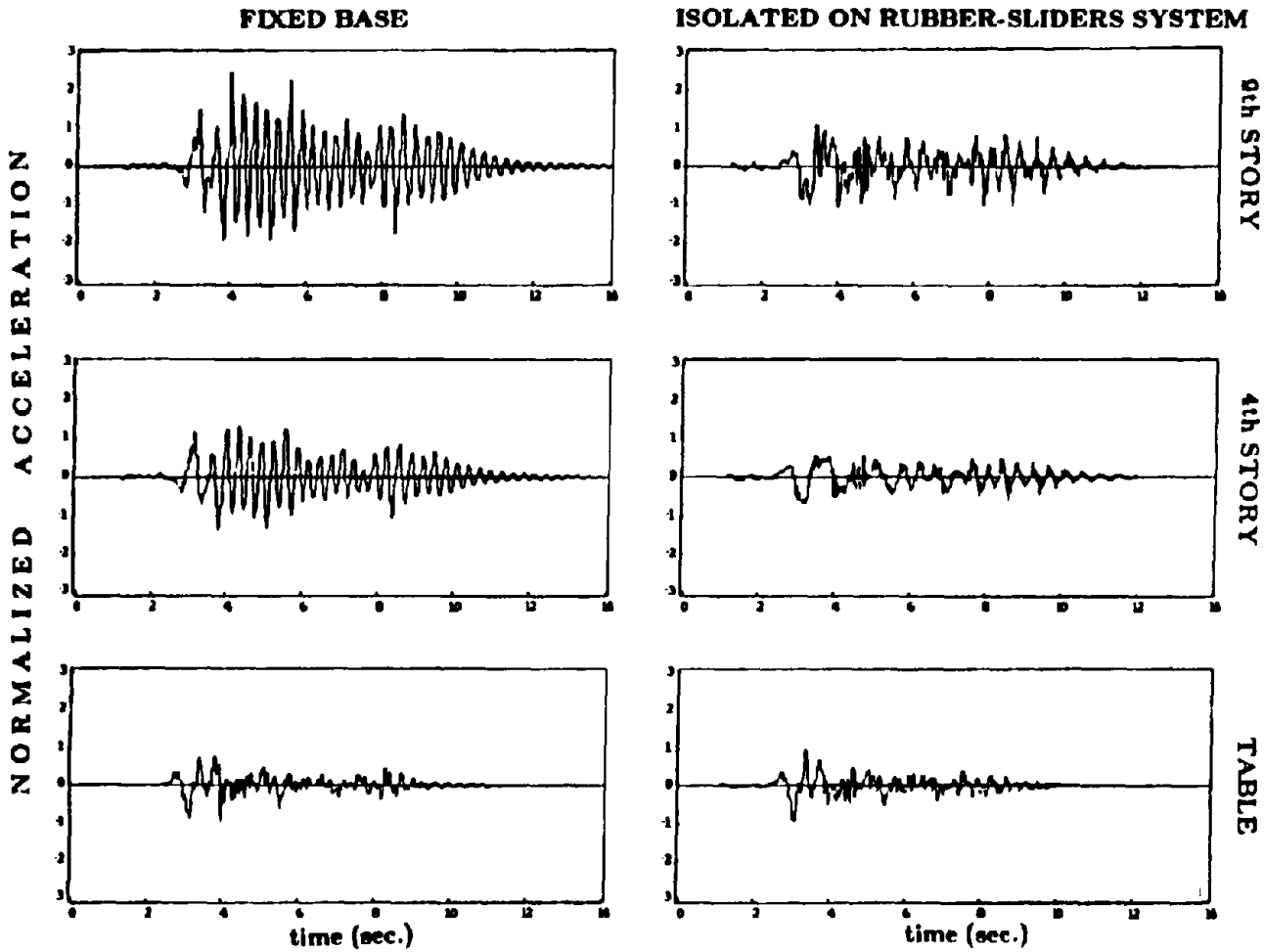

Figure 7.22 Acceleration time histories normalized to peak table acceleration for Bucharest record 175 horizontal span (PTA=0.17g, left) and 300 horizontal span (PTA=0.27g, right).

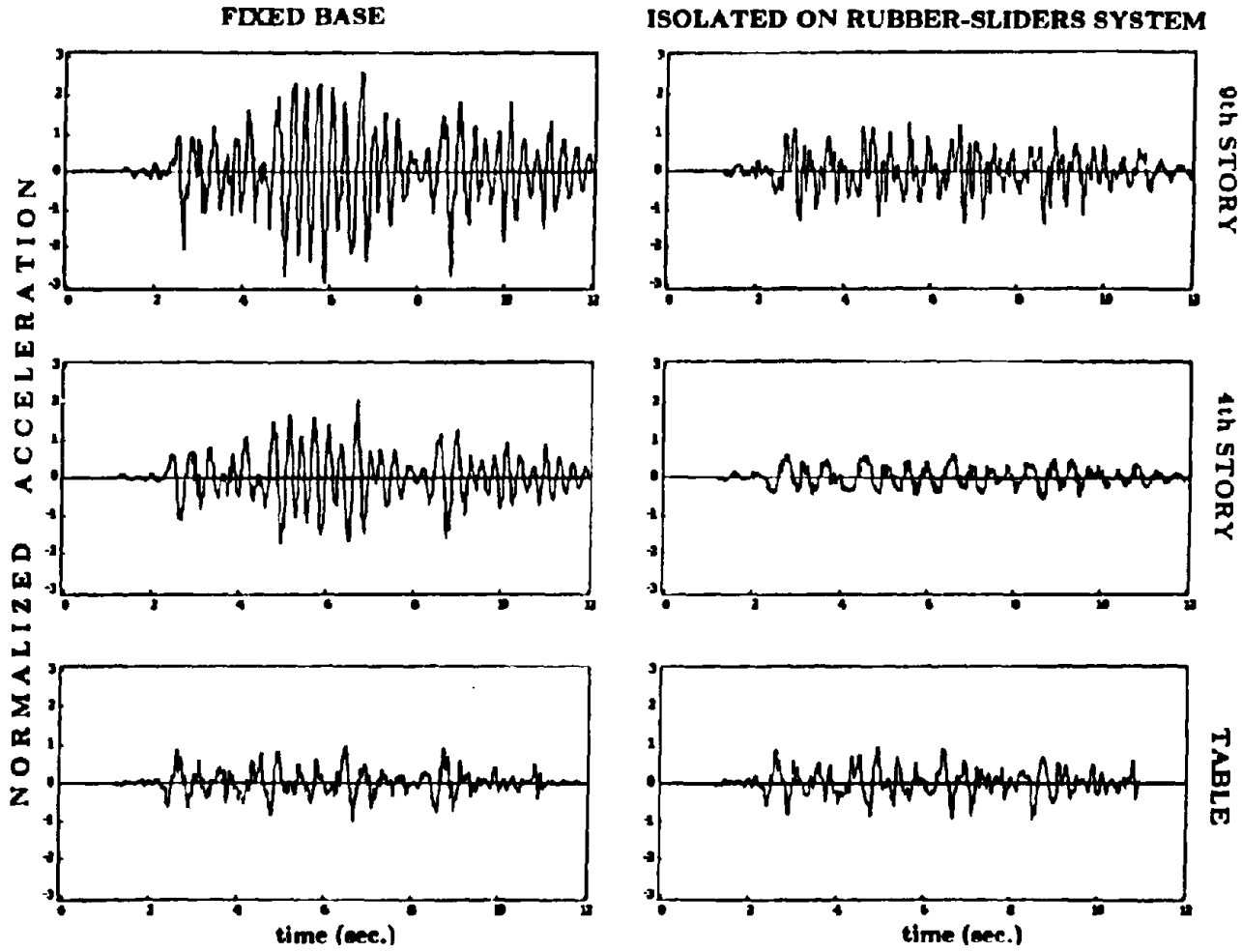

Figure 7.23 Acceleration time histories normalized to peak table acceleration for Miyagi-Ken-Oki record 150 horizontal span (PTA=0.16g, left) and 350 horizontal span (PTA=0.33g, right).

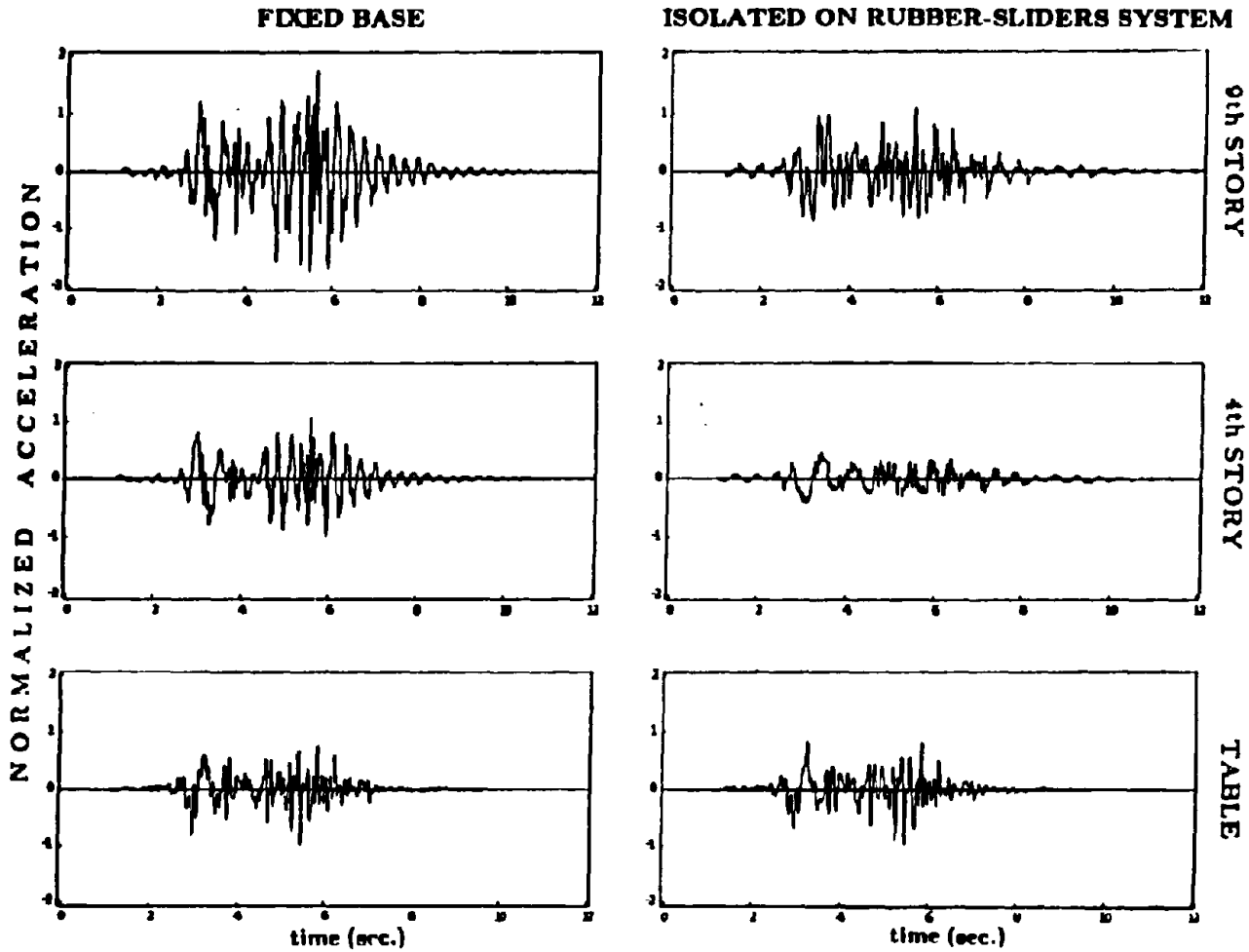

Figure 7.24 Acceleration time histories normalized to peak table acceleration for Pacoima Dam record 125 horizontal span (PTA=0.18g, left) and 350 horizontal span (PTA=0.49g, right).

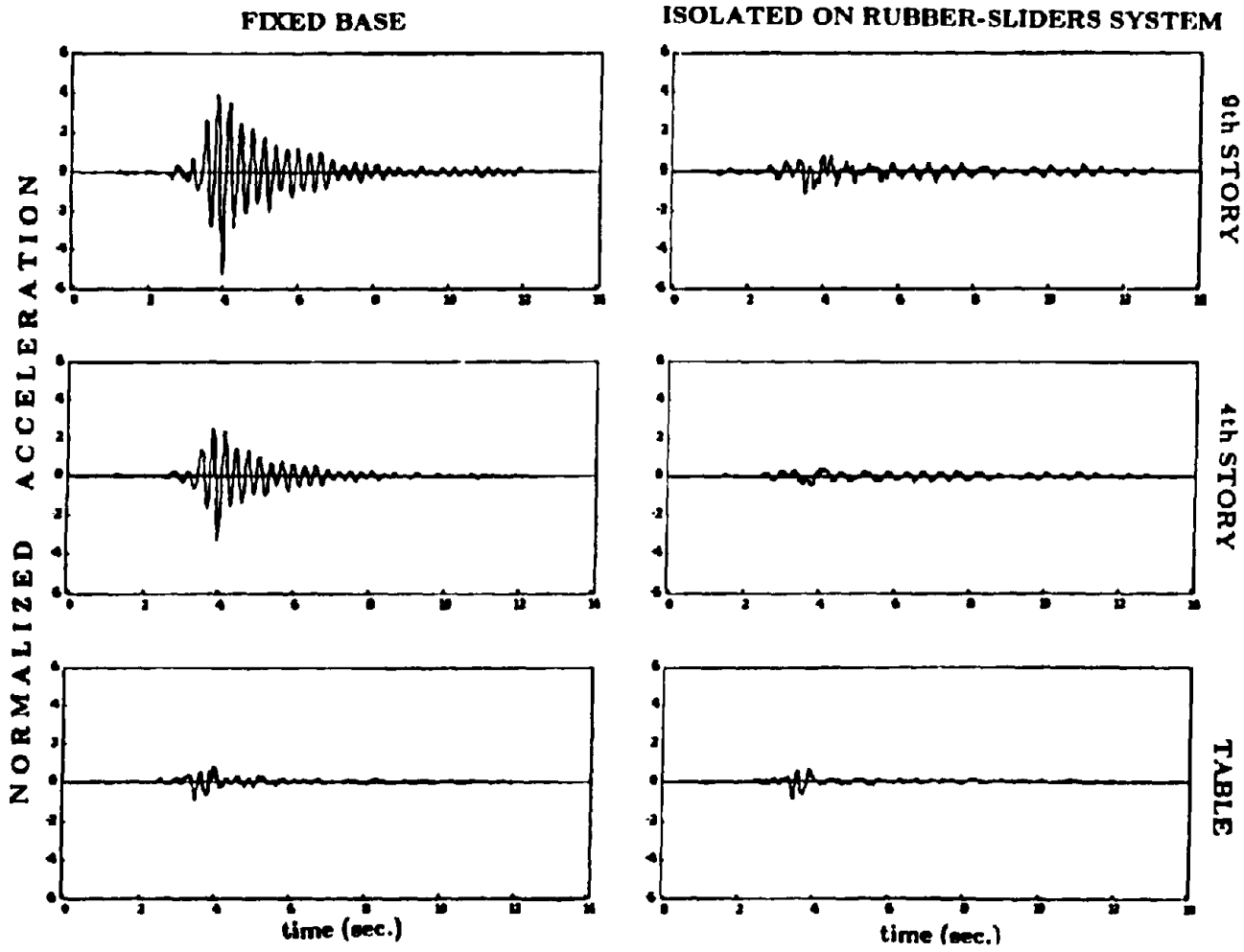

Figure 7.25 Acceleration time histories normalized to peak table acceleration for Parkfield record 125 horizontal span (PTA=0.14g, left) and 350 horizontal span (PTA=0.41g, right).

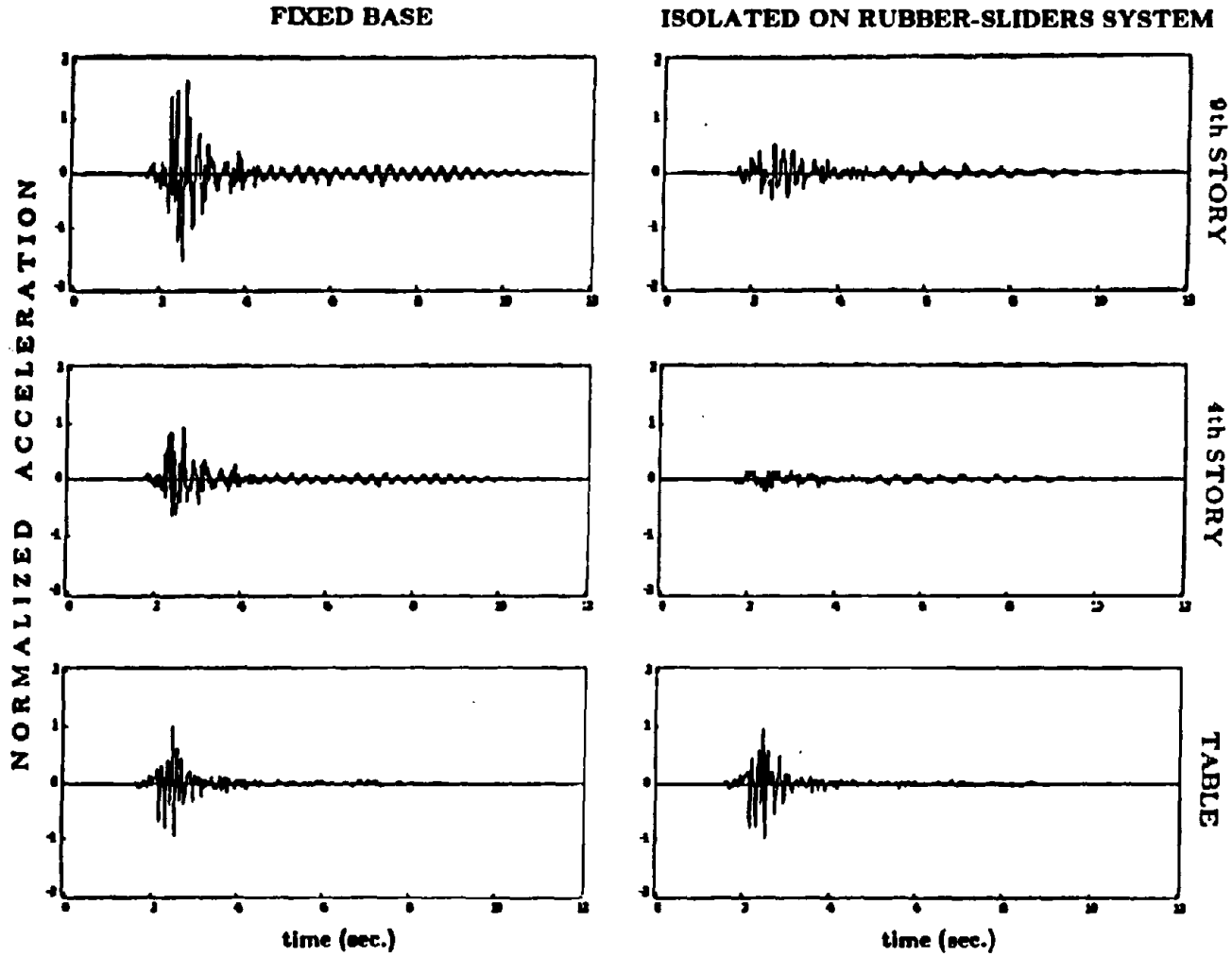

Figure 7.26 Acceleration time histories normalized to peak table acceleration for San Francisco record 100 horizontal span (PTA=0.73g, left) and 200 horizontal span (PTA=1.20g, right).

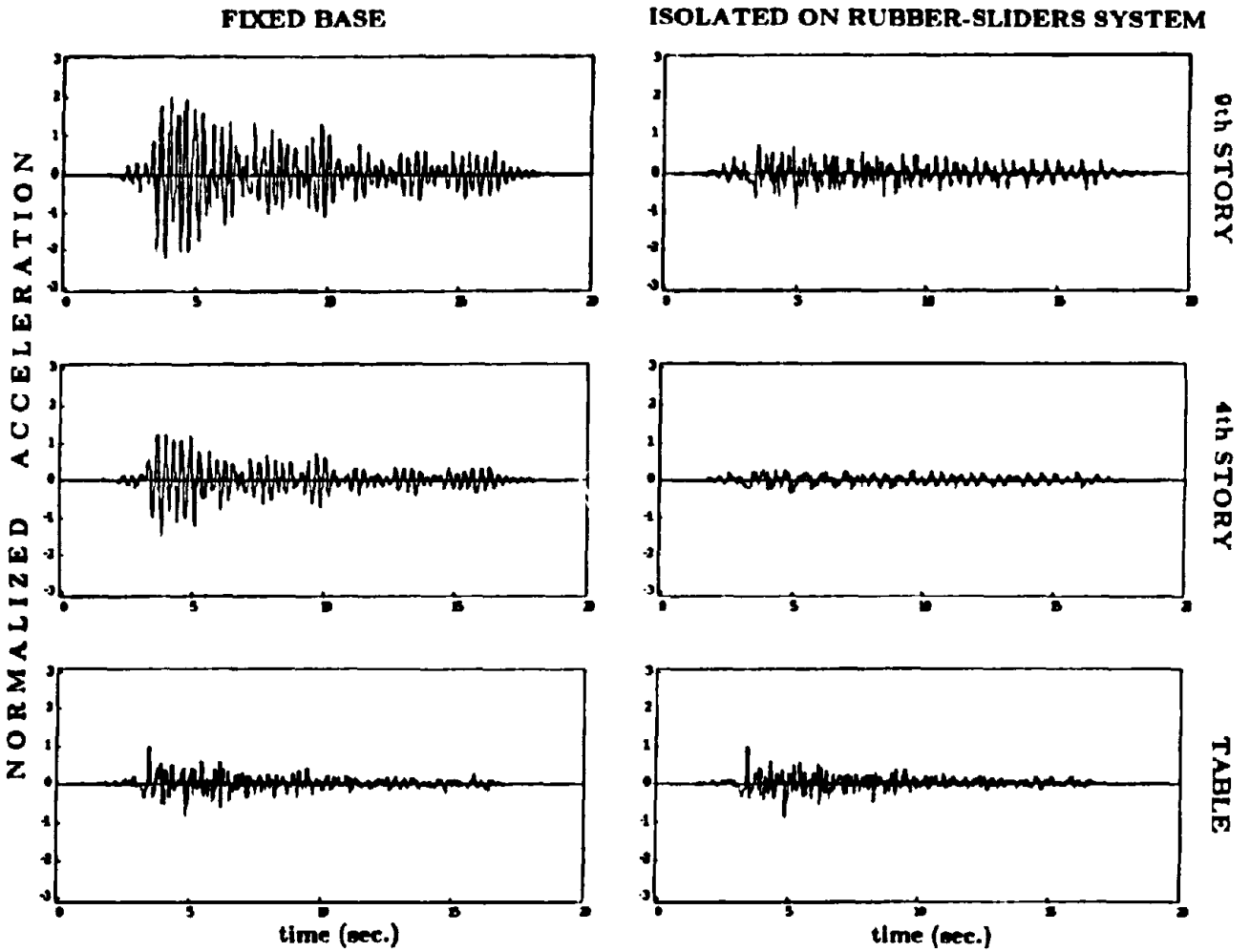

Figure 7.27 Acceleration time histories normalized to peak table acceleration for Taft record 100 horizontal span (PTA=0.20g, left) and 350 horizontal span (PTA=0.71g, right).

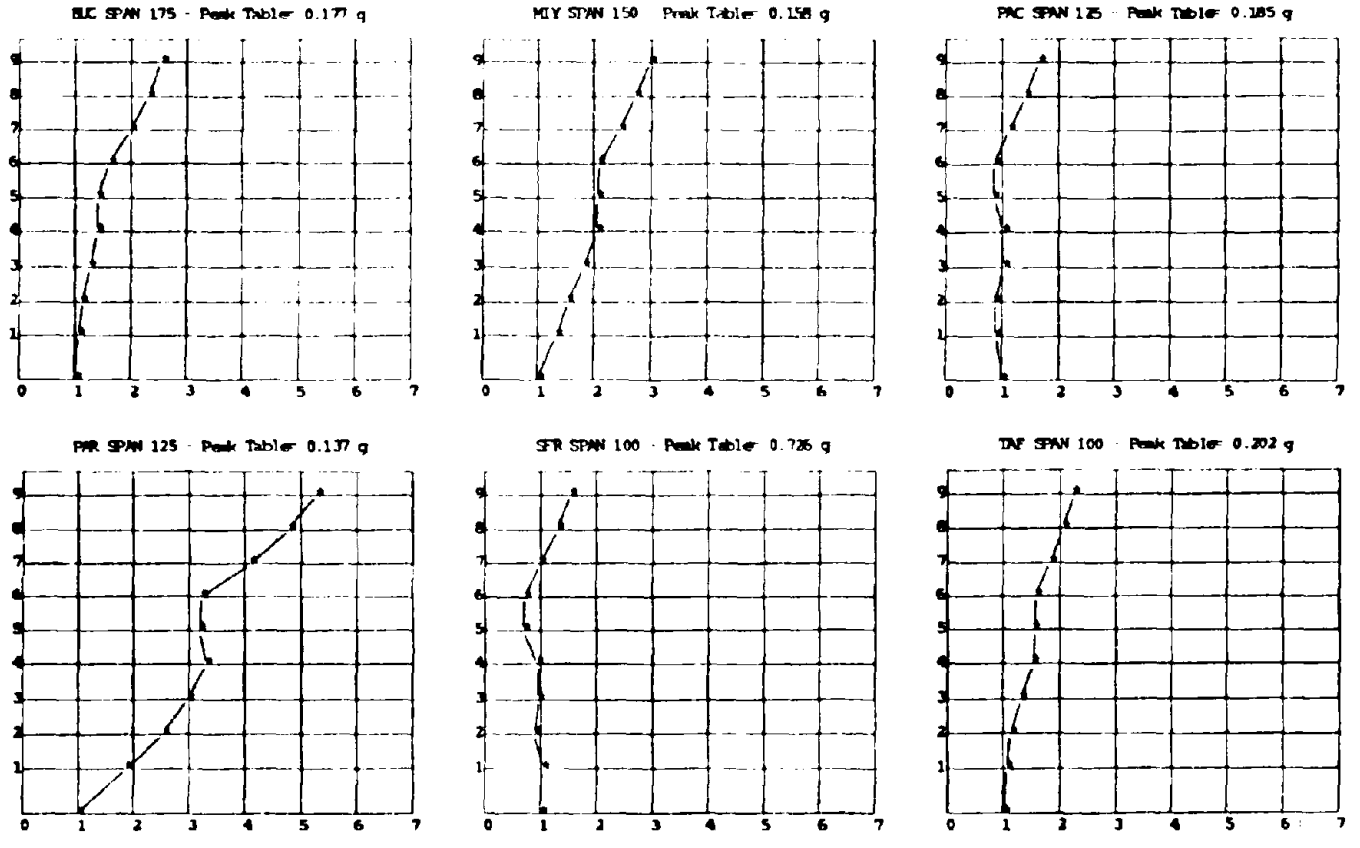

Figure 7.28 Acceleration amplification ratios along elevation of fixed base structure for Bucharest (PTA=0.17g), Miyagi-Ken-Oki (PTA=0.16g), Pacoima (PTA=0.18g), Parkfield (PTA=0.14g), San Francisco (PTA=0.73g), and Taft (PTA=0.20g), input motions.

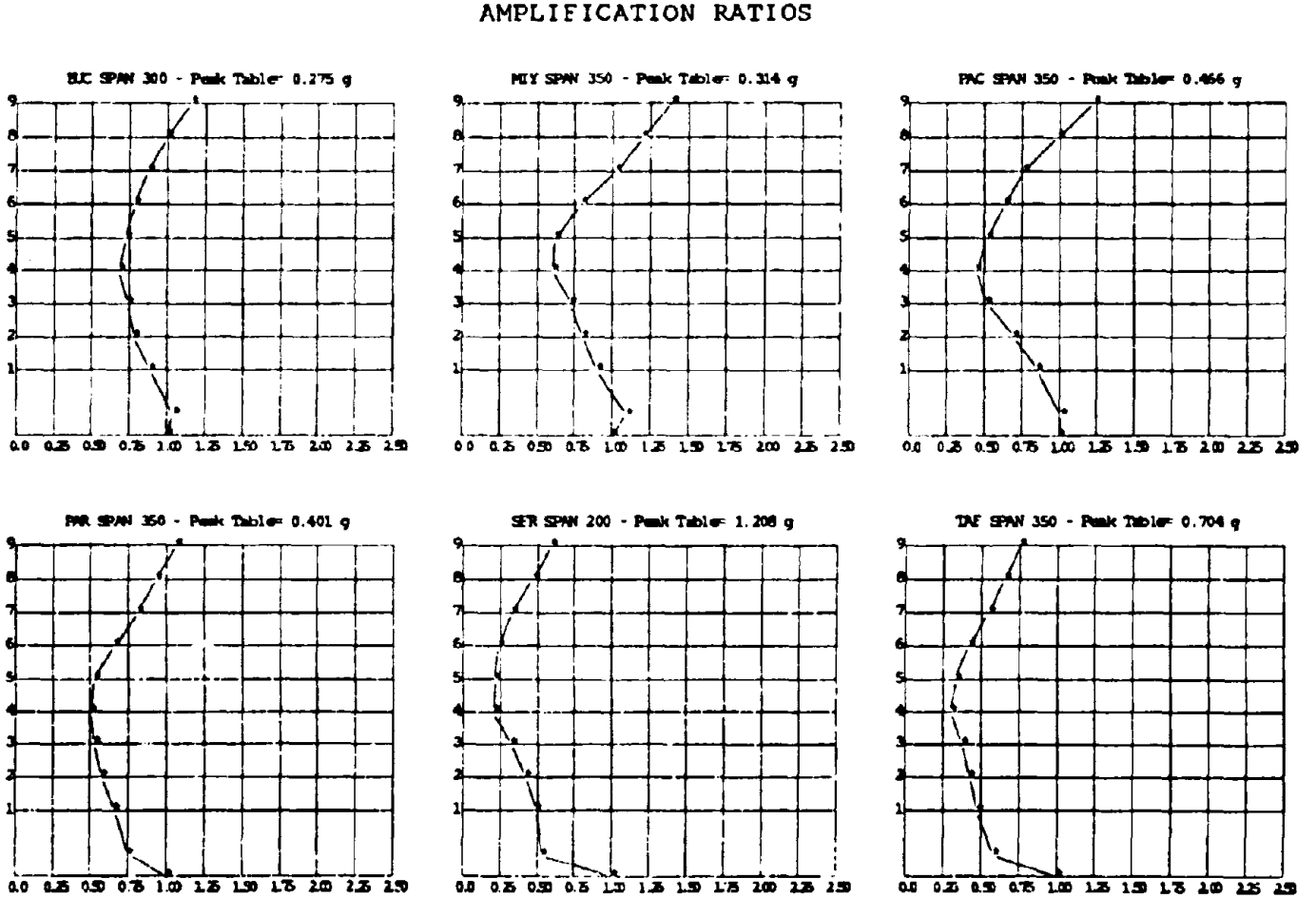

Figure 7.29 Acceleration amplification ratios along elevation of base isolated structure on rubber-sliders system for Bucharest (PTA=0.25g), Miyagi-Ken-Oki (PTA=0.33g), Pacoima (PTA=0.49g), Parkfield (PTA=0.41g), San Francisco (PTA=1.20g), and Taft (PTA=0.72g), input motions.

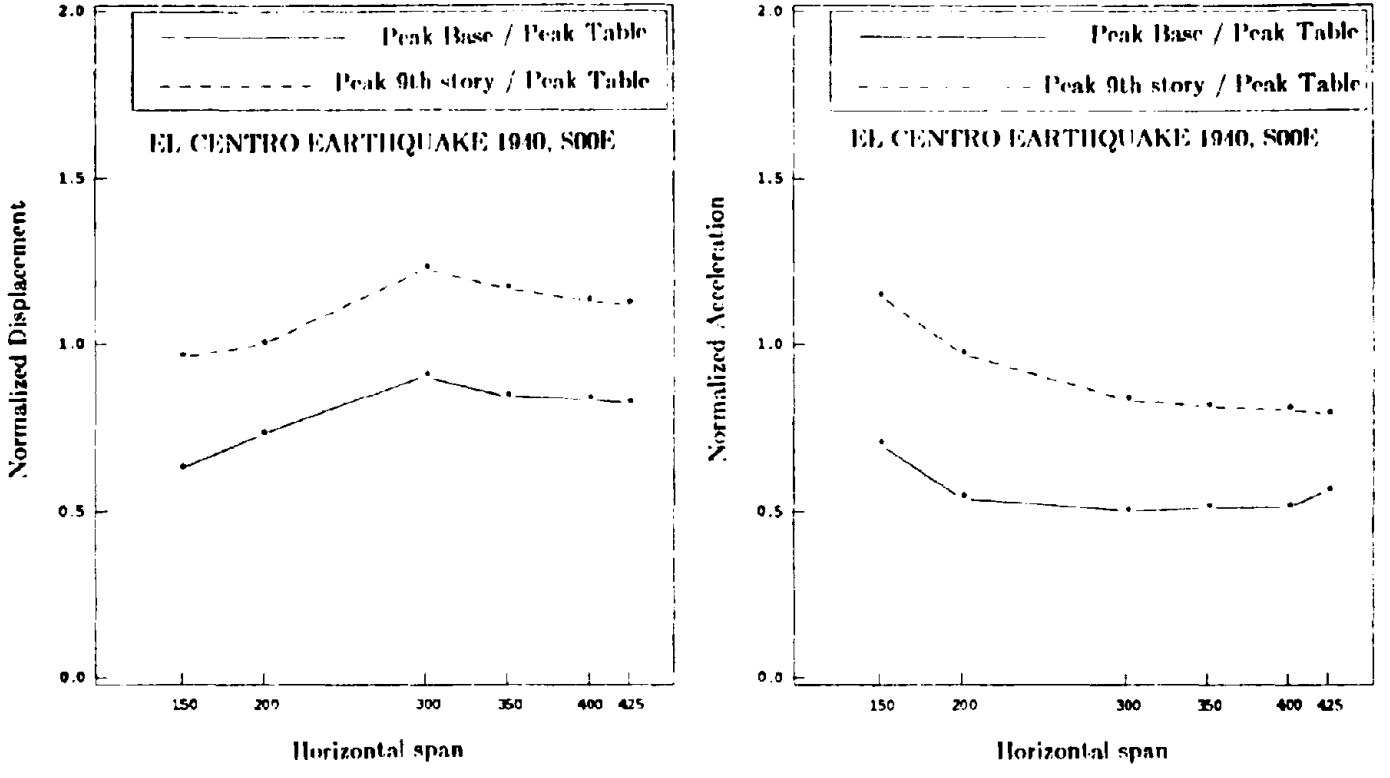

Figure 7.30 **Performance of the rubber bearing slider bearing combined system with increasing input magnitude, under √4 time scaled El Centro record between 150 and 425 horizontal span.**

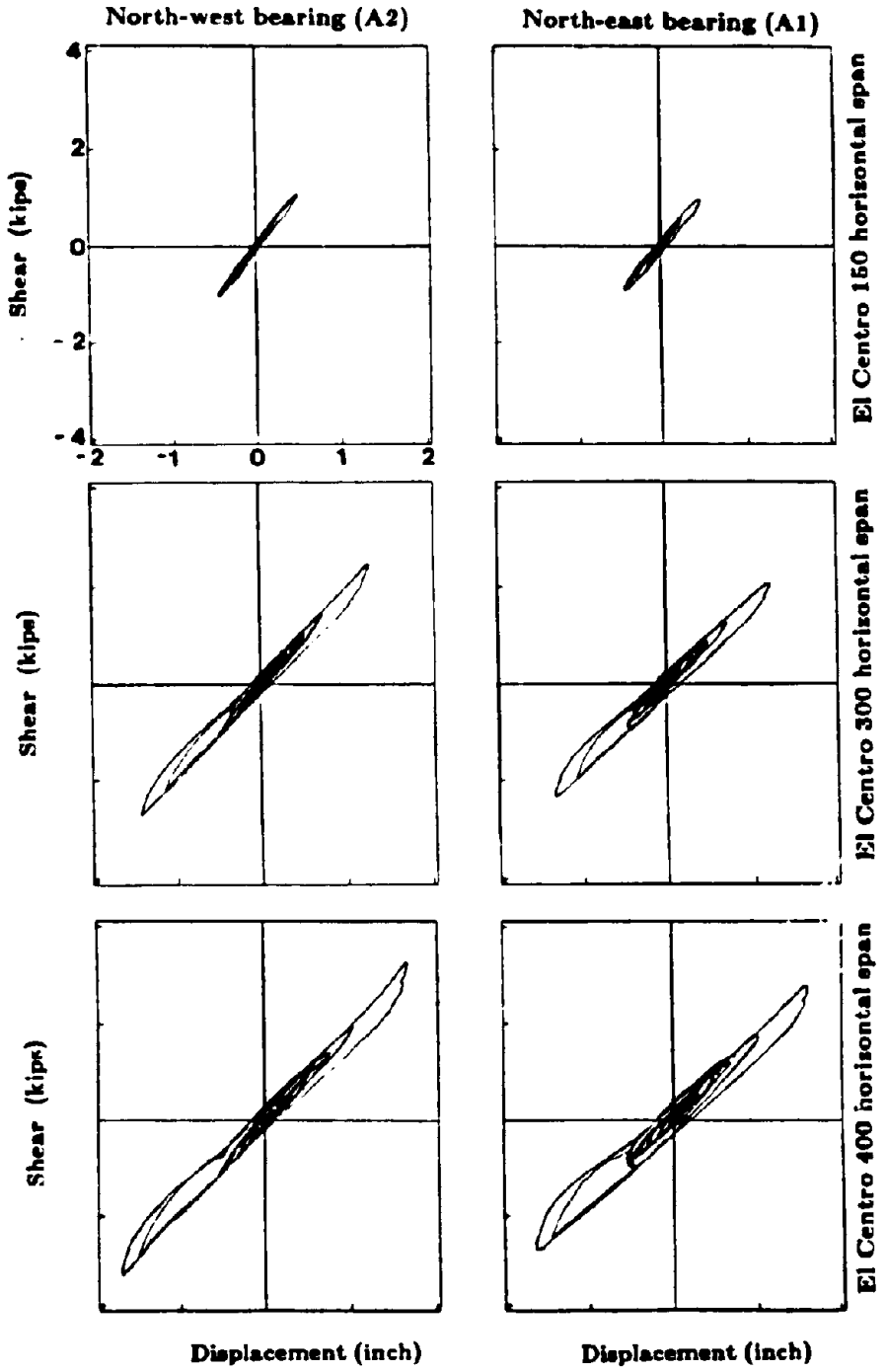

Figure 7.31 North-west (left) and north-east (right) rubber bearings hysteresis loops under El Centro 150, 300, and 400 horizontal span showing stiffening due to tension device.

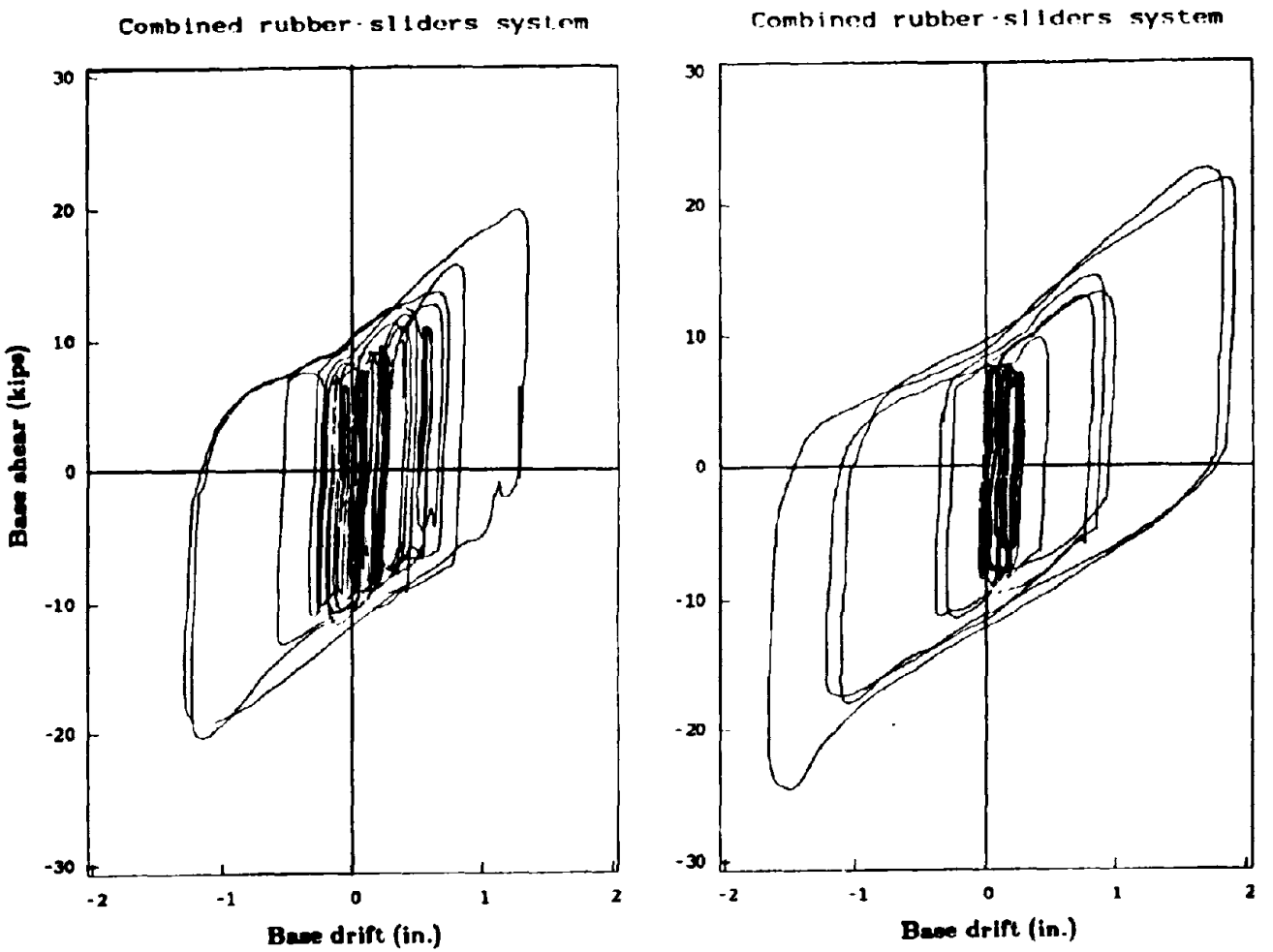

Figure 7.32 Base shear hysteresis loop at isolation interface for El Centro 375 horizontal span (PTA=0.73g, left) and Mexico City 375 horizontal span (PTA=0.18g, right).

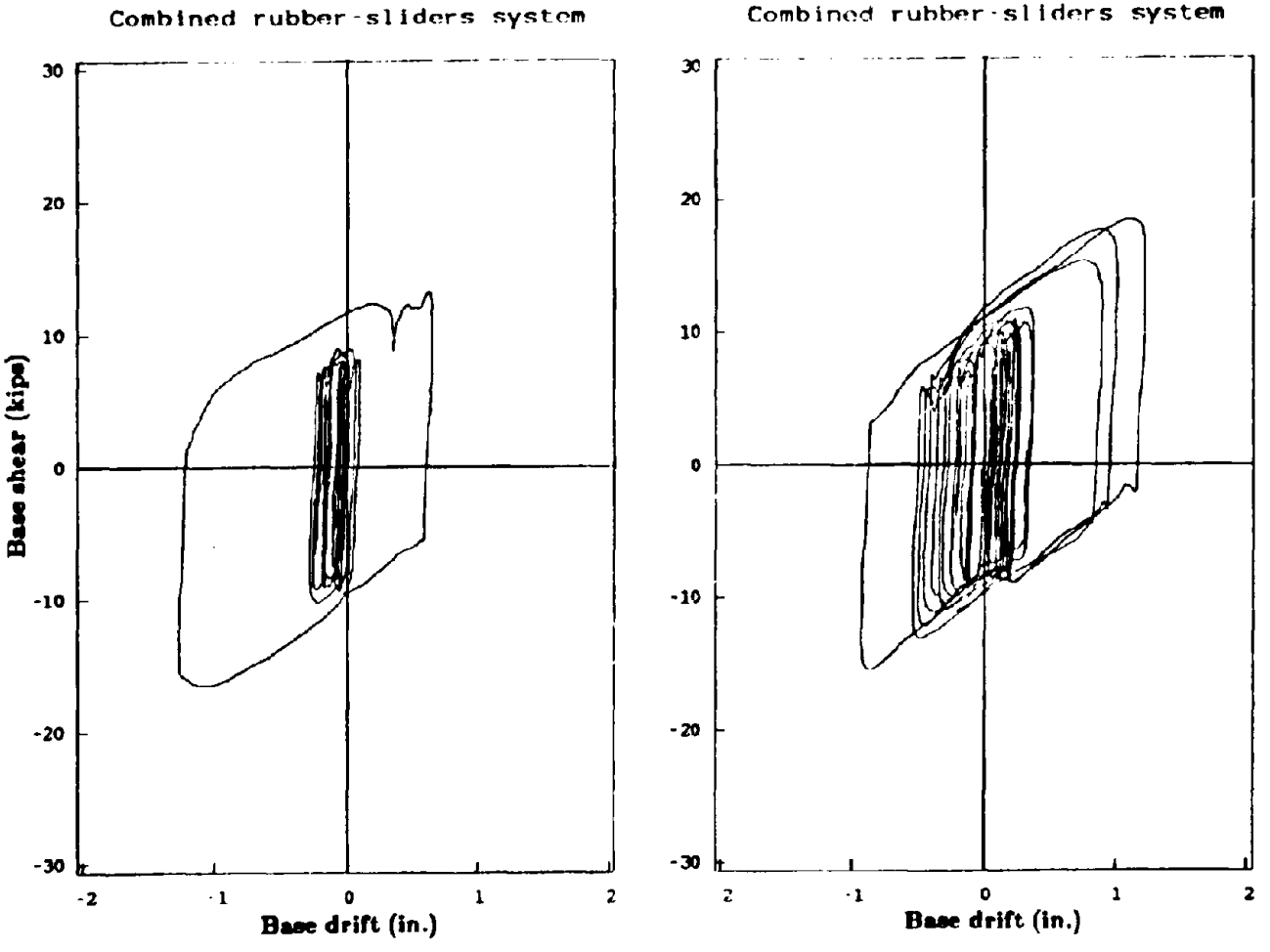

Figure 7.33 Base shear hysteresis loop at isolation interface for Bucharest 300 horizontal span (PTA=0.27g, left) and Miyagi-Ken-Oki 350 horizontal span (PTA=0.33g, right).

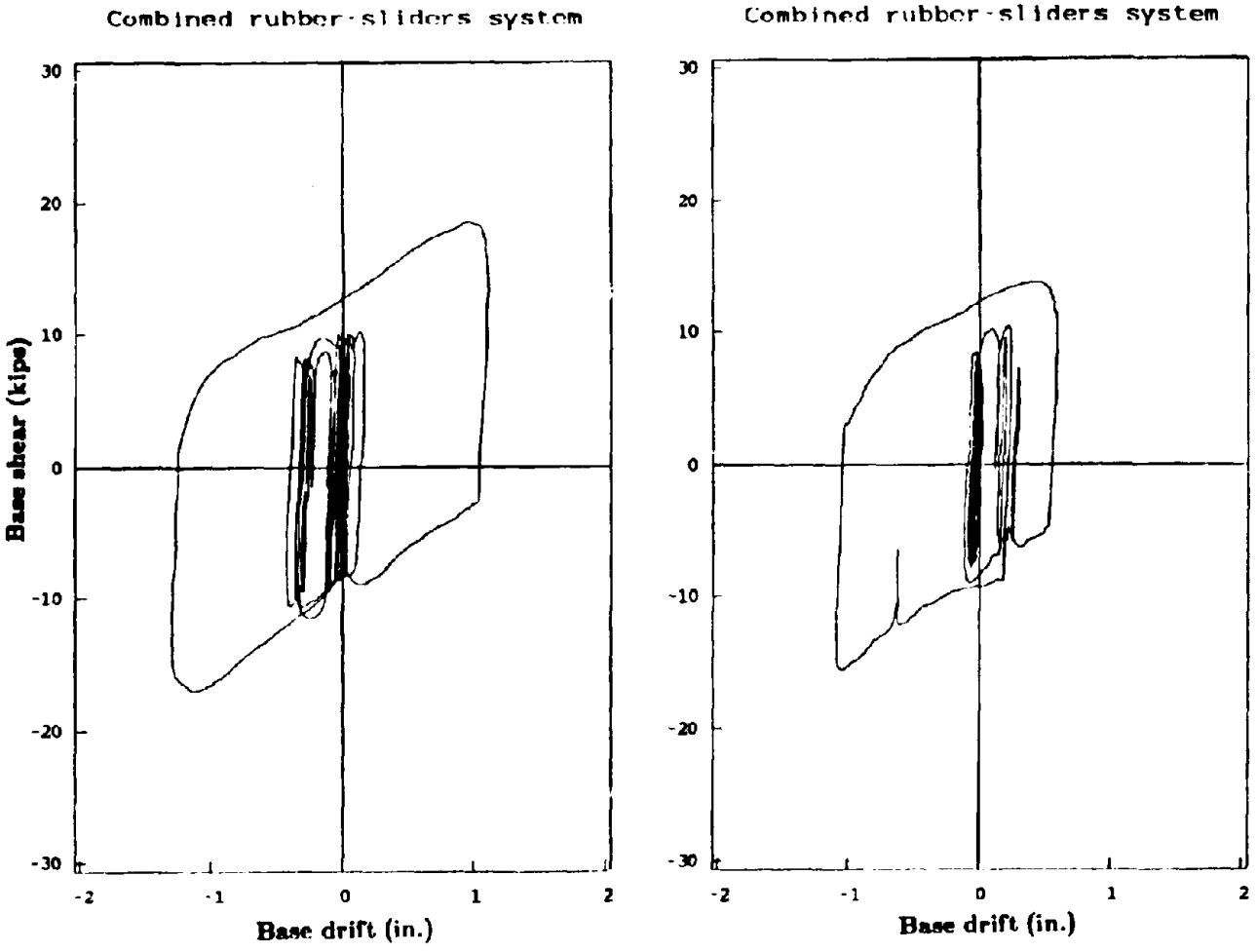

Figure 7.34 Base shear hysteresis loop at isolation interface for Pacoima Dam 350 horizontal span (PTA=0.49g, left) and Parkfield 350 horizontal span (PTA=0.41g, right).

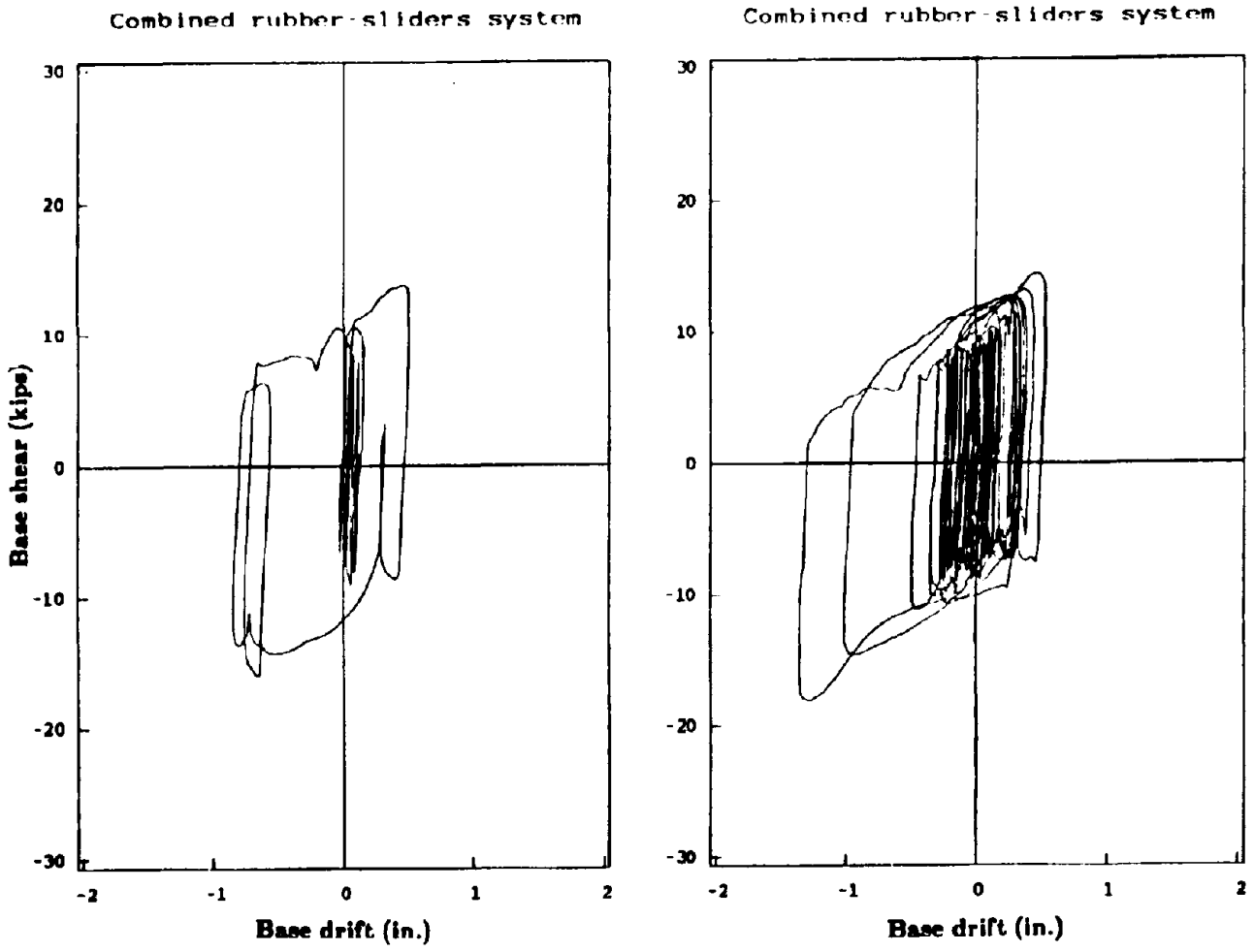

Figure 7.35 Base shear hysteresis loop at isolation interface for San Francisco 200 horizontal span (PTA=1.20g, left) and Taft 350 horizontal span (PTA=0.71g, right).

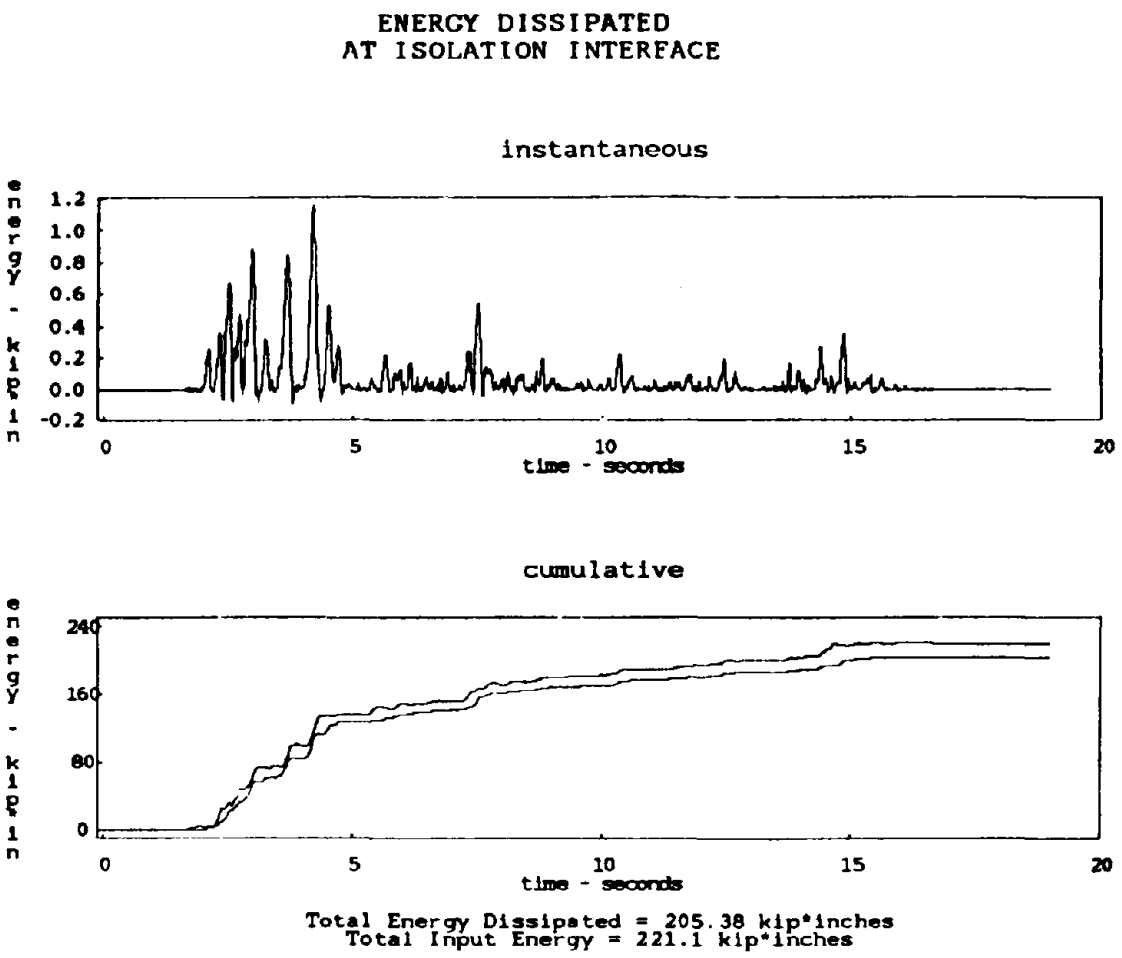

Figure 7.36 Energy dissipation at isolation interface for $\sqrt{4}$ time scaled El Centro record at 375 horizontal span (PTA=0.73g).

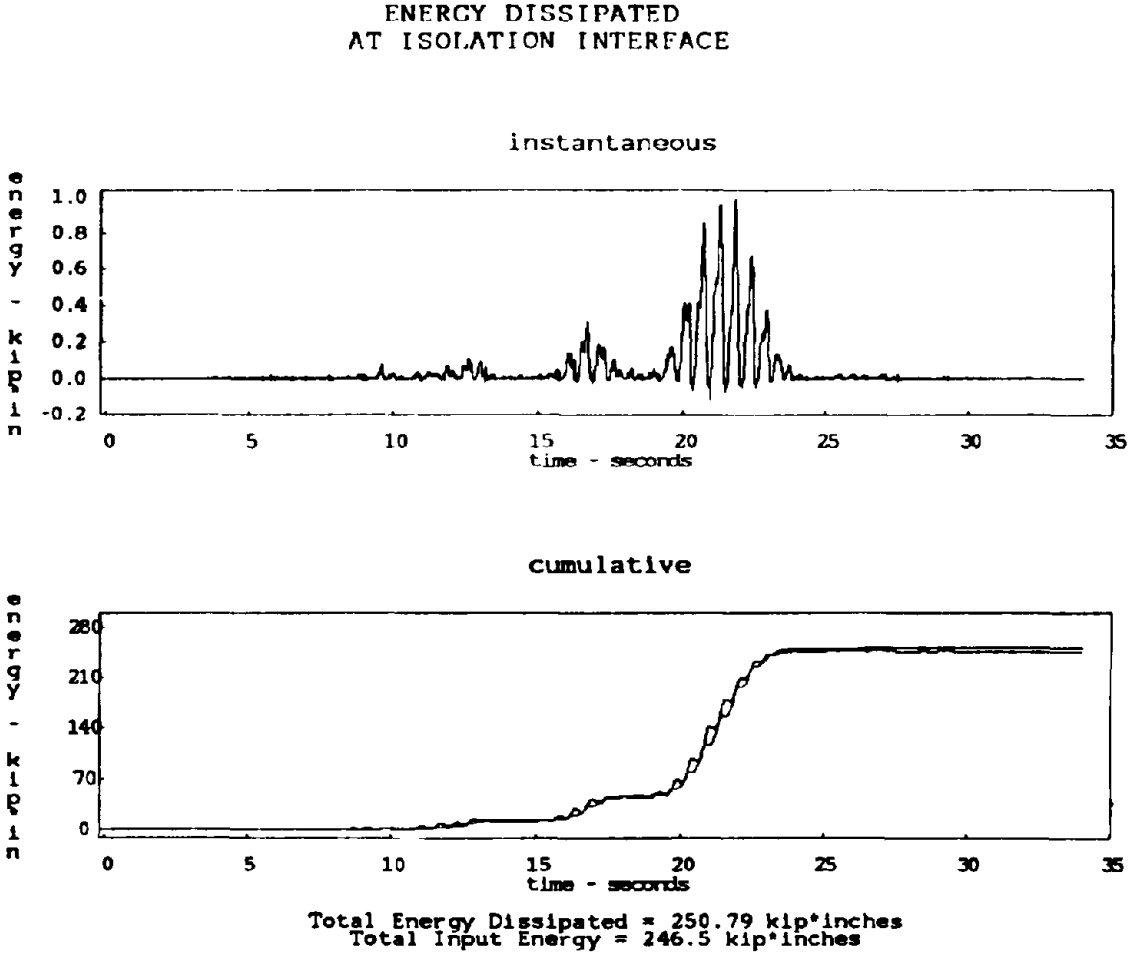

Figure 7.37 Energy dissipation at isolation interface for $\sqrt{4}$ time scaled Mexico City record at 375 horizontal span (PTA=0.18g).

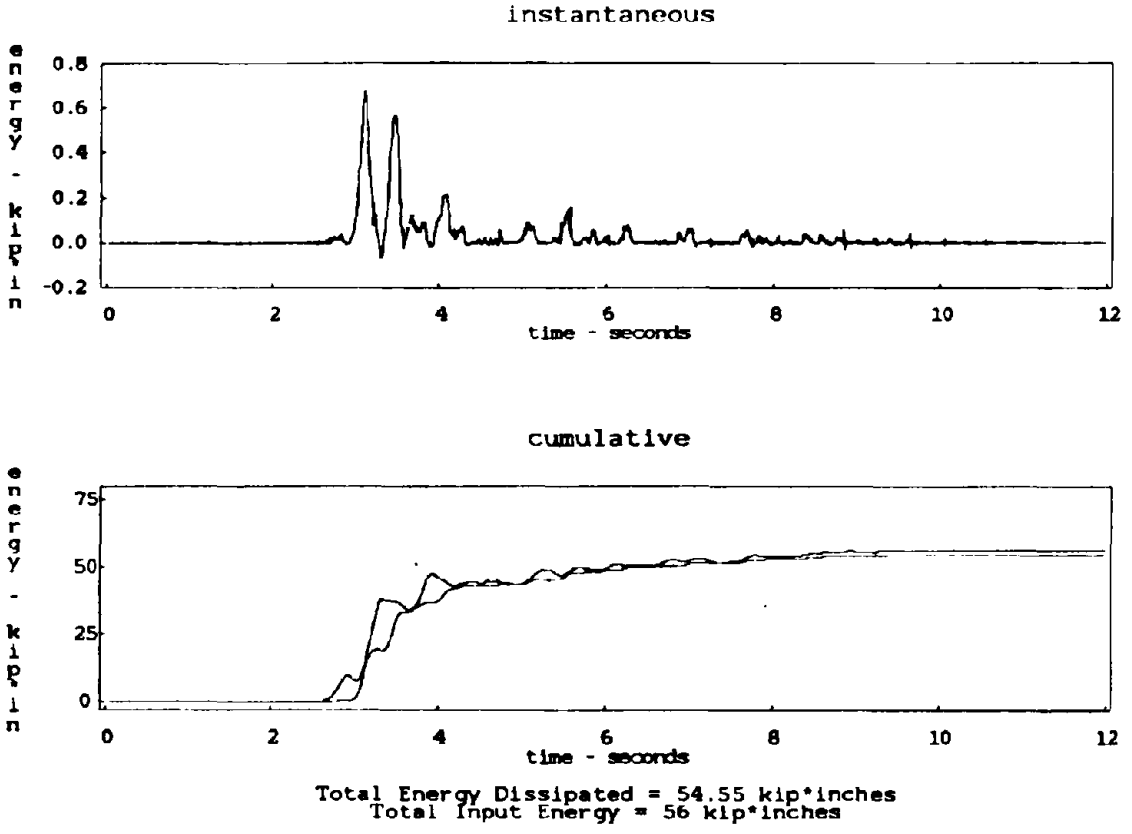

Figure 7.38 Energy dissipation at isolation interface for $\sqrt{4}$ time scaled Bucharest record at 300 horizontal span (PTA=0.27g).

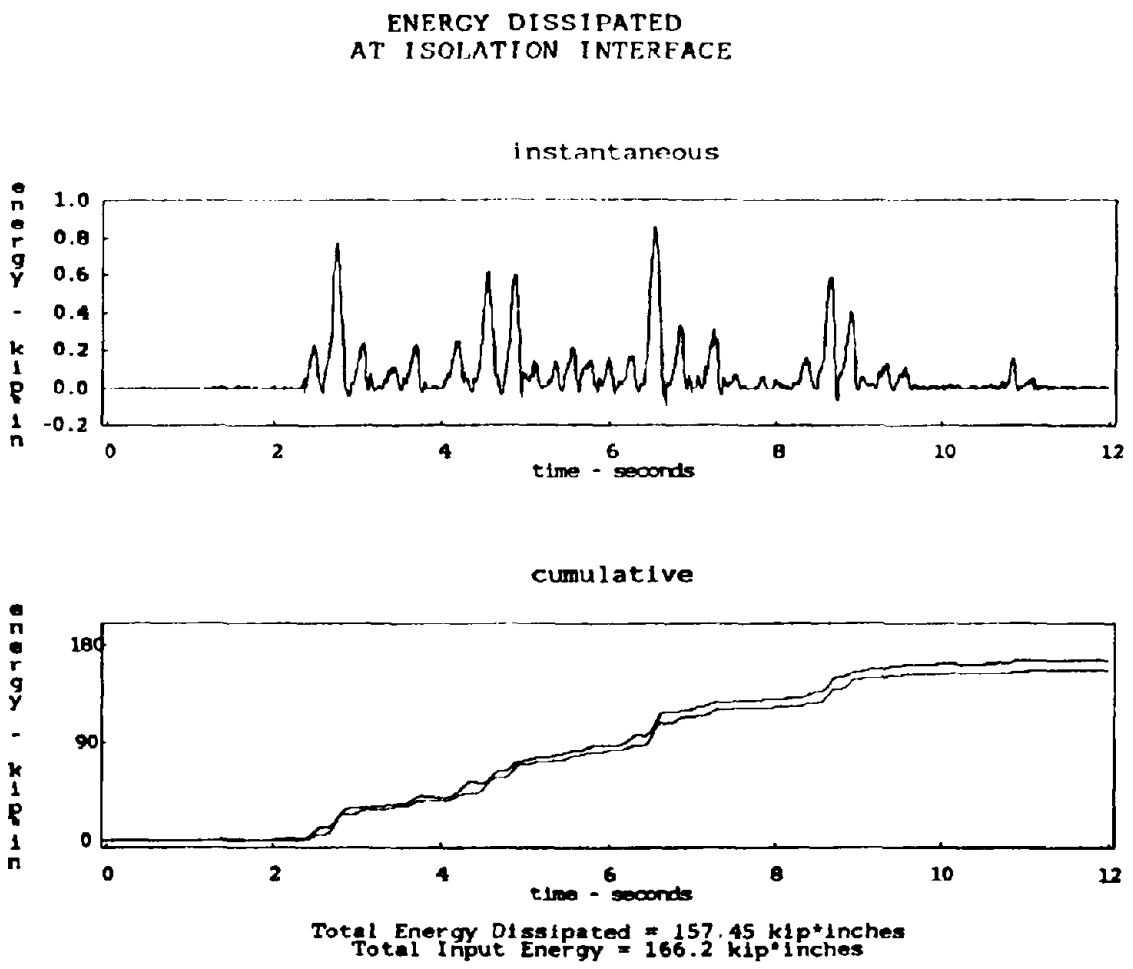

Figure 7.39 **Energy dissipation at isolation interface for $\sqrt{4}$ time scaled Miyagi-Ken-Oki record at 350 horizontal span (PTA=0.33g).**

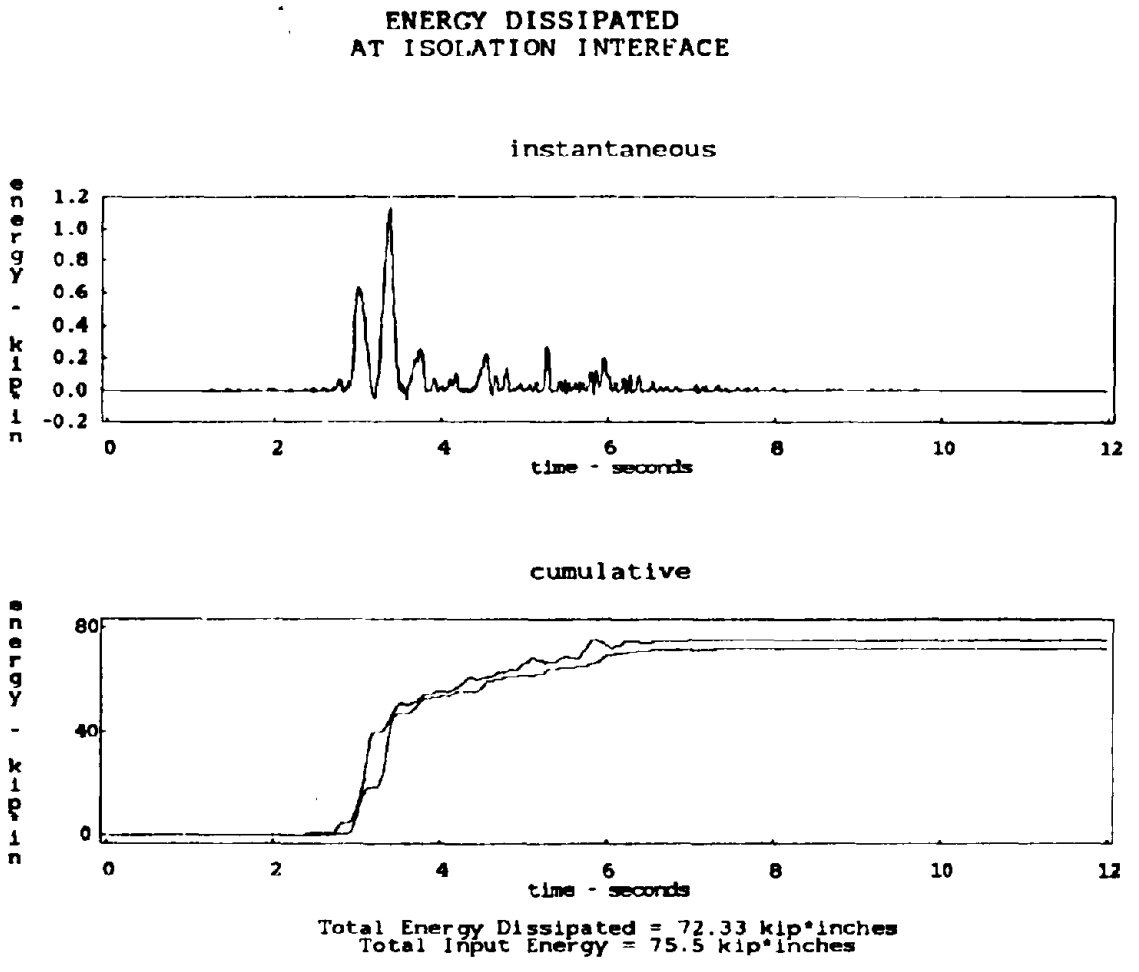

Figure 7.40 **Energy dissipation at isolation interface for √4 time scaled Pacoima Dam record at 350 horizontal span (PTA=0.49g).**

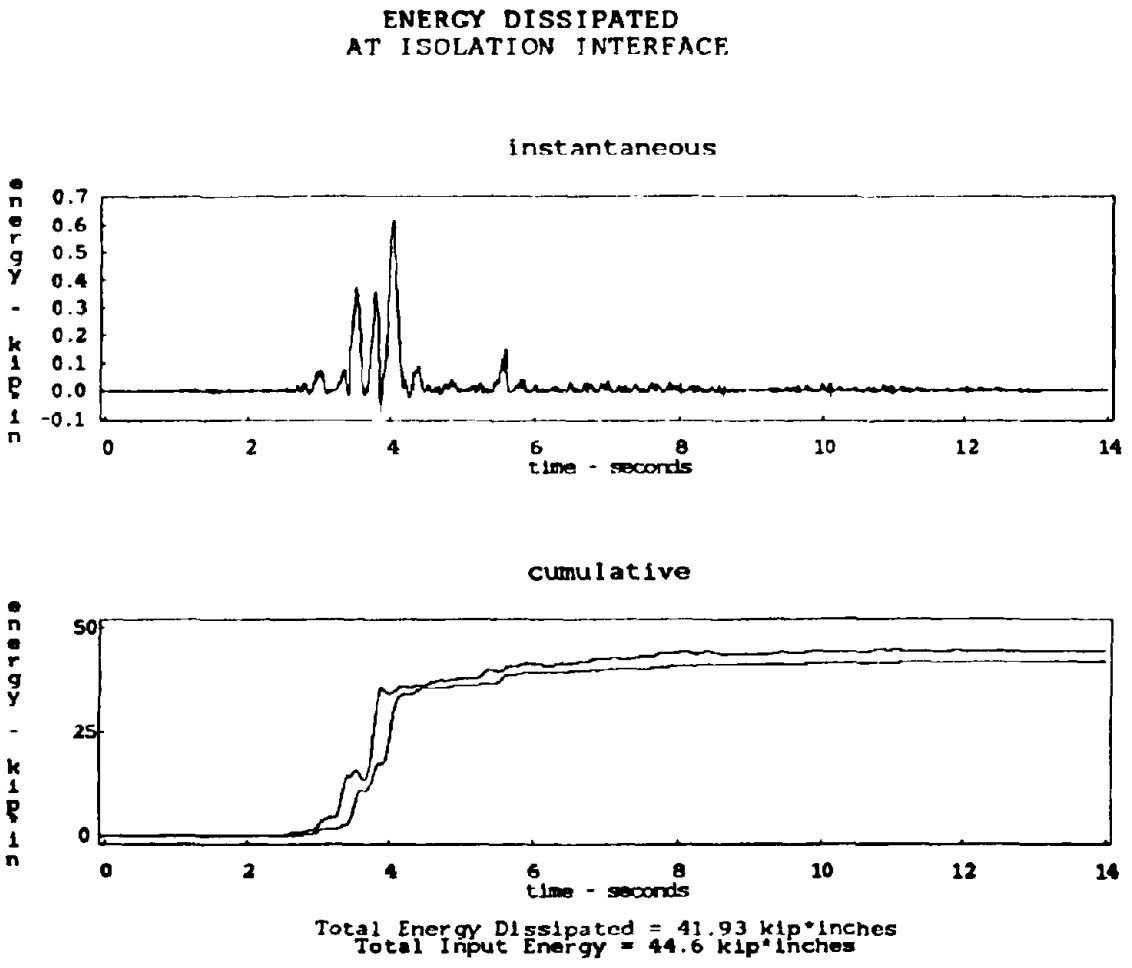

Figure 7.41 **Energy dissipation at isolation interface for $\sqrt{4}$ time scaled Parkfield record at 350 horizontal span (PTA=0.41g).**

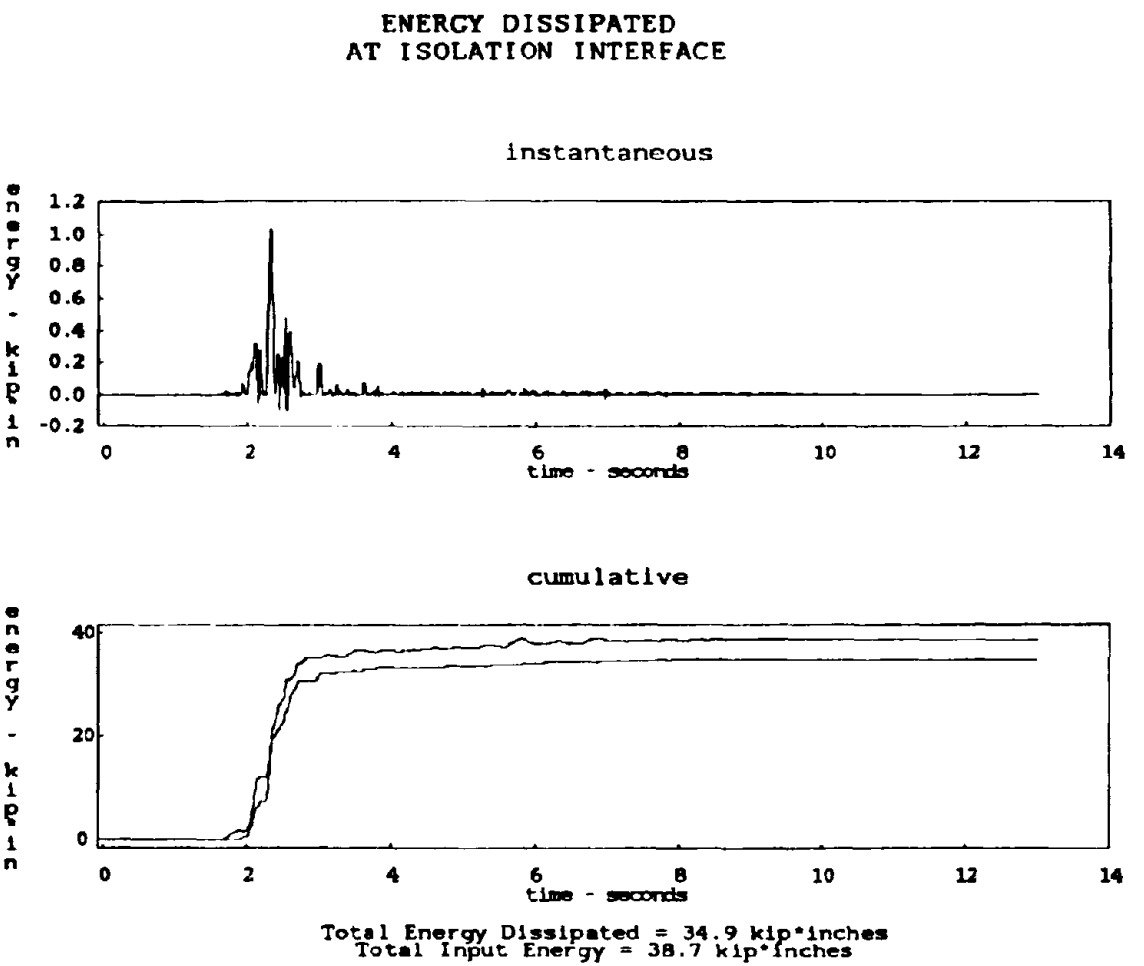

Figure 7.42 Energy dissipation at isolation interface for $\sqrt{4}$ time scaled San Francisco record at 200 horizontal span (PTA=1.20g).

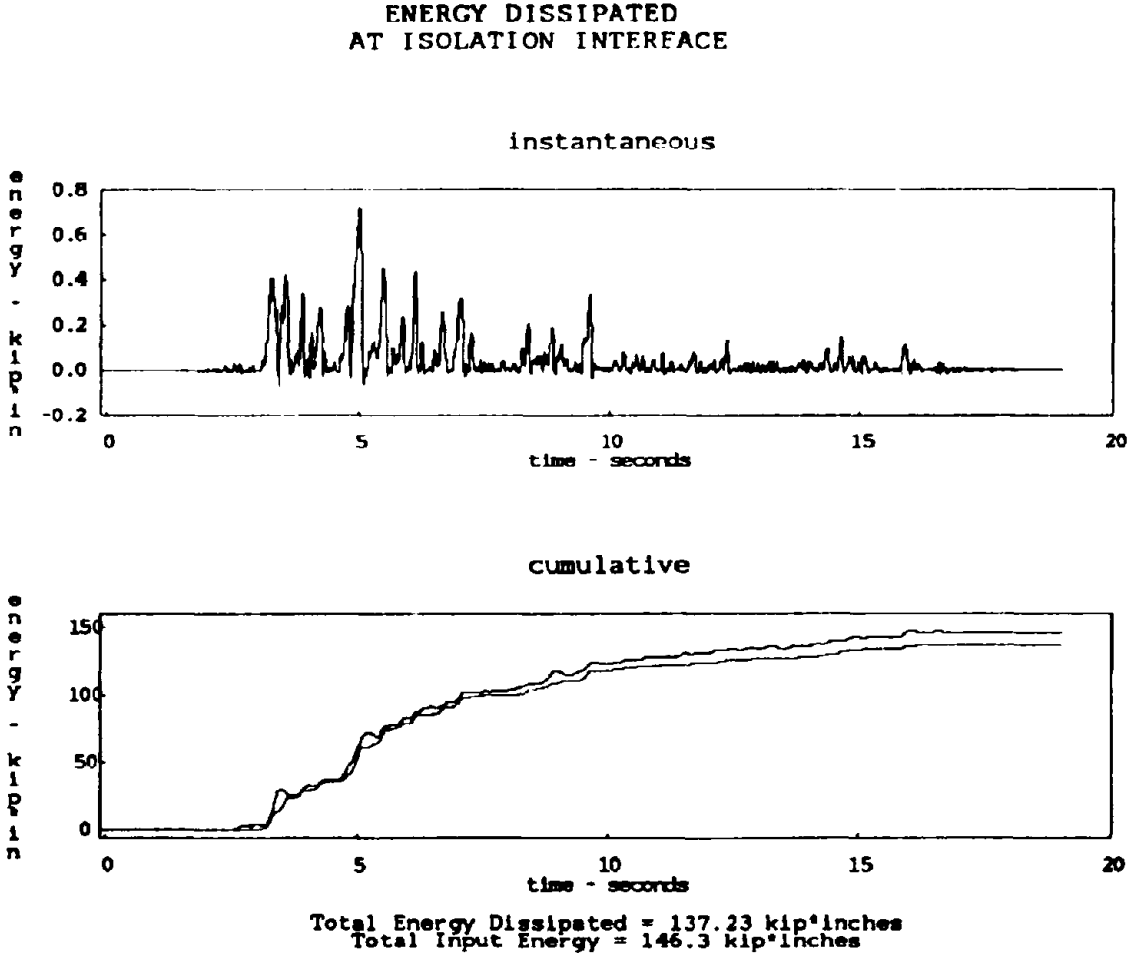

Figure 7.43 **Energy dissipation at isolation interface for $\sqrt{4}$ time scaled Taft record at 350 horizontal span (PTA=0.72g).**

CHAPTER EIGHT

COMPARISON OF EARTHQUAKE SIMULATOR TEST RESULTS WITH SEAONC TENTATIVE CODE

1. General

The Base Isolation Subcommittee of the Seismology Committee of the Structural Engineers Association of Northern California (SEAONC) prepared a tentative code in 1986, for base-isolated structures [14]. This tentative code proposed two main procedures for the seismic analysis of base-isolated structures. The first approach uses simplified formulas similar to the equivalent static analysis formulas recommended by the Uniform Building Code. The second approach uses dynamic analysis procedures (time history and response spectra analyses). In this chapter, the values obtained from code simplified formulas are compared with experimental results from shaking table tests.

2. Displacements

The requirement for the minimum base displacement of an isolated structure to be accommodated by its isolation system, as recommended in the tentative code is

$$D = \frac{10ZNST}{B} \tag{8.1}$$

where S is a soil factor, ranging from 1.0 for hard soils to 2.7 for very soft soils, T is the fundamental period of the building obtained by considering the structure as a single degree-of-freedom oscillator, and B is a factor related to the damping in the isolation system. The code provides tables for the above coefficients.

ZN is interpreted as a "Design Ground Shaking" parameter. ATC 3-06 recommends a smoothed elastic response spectrum for 5 % damping to be used as a basic tool for the quantitative description of the intensity and the frequency content of the effects of local ground conditions [15]. ATC 3-06 also suggests the better solution that consists of using four or more acceleration time histories from which an average response spectrum is extracted. Both approaches are based on response spectra and do not account for ground motion duration which is an important factor in the loss of strength of structures.

The use of base isolation provides a system that can withstand the repeated loading, thus eliminating the concern about the loss of strength of the superstructure, if it were to be conventionally designed.

The intensity of "Design Ground Shaking" is represented by two parameters the Effective Peak Acceleration (EPA), A_a, and the Effective Peak Velocity (EPV), which yields the Velocity Related Acceleration coefficient, A_v. The EPA is obtained by averaging the spectral accelerations between the periods of 0.1 and 0.5 second and reducing the average by a factor of 2.5. For the one-fourth scale steel model used in the present experiment, the period limits are replaced by 0.05 and 0.25 second, respectively. A_a is then the numerical value of EPA divided by g. The EPV is obtained by taking the spectral velocity at 1 second period and reducing it by a factor of 2.5. Instead, the ordinate at 0.5 second is used here for comparison with the model response. A_v is then obtained from EPV/30. Maps representing the EPA and EPV for various seismic regions are available and are discussed in ATC 3-06 1984; in the present comparison, however, the numerical procedure described above is used.

The A_a and A_v coefficients of the eight records used were computed for different ranges of periods and tabulated in Table T-8.1. The response spectra of the $\sqrt{4}$ time scaled earthquake records used in the calculation of A_a and A_v are shown in Figures 5.1b-5.8b.

Equation (8.1) approximates long-period displacements obtained from 5 % damped response spectra and was developed for full scale structures. For a one-fourth scale structural model, equation (8.1) becomes

$$D = \frac{5ZNST}{B} \tag{8.2}$$

T is obtained from equation (8.3), using the minimum effective stiffness, K_{min}, of the isolation system, and the total weight of the structure, W:

$$T = 2\pi \sqrt{W/g\, K_{min}} \tag{8.3}$$

In the case of the slider-bearing system, the effective stiffness depended on the base relative displacement, which changed with the type of excitation. For the various records applied to the system, the lowest effective stiffness was 11.8 k/in.; with a total weight of 91 kips the effective period

would be 0.89 second. Note that the horizontal drift was limited by tension devices installed in the corner rubber bearings, and that the maximum allowed displacement of the isolation system could be used to obtain the lowest equivalent stiffness of the system.

The soil factor was taken as $S_4 = 2.7$ for the Mexico City record, $S_1 = 1.0$ for the San Francisco record, $S_3 = 2.0$ for the Bucharest record, and $S_2 = 1.5$ for the rest of the signals.

The factor ZN in equation (8.2) was obtained from two different considerations: from recorded peak table acceleration, and from the EPA and EPV calculations suggested in the ATC 3-06 1984 Building Code and listed in Table T-8.1. For the sake of observation different combinations were used to determine the displacements. The D_{ij} values were obtained using the controlling value of A_{a_i} and A_{v_i}. In order to compare the present code recommendations with the experimental results, D_{11} obtained from A_{a_1} (EPA for $T_1 = 0.05$ second and $T_2 = 0.25$ second) or A_{v_1} (EPV for $T = 0.5$ second) was used and the ratios D_{11}/D_{test} are listed in Table T-8.2.

It was noticed that the code formula is slightly conservative for records of intermediate frequency content, and overestimates the recorded base displacement for high frequency excitations. For instance, D_{11}/D_{test} is about 4 for the San Francisco record. There was a major concern about the underestimated result for low frequency inputs such as the Mexico City record for which D_{11}/D_{test} is about 0.5. This is due to the dependence of the factor ZN on the ground acceleration. For the Mexico City signal those accelerations were very low, nevertheless it was the most severe input for base isolation systems. One interpretation is that buildings on soft soil need not be isolated, but it is preferable to introduce a factor that makes the code displacement increase substantially for this case in order to translate the severity of low frequency ground motions for isolation systems.

The period range recommended by the code does not relate to the particular structure under consideration, and thus ignores the crucial period band in which amplification in the response might occur. For this reason, the code formula was also used with an EPA obtained from the average spectral acceleration between 0.29 and 1.4 seconds which correspond to the fixed base and to the sliding conditions, respectively. The response spectra used was for 20% damping to match the

equivalent damping of the system calculated from the base shear hysteresis loops. This approach still needs some improvement but it gave results that were more consistent with the measured displacements. When the average spectral acceleration $\overline{S}_a$ (0.29 sec < T < 1.4 sec) was used, the ratios of code displacement to test displacement were 1.32 for El Centro, 1.05 for Mexico City, 1.10 for Bucharest, 1.01 for Parkfield, 1.03 for Taft and about 0.95 for the Miyagi, Pacoima and San Francisco records. Furthermore, the average spectral displacement $\overline{S}_d$ was very close to the measured base displacement. These results are listed in Table T-8.3.

3. Base Shear

According to the tentative code, the part of the structure that is above the isolation interface, should be designed to withstand a minimum shear force of

$$V_s = \frac{K_{max} D}{R_w/2} \tag{8.4}$$

where the values for the factor R_w, which takes into account the structural system used, according to the code are the same as for a non-isolated structure but should not be taken more than 8. $R_w/2$ can be regarded as a base shear reduction coefficient that accounts for the ductility of the superstructure. Since one of the important advantages of base isolation is to protect the structure from deforming into the inelastic range, the expression $K_{eff}D_{code}$ was used for comparison with the maximum base shear obtained from shake table tests. This is equivalent to taking $R_w/2=1$. The stiffness used in the code base shear calculation is the average equivalent stiffness for the eight records listed in Table T-7.6. It was noticed that the code overestimates the base shear for high frequency excitations (San Francisco), and might underestimate it for low frequency signals (Mexico City). The values are shown in Table T-8.4.

4. Lateral Force Distribution

From the experimental data, the force at a given story level was obtained by summing the inertia force time histories acting on the part of the structure above this level. Since the damping in the

structure is very small this should yield the story shear (elastic force f_s). This approach was verified at the base; the base shear obtained by adding up the inertia forces compares well (4 % relative error) with the forces recorded by the load cells located under the base. From the recorded story shear time histories of all floors, an envelope for the shear distribution along the elevation of the model was obtained. SEAONC provides a simplified formula for the lateral force distribution along the elevation of the building. The distribution is given by

$$F_x = \frac{V_s W_x}{\sum_{i=1}^{n} W_i} \tag{8.5}$$

where W_x is the weight at level x, and V_s is the base shear obtained from equation (8.4) with the reduction coefficient $R_w/2$ taken as unity.

5. Comparison with Response Spectra Analysis

Despite the nonlinearity introduced by the sliders in the properties of the isolation system, the basic feature of base isolation of causing the building motion to be controlled by merely one mode shape, was preserved. For instance, by considering Figures 7.7-7.14 which show the deflected shape of the structure at maximum story displacements, it was noticed that they followed a certain pattern independent of the excitation. The vectors containing the story displacements relative to the table, normalized to the highest story displacement (seventh story) varied slightly with the type of excitation and span. The vector containing the average values for all eight records is

$$\Phi = [\ 0.68\ \ 0.74\ \ 0.77\ \ 0.80\ \ 0.94\ \ \ 0.96\ \ 0.98\ \ 1.00\ \ 0.92\ \ 0.93\ ]^T \tag{8.6}$$

where the average displacement normalized to the seventh story displacement is 0.68 at the base and 0.93 at the ninth story. Thus the distribution is close to constant along the height of the building and a vector of ones can be used. However, the vector in equation (8.6) will be used here in a response spectrum analysis, treating the 9 DOF structure and the isolated base as a 10 DOF linear system.

the response quantity is then given by

$$L = \Phi^T \mathbf{m}\ [1] = 0.21 \tag{8.7}$$

where [1] is a 10x1 vector of ones and **m** is the mass matrix. The modal mass is given by

$$M = \Phi^T \mathbf{m} \Phi = 0.18 \tag{8.8}$$

the story displacements and story shears vectors are given by:

$$v_{max} = \Phi\ \frac{L}{M}\ S_d(\xi, T) \tag{8.9}$$

$$f_{max} = \mathbf{m}\ \Phi\ \frac{L}{M}\ S_a(\xi, T) \tag{8.10}$$

where S_d and S_a are the displacement and pseudo-acceleration spectral values. These can be obtained from Figures 5.1b-5.8b for a damping ratio of 20 %, since this level of damping was experimentally determined for almost all applied table motions (Table T-7.6). In the choice of the spectral quantities, it was taken into account that the isolation system had two distinct stiffnesses, one infinite and corresponding to no sliding when the base shear is below the sliding threshold, and one that equals the stiffness of the four rubber bearings. For this reason, the average spectral value $\overline{S_a}$ was used in equation (8.10). This approach might be conservative since it uses a non reduced linear response spectrum, nevertheless it yielded better correlation with the test results than the code formula. The story shear distribution for test, code formula, and response spectrum analysis are shown in Figures 8.1-8.8.

Generally, the analysis using a response spectrum with 20% damping along with the average spectral values at a period band pertinent to the properties of the structure yielded results closer to the experimental ones than the code formula did.

6. Future Research and Conclusions

Earthquake records of low frequency content generally contain low accelerations, and thus would result in low values of Peak Table Acceleration (PTA) and/or Effective Peak Acceleration (EPA).

When these values are used in the code formulas they yield underestimated base displacements which contradict theoretical and experimental results that low frequency inputs are extremely severe to base isolation systems and produce excessive base drift. ATC 3-06 recommended using the controlling value of either A_a or A_v in order to account for the high velocities caused by low frequency large amplitude displacements, however, A_v was introduced as a spectral velocity ordinate corresponding to one period value. This approach seemed insufficient in describing the "Design Ground Shaking" corresponding to the low frequency inputs used in the present experiment. Instead, a range of periods of the same width as the one used for EPA but centered around a 1 second period (0.5 seconds for the model) was used in the pseudo-velocity response spectra. The factor 30 by which the EPV was reduced to yield A_v as was concluded from ATC 3-06 Section C1.4.1 F, p. 301, caused low values of A_v. It is suggested that for correlation with dynamic test results, the reducing factor 30 should be replaced by $30/\sqrt{S}$ where S is the geometric scale of the structural model used.

Approximate preliminary design of base isolated structures can be performed by using simplified formulas. Despite the non-linearity in the properties of the sliding bearing and rubber bearing combined system it was shown that simplified formulas can predict displacements and forces within 40 % of overestimation. This amount of uncertainty is unavoidable in most preliminary designs. However, the parameters used to characterize the "Design Ground Shaking" need to be studied in more detail. In the case of base isolated structures it is necessary that the Velocity Related Acceleration Coefficient be given a more careful treatment. Also, for structural systems that might be influenced by repeated loading, a special coefficient representing the duration of ground motion should be defined. In general, however, isolation systems are tested against cyclic loading before gaining acceptance. In a response spectra analysis, where the structure was expected to possess varying fundamental period, the average value of the spectral ordinates between these two periods was used and yielded good results.

Table T-8.1 EPA and EPV values with the corresponding code displacements for the eight records used.

file	A_{a1}	A_{a2}	A_{v1}	A_{v2}	A_{v3}	A_{v4}	D_{11}	D_{12}	D_{23}	D_{24}
ELC375	0.570	0.618	0.502	0.449	0.349	0.367	2.57	2.57	2.78	2.78
MEX375	0.128	0.103	0.088	0.097	0.763	0.564	1.04	1.04	6.18	4.57
BUC300	0.192	0.212	0.243	0.239	0.290	0.286	1.46	1.43	1.74	1.72
MIY350	0.255	0.319	0.453	0.369	0.247	0.233	2.72	2.21	1.91	1.91
PAC350	0.468	0.337	0.288	0.289	0.229	0.225	2.12	2.11	1.52	1.52
PAR350	0.308	0.309	0.146	0.151	0.216	0.219	1.39	1.39	1.39	1.39
SFR200	1.096	0.592	0.249	0.231	0.091	0.096	3.29	3.29	1.78	1.78
TAF350	0.569	0.464	0.223	0.252	0.258	0.280	2.56	2.56	2.09	2.09

A_{a1} between T_1=0.05*s*. and T_2=0.25*s*.

A_{a2} between T_1=0.10*s*. and T_2=0.50*s*.

A_{v1} at T_1=0.50*s*. (/30)

A_{v2} between T_1=0.40*s*. and T_2=0.60*s*.

A_{v3} at T_1=1.0*s*. (/30)

A_{v4} between T_1=0.80*s*. and T_2=1.20*s*.

Table T-8.2 Comparison of code displacement with test displacement showing overestimation for high frequency inputs and underestimation for low frequency inputs.

input	Soil Factor S	PTA	D_{PTA}	D_{11}	D_{test}	$\frac{D_{PTA}}{D_{test}}$	$D\frac{sub\,11}{D_{test}}$
ELC375	1.5	0.73	3.25	2.57	1.36	2.39	1.89
MEX375	2.7	0.18	1.44	1.04	1.91	0.75	0.54
BUC300	2.0	0.27	1.60	1.46	1.27	1.26	1.15
MIY350	1.5	0.33	1.47	2.72	1.22	1.20	2.23
PAC350	1.5	0.49	2.18	2.12	1.30	1.68	1.63
PAR350	1.5	0.41	1.82	1.39	1.09	1.67	1.28
SFR200	1.0	1.20	3.56	3.29	0.84	4.24	3.92
TAF350	1.5	0.72	3.20	2.56	1.36	2.35	1.88

Table T-8.3 Measured base displacement, average spectral displacement, and average spectral acceleration over 0.29 sec < T < 1.4 sec.

	D_{test} (in)	$\overline{S_d}$ (in)	$\overline{S_a}$ (in/sec^2)
ELC375	1.36	2.27	162.0
MEX375	1.91	2.19	96.5
BUC300	1.27	1.55	91.1
MIY350	1.22	1.36	100.3
PAC350	1.30	1.55	106.1
PAR350	1.09	1.42	92.5
SFR200	0.84	0.87	81.9
PAR350	1.36	1.53	110.2

Table T-8.4 Maximum base shear from Code Formula, Test, and Response Spectra Analysis.

-	Maximum Base shear			
filename	F_{code} (k.)	F_{test} (k.)	F'_{test} (k.)	F_{rspct} (k.)
861119.03 ELC375	36.5	20.2	20.7	38.3
861119.04 MEX375	14.8	24.3	24.5	22.8
861119.05 BUC300	20.7	16.3	16.6	21.6
861119.06 MIY350	38.6	16.5	16.7	23.7
861119.07 PAC350	30.1	17.2	17.4	25.1
861119.08 PAR350	19.7	15.6	16.0	21.9
861119.09 SFR200	46.7	16.0	15.9	16.0
861119.10 TAF350	36.4	18.2	18.5	26.1

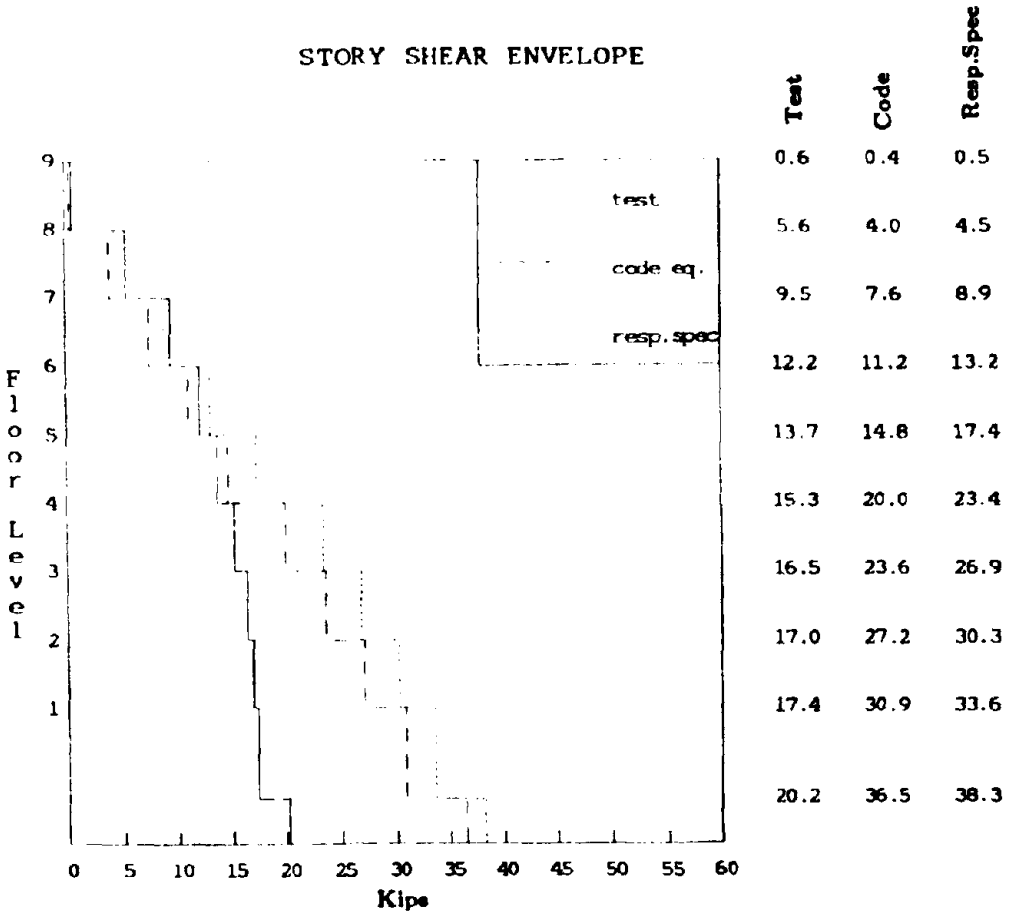

Figure 8.1 **Story shear envelope from test, code formula, and response spectra analysis. Table input: $\sqrt{4}$ time scaled El Centro, horizontal span 375, PTA=0.73 g.**

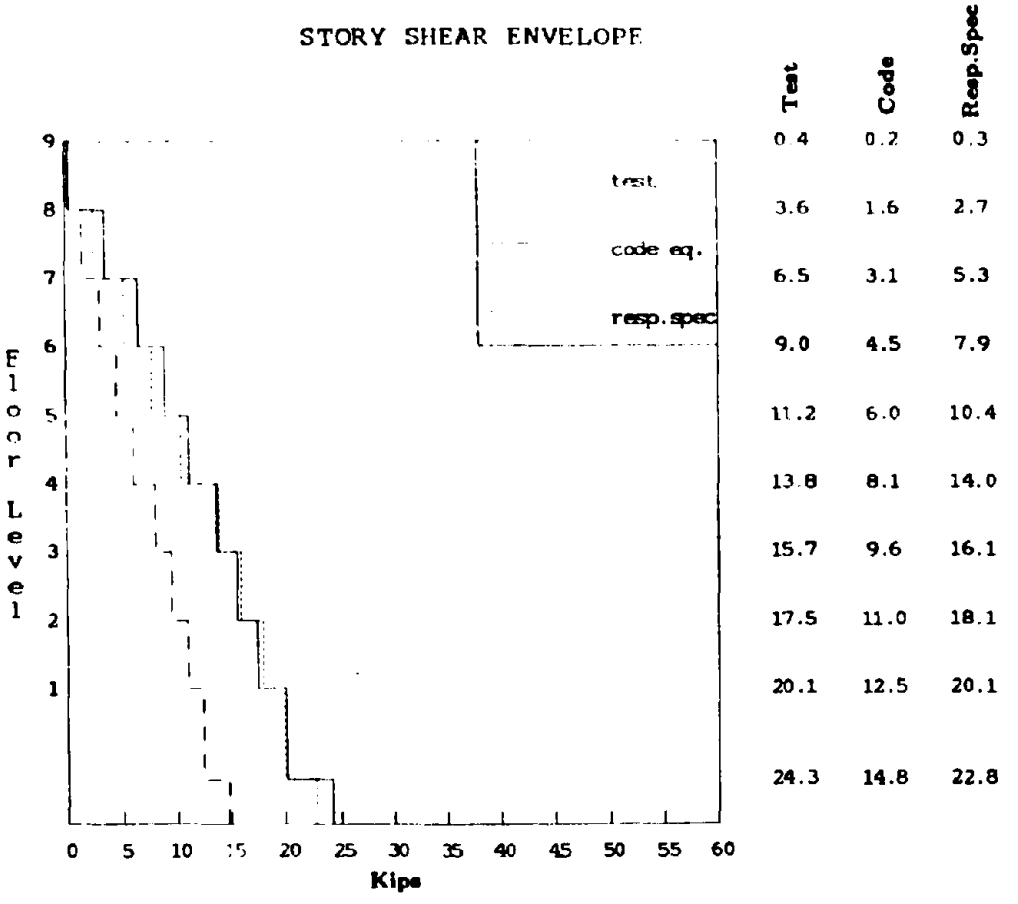

Figure 8.2 Story shear envelope from test, code formula, and response spectra analysis. Table input: √4 time scaled Mexico City, horizontal span 375, PTA=0.18 g.

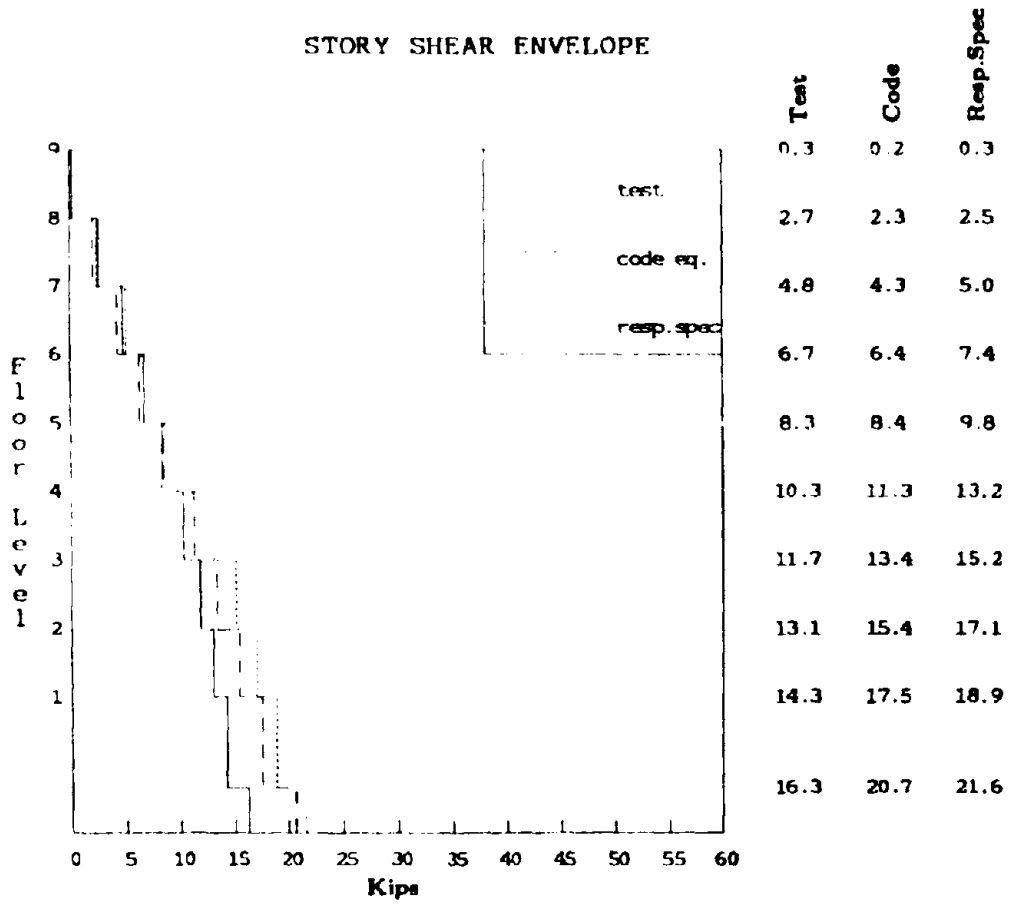

Figure 8.3 Story shear envelope from test, code formula, and response spectra analysis. Table input: √4 time scaled Bucharest, horizontal span 300, PTA=0.27 g.

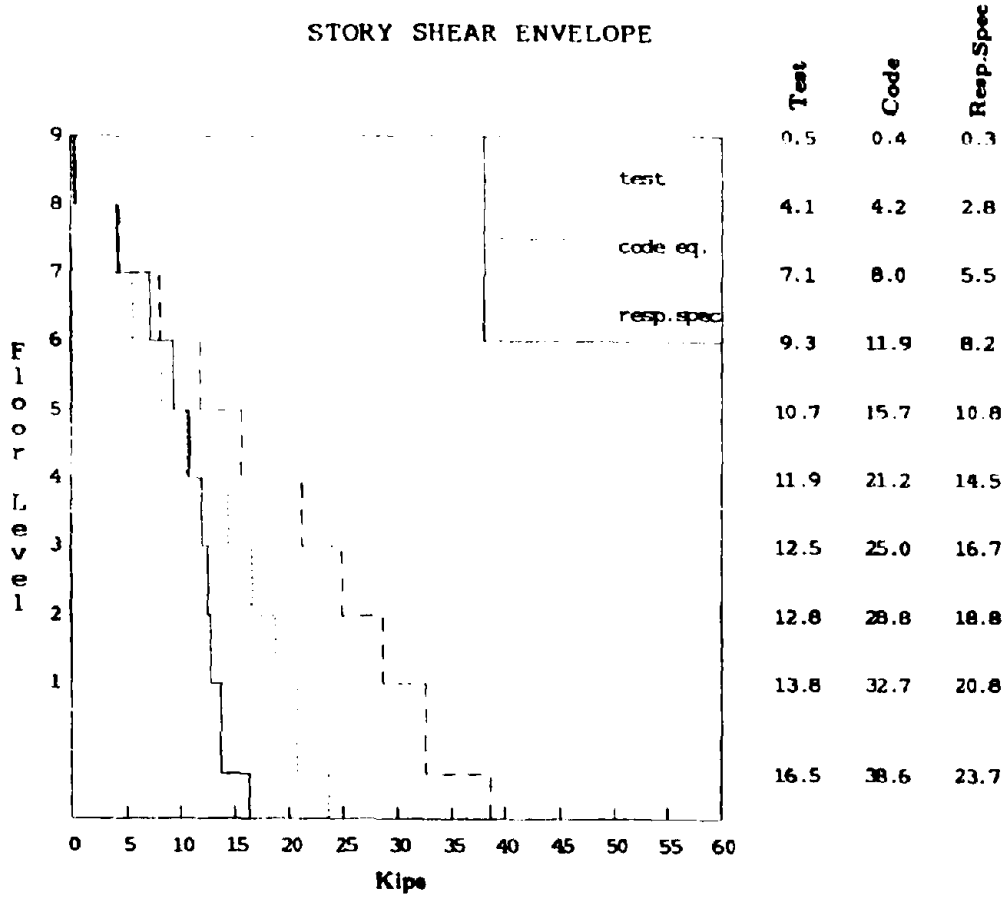

Figure 8.4 Story shear envelope from test, code formula, and response spectra analysis. Table input: √4 time scaled Miyagi-Ken-Oki, horizontal span 350, PTA=0.33 g.

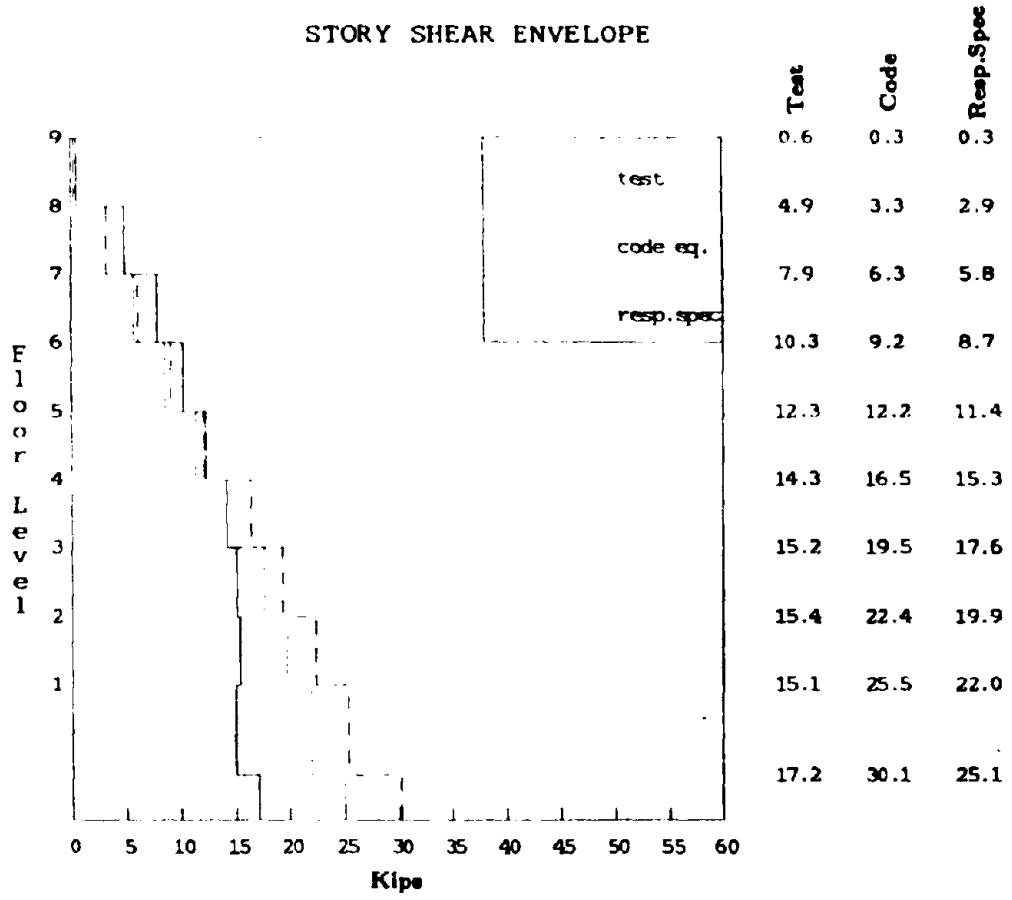

Figure 8.5 Story shear envelope from test, code formula, and response spectra analysis. Table input: $\sqrt{4}$ time scaled Pacoima Dam, horizontal span 350, PTA=0.49 g.

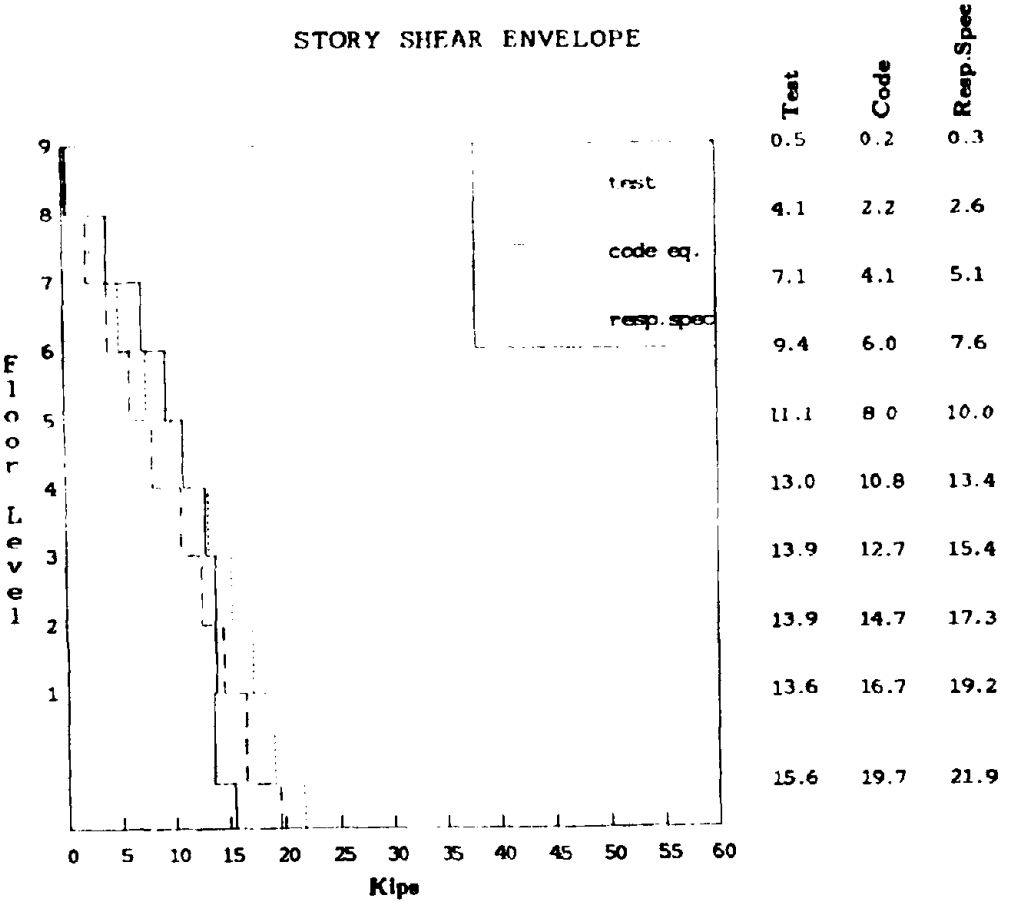

Figure 8.6 Story shear envelope from test, code formula, and response spectra analysis. Table input: $\sqrt{4}$ time scaled Parkfield, horizontal span 350, PTA=0.41 g.

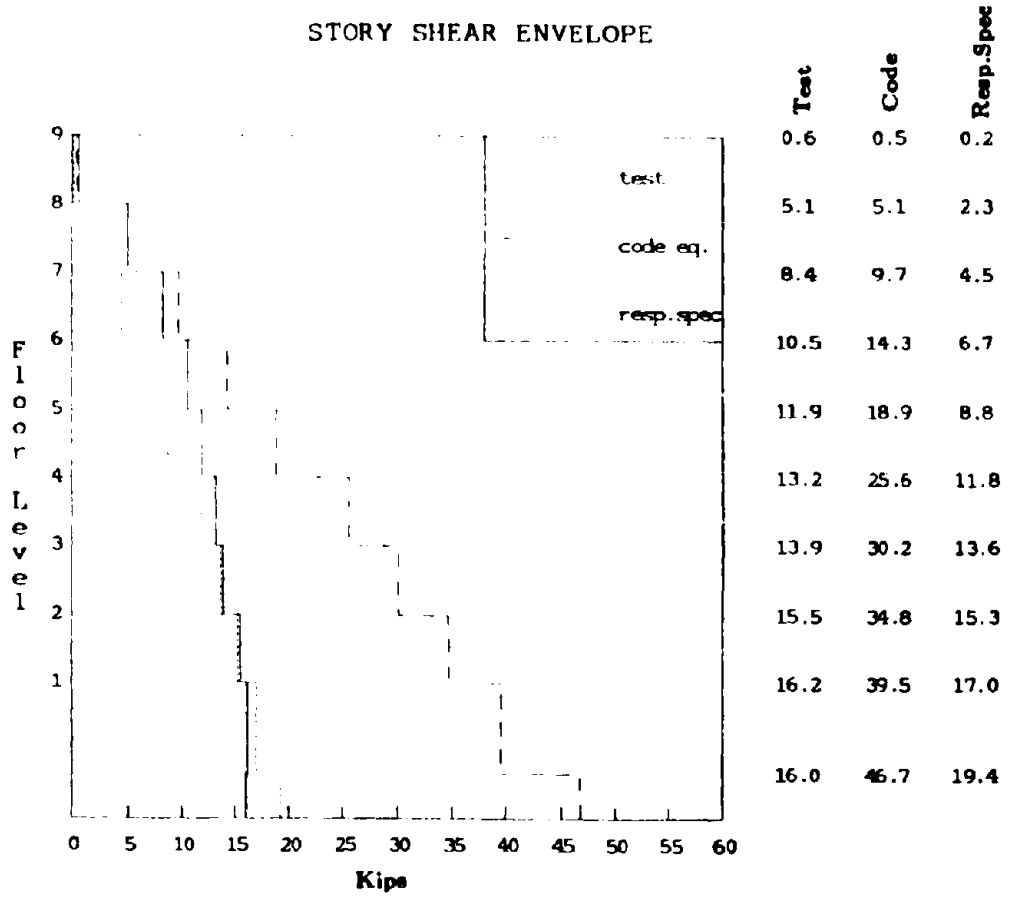

Figure 8.7 Story shear envelope from test, code formula, and response spectra analysis. Table input: $\sqrt{4}$ time scaled San Francisco, horizontal span 200, PTA=1.20 g.

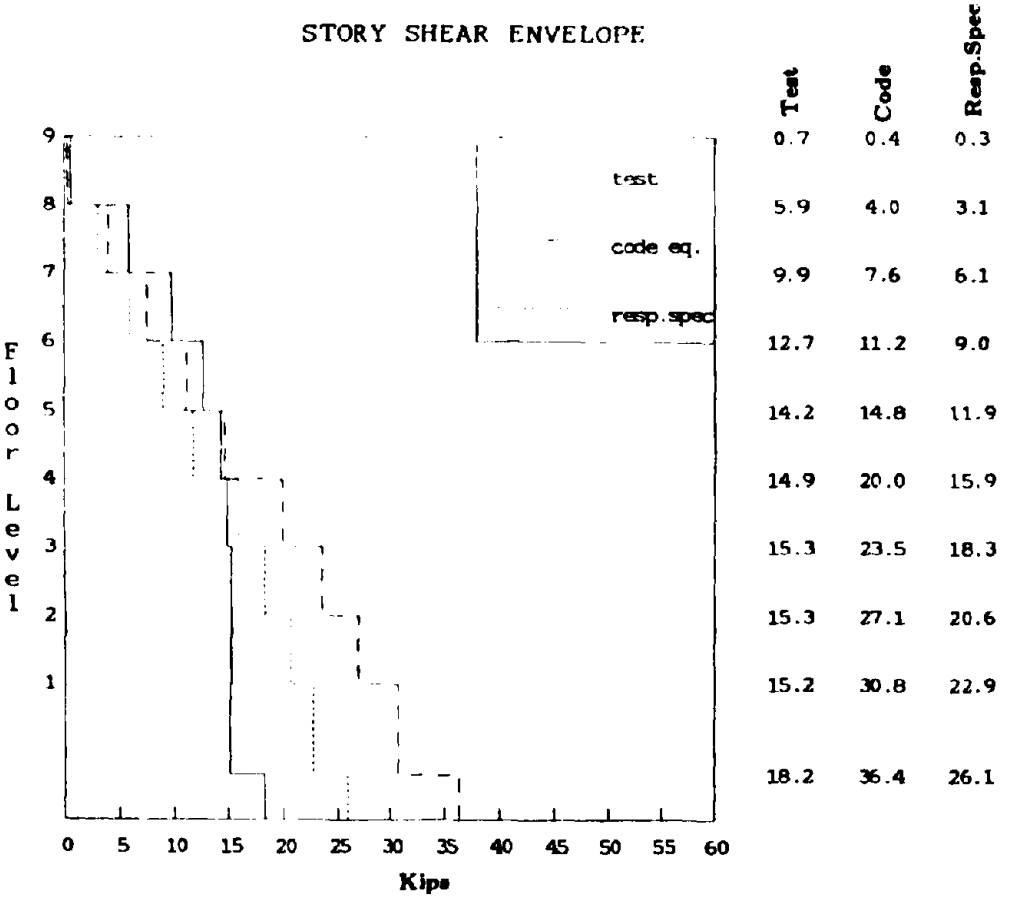

Figure 8.8 Story shear envelope from test, code formula, and response spectra analysis. Table input: $\sqrt{4}$ time scaled Taft, horizontal span 350, PTA=0.72 g.

CHAPTER NINE
CONCLUSIONS

Various base isolation systems have previously been proposed but most of them need separate accessories to provide wind restraint, displacement control, stability and fail-safe capacity. Systems that provide large reduction of ground accelerations usually consist of horizontally flexible rubber bearings solely. These, however, might present stability problems in case of accidental excessive base drift, and thus need a support on which the structure can depend in case of bearing buckling or roll-out. Furthermore, the damping that elastomers provide does not always meet the level of energy dissipation needed. On the other hand, a system that is very economical and close to existing practice consists of frictional elements currently used for purposes other than earthquake protection. In this study, these two systems were combined into a new one that satisfies all requirements for the earthquake isolation of structures. The threshold of sliding provides wind restraint, the friction provides energy dissipation, the reinforced rubber bearings carry part of the vertical load and recenter the structure, and the tension restraint keeps the structure from uplifting. Furthermore, since the base is constantly resting on the sliders, the fail-safe capacity is inherent.

The earthquake simulator testing showed that the inclusion of teflon sliders in the base-isolation system drastically improves the control of displacements at the cost of slightly reducing the acceleration reduction efficiency of a solely rubber system. For the same model, where fixed base tests resulted in acceleration amplification ratios as high as 6, the combined slider-rubber system yielded ratios around 1, whereas a solely rubber system typically yields ratios around 0.5. The solely rubber systems, however, resulted in base displacements around 3 times the ones that correspond to the combined slider-rubber system.

The high energy dissipation is characterized by the large area enclosed in the base shear hysteresis loops, and on the average the system provided an equivalent damping of about 20%.

The so-called Alexisismon system uses sliders combined with unreinforced neoprene pads that act as restoring springs [16]. This system has two major differences from the one described in this report. The neoprene springs in that system are not allowed to carry any axial load and all the weight of the

building is carried by the sliders. This causes the base response, specifically the base shear sliding threshold, to be totally controlled by the weight of the building and by the friction coefficient of the sliders which changes with velocity, temperature and pressure. Thus, the above arrangement does not allow the designer to distribute the weight of the building on both sliders and reinforced bearings. In the present system, the base shear threshold can be better controlled by appropriate choice of the size of the sliding area which can be decreased to a very low percentage, since sliders here are not required to carry the total weight of the building. On the other hand, excessive drift of the base may cause tension in the neoprene springs and thus make them more vulnerable to external factors such as ozone attacks, while in the case of the reinforced rubber bearings used here, they are initially under compression by carrying a fraction of the weight of the structure and this risk is eliminated. In the case of accidental excessive base drift, part of the vertical load that is initially carried by the rubber is transferred to the sliders and prevents the rubber bearings from buckling.

Many analytical studies have been performed on such systems and mathematical models using equivalent linear systems have been proposed but none of them accounted for the varying friction coefficient. The dependence of this coefficient on the velocity of sliding is important since it causes stiffening in the system as the base relative velocity increases. Numerical derivation of the measured base displacements on the shake table yielded sliding velocities of up to 12 in./sec. A variation of this magnitude causes the teflon coefficient of friction to change by a factor as high as two, thus doubling the shear resistance of the sliders.

When the results from formulas recommended in 1986 by the SEAONC seismology subcommittee for the design of base isolated structures were compared with the measured values, the displacements were found to be overly conservative for earthquakes of high accelerations and frequencies, and were underestimated for low frequency inputs. The base shear and the force distribution code formulas need to be examined in more detail since they yielded values as high as three times the measured forces for some earthquake inputs. More specifically, the coefficient R_w needs a more careful interpretation since it was initially defined for conventionally designed fixed base structures that are expected to dissipate energy by yielding. A simplified approach using a response

spectra analysis, that was considered, yielded satisfactory results.

REFERENCES

[1] Kelly J. M., "Aseismic Base Isolation: review and bibliography", *Soil Dynamics and Earthquake Engineering*, Vol. 5, No. 3, 1986.

[2] Kelly J. M., and Tsztoo D. F., "The Development of Energy-Absorbing Devices for Aseismic Base Isolation Systems", *Report No. UCB/EERC-78/01*, Earthquake Engineering Research Center, University of California, Berkeley, California, 1978.

[3] Kelly J. M., and Chitty D. E., "Testing of a Wind Restraint for Aseismic Base Isolation", *Report No. UCB/EERC-78/20*, Earthquake Engineering Research Center, University of California, Berkeley, California, 1978.

[4] Kelly J. M., Beucke K. E., and Skinner M., "Experimental Testing of a Friction Damped Aseismic Base Isolation System with Fail-Safe Characterisitics", *Report No. UCB/EERC-80/18*, Earthquake Engineering Research Center, University of California, Berkeley, California, 1980.

[5] Delfosse G. C., "Full Earthquake Protection through Base Isolation System", *7th World Conference on Earthquake Engineering*, Istanbul, Turkey, Vol. 8, p. 61, 1980.

[6] Plichon C., Gueraud R., Richli M. H., and Casagrande J. F., "Protection of Nuclear Power Plants against Seism", *Nuclear Technology* Vol. 49, pp. 295-306, 1980.

[7] Tarics A. G., "The Implementation of Base Isolation for the Foothill Communities Law and Justice Center", *Report to the National Science Foundation and the County of San Bernardino*, Reid and Tarics Associates, San Francisco, CA, 1984.

[8] Walter M., Elsesser E., and Allen E. W., "Base Isolation of the Existing City and County Building in Salt Lake City", *Proceedings, Seminar on Base Isolation and Passive Energy Dissipation*, ATC-17, Applied Technology Council, San Francisco, pp. 113-122, 1986.

[9] Stanton J. F., and Roeder C. W., "Elastomeric Bearing Design, Construction and material", *Report No. 248, Transportation Research Board, National Research Council*, pp. 17-27, Washington D. C., 1982.

[10] Chalhoub M. S., and Kelly J. M., "Reduction of the Stiffness of Rubber Bearings due to Compressibility", *Report No. SESM-86/06*, University of California, Berkeley, 1986.

[11] Aslam M., Godden W. G., and Scalise D. T., "Sliding Response of Rigid Bodies to Earthquake Motions", *Report to the U.S. Energy Research and Development Administration*, Lawrence Berkeley Laboratory, 1975.

[12] Tyler R. G., "Dynamic Tests on PTFE Sliding Layers under Earthquake Conditions", *Bulletin of the New Zealand National Society for Earthquake Engineering*, Vol.10, No.3, September 1977.

[13] Taylor M. E., "PTFE in Highway Bridge Bearings", *Report No. LR 491, Transport and Road Research Laboratory*, Department of the Environment, Crowthorne, Berkshire, 1972.

[14] Base Isolation Committee of the Seismological Committee of the Structural Engineers Association of Northern California, "Tentative Seismic Isolation Design Requirements", SEAONC, 1986.

[15] Applied Technology Council, "Tentative Provisions for the Development of Seismic Regulations for Buildings", ATC 3-06, June 1978.

[16] Ikonomou A. S., "Alexisismon Isolation Engineering for Nuclear Power Plants", *Nuclear Engineering and Design*, Vol. 85, 2, pp. 210-216, 1985.

EARTHQUAKE ENGINEERING RESEARCH CENTER REPORT SERIES

EERC reports are available from the National Information Service for Earthquake Engineering(NISEE) and from the National Technical Information Service(NTIS). Numbers in parentheses are Accession Numbers assigned by the National Technical Information Service; these are followed by a price code. Contact NTIS, 5285 Port Royal Road, Springfield Virginia, 22161 for more information. Reports without Accession Numbers were not available from NTIS at the time of printing. For a current complete list of EERC reports (from EERC 67-1) and availability information, please contact University of California, EERC, NISEE, 1301 South 46th Street, Richmond, California 94804.

UCB/EERC-81/01 "Control of Seismic Response of Piping Systems and Other Structures by Base Isolation," by Kelly, J.M., January 1981, (PB81 200 735)A05.

UCB/EERC-81/02 "OPTNSR- An Interactive Software System for Optimal Design of Statically and Dynamically Loaded Structures with Nonlinear Response," by Bhatti, M.A., Ciampi, V. and Pister, K.S., January 1981, (PB81 218 851)A09.

UCB/EERC-81/03 "Analysis of Local Variations in Free Field Seismic Ground Motions," by Chen, J.-C., Lysmer, J. and Seed, H.B., January 1981, (AD-A099508)A13.

UCB/EERC-81/04 "Inelastic Structural Modeling of Braced Offshore Platforms for Seismic Loading," by Zayas, V.A., Shing, P.-S.B., Mahin, S.A. and Popov, E.P., January 1981, (PB82 138 777)A07.

UCB/EERC-81/05 "Dynamic Response of Light Equipment in Structures," by Der Kiureghian, A., Sackman, J.L. and Nour-Omid, B., April 1981, (PB81 218 497)A04.

UCB/EERC-81/06 "Preliminary Experimental Investigation of a Broad Base Liquid Storage Tank," by Bouwkamp, J.G., Kollegger, J.P. and Stephen, R.M., May 1981, (PB82 140 385)A03.

UCB/EERC-81/07 "The Seismic Resistant Design of Reinforced Concrete Coupled Structural Walls," by Aktan, A.E. and Bertero, V.V., June 1981, (PB82 113 358)A11.

UCB/EERC-81/08 "Unassigned," by Unassigned, 1981.

UCB/EERC-81/09 "Experimental Behavior of a Spatial Piping System with Steel Energy Absorbers Subjected to a Simulated Differential Seismic Input," by Stiemer, S.F., Godden, W.G. and Kelly, J.M., July 1981, (PB82 201 898)A04.

UCB/EERC-81/10 "Evaluation of Seismic Design Provisions for Masonry in the United States," by Sveinsson, B.I., Mayes, R.L. and McNiven, H.D., August 1981, (PB82 166 075)A08.

UCB/EERC-81/11 "Two-Dimensional Hybrid Modelling of Soil-Structure Interaction," by Tzong, T.-J., Gupta, S. and Penzien, J., August 1981, (PB82 142 118)A04.

UCB/EERC-81/12 "Studies on Effects of Infills in Seismic Resistant R/C Construction," by Brokken, S. and Bertero, V.V., October 1981, (PB82 166 190)A09.

UCB/EERC-81/13 "Linear Models to Predict the Nonlinear Seismic Behavior of a One-Story Steel Frame," by Valdimarsson, H., Shah, A.H. and McNiven, H.D., September 1981, (PB82 138 793)A07.

UCB/EERC-81/14 "TLUSH: A Computer Program for the Three-Dimensional Dynamic Analysis of Earth Dams," by Kagawa, T., Mejia, L.H., Seed, H.B. and Lysmer, J., September 1981, (PB82 139 940)A06.

UCB/EERC-81/15 "Three Dimensional Dynamic Response Analysis of Earth Dams," by Mejia, L.H. and Seed, H.B., September 1981, (PB82 137 274)A12.

UCB/EERC-81/16 "Experimental Study of Lead and Elastomeric Dampers for Base Isolation Systems," by Kelly, J.M. and Hodder, S.B., October 1981, (PB82 166 182)A05.

UCB/EERC-81/17 "The Influence of Base Isolation on the Seismic Response of Light Secondary Equipment," by Kelly, J.M., April 1981, (PB82 255 266)A04.

UCB/EERC-81/18 "Studies on Evaluation of Shaking Table Response Analysis Procedures," by Blondet, J. M., November 1981, (PB82 197 278)A10.

UCB/EERC-81/19 "DELIGHT.STRUCT: A Computer-Aided Design Environment for Structural Engineering," by Balling, R.J., Pister, K.S. and Polak, E., December 1981, (PB82 218 496)A07.

UCB/EERC-81/20 "Optimal Design of Seismic-Resistant Planar Steel Frames," by Balling, R.J., Ciampi, V. and Pister, K.S., December 1981, (PB82 220 179)A07.

UCB/EERC-82/01 "Dynamic Behavior of Ground for Seismic Analysis of Lifeline Systems," by Sato, T. and Der Kiureghian, A., January 1982, (PB82 218 926)A05.

UCB/EERC-82/02 "Shaking Table Tests of a Tubular Steel Frame Model," by Ghanaat, Y. and Clough, R.W., January 1982, (PB82 220 161)A07.

UCB/EERC-82/03 "Behavior of a Piping System under Seismic Excitation: Experimental Investigations of a Spatial Piping System supported by Mechanical Shock Arrestors," by Schneider, S., Lee, H.-M. and Godden, W. G., May 1982, (PB83 172 544)A09.

UCB/EERC-82/04 "New Approaches for the Dynamic Analysis of Large Structural Systems," by Wilson, E.L., June 1982, (PB83 148 080)A05.

UCB/EERC-82/05 "Model Study of Effects of Damage on the Vibration Properties of Steel Offshore Platforms," by Shahrivar, F. and Bouwkamp, J.G., June 1982, (PB83 148 742)A10.

UCB/EERC-82/06 "States of the Art and Pratice in the Optimum Seismic Design and Analytical Response Prediction of R/C Frame Wall Structures," by Aktan, A.E. and Bertero, V.V., July 1982, (PB83 147 736)A05.

UCB/EERC-82/07 "Further Study of the Earthquake Response of a Broad Cylindrical Liquid-Storage Tank Model," by Manos, G.C. and Clough, R.W., July 1982, (PB83 147 744)A11.

UCB/EERC-82/08 "An Evaluation of the Design and Analytical Seismic Response of a Seven Story Reinforced Concrete Frame," by Charney, F.A. and Bertero, V.V., July 1982, (PB83 157 628)A09.

UCB/EERC-82/09 "Fluid-Structure Interactions: Added Mass Computations for Incompressible Fluid," by Kuo, J.S.-H., August 1982, (PB83 156 281)A07.

UCB/EERC-82/10 "Joint-Opening Nonlinear Mechanism: Interface Smeared Crack Model," by Kuo, J.S.-H., August 1982, (PB83 149 195)A05.

UCB/EERC-82/11 "Dynamic Response Analysis of Techi Dam," by Clough, R.W., Stephen, R.M. and Kuo, J.S.-H., August 1982, (PB83 147 496)A06

UCB/EERC-82/12 "Prediction of the Seismic Response of R/C Frame-Coupled Wall Structures," by Aktan, A.E., Bertero, V.V. and Piazzo, M., August 1982, (PB83 149 203)A09.

UCB/EERC-82/13 "Preliminary Report on the Smart 1 Strong Motion Array in Taiwan," by Bolt, B.A., Loh, C.H., Penzien, J. and Tsai, Y.B., August 1982, (PB83 159 400)A10.

UCB/EERC-82/14 "Seismic Behavior of an Eccentrically X-Braced Steel Structure," by Yang, M.S., September 1982, (PB83 260 778)A12.

UCB/EERC-82/15 "The Performance of Stairways in Earthquakes," by Roha, C., Axley, J.W. and Bertero, V.V., September 1982, (PB83 157 693)A07.

UCB/EERC-82/16 "The Behavior of Submerged Multiple Bodies in Earthquakes," by Liao, W.-G., September 1982, (PB83 158 709)A07.

UCB/EERC-82/17 "Effects of Concrete Types and Loading Conditions on Local Bond-Slip Relationships," by Cowell, A.D., Popov, E.P. and Bertero, V.V., September 1982, (PB83 153 577)A04.

UCB/EERC-82/18 "Mechanical Behavior of Shear Wall Vertical Boundary Members: An Experimental Investigation," by Wagner, M.T. and Bertero, V.V., October 1982, (PB83 159 764)A05.

UCB/EERC-82/19 "Experimental Studies of Multi-support Seismic Loading on Piping Systems," by Kelly, J.M. and Cowell, A.D., November 1982, (PB90 262 684)A07.

UCB/EERC-82/20 "Generalized Plastic Hinge Concepts for 3D Beam-Column Elements," by Chen, P. F.-S. and Powell, G.H., November 1982, (PB83 247 981)A13.

UCB/EERC-82/21 "ANSR-II: General Computer Program for Nonlinear Structural Analysis," by Oughourlian, C.V. and Powell, G.H., November 1982, (PB83 251 330)A12.

UCB/EERC-82/22 "Solution Strategies for Statically Loaded Nonlinear Structures," by Simons, J.W. and Powell, G.H., November 1982, (PB83 197 970)A06.

UCB/EERC-82/23 "Analytical Model of Deformed Bar Anchorages under Generalized Excitations," by Ciampi, V., Eligehausen, R., Bertero, V.V. and Popov, E.P., November 1982, (PB83 169 532)A06.

UCB/EERC-82/24 "A Mathematical Model for the Response of Masonry Walls to Dynamic Excitations," by Sucuoglu, H., Mengi, Y. and McNiven, H.D., November 1982, (PB83 169 011)A07.

UCB/EERC-82/25 "Earthquake Response Considerations of Broad Liquid Storage Tanks," by Cambra, F.J., November 1982, (PB83 251 215)A09.

UCB/EERC-82/26 "Computational Models for Cyclic Plasticity, Rate Dependence and Creep," by Mosaddad, B. and Powell, G.H., November 1982, (PB83 245 829)A08.

UCB/EERC-82/27 "Inelastic Analysis of Piping and Tubular Structures," by Mahasuverachai, M. and Powell, G.H., November 1982, (PB83 249 987)A07.

UCB/EERC-83/01 "The Economic Feasibility of Seismic Rehabilitation of Buildings by Base Isolation," by Kelly, J.M., January 1983, (PB83 197 988)A05.

UCB/EERC-83/02 "Seismic Moment Connections for Moment-Resisting Steel Frames," by Popov, E.P., January 1983, (PB83 195 412)A04.

UCB/EERC-83/03 "Design of Links and Beam-to-Column Connections for Eccentrically Braced Steel Frames," by Popov, E.P. and Malley, J.O., January 1983, (PB83 194 811)A04.

UCB/EERC-83/04 "Numerical Techniques for the Evaluation of Soil-Structure Interaction Effects in the Time Domain," by Bayo, E. and Wilson, E.L., February 1983, (PB83 245 605)A09.

UCB/EERC-83/05 "A Transducer for Measuring the Internal Forces in the Columns of a Frame-Wall Reinforced Concrete Structure," by Sause, R. and Bertero, V.V., May 1983, (PB84 119 494)A06.

UCB/EERC-83/06 "Dynamic Interactions Between Floating Ice and Offshore Structures," by Croteau, P., May 1983, (PB84 119 486)A16.

UCB/EERC-83/07 "Dynamic Analysis of Multiply Tuned and Arbitrarily Supported Secondary Systems," by Igusa, T. and Der Kiureghian, A., July 1983, (PB84 118 272)A11.

UCB/EERC-83/08 "A Laboratory Study of Submerged Multi-body Systems in Earthquakes," by Ansari, G.R., June 1983, (PB83 261 842)A17.

UCB/EERC-83/09 "Effects of Transient Foundation Uplift on Earthquake Response of Structures," by Yim, C.-S. and Chopra, A.K., June 1983, (PB83 261 396)A07.

UCB/EERC-83/10 "Optimal Design of Friction-Braced Frames under Seismic Loading," by Austin, M.A. and Pister, K.S., June 1983, (PB84 119 288)A06.

UCB/EERC-83/11 "Shaking Table Study of Single-Story Masonry Houses: Dynamic Performance under Three Component Seismic Input and Recommendations," by Manos, G.C., Clough, R.W. and Mayes, R.L., July 1983, (UCB/EERC-83/11)A08.

UCB/EERC-83/12 "Experimental Error Propagation in Pseudodynamic Testing," by Shiing, P.B. and Mahin, S.A., June 1983, (PB84 119 270)A09.

UCB/EERC-83/13 "Experimental and Analytical Predictions of the Mechanical Characteristics of a 1/5-scale Model of a 7-story R/C Frame-Wall Building Structure," by Aktan, A.E., Bertero, V.V., Chowdhury, A.A. and Nagashima, T., June 1983, (PB84 119 213)A07.

UCB/EERC-83/14 "Shaking Table Tests of Large-Panel Precast Concrete Building System Assemblages," by Oliva, M.G. and Clough, R.W., June 1983, (PB86 110 210/AS)A11.

UCB/EERC-83/15 "Seismic Behavior of Active Beam Links in Eccentrically Braced Frames," by Hjelmstad, K.D. and Popov, E.P., July 1983, (PB84 119 676)A09.

UCB/EERC-83/16 "System Identification of Structures with Joint Rotation," by Dimsdale, J.S., July 1983, (PB84 192 210)A06.

UCB/EERC-83/17 "Construction of Inelastic Response Spectra for Single-Degree-of-Freedom Systems," by Mahin, S. and Lin, J., June 1983, (PB84 208 834)A05.

UCB/EERC-83/18 "Interactive Computer Analysis Methods for Predicting the Inelastic Cyclic Behaviour of Structural Sections," by Kaba, S. and Mahin, S., July 1983, (PB84 192 012)A06.

UCB/EERC-83/19 "Effects of Bond Deterioration on Hysteretic Behavior of Reinforced Concrete Joints," by Filippou, F.C., Popov, E.P. and Bertero, V.V., August 1983, (PB84 192 020)A10.

UCB/EERC-83/20 "Correlation of Analytical and Experimental Responses of Large-Panel Precast Building Systems," by Oliva, M.G., Clough, R.W., Velkov, M. and Gavrilovic, P., May 1988, (PB90 262 692)A06.

UCB/EERC-83/21 "Mechanical Characteristics of Materials Used in a 1/5 Scale Model of a 7-Story Reinforced Concrete Test Structure," by Bertero, V.V., Aktan, A.E., Harris, H.G. and Chowdhury, A.A., October 1983, (PB84 193 697)A05.

UCB/EERC-83/22 "Hybrid Modelling of Soil-Structure Interaction in Layered Media," by Tzong, T.-J. and Penzien, J., October 1983, (PB84 192 178)A08.

UCB/EERC-83/23 "Local Bond Stress-Slip Relationships of Deformed Bars under Generalized Excitations," by Eligehausen, R., Popov, E.P. and Bertero, V.V., October 1983, (PB84 192 848)A09.

UCB/EERC-83/24 "Design Considerations for Shear Links in Eccentrically Braced Frames," by Malley, J.O. and Popov, E.P., November 1983, (PB84 192 186)A07.

UCB/EERC-84/01 "Pseudodynamic Test Method for Seismic Performance Evaluation: Theory and Implementation," by Shing, P.-S.B. and Mahin, S.A., January 1984, (PB84 190 644)A08.

UCB/EERC-84/02 "Dynamic Response Behavior of Kiang Hong Dian Dam," by Clough, R.W., Chang, K.-T., Chen, H.-Q. and Stephen, R.M., April 1984, (PB84 209 402)A08.

UCB/EERC-84/03 "Refined Modelling of Reinforced Concrete Columns for Seismic Analysis," by Kaba, S.A. and Mahin, S.A., April 1984, (PB84 234 384)A06.

UCB/EERC-84/04 "A New Floor Response Spectrum Method for Seismic Analysis of Multiply Supported Secondary Systems," by Asfura, A. and Der Kiureghian, A., June 1984, (PB84 239 417)A06.

UCB/EERC-84/05 "Earthquake Simulation Tests and Associated Studies of a 1/5th-scale Model of a 7-Story R/C Frame-Wall Test Structure," by Bertero, V.V., Aktan, A.E., Charney, F.A. and Sause, R., June 1984, (PB84 239 409)A09.

UCB/EERC-84/06 "Unassigned," by Unassigned, 1984.

UCB/EERC-84/07 "Behavior of Interior and Exterior Flat-Plate Connections subjected to Inelastic Load Reversals," by Zee, H.L. and Moehle, J.P., August 1984, (PB86 117 629/AS)A07.

UCB/EERC-84/08 "Experimental Study of the Seismic Behavior of a Two-Story Flat-Plate Structure," by Moehle, J.P. and Diebold, J.W., August 1984, (PB86 122 553/AS)A12.

UCB/EERC-84/09 "Phenomenological Modeling of Steel Braces under Cyclic Loading," by Ikeda, K., Mahin, S.A. and Dermitzakis, S.N., May 1984, (PB86 132 198/AS)A08.

UCB/EERC-84/10 "Earthquake Analysis and Response of Concrete Gravity Dams," by Fenves, G. and Chopra, A.K., August 1984, (PB85 193 902/AS)A11.

UCB/EERC-84/11 "EAGD-84: A Computer Program for Earthquake Analysis of Concrete Gravity Dams," by Fenves, G. and Chopra, A.K., August 1984, (PB85 193 613/AS)A05.

UCB/EERC-84/12 "A Refined Physical Theory Model for Predicting the Seismic Behavior of Braced Steel Frames," by Ikeda, K. and Mahin, S.A., July 1984, (PB85 191 450/AS)A09.

UCB/EERC-84/13 "Earthquake Engineering Research at Berkeley - 1984," by EERC, August 1984, (PB85 197 341/AS)A10.

UCB/EERC-84/14 "Moduli and Damping Factors for Dynamic Analyses of Cohesionless Soils," by Seed, H.B., Wong, R.T., Idriss, I.M. and Tokimatsu, K., September 1984, (PB85 191 468/AS)A04.

UCB/EERC-84/15 "The Influence of SPT Procedures in Soil Liquefaction Resistance Evaluations," by Seed, H.B., Tokimatsu, K., Harder, L.F. and Chung, R.M., October 1984, (PB85 191 732/AS)A04.

UCB/EERC-84/16 "Simplified Procedures for the Evaluation of Settlements in Sands Due to Earthquake Shaking," by Tokimatsu, K. and Seed, H.B., October 1984, (PB85 197 887/AS)A03.

UCB/EERC-84/17 "Evaluation of Energy Absorption Characteristics of Highway Bridges Under Seismic Conditions - Volume I (PB90 262 627)A16 and Volume II (Appendices) (PB90 262 635)A13," by Imbsen, R.A. and Penzien, J., September 1986.

UCB/EERC-84/18 "Structure-Foundation Interactions under Dynamic Loads," by Liu, W.D. and Penzien, J., November 1984, (PB87 124 889/AS)A11.

UCB/EERC-84/19 "Seismic Modelling of Deep Foundations," by Chen, C.-H. and Penzien, J., November 1984, (PB87 124 798/AS)A07.

UCB/EERC-84/20 "Dynamic Response Behavior of Quan Shui Dam," by Clough, R.W., Chang, K.-T., Chen, H.-Q., Stephen, R.M., Ghanaat, Y. and Qi, J.-H., November 1984, (PB85 115177/AS)A07.

UCB/EERC-85/01 "Simplified Methods of Analysis for Earthquake Resistant Design of Buildings," by Cruz, E.F. and Chopra, A.K., February 1985, (PB86 112299/AS)A12.

UCB/EERC-85/02 "Estimation of Seismic Wave Coherency and Rupture Velocity using the SMART 1 Strong-Motion Array Recordings," by Abrahamson, N.A., March 1985, (PB86 214 343)A07.

UCB/EERC-85/03 "Dynamic Properties of a Thirty Story Condominium Tower Building," by Stephen, R.M., Wilson, E.L. and Stander, N., April 1985, (PB86 118965/AS)A06.

UCB/EERC-85/04 "Development of Substructuring Techniques for On-Line Computer Controlled Seismic Performance Testing," by Dermitzakis, S. and Mahin, S., February 1985, (PB86 132941/AS)A08.

UCB/EERC-85/05 "A Simple Model for Reinforcing Bar Anchorages under Cyclic Excitations," by Filippou, F.C., March 1985, (PB86 112 919/AS)A05.

UCB/EERC-85/06 "Racking Behavior of Wood-framed Gypsum Panels under Dynamic Load," by Oliva, M.G., June 1985, (PB90 262 643)A04.

UCB/EERC-85/07 "Earthquake Analysis and Response of Concrete Arch Dams," by Fok, K.-L. and Chopra, A.K., June 1985, (PB86 139672/AS)A10.

UCB/EERC-85/08 "Effect of Inelastic Behavior on the Analysis and Design of Earthquake Resistant Structures," by Lin, J.P. and Mahin, S.A., June 1985, (PB86 135340/AS)A08.

UCB/EERC-85/09 "Earthquake Simulator Testing of a Base-Isolated Bridge Deck," by Kelly, J.M., Buckle, I.G. and Tsai, H.-C., January 1986, (PB87 124 152/AS)A06.

UCB/EERC-85/10 "Simplified Analysis for Earthquake Resistant Design of Concrete Gravity Dams" by Fenves, G. and Chopra, A.K., June 1986. (PB87 124 160/AS)A08.

UCB/EERC-85/11 "Dynamic Interaction Effects in Arch Dams." by Clough, R.W., Chang, K.-T., Chen, H.-Q. and Ghanaat, Y., October 1985. (PB86 135027/AS)A05.

UCB/EERC-85/12 "Dynamic Response of Long Valley Dam in the Mammoth Lake Earthquake Series of May 25-27, 1980," by Lai, S. and Seed, H.B., November 1985. (PB86 142304/AS)A05.

UCB/EERC-85/13 "A Methodology for Computer-Aided Design of Earthquake-Resistant Steel Structures," by Austin, M.A., Pister, K.S. and Mahin, S.A., December 1985. (PB86 159480/AS)A10.

UCB/EERC-85/14 "Response of Tension-Leg Platforms to Vertical Seismic Excitations," by Liou, G.-S., Penzien, J. and Yeung, R.W., December 1985. (PB87 124 871/AS)A08.

UCB/EERC-85/15 "Cyclic Loading Tests of Masonry Single Piers, Volume 4 - Additional Tests with Height to Width Ratio of 1," by Sveinsson, B., McNiven, H.D. and Sucuoglu, H., December 1985.

UCB/EERC-85/16 "An Experimental Program for Studying the Dynamic Response of a Steel Frame with a Variety of Infill Partitions," by Yanev, B. and McNiven, H.D., December 1985. (PB90 262 676/AS)A05.

UCB/EERC-86/01 "A Study of Seismically Resistant Eccentrically Braced Steel Frame Systems," by Kasai, K. and Popov, E.P., January 1986. (PB87 124 178/AS)A14.

UCB/EERC-86/02 "Design Problems in Soil Liquefaction," by Seed, H.B., February 1986. (PB87 124 186/AS)A03.

UCB/EERC-86/03 "Implications of Recent Earthquakes and Research on Earthquake-Resistant Design and Construction of Buildings," by Bertero, V.V., March 1986. (PB87 124 194/AS)A05.

UCB/EERC-86/04 "The Use of Load Dependent Vectors for Dynamic and Earthquake Analyses," by Leger, P., Wilson, E.L. and Clough, R.W., March 1986. (PB87 124 202/AS)A12.

UCB/EERC-86/05 "Two Beam-To-Column Web Connections," by Tsai, K.-C. and Popov, E.P., April 1986. (PB87 124 301/AS)A04.

UCB/EERC-86/06 "Determination of Penetration Resistance for Coarse-Grained Soils using the Becker Hammer Drill," by Harder, L.F. and Seed, H.B., May 1986. (PB87 124 210/AS)A07.

UCB/EERC-86/07 "A Mathematical Model for Predicting the Nonlinear Response of Unreinforced Masonry Walls to In-Plane Earthquake Excitations," by Mengi, Y. and McNiven, H.D., May 1986. (PB87 124 780/AS)A06.

UCB/EERC-86/08 "The 19 September 1985 Mexico Earthquake: Building Behavior," by Bertero, V.V., July 1986.

UCB/EERC-86/09 "EACD-3D: A Computer Program for Three-Dimensional Earthquake Analysis of Concrete Dams," by Fok, K.-L., Hall, J.F. and Chopra, A.K., July 1986. (PB87 124 228/AS)A08.

UCB/EERC-86/10 "Earthquake Simulation Tests and Associated Studies of a 0.3-Scale Model of a Six-Story Concentrically Braced Steel Structure," by Uang, C.-M. and Bertero, V.V., December 1986. (PB87 163 564/AS)A17.

UCB/EERC-86/11 "Mechanical Characteristics of Base Isolation Bearings for a Bridge Deck Model Test," by Kelly, J.M., Buckle, I.G. and Koh, C.-G., November 1987. (PB90 262 668)A04.

UCB/EERC-86/12 "Effects of Axial Load on Elastomeric Isolation Bearings," by Koh, C.-G. and Kelly, J.M., November 1987.

UCB/EERC-87/01 "The FPS Earthquake Resisting System: Experimental Report," by Zayas, V.A., Low, S.S. and Mahin, S.A., June 1987.

UCB/EERC-87/02 "Earthquake Simulator Tests and Associated Studies of a 0.3-Scale Model of a Six-Story Eccentrically Braced Steel Structure," by Whittaker, A., Uang, C.-M. and Bertero, V.V., July 1987.

UCB/EERC-87/03 "A Displacement Control and Uplift Restraint Device for Base-Isolated Structures," by Kelly, J.M., Griffith, M.C. and Aiken, I.D., April 1987.

UCB/EERC-87/04 "Earthquake Simulator Testing of a Combined Sliding Bearing and Rubber Bearing Isolation System," by Kelly, J.M. and Chalhoub, M.S., 1987.

UCB/EERC-87/05 "Three-Dimensional Inelastic Analysis of Reinforced Concrete Frame-Wall Structures," by Moazzami, S. and Bertero, V.V., May 1987.

UCB/EERC-87/06 "Experiments on Eccentrically Braced Frames with Composite Floors," by Ricles, J. and Popov, E., June 1987.

UCB/EERC-87/07 "Dynamic Analysis of Seismically Resistant Eccentrically Braced Frames," by Ricles, J. and Popov, E., June 1987.

UCB/EERC-87/08 "Undrained Cyclic Triaxial Testing of Gravels-The Effect of Membrane Compliance," by Evans, M.D. and Seed, H.B., July 1987.

UCB/EERC-87/09 "Hybrid Solution Techniques for Generalized Pseudo-Dynamic Testing," by Thewalt, C. and Mahin, S.A., July 1987.

UCB/EERC-87/10 "Ultimate Behavior of Butt Welded Splices in Heavy Rolled Steel Sections," by Bruneau, M., Mahin, S.A. and Popov, E.P., September 1987.

UCB/EERC-87/11 "Residual Strength of Sand from Dam Failures in the Chilean Earthquake of March 3, 1985," by De Alba, P., Seed, H.B., Retamal, E. and Seed, R.B., September 1987.

UCB/EERC-87/12 "Inelastic Seismic Response of Structures with Mass or Stiffness Eccentricities in Plan," by Bruneau, M. and Mahin, S.A., September 1987. (PB90 262 650)A14.

UCB/EERC-87/13 "CSTRUCT: An Interactive Computer Environment for the Design and Analysis of Earthquake Resistant Steel Structures," by Austin, M.A., Mahin, S.A. and Pister, K.S., September 1987.

UCB/EERC-87/14 "Experimental Study of Reinforced Concrete Columns Subjected to Multi-Axial Loading," by Low, S.S. and Moehle, J.P., September 1987.

UCB/EERC-87/15 "Relationships between Soil Conditions and Earthquake Ground Motions in Mexico City in the Earthquake of Sept. 19, 1985," by Seed, H.B., Romo, M.P., Sun, J., Jaime, A. and Lysmer, J., October 1987.

UCB/EERC-87/16 "Experimental Study of Seismic Response of R. C. Setback Buildings," by Shahrooz, B.M. and Moehle, J.P., October 1987.

UCB/EERC-87/17 "The Effect of Slabs on the Flexural Behavior of Beams," by Pantazopoulou, S.J. and Moehle, J.P., October 1987, (PB90 262 700)A07.

UCB/EERC-87/18 "Design Procedure for R-FBI Bearings," by Mostaghel, N. and Kelly, J.M., November 1987, (PB90 262 718)A04

UCB/EERC-87/19 "Analytical Models for Predicting the Lateral Response of R C Shear Walls: Evaluation of their Reliability," by Vulcano, A. and Bertero, V.V., November 1987

UCB/EERC-87/20 "Earthquake Response of Torsionally-Coupled Buildings," by Hejal, R. and Chopra, A.K., December 1987.

UCB/EERC-87/21 "Dynamic Reservoir Interaction with Monticello Dam," by Clough, R.W., Ghanaat, Y. and Qiu, X-F., December 1987.

UCB/EERC-87/22 "Strength Evaluation of Coarse-Grained Soils," by Siddiqi, F.H., Seed, R.B., Chan, C.K., Seed, H.B. and Pyke, R.M., December 1987.

UCB/EERC-88/01 "Seismic Behavior of Concentrically Braced Steel Frames," by Khatib, I., Mahin, S.A. and Pister, K.S., January 1988.

UCB/EERC-88/02 "Experimental Evaluation of Seismic Isolation of Medium-Rise Structures Subject to Uplift," by Griffith, M.C., Kelly, J.M., Coveney, V.A. and Koh, C.G., January 1988.

UCB/EERC-88/03 "Cyclic Behavior of Steel Double Angle Connections," by Astaneh-Asl, A. and Nader, M.N., January 1988.

UCB/EERC-88/04 "Re-evaluation of the Slide in the Lower San Fernando Dam in the Earthquake of Feb. 9, 1971," by Seed, H.B., Seed, R.B., Harder, L.F. and Jong, H.-L., April 1988.

UCB/EERC-88/05 "Experimental Evaluation of Seismic Isolation of a Nine-Story Braced Steel Frame Subject to Uplift," by Griffith, M.C., Kelly, J.M. and Aiken, I.D., May 1988.

UCB/EERC-88/06 "DRAIN-2DX User Guide," by Allahabadi, R. and Powell, G.H., March 1988.

UCB/EERC-88/07 "Theoretical and Experimental Studies of Cylindrical Water Tanks in Base-Isolated Structures," by Chalhoub, M.S. and Kelly, J.M., April 1988.

UCB/EERC-88/08 "Analysis of Near-Source Waves: Separation of Wave Types using Strong Motion Array Recordings," by Darragh, R.B., June 1988.

UCB/EERC-88/09 "Alternatives to Standard Mode Superposition for Analysis of Non-Classically Damped Systems," by Kusainov, A.A. and Clough, R.W., June 1988.

UCB/EERC-88/10 "The Landslide at the Port of Nice on October 16, 1979," by Seed, H.B., Seed, R.B., Schlosser, F., Blondeau, F. and Juran, I., June 1988.

UCB/EERC-88/11 "Liquefaction Potential of Sand Deposits Under Low Levels of Excitation," by Carter, D.P. and Seed, H.B., August 1988.

UCB/EERC-88/12 "Nonlinear Analysis of Reinforced Concrete Frames Under Cyclic Load Reversals," by Filippou, F.C. and Issa, A., September 1988.

UCB/EERC-88/13 "Implications of Recorded Earthquake Ground Motions on Seismic Design of Building Structures," by Uang, C.-M. and Bertero, V.V., November 1988.

UCB/EERC-88/14 "An Experimental Study of the Behavior of Dual Steel Systems," by Whittaker, A.S., Uang, C.-M. and Bertero, V.V., September 1988.

UCB/EERC-88/15 "Dynamic Moduli and Damping Ratios for Cohesive Soils," by Sun, J.I., Golesorkhi, R. and Seed, H.B., August 1988.

UCB/EERC-88/16 "Reinforced Concrete Flat Plates Under Lateral Load: An Experimental Study Including Biaxial Effects," by Pan, A. and Moehle, J., October 1988.

UCB/EERC-88/17 "Earthquake Engineering Research at Berkeley - 1988," by EERC, November 1988.

UCB/EERC-88/18 "Use of Energy as a Design Criterion in Earthquake-Resistant Design," by Uang, C.-M. and Bertero, V.V., November 1988.

UCB/EERC-88/19 "Steel Beam-Column Joints in Seismic Moment Resisting Frames," by Tsai, K.-C. and Popov, E.P., November 1988.

UCB/EERC-88/20 "Base Isolation in Japan, 1988," by Kelly, J.M., December 1988.

UCB/EERC-89/01 "Behavior of Long Links in Eccentrically Braced Frames," by Engelhardt, M.D. and Popov, E.P., January 1989.

UCB/EERC-89/02 "Earthquake Simulator Testing of Steel Plate Added Damping and Stiffness Elements," by Whittaker, A., Bertero, V.V., Alonso, J. and Thompson, C., January 1989.

UCB/EERC-89/03 "Implications of Site Effects in the Mexico City Earthquake of Sept. 19, 1985 for Earthquake-Resistant Design Criteria in the San Francisco Bay Area of California," by Seed, H.B. and Sun, J.I., March 1989.

UCB/EERC-89/04 "Earthquake Analysis and Response of Intake-Outlet Towers," by Goyal, A. and Chopra, A.K., July 1989.

UCB/EERC-89/05 "The 1985 Chile Earthquake: An Evaluation of Structural Requirements for Bearing Wall Buildings," by Wallace, J.W. and Moehle, J.P., July 1989.

UCB/EERC-89/06 "Effects of Spatial Variation of Ground Motions on Large Multiply-Supported Structures," by Hao, H., July 1989.

UCB/EERC-89/07 "EADAP - Enhanced Arch Dam Analysis Program: Users's Manual," by Ghanaat, Y. and Clough, R.W., August 1989.

UCB/EERC-89/08 "Seismic Performance of Steel Moment Frames Plastically Designed by Least Squares Stress Fields," by Ohi, K. and Mahin, S.A., August 1989.

UCB/EERC-89/09 "Feasibility and Performance Studies on Improving the Earthquake Resistance of New and Existing Buildings Using the Friction Pendulum System," by Zayas, V., Low, S., Mahin, S.A. and Bozzo, L., July 1989.

UCB/EERC-89/10 "Measurement and Elimination of Membrane Compliance Effects in Undrained Triaxial Testing," by Nicholson, P.G., Seed, R.B. and Anwar, H., September 1989.

UCB/EERC-89/11 "Static Tilt Behavior of Unanchored Cylindrical Tanks," by Lau, D.T. and Clough, R.W., September 1989.

UCB/EERC-89/12 "ADAP-88: A Computer Program for Nonlinear Earthquake Analysis of Concrete Arch Dams," by Fenves, G.L., Mojtahedi, S. and Reimer, R.B., September 1989.

UCB/EERC-89/13 "Mechanics of Low Shape Factor Elastomeric Seismic Isolation Bearings," by Aiken, I.D., Kelly, J.M. and Tajirian, F.F., November 1989.

UCB/EERC-89/14 "Preliminary Report on the Seismological and Engineering Aspects of the October 17, 1989 Santa Cruz (Loma Prieta) Earthquake," by EERC, October 1989.

UCB/EERC-89/15 "Experimental Studies of a Single Story Steel Structure Tested with Fixed, Semi-Rigid and Flexible Connections," by Nader, M.N. and Astaneh-Asl, A., August 1989.

UCB/EERC-89/16 "Collapse of the Cypress Street Viaduct as a Result of the Loma Prieta Earthquake," by Nims, D.K., Miranda, E., Aiken, I.D., Whittaker, A.S. and Bertero, V.V., November 1989.

UCB/EERC-90/01 "Mechanics of High-Shape Factor Elastomeric Seismic Isolation Bearings," by Kelly, J.M., Aiken, I.D. and Tajirian, F.F., March 1990.

UCB/EERC-90/02 "Javid's Paradox: The Influence of Preform on the Modes of Vibrating Beams," by Kelly, J.M., Sackman, J.L. and Javid, A., May 1990.

UCB/EERC-90/03 "Earthquake Simulator Testing and Analytical Studies of Two Energy-Absorbing Systems for Multistory Structures," by Aiken, I.D. and Kelly, J.M., October 1990.

UCB/EERC-90/04 "Damage to the San Francisco-Oakland Bay Bridge During the October 17, 1989 Earthquake," by Astaneh, A., June 1990.

UCB/EERC-90/05 "Preliminary Report on the Principal Geotechnical Aspects of the October 17, 1989 Loma Prieta Earthquake," by Seed, R.B., Dickenson, S.E., Riemer, M.F., Bray, J.D., Sitar, N., Mitchell, J.K., Idriss, I.M., Kayen, R.E., Kropp, A., Harder, L.F., Jr. and Power, M.S., April 1990.

UCB/EERC-90/06 "Models of Critical Regions in Reinforced Concrete Frames Under Seismic Excitations," by Zulfiqar, N. and Filippou, F., May 1990.

UCB/EERC-90/07 "A Unified Earthquake-Resistant Design Method for Steel Frames Using ARMA Models," by Takewaki, I., Conte, J.P., Mahin, S.A. and Pister, K.S., June 1990.

UCB/EERC-90/08 "Soil Conditions and Earthquake Hazard Mitigation in the Marina District of San Francisco," by Mitchell, J.K., Masood, T., Kayen, R.E. and Seed, R.B., May 1990.

UCB/EERC-90/09 "Influence of the Earthquake Ground Motion Process and Structural Properties on Response Characteristics of Simple Structures," by Conte, J.P., Pister, K.S. and Mahin, S.A., July 1990.

UCB/EERC-90/10 "Experimental Testing of the Resilient-Friction Base Isolation System," by Clark, P.W. and Kelly, J.M., July 1990.

UCB/EERC-90/11 "Seismic Hazard Analysis: Improved Models, Uncertainties and Sensitivities," by Araya, R. and Der Kiureghian, A., March 1988.

UCB/EERC-90/12 "Effects of Torsion on the Linear and Nonlinear Seismic Response of Structures," by Sedarat, H. and Bertero, V.V., September 1989.

UCB/EERC-90/13 "The Effects of Tectonic Movements on Stresses and Deformations in Earth Embankments," by Bray, J.D., Seed, R.B. and Seed, H.B., September 1989.

UCB/EERC-90/14 "Inelastic Seismic Response of One-Story, Asymmetric-Plan Systems," by Goel, R.K. and Chopra, A.K., October 1990.

UCB/EERC-90/15 "Dynamic Crack Propagation: A Model for Near-Field Ground Motion," by Seyyedian, H. and Kelly, J.M., 1990.

UCB/EERC-90/16 "Sensitivity of Long-Period Response Spectra to System Initial Conditions," by Blasquez, R., Ventura, C. and Kelly, J.M., 1990.

UCB/EERC-90/17 "Behavior of Peak Values and Spectral Ordinates of Near-Source Strong Ground-Motion over a Dense Array," by Niazi, M., June 1990.

UCB/EERC-90/18 "Material Characterization of Elastomers used in Earthquake Base Isolation," by Papoulia, K.D. and Kelly, J.M., 1990.

UCB/EERC-90/19 "Cyclic Behavior of Steel Top-and-Bottom Plate Moment Connections," by Harriott, J.D. and Astaneh, A., August 1990.

UCB/EERC-90/20 "Seismic Response Evaluation of an Instrumented Six Story Steel Building," by Shen, J.-H. and Astaneh, A., December 1990.

UCB/EERC-90/21 "Observations and Implications of Tests on the Cypress Street Viaduct Test Structure," by Bollo, M., Mahin, S.A., Moehle, J.P., Stephen, R.M. and Qi, X., December 1990.

UCB/EERC-91/01 "Experimental Evaluation of Nitinol for Energy Dissipation in Structures," by Nims, D.K., Sasaki, K.K. and Kelly, J.M., 1991.

UCB/EERC-91/02 "Displacement Design Approach for Reinforced Concrete Structures Subjected to Earthquakes," by Qi, X. and Moehle, J.P., January 1991.

UCB/EERC-91/03 "Shake Table Tests of Long Period Isolation System for Nuclear Facilities at Soft Soil Sites," by Kelly, J.M., March 1991.

UCB/EERC-91/04 "Dynamic and Failure Characteristics of Bridgestone Isolation Bearings," by Kelly, J.M., April 1991.

UCB/EERC-91/05 "Base Sliding Response of Concrete Gravity Dams to Earthquakes," by Chopra, A.K. and Zhang, L., May 1991.

UCB/EERC-91/06 "Computation of Spatially Varying Ground Motion and Foundation-Rock Impedance Matrices for Seismic Analysis of Arch Dams," by Zhang, L. and Chopra, A.K., May 1991.

UCB/EERC-91/07 "Estimation of Seismic Source Processes Using Strong Motion Array Data," by Chiou, S.-J., July 1991.